JOHANNES GUTENBERG UNIVERSITÄT MAINZ

Synthese, Radiomarkierung sowie *in vitro*- und *in vivo*-Evaluierung verschiedener Chelator-Biomolekül-Systeme mit den Radionukliden ^{68}Ga, ^{89}Zr und ^{177}Lu

Dissertation

zur Erlangung des Grades eines
„Doktor rerum naturalium (Dr. rer. nat.)“
im Promotionsfach Chemie

am Fachbereich Chemie, Pharmazie und Geowissenschaften
der Johannes Gutenberg-Universität Mainz
vorgelegt von

Johannes Nagel
geboren in Lugowoje/Kasachstan

Mainz, August 2017

Dekan: [redacted]

Erster Berichterstatter: [redacted]

Zweiter Berichterstatter: [redacted]

Tag der mündlichen Prüfung: 17.08.2017

Zusammenfassung

Die Synthese und Radiometallmarkierung von Chelator-Biomolekül-Systemen (CBS) ist ein wichtiges Gebiet der onkologischen Radiopharmazie. Diese Konjugate ermöglichen eine nicht-invasive Diagnostik mittels Positronenemissionstomographie (PET) als auch Radionuklidtherapie von malignen Tumoren durchzuführen.

Der allgemeine Vorteil der CBSs liegt in der einfachen radiochemischen Handhabung, wodurch das jeweilige Radionuklid unter geringem Zeit- und Arbeitsaufwand koordiniert und für *in vitro*- und *in vivo*-Untersuchungen zugänglich gemacht werden kann. Schlüsselkomponente hierfür ist die Verwendung eines geeigneten Chelators im Hinblick auf das Nuklide und dessen Halbwertszeiten. Neben der Reaktionsdauer ist die physiologische Verteilungs- und Zirkulationszeit des Biomoleküls relevant. So muss z. B. für einen Antikörper mit einer Zirkulationszeit von bis zu 3 Tagen ein Radionuklid mit einer Halbwertszeit von mehreren Stunden oder Tagen (wie z. B. ^{89}Zr ($t_{1/2}$=78,4 h) oder ^{177}Lu ($t_{1/2}$=6,7 d)) gewählt werden, um eine Anreicherung des Antikörper-Radionuklid-Konjugats selbst nach einigen Tagen detektieren zu können.

Basierend auf diesen Grundlagen wurden zunächst die thermodynamischen und kinetischen Komplexstabilitäten des neuen Chelators DATA^{m} und des bifunktionellen DATA^{5m} mit ^{nat}Ga sowie Transmetallierungsuntersuchungen durchgeführt. Beide Chelatoren wiesen eine hohe thermodynamische Stabilität mit einem logK > 21 auf. Die Transchelatisierungsstudien gegen Transferrin zeigten, dass das bifunktionelle Derivat eine Halbwertszeit von über 46 h und das DATA^{m} 9,4 h besaß. Diese grundlegenden Daten belegen einen stabilisierenden Effekt durch den n-Valeriansäurespacer am bifunktionellen Derivat (Teilprojekt A).

Im Teilprojekt B wurde DATA^{5m} mit dem Somatostatin-Analogon [DPhe^{1}][Tyr^{3}]-Octreotid (TOC), welches ein etablierter Targetingvektor für neuroendokrine Tumore (NET) ist, gekoppelt (DATA-TOC). Das DATA-TOC wurde als ^{nat}Ga-Komplex in *in vitro*-Studien bzgl. der Rezeptoraffinität sowie als ^{68}Ga-Komplex in präklinischen als auch klinischen *in vivo*-Studien hinsichtlich der Akkumulation des Konjugats untersucht. Um die Potenz des [^{68}Ga]Ga-DATA-TOC einzuordnen, wurden alle *in vitro*- und *in vivo*-Untersuchungen mit dem bisherigen Standard DOTA-TOC verglichen. Es konnte gezeigt werden, dass das [^{nat}Ga]Ga-DATA-TOC eine hohe Affinität von 1.03±0.08 nM gegenüber dem humanen Somatostatin-Rezeptor 2 (hsst$_2$) auf HEK293 Zellmembranen aufweist. Am Tumor-Mausmodell (SCID/beige sst2+ MPC-EGFP-Luc) verhält sich das [^{68}Ga]Ga-DATA-TOC ähnlich wie das [^{68}Ga]Ga-DOTA-TOC mit einer spezifischen Anreicherung im Tumorgewebe von über 2 %ID. Die ersten klinischen Studien an einem 46-Jährigen Patienten mit differenzierbaren NET im Pankreas zeigten, dass das [^{68}Ga]Ga-DATA-TOC zwar eine geringere Anreicherung im Tumor besitzt (SUV([^{68}Ga]Ga-DATA-TOC)=46,9 vs. SUV([^{68}Ga]Ga-DOTA-TOC)=71,1), jedoch auf Grund geringerer Aufnahme in der Leber einen besseren Kontrast zur

Differenzierung zwischen gesundem und tumorösem Gewebe bietet.

Im Teilprojekt C wurden mehrere bifunktionelle Derivate ($DATA^{5m}$-Bz-NCS, $DATA^{5m}$-TEG-N_3, $DATA^{5m}$-en-QS) des $DATA^{5m}$ synthetisiert, charakterisiert und deren ^{68}Ga-markierte Komplexe bezüglich ihrer *in vitro*-Stabilität untersucht. Alle Derivate zeigten quantitative radiochemische Ausbeuten (>95 %) innerhalb von 10 min bei RT innerhalb verschiedener Puffersysteme. Die ^{68}Ga-Komplexe des $DATA^{5m}$-en-QS und $DATA^{5m}$-TEG-N_3 besaßen zudem eine hohe *in vitro*-Stabilität (gegenüber humanem Serum, DTPA, EDTA und PBS), was beide Derivate zu hervorragenden Kandidaten für die Anwendung an Targetingvektoren wie Peptiden, Bisphosphonaten oder makromolekularen Systemen wie Antikörper oder Polymeren.

Analog zu den Derivaten aus Teilprojekt C sollten im Teilprojekt D bifunktionelle Derivate des literaturbekannten Chelators AAZTA (6-Amino-6-methylperhydro-1,4-diazepin-tetraacetat) synthetisiert und charakterisiert werden. Da dieser Chelator das gleiche Grundgerüst wie die DATA-Chelatoren besitzt, hierbei jedoch in der Lage ist das Therapienuklid ^{177}Lu zu komplexieren, sollte auch hier das Anwendungsgebiet dieses Chelatorgrundgerüsts erweitert werden. Die Radiomarkierungen zeigten die hohe Affinität des Chelators gegenüber dem ^{177}Lu, da das Lutetium durch alle Derivate bei einem Chelator-zu-Lutetium-Verhältnis von 2:1 quantitative komplexiert werden konnte. Analog zu den DATA-Derivaten zeigte sich auch hier eine hohe Stabilität der ^{177}Lu-Komplexe für die Derivate $AAZTA^5$-en-QS und $AAZTA^5$-TEG-N_3.

Im Teilprojekt E sollte ein durch Vakzinierung generierter Antikörper (GGSK-1/30), welcher spezifisch am humanen Antigen MUC1 anbindet, mit dem Chelator Desferrioxamin (Df) konjugiert werden. Die Konjugation von bis zu 4 Df-Einheiten pro Antikörper zeigte keine Verringerung der Immunoreaktivität des Antikörpers gegenüber dem MUC1. Das Konjugat wurde mit ^{89}Zr ($t_{1/2}$=3,3 d) markiert, aufgereinigt und in Zellbindungsstudien an verschiedenen Zelllinien untersucht. Hierbei zeigte sich eine hohe Affinität gegenüber humanen Brustkrebszellen mit einer Anbindung von über 30 %. Erste präklinische *in vivo*-Studien zeigten, dass der radiomarkierte Antikörper eine hohe Anreicherung mit über 55 %ID/g im Tumorgewebe aufwies. Die Spezifizität gegenüber dem MUC1 konnte durch Blockadestudien dargelegt werden, was sich in einer verringerten Anreicherung des Tumors widerspiegelte (<10 %ID/g).

Abstract

The synthesis and radio metal labelling of chelator biomolecule systems (CBS) is an important field within the oncological radiopharmacy. These conjugates offer non-invasive diagnostics via positron emission tomography (PET) as well as radionuclide therapy of malign tumours – depending on radio metal and chelator used.

The general advantage of CBSs is their simple radio chemical handling. They allow radio labelling of the system within a short time period and a low amount of work, which makes them easily accessible for *in vitro* and *in vivo* studies. Key component is the application of suitable chelate in respect to the used nuclide and its half-life. Besides the reaction time the physiological circulation time of a biomolecule have to be taken into account. Antibodies, for example, with a circulation time of 3 days have to be radio labelled with radio metals offering half lifes of several hours or days (e. g. ^{89}Zr ($t_{1/2}$=78,4 h) or ^{177}Lu ($t_{1/2}$=6,7 d)) to provide detectable amounts of the antibody-radionuclide-conjugate after several days.

Based on this background subproject A deals with thermodynamic and kinetic complex stabilities of the novel chelators DATA^{m} and DATA^{5m} with ^{nat}Ga as well as the trans metalation studies of these. Both chelators have shown a high thermodynamic stability with logK values > 21. The transchelation studies versus transferrin obtained a half life of 46 h for the DATA^{5m} and 9.4 h for the DATA^{m}. These findings proof the stabilizing effect due to the n-valeric acid spacers on the bifunctional derivative.

In subproject B the bifunctional derivative DATA^{5m} was coupled with the somatostatin analogue [DPhe^{1}][Tyr^{3}]-octreotide (TOC), which is a well-established targeting vector for neuroendocrine tumor (NET). The DATA-TOC was evaluated as [^{nat}Ga]Ga-complex in *in vitro* studies in respect to its receptor affinities as well as [^{68}Ga]Ga-complex in *in vivo* studies within preclinical and clinical studies concerning its accumulation in target tissue. To classify the potency of [^{68}Ga]Ga-DATA-TOC all *in vitro* and *in vivo* studies were compared with the gold standard DOTA-TOC. It was shown that [^{nat}Ga]Ga-DATA-TOC offers a high affinity of 1.03±0.08 nM to human somatostatin receptor ($hsst_2$) on HEK293 cell membranes. Within tumor mouse model (SCID/beige sst2+ MPC-EGFP-Luc) the preclinical *in vivo* studies ^{68}Ga-DATA-TOC demonstrated similar specific enrichment in tumor tissue as [^{68}Ga]Ga-DOTA-TOC with uptake values of 2 %ID. First clinical studies in a 46 year old patient with well-differentiated NETs in pancreas displayed, that [^{68}Ga]Ga-DATA-TOC represents a decreased tumor uptake (SUV([^{68}Ga]Ga-DATA-TOC)=46.9 vs. SUV([^{68}Ga]Ga-DOTA-TOC)=71.1) resulting in a higher contrast for differentiating between healthy and tumor tissue.

In subproject C several bifunctional chelators of the DATA^{5m} were synthesized, characterized and the ^{68}Ga-complexes evaluated regarding their *in vitro* stability. All derivatives offered quantitative radiolabelling yields (>95 %) within 10 min at RT within different buffer systems. ^{68}Ga-complexes of DATA^{5m}-

en-QS and DATA^{5m}-TEG-N_3 come with high *in vitro* stability (vs. human serum, DTPA, EDTA and PBS), which makes both derivatives excellent candidates for the application on targeting vectors like peptides, bisphosphonates or macromolecular systems like antibodies or polymers.

For subproject D same bifunctional chelators as in subproject C were synthesized of the known chelator AAZTA (6-Amino-6-methylperhydro-1,4-diazepine-tetraacetate). With the ability of AAZTA to complex the therapy nuclide ^{177}Lu the goal of this project was to broaden the application spectrum of this ligand. Radio labellings showed a high affinity of the chelators to ^{177}Lu since all derivatives could be quantitatively complexed with chelator-to-lutetium ratio of 2:1. Same as for the DATA derivatives, a high stability could be obtained for the ^{177}Lu-complexes of AAZTA^5-en-QS und AAZTA^5-TEG-N_3.

In subproject E a novel antibody (GGSK-1/30), which was generated by vaccination and demonstrated a specific affinity to human MUC1, was modified with desferrioxamine (Df). It could be shown that the conjugate had up to 4 Df units per antibody without loss of immunoreactivity against MUC1. The conjugate was radio labelled with ^{89}Zr ($t_{1/2}$=3.3 d), purified and tested in cell binding studies to different cell lines. The radio labelled compound offered more than 30 % binding to human breast cancer cells. First preclinical *in vivo* studies showed, that uptake over 55 %ID/g was observed in tumor tissue. The specificity to MUC1 was proofed by blocking experiments, displayed by a reduced tumor uptake of less than 10 %ID/g.

Für meine Liebsten

Inhalt

1. Einleitung

Laut einer durch die Weltgesundheitsorganisation WHO erhobenen Statistik aus dem Jahr 2011 ist Krebs die weltweit häufigste Todesursache. Der demografische und epidemiologische Wandel wird hierbei in den nächsten Jahrzehnten zu stetig steigenden Todesfällen durch Krebs führen. Laut Stewart *et al.* werden schon ab dem Jahr 2025 jährlich über 20 Millionen neue Krebsfälle in Ländern mit niedrigen und mittleren Einkommen erwartet [1,2]. Vermeidbare Risikofaktoren für Krebserkrankungen sind der Konsum von Tabak, eine ungesunde Ernährungsweise, UV-Strahlung des Sonnenlichtes sowie chronische, virale Infektionen [3,4]. Als unvermeidbare Risikofaktoren sind genetische Prädisposition sowie das voranschreitende Alter zu nennen [5]. Die wichtigsten Ziele der Krebsforschung heutzutage sind die frühzeitige Diagnose sowie eine effiziente Therapie malignen Tumorgewebes. Innerhalb der Nuklearmedizin haben sich die Positronenemissionstomographie (PET) sowie die Einzel-photonenemissionstomographie (engl.: *single photon emission computed tomography*, SPECT) als nicht-invasive Bildgebungsverfahren in der klinischen Anwendung etabliert. Hierbei wird dem Patienten ein sogenannter Radiotracer verabreicht. Prinzipiell bauen sich Radiotracer aus einem Biomolekül (wie z. B. einem Peptid) und dem Radioaktivstrahlung emittierenden Teil auf. Bei letzterem unterscheidet man zwischen Radionukliden, welche direkt (kovalent) am Biomolekül gebunden werden können (wie z. B. das ^{11}C oder ^{18}F) oder mittels eines sogenannten Chelators koordiniert werden (wie z. B. das ^{68}Ga, ^{89}Zr oder ^{177}Lu). Durch die spezifische Anreicherung und die vom Radiotracer emittierte Strahlung in Form von γ-Strahlen ist eine Visualisierung und Lokalisierung des Tumorgewebes möglich. Durch die Kombination aus PET bzw. SPECT mit Computertomographen (CT) oder Magnetresonanztomographen (MRT), welche morphologische Informationen liefern, ist es möglich, die Lage des Tumors einem Organ/Gewebe zuzuordnen. Diese Diagnostikmethode erleichtert den operativen Eingriff am Tumor, da eine präzisere Auskunft gegenüber den reinen CT-/MRT-Messungen gewonnen wird und ein unmittelbarer Vergleich zwischen prä- und postoperativer Diagnostik gezogen werden kann [6–10].

Neben der Diagnostik hat die nuklearmedizinische Therapie in den letzten Jahren an großer Aufmerksamkeit gewonnen. Beruhend auf dem Prinzip der peptidrezeptorvermittelten Radiotherapie (PRRT) kommen immer mehr Radiotracer basierend auf regulatorischen Peptiden wie dem Octreotid in Kombination mit Radioisotopen wie ^{90}Y oder ^{177}Lu als Therapienuklide zum Einsatz [11–15]. Wie auch bei der Diagnostik, ist auch hier der nicht-invasive Einsatz der Verbindung von Vorteil. Des Weiteren sorgt die spezifische und selektive Anreicherung des Tracers dafür, dass ausschließlich tumoröses Gewebe durch die emittierte Strahlung zerstört wird und gesundes Gewebe weitestgehend verschont bleibt [11,13,16].

1.1 Chelatoren / Bifunktionelle Chelatoren (BFC)

Chelatoren sind Liganden, welche mittels mehrerer koordinativer Bindungsstellen ein Metallion komplexieren können. Die Geometrie des dabei entstehenden Komplexes (tetraedrisch, oktaedrisch, quadratisch-planar, etc.) ist einerseits abhängig von der Zähnigkeit des Liganden, d. h. von der Anzahl der Ligandatome, die der Chelator liefert. Andererseits bestimmt auch die Elektronenkonfiguration und die damit zusammenhängende Ionenladung des Ions die Komplexierungsgeometrie.
Systematisch können die Chelatoren in zwei Klassen aufgeteilt werden: (makro)-zyklische und azyklische Chelatoren. Durch Erweiterungen am Rückgrat können diese noch funktionalisiert werden, sodass ein sogenannter bifunktioneller Chelator (BFC) erhalten wird. Durch diese Funktionalisierung ist der Ligand in der Lage, simultan ein Radionuklid zu komplexieren und ein Biomolekül als Targetingvektor (TV) zu tragen. Unter einem bifunktionellen Chelator (BFC) versteht man ein System, bei dem der Chelator sowohl für die Komplexierung des Radiometalls als auch für der Kopplung an Biomoleküle wie Peptide befähigt ist. Abbildung 1 zeigt schematisch den grundlegenden Aufbau eines BFC gekoppelt an einem TV.

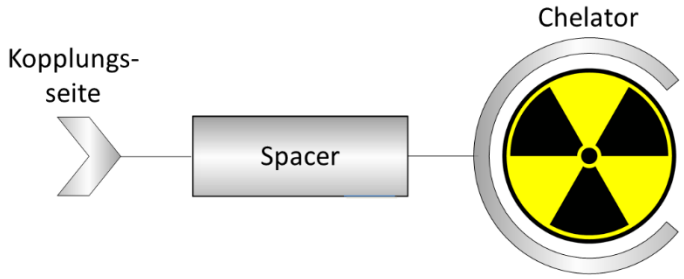

Abbildung 1: Grundstruktur eines BFC-TV-Systems basierend auf dem Komplexbildner (rechts), einem Spacer (mitte) und der Kopplungsseite zum Targetingvektor (links)

Die Vielfalt an bifunktionellen Chelatoren ermöglicht die Radiomarkierung verschiedenster biologisch relevanter Vektoren. Es können Peptide wie das PSMA [17,18] oder Octreotid-Analoga [19–21] als auch Polypeptide wie das Exendin-4 [22] oder nanodimensionale Systeme wie Antikörper [23,24] und Nanopartikel [25,26] unter milden Bedingungen an die BFCs angebracht werden. Die wichtigsten funktionellen Gruppen für Chelatoren und deren Kopplungspartner sind in Abbildung 2 aufgelistet.

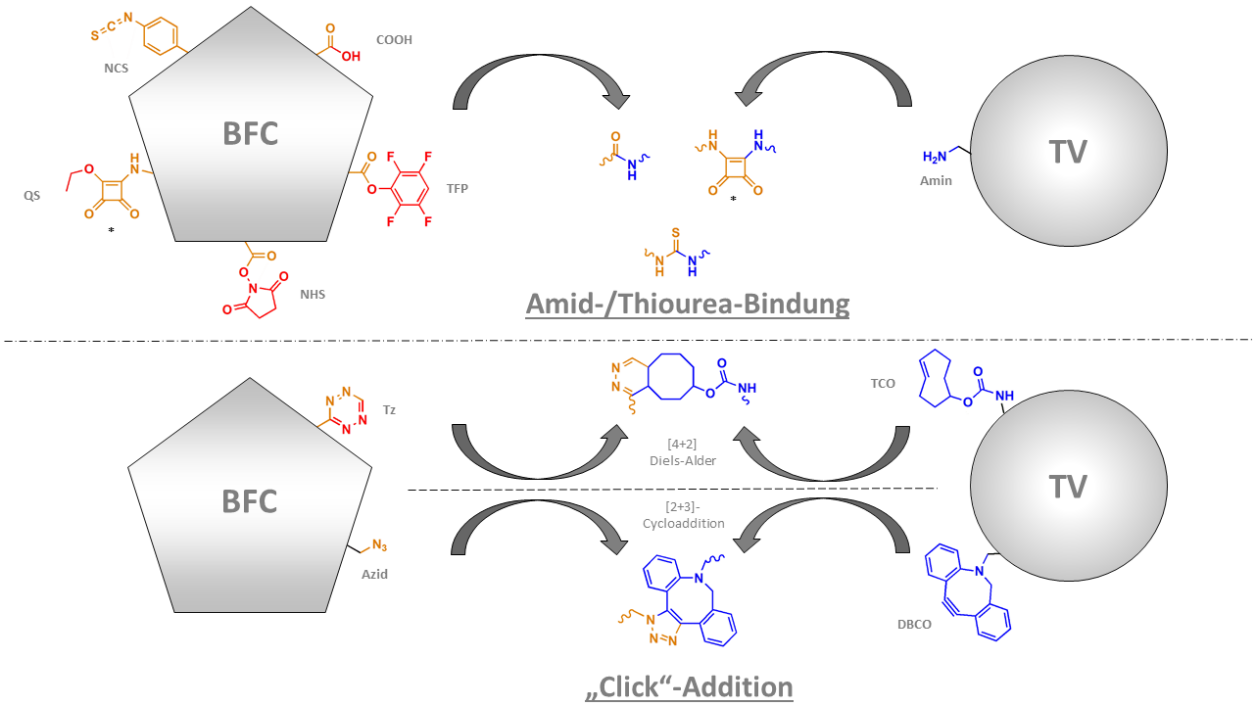

Abbildung 2: Kopplungsvarianten zwischen bifunktionellen Chelatoren (BFC) und modifizierten Targetingvektoren (TV); NHS: Succinimidylester, QS: Quadratsäureester, NCS: Isothiocyanat, COOH: Carbonsäure, TFP: Tetrafluorphenolester, Tz: Tetrazin, N_3: Azid, TCO: *trans*-Cycloocten, DBCO: Dibenzylcyclooctin

Mittels einer zusätzlichen Carbonsäureeinheit (-COOH) kann ein BFC unter klassischen Amidbindungsbedingungen an die Biomoleküle angebunden werden [27]. Alternativ wurde die Succinimidyleinheit als Aktivester von Carbonsäuren eingeführt, um eine Kopplung unter milden Bedingungen sowie innerhalb von wenigen Minuten an primären Aminen zu erreichen [28]. Eine Weiterentwicklung im Hinblick auf die Stabilität dieser Ester ist das Tetrafluorphenol-Derivat. Dieses zeigt im Vergleich zu den NHS-Estern eine verringerte Hydrolyseempfindlichkeit und somit eine effizientere Umsetzung zum gewünschten Produkt [29]. Eine elegante Kopplungschemie bietet die sogenannte Quadratsäure (QS). Mit diesem vinylogen System ist es durch die Variation des pH-Wertes möglich innerhalb eines Moleküls zwei Amidbindungen auszubilden. Ein weiterer Vorteil ist die hohe Selektivität des Esters gegenüber primären Aminen, d. h. weder alkoholische noch phenolische Hydroxylgruppe sind in der Lage mit der Quadratsäure zu reagieren [30]. Entsprechend muss ein primäres Amin am Chelator zugegen sein, um diesen mit der QS zu funktionalisieren. Enorme Bedeutung haben die Benzyl-NCS-Ester zur Funktionalisierung verschiedener Chelatoren erhalten, da diese unter milden Bedingungen (pH 8-9, RT) an Biomoleküle mit freien, primären Aminen geknüpft werden können. Die dabei gebildete Thiourea-Einheit weist eine hohe Stabilität auf, was Grundvoraussetzung für *in vitro*- und *in vivo*-Studien ist [31–34].

Die beiden letztgenannten Systeme eignen sich für eine kupferfreie, spannungsvermittelte Clickchemie. Während beim Azid/DBCO-System eine [2+3]-Cycloaddition als Kopplungsreaktion stattfindet,

handelt es sich beim Tetrazin/*trans*-Cycloocten-System um eine [4+2]-Diels-Alder-Cycloaddition [35]. Beide Methoden ermöglichen es, den bifunktionellen Chelator radioaktiv zu markieren, aufzureinigen und anschließend am Biomolekül anzukoppeln. Das Azid/DBCO-System kann variabel verwendet werden, da das Azid sowohl am Chelator als auch am Biomolekül angekoppelt werden kann. Bisherige Untersuchungen bezüglich der Reaktionsgeschwindigkeit zeigten, dass das Cyclooctin eine geringere Geschwindigkeit aufweist als das *trans*-Cycloocten [36–40]. Während unterschiedliche DBCO-Derivate mit Benzylazid Ratenkonstanten von bis zu 0,96 $M^{-1}s^{-1}$ erreichten [36], konnten mit 3,6-Diaryltetrazinen und verschiedenen *trans*-Cyclooctenen Reaktionsgeschwindigkeiten von bis zu 22000 $M^{-1}s^{-1}$ erreicht werden. Aufgrund dieser hohen Geschwindigkeitsrate haben Tetrazin/*trans*-Cycloocten-Systeme innerhalb der letzten Jahre eine Anwendung in sogenannten *in vivo*-Click-Reaktionen gefunden [41,42].

Im Hinblick auf den Anwendungsbereich innerhalb der Nuklearmedizin ist die Stabilität solcher Komplexe von enormer Wichtigkeit. Man unterscheidet zwischen der thermodynamischen und der kinetischen Stabilität. Die thermodynamische Stabilität spiegelt sich in der Komplexstabilitätskonstanten K_{ML} zwischen Ligand (L) und Radionuklid (M) wider und wird durch den $\log K_{ML}$ beschrieben. Die kinetische Stabilität ist ein Maß für die Transmetallierung des Komplexes durch Fremdmetalle wie Eisen oder durch Glykoproteine wie dem *apo*-Transferrin. Für die Anwendung in der Nuklearmedizin wird der kinetischen Stabilität eine größere Bedeutung beigemessen, da innerhalb der *in vivo*-Experimente ein stabiler Komplex unabdingbar ist.

1.1.1 Makrozyklische Chelatoren

Die wichtigsten makrozyklischen Chelatoren und deren bifunktionelle Derivate für 3-wertige Radiometale sind das DOTA (1,4,7,10-Tetraazacyclododecan-1,4,7,10-tetraessigsäure, Abbildung 3) und das NOTA (1,4,7-Triazacyclononan-1,4,7-triessigsäure, Abbildung 4). Das DOTA bietet durch sein N_4O_4-Komplexierungsgerüst eine ausreichende Anzahl an Ligandatomen zur Komplexierung verschiedenster Radionuklide wie ^{68}Ga, $^{44/47}$Sc oder ^{177}Lu [43–48]. Hierbei wird eine der vier Säureeinheiten für die Kopplung am Biomolekül verwendet, wodurch eine Acetatgruppe für die Komplexierung des Nuklids entfällt. Für die Anwendung des DOTA-Chelators im Bereich der Radiotherapie mit ^{225}Ac werden bifunktionelle Derivate wie das *p*-SCN-Bz-DOTA eingesetzt (Abbildung 3), um die 8-fache Komplexierungsgeometrie zu erhalten und damit eine erhöhte Stabilität des [^{225}Ac]Ac-DOTA-Komplexes zu gewährleisten [49,50].

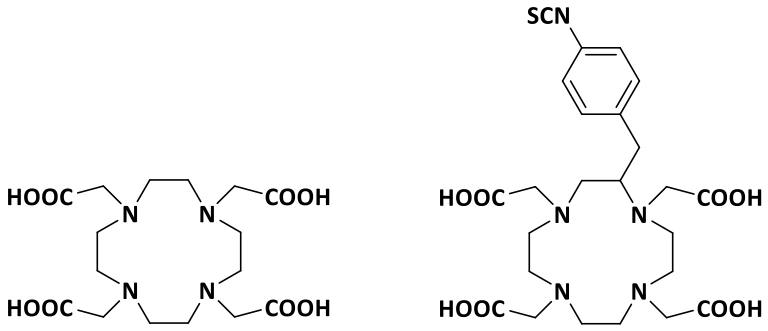

DOTA **p-SCN-Bz-DOTA**

Abbildung 3: Struktur des Chelators DOTA und dessen Derivates *p*-SCN-Bz-DOTA

NOTA zeigt hervorragende Markierungseigenschaften mit ^{64}Cu und ^{68}Ga, ist jedoch als solches für die Anwendung innerhalb der Nuklearmedizin ungeeignet [51–53]. Daher wurden bifunktionelle Derivate wie das *p*-SCN-Bz-NOTA als auch das NODAGA-NHS entwickelt (Abbildung 4) und an Peptide oder an Antikörper gekoppelt [54–56]. Zwar besitzt das NOTA im Vergleich zu DOTA für die Radiomarkierung von ^{64}Cu und ^{68}Ga den Vorteil einer höheren Stabilität und einer milden Markierungschemie, jedoch beschränkt sich die Anwendung des NOTAs auf Grund seiner kleineren Käfiggeometrie und der hexadentalen Ligandenstruktur nur auf wenige Nuklide [57]. Ein vielversprechendes Derivat des NOTA ist das TRAP (1,4,7-triazacyclononan-1,4,7-tris[methyl(2-carboxyethyl)phosphinsäure], Abbildung 4), welches eine hohe Spezifizität gegenüber dem PET-Nuklid ^{68}Ga aufweist [58,59]. Erste präklinische Evaluierungen trimerer RGD-Derivate (TRAP(RGD)$_3$) zeigten eine einfache Radiomarkierung sowie eine hohe Anreicherungen des Tracers in Mammakarzinom tragenden Mäusen [21,60].

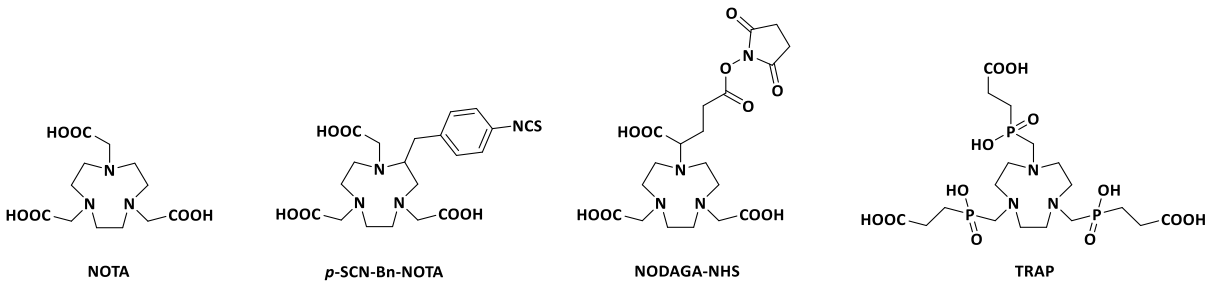

NOTA ***p*-SCN-Bn-NOTA** **NODAGA-NHS** **TRAP**

Abbildung 4: Struktur des Chelators NOTA und dessen Derivate *p*-SCN-Bz-NOTA, NODAGA-NHS und TRAP

1.1.2 Azyklische Chelatoren

Die Entwicklung azyklischer Chelatoren begann mit DTPA (Diethylentriaminpentaacetat). Sein N_3O_5-Ligandenfeld ermöglicht die Radiomarkierung dreiwertiger Radiometalle wie ^{68}Ga, ^{90}Y, ^{111}In oder ^{177}Lu [57,61–64].

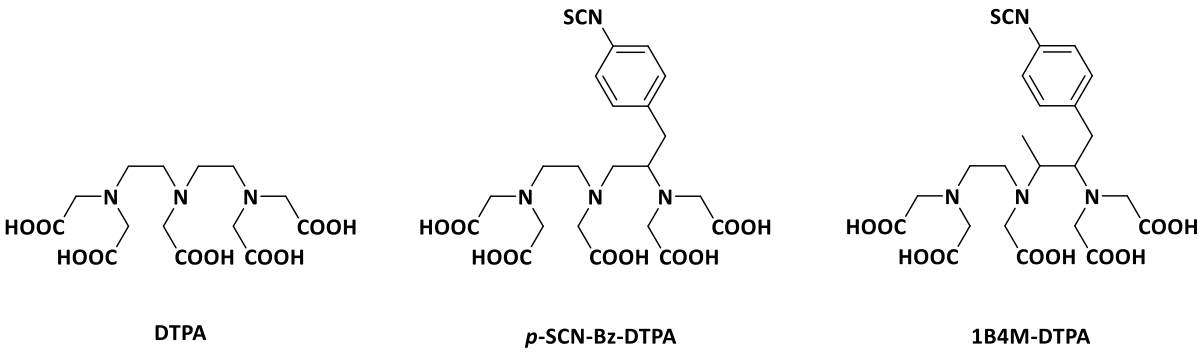

Abbildung 5: Struktur des Chelators DTPA und dessen bifunktionellem Derivate 1B4M-DTPA

Das in Bakterien auftretende Siderophor Desferrioxamin (Df) wurde zur Radiomarkierung mit ^{68}Ga und ^{89}Zr in mehreren Studien untersucht [23,65–69]. Aufgrund der harten Hydroxamat-Gruppen und der O_6-Ligandengeometrie weist das Df eine hohe Stabilität der Zr-markierten Konjugate auf und brachte dem Df in den letzten beiden Jahrzehnten ein Alleinstellungsmerkmal für die Anwendung innerhalb der ImmunoPET-Diagnostik mittels ^{89}Zr [70]. Es muss jedoch berücksichtigt werden, dass zum einen das Df nur 6 der 8 Koordinantionsstellen des Zirkoniums besetzen kann, zum anderen weist das Zirkonium eine erhöhte Oxophilie auf, welche sich in einer Anreicherung des Nuklids 72 h p.i. im Knochen- und Gelenkgewebe niederschlägt. Um eine erhöhte Stabilität zu gewährleisten, entwickelten Patra und Mitarbeiter ein Df-Derivat (Df*), welches um eine weitere Hydroxamat-Einheit verlängert wurde [71]. Vugts *et al.* synthetisierten und verglichen das Df*-Bz-NCS mit dem bisherigen Df-Bz-NCS (Abbildung 6) unter Verwendung beider Chelatoren am Antikörper Trastuzumab. Hierbei zeigte sich eine verbesserte Tumorakkumlation sowie eine erhöhte Stabilität des Df*-Trastuzumab [24].

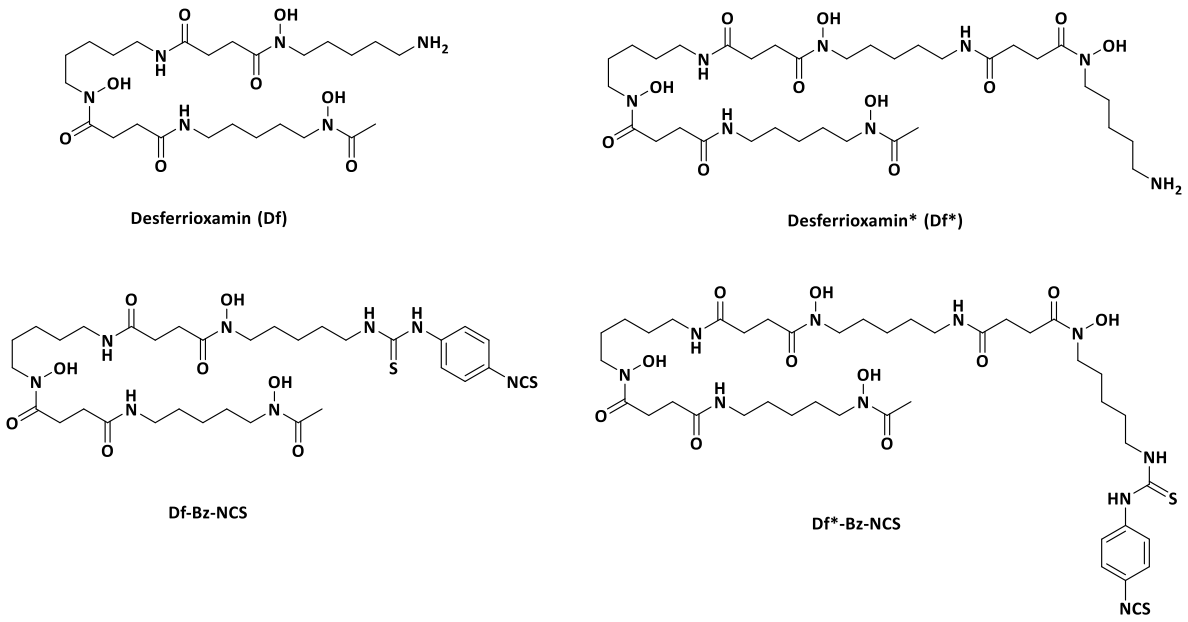

Abbildung 6: Struktur der Chelatoren Desferrioxamin (Df), Desferrioxamin* (Df*) sowie deren bifunktionellen Derivate Df-Bz-NCS und Df*-Bz-NCS

Chelatoren wie das H_2dedpa, HBED und CP256 (Abbildung 7) zeigen gegenüber ^{68}Ga eine schnelle Markierung und eine hohe Stabilität innerhalb von *in vitro*- und *in vivo*-Studien [72–75].

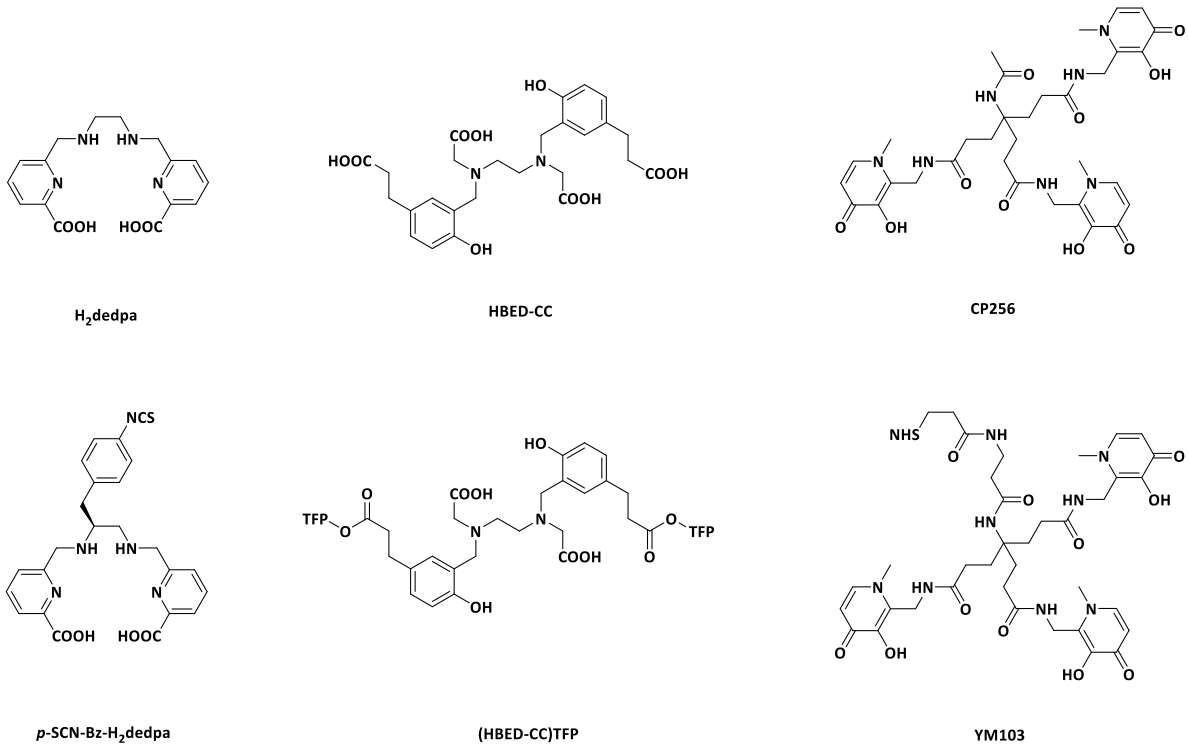

Abbildung 7: Struktur der azyklischen Chelatoren H_2dedpa, HBED-CC und CP256 sowie deren bifunktionelle Derivate *p*-SCN-Bz-H_2dedpa, (HBED-CC)TFP und YM103

Besonders das HBED gewann in den letzten Jahren als bifunktionelles Derivat, gekoppelt am PSMA, an großer Bedeutung [17,18].

Der heptadentale Chelator AAZTA (1,4-bis(hydroxycarbonylmethyl)-6-[bis(hydroxycarbonylmethyl)]-

amino-6-methylperhydro-1,4-diazepin) besitzt eine Hybridstruktur mit azyklischen und zyklischen Charakter. Dieser bietet eine schnelle Komplexierungskinetik von dreiwertigen Lanthaniden sowie Übergangsmetallen wie Scandium und Kupfer [76–79]. Basierend auf diesem Liganden wurde das hexadentale Derivat (DATA^{m}) von Waldron *et al.* bzgl. der Komplexierungseigenschaften von ^{68}Ga evaluiert [80–82]. Aufgrund der ebenfalls vorhandenen Hybridstruktur bietet dieser Chelator eine Markierungschemie mit ^{68}Ga unter milden Bedingungen (pH 5, RT, 10 min), die einen Einsatz für temperatursensitive TVs anbietet [83]. Basierend auf diesen Grundlagen wurde ein bifunktionelles Derivat des DATA^{m} entwickelt, das DATA^{5m}, welches durch Seemann *et al.* in einer *proof-of-concept*-Studie bzgl. der Radiomarkierungseigenschaften sowie der *in vitro*-Stabilität evaluiert wurde [84].

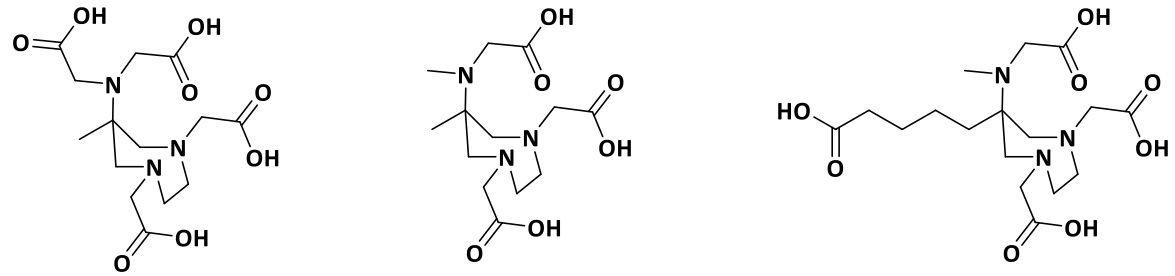

Abbildung 8: Struktur des AAZTA sowie des DATA^{m} und des bifunktionellen Derivates DATA^{5m}

1.2 Komplexchemie

1.2.1 Komplexierungsgleichgewicht

Die Ausbildung des Komplexierungsgleichgewichts zwischen einem Metall (M) und einem Chelator bzw. Liganden (L) kann durch die thermodynamische Stabilitätskonstante K_{ML} definiert werden:

$$K_{ML} = \frac{[ML]}{[M][L]} \quad (1)$$

wobei [ML], [M] und [L] jeweils die Gleichgewichtskonzentration des Metall-Ligand-Komplexes, des Metallions und des deprotonierten Liganden sind. Für multidentale Liganden, wie sie in dieser Arbeit verwendet werden, muss berücksichtigt werden, dass diese aufgrund der Vielzahl an Donoratomen bei geringen pH-Werten mehrfach protoniert vorliegen können. Daher muss für diese Art von Liganden eine pH-Wert-abhängige Gleichgewichtskonstante beschrieben werden (2)

$$K_{MH_iL} = \frac{[MH_iL]}{[MH_{i-1}L][H^+]} \quad (2)$$

wobei i = 1, 2,..., n und $[H^+]$, $[MH_{i-1}L]$ und $[MH_iL]$ die Gleichgewichtskonzentration der Protonen sowie der Metall-Ligand-Komplex-Spezies mit der i-ten Protonierungsstufe sind. Um die Konstante K_{MH_iL} berechnen zu können, müssen die Protonierungskonstanten K_i^H des Liganden bekannt sein (3).

$$K_i^H = \frac{[H_iL]}{[H_{i-1}L][H^+]} \quad (3)$$

Um die Stabilitäts- als auch Protonierungskonstanten der Liganden zu ermitteln, gibt es drei experimentelle Methoden. Von enormer Wichtigkeit für alle Methoden ist hierbei, dass ein konstanter Aktivitätskoeffizient aller Teilchen eingehalten wird, um die konzentrationsabhängigen Konstanten ermitteln zu können. Dies wird durch die Zugabe eines inerten Elektrolyten wie KCl, KNO_3 oder NaCl erreicht (0,1 oder 1 M), welcher für eine konstante Ionenstärke innerhalb des Mediums sorgt.

1.2.2 pH-Potentiometrie

Da die Komplexbildung zwischen Metallion und Ligand ein Konkurrenzprozess zwischen Metall- und H^+-Ionen bezüglich der Donoratome des Liganden ist, kann hierbei eine Änderung des pH-Wertes beobachtet werden. In Anbetracht dieser Tatsache bietet sich eine pH-potentiometrische Titration an, um sowohl den K_{MH_iL} als auch den K_i^H zu ermitteln. Mittels eines pH-Meters mit Glas- und Referenzelektrode und einer Autobürette kann durch Titration die Änderung der Protonenaktivität pH_r bzw. der elektromotorischen Kraft E bestimmt werden. Aus beiden Werten kann der pH-Wert bzw. die damit zusammenhängende Konzentration der Protonen berechnet werden [85,86]. Es gilt

$$p[H^+] = pH_r + \log(f) \tag{4}$$

mit f als Aktivitätskoeffizient der Hintergrundelektrolyte und

$$E = E_0' + Q\log(H^+) + j_H[H^+] + j_{OH}\frac{K_W}{[H^+]} \tag{5}$$

mit E_0', welches das Standardpotential, den Aktivitätskoeffizienten und das Diffusionspotential des inerten Elektrolyten beinhaltet, Q der Nernst-Steilheit, K_W dem Ionenprodukt des Wassers und $j_H[H^+]$ und $j_{OH}[OH^-]$ als Beitrag der H^+- und OH^--Ionen zum Diffusionspotential.

1.2.3 UV/Vis-Spektrometrie

Da Komplexbildungsreaktionen makrozyklischer Liganden bei geringem pH-Wert langsam ablaufen und die pH-potentiometrische Bestimmung nur einen pH-Werte-Bereich von 1,7-12 abdeckt, können alternativ UV/Vis-spektrometrische Messungen an den Metall-Ligand-Komplexen durchgeführt werden. Hierbei wird das zu untersuchende Metall aus dem Komplex durch ein UV/Vis-aktives Metall (z. B. Kupfer) verdrängt und dessen Absorptivität bei unterschiedlichen pH-Werten untersucht [87]. Voraussetzung für diese Methodik ist die Kenntnis über die Stabilitätskonstante des neuen Metall-Ligand-Komplexes. Die Absorptivitätswerte können wie folgt beschrieben werden:

$$A = \sum_{l}^{n} \varepsilon_i \chi_i l \tag{6}$$

mit l als Länge der Messzelle und ε_i und χ_i der molaren Absorptivität und molaren Fraktion der Spezies i. Um die Protonierungs- oder Stabilitätskonstanten aus Gleichung (6) bestimmen zu können, müssen die molaren Fraktionen χ_i als Protonierungs- und Stabilitätskonstanten ausgedrückt und die spektrophotometrischen Messungen bei unterschiedlichen pH-Werten durchgeführt werden. Der Vorteil der spektrophotometrischen Methode gegenüber der pH-Potentiometrie liegt in dem höheren Konzentrationsmessbereich der H^+- und OH^--Ionen.

1.2.4 NMR-Spektroskopie

Multinukleare NMR-Spektroskopie (NMR = nuclear magnetic resonance) eignet sich ebenfalls für Untersuchungen der Protonierungsstufen und Komplexbildungen von Liganden. Hierbei werden pH-abhängige Spektren NMR-aktiver Kerne (z. B. ^1H, ^{13}C, ^{31}P, ^{71}Ga) bei konstanter Temperatur aufgenommen, um die einzelnen Protonierungsstellen sowie die Protonierungskonstanten zu ermitteln. Die Änderungen des Spektrums, genauer der chemischen Verschiebungen, kann anschließend den zuvor erwähn-

ten Protonierungsstellen und -konstanten zugeordnet werden. Die chemischen Verschiebungen stellen dabei den gewichteten Mittelwert der Verschiebungen der verschiedenen H_iL-Spezies, welche innerhalb eines Protonierungsschritts involviert sind, dar [88].

$$\delta_{obs} = \sum_{I}^{n} \chi_{H_iL} \delta^{H_iL} \tag{7}$$

mit i = 0, 1, 2,…, n, δ_{obs} der ermittelten chemischen Verschiebung für ein gegebenes Signal, χ_{H_iL} der molaren Fraktion und δ^{H_iL} der chemischen Verschiebung der involvierten Spezies. Drückt man die molare Fraktion durch $[L]_t$ und die Protonierungskonstanten aus, können sowohl die Protonierungskonstanten als auch die chemischen Verschiebungen δ^{H_iL} ermittelt werden (wobei $[L]_t$ = [L] + [HL] + $[H_2L]$ + … $[H_nL]$ + [CaL] + [CaHL] + … [ZnL] + [ZnHL] + …) [88].

1.3 Radiometalle für die nuklearmedizinische Anwendung

1923 verwendete Georg de Hevesy (1885-1966) als Erster das natürlich vorkommende Bleiisotop ^{212}Pb, um die Absorption und Verteilung von Blei in Wurzel, Stiel und Blättern der Ackerbohne *Vicia Faba* zu untersuchen [89]. Hiermit formulierte Hevesy das Radiotracerprinzip, welches heutzutage für die Untersuchung chemischer, biochemischer sowie pharmakologischer Prozesse von enormer Bedeutung ist.

Für die nuklearmedizinische Anwendung wird die von den Radioisotopen ausgehende Strahlung genutzt. Hierbei unterscheidet man zwischen Radioisotopen mit gewebe-durchdringender Strahlung (γ-Strahlung) für die Diagnostik und Partikel-emittierender Strahlung (α-/β-Strahlung) für die Therapie. Wichtige Radiometalle für die diagnostische Anwendung sind ^{68}Ga (für die PET) und ^{99m}Tc (für die SPECT) [90–92]. Für den therapeutischen Aspekt werden Radioisotope wie z. B. ^{90}Y, ^{153}Sm, ^{177}Lu, $^{186/188}$Re, ^{213}Bi und ^{225}Ac verwendet.

Tabelle 1: Wichtige, für BFCs relevante Radionuklide für den diagnostischen und therapeutischen Ansatz [93–99]

Radionuklid	$t_{1/2}$	Produktionsroute	Einsatz
^{64}Cu	12,7 h	^{64}Ni(p,n)^{64}Cu ^{64}Ni(d,2n)^{64}Cu	**Diagnostik**
^{67}Ga	78,3 h	^{67}Zn(p,n)^{67}Ga	
^{68}Ga	67,7 min	^{68}Ge/^{68}Ga-Generator	
^{86}Y	14,7 h	^{86}Sr(p,n)^{86}Y	
^{89}Zr	78,4 h	^{89}Y(p,n)^{89}Zr ^{89}Y(d,2n)^{89}Zr	
^{90}Nb	14,6 h	^{90}Zr(p,n)^{90}Nb	
^{99m}Tc	6,0 h	^{99}Mo/^{99m}Tc-Generator	
^{90}Y	64,2 h	^{89}Y(n, γ)^{90}Y ^{90}Sr/^{90}Y-Generator	**Therapie**
^{153}Sm	50,5 d	^{152}Sm(n, γ)^{153}Sm	
^{177}Lu	6,7 d	^{176}Lu(n,γ)^{177}Lu ^{176}Yb(n,γ)^{177}Y→^{177}Lu	
^{186}Re	3,72 d	^{186}W(p, n)^{186}Re	
^{188}Re	16,9 h	^{188}W/^{188}Re-Generator	
^{213}Bi	45,6 min	^{225}Ac/^{213}Bi-Generator	
^{225}Ac	10,0 d	^{228}Th-Zerfallsreihe	

Im Gegensatz zu Hevesys Ansatz werden all diese Nuklide für eine spezifische Anreicherung im Zielgewebe innerhalb von Chelator-TV-Systemen komplexiert und verabreicht. Tabelle 2 listet die relevante Nuklide sowie deren Halbwertszeiten und Produktionsrouten für den diagnostischen als auch den therapeutischen Einsatz auf.

1.3.1 Radiometalle für die Diagnostik

Radiometalle wie das ^{68}Ga, ^{89}Zr oder ^{99m}Tc ermöglichen durch ihre kernchemischen Eigenschaften eine nicht-invasive Bildgebung auf molekularer Ebene. Die von den Nukliden emittierte Strahlung (γ-Strahlung) kann mittels PET oder SPECT detektiert werden.

Wichtigster Vertreter innerhalb dieser Isotope ist das ^{99m}Tc, welches als Generator-produziertes Nuklid eine ortsunabhängige Verfügbarkeit bietet. Zudem deckt das ^{99m}Tc in Kombination mit diversen Pharmazeutika ein breites Spektrum für die Bildgebung ab - von Knochen-, Hirn- und Herzperfusions- bis hin zur Tumordarstellung [91]. Eine weitere Eigenschaft des ^{99m}Tc und seiner Verbindungen ist deren

leichte Synthese und Aufarbeitung. Durch sogenannte „Kits“ wird erreicht, dass hohe, reproduzierbare Ausbeuten des Radiopharmazeutikums innerhalb kurzer Zeit (ca. 30 min) erhalten und unmittelbar für die Bildgebung verwendet werden können.
Wichtige und für diese Arbeit relevante Vertreter für die PET sind das ^{68}Ga und ^{89}Zr. Diese Nuklide emittieren Positronen, deren 511 keV-Strahlen mittels PET registriert werden kann. In den nachfolgenden Kapiteln soll auf die Eigenschaften beider Nuklide und auf das Prinzip der PET eingegangen werden.

1.3.1.1 Gallium-67/Gallium-68

Das Gallium ist ein in der Natur selten auftretendes Metall, welches vergesellschaftet mit Zink, Germanium oder Aluminium auftritt [100]. In wässrigen Lösungen besitzt das Gallium die Oxidationszahl +III und wird als harte Lewis-Säure eingestuft. Damit ist das Gallium in der Lage, mit harten Lewis-Basen, wie z. B. Amino-, Carboxyl- oder Hydroxyl-Gruppen stabile, oktaedrische Komplexe mit einer Koordinationszahl von 6 auszubilden. Aufgrund vergleichbarer Eigenschaften (Ladung, Ionenradius) zwischen Ga^{3+} und Fe^{3+} bilden beide ähnlich stabile Komplexe aus. Dies ist ein Faktor, welcher bei der Darstellung von Gallium-Verbindungen berücksichtig werden muss [101].
Hinsichtlich der Isotopenverteilung sind zunächst die stabilen, NMR-aktiven Isotope ^{69}Ga und ^{71}Ga zu nennen. Neben den stabilen Isotopen ist es eine Vielzahl radioaktiver Isotope bekannt (^{66}Ga, ^{67}Ga, ^{68}Ga, ^{73}Ga, ^{74}Ga), welche sich durch verschiedene Zerfallsarten (β^+, β^- oder EC) stabilisieren. Neben dem ^{67}Ga (SPECT) wird vor allem das ^{68}Ga für nuklearmedizinische Diagnostik mittels PET eingesetzt. Im Gegensatz zum ^{67}Ga, welches am Zyklotron produziert wird, kann das ^{68}Ga sowohl am Zyklotron als auch mit Hilfe eines ^{68}Ge/^{68}Ga-Nuklidgenerators gewonnen werden. Der Nuklidgenerator ermöglicht eine täglich mehrfache Verfügbarkeit des ^{68}Ga, was im Hinblick auf die Anwendung und die damit verbundenen Kosten für eine nuklearmedizinische Einrichtung ein enormer Vorteil gegenüber zyklotronproduzierten Nukliden ist.

1.3.1.2 ^{68}Ge/^{68}Ga-Nuklidgenerator

Die grundlegende Kernreaktion innerhalb des ^{68}Ge/^{68}Ga-Nuklidgenerators ist der Zerfall des Mutternuklids ^{68}Ge ($t_{1/2}$=271 d) unter Elektroneneinfang zum Tochternuklid ^{68}Ga. Das ^{68}Ga zerfällt anschließend mit einer Halbwertszeit von 67,7 min in das stabile ^{68}Zn unter Aussendung eines Positrons (89,14 %, $E_{\beta,max}$=1,9 MeV).

$$^{68}\mathrm{Ge} \xrightarrow{\mathrm{EC}} {}^{68}\mathrm{Ga} \xrightarrow{\beta^+} {}^{68}\mathrm{Zn} + \beta^+ + \nu_e + Q \qquad (8)$$

Das zugrundeliegende radiochemische Gleichgewicht wird säkulares Gleichgewicht genannt, da die Halbwertszeit des Mutternuklids um mehr als den Faktor 1000 größer ist als die des Tochternuklids. Das ^{68}Ge wird innerhalb einer ^{69}Ga(p,2n)^{68}Ge-Kernreaktion unter Verwendung von Protonenenergien von 23 MeV hergestellt [102,103]. Nach radiochemischer Abtrennung wird das Germanium auf einer anorganischen (TiO_2 oder SnO_2) oder organischen Matrix fixiert. Unter Verwendung von Salzsäure (0,05-0,6 M) kann das ^{68}Ga vom ^{68}Ge/^{68}Ga-Generator eluiert werden. Ein geringer Anteil des Germaniums sowie Verunreinigungen wie ^{68}Zn, Fe^{3+}- oder Trägermaterial-Ionen (Ti^{4+} oder Sn^{4+}) werden mit der salzsauren Lösung miteluiert. Mittels dreier Methoden (Fraktionierung, anionische oder kationische Ausstauscherfixierung; Abbildung 9) kann anschließend das Eluat aufgearbeitet [90,104].

Bei der Fraktionierung wird lediglich das Eluat mit der höchsten Volumenaktivität A_V(^{68}Ga) verwendet. Durch das geringe Volumen von bis zu 2 mL wird die Konzentration an ^{68}Ge minimiert, zeitgleich aber auch die Ausbeute an ^{68}Ga reduziert. Zudem werden die oben genannten Fremdionen nicht entfernt (Abbildung 9, rechts) [19].

Bei der Methode mit Anionenaustauscher wird das Eluat durch Zugabe von konzentrierter Salzsäure angesäuert und das Gallium als [$^{68}GaCl_4$]$^-$-Komplex gebunden, wobei die Fremdionen kaum oder nur geringfügig am Austauschermaterial retiniert werden. Der Tetrachlorokomplex des Galliums kann anschließend wässrig vom Austauscher eluiert werden (Abbildung 9, mitte) [105].

Die kationische Austauschermethode basiert auf der Fixierung des im Eluat als Kation vorliegenden Galliums Ga^{3+} und dem Abtrennen der Fremdionen. Es kann danach mittels verschiedener Lösungen eluiert werden [90,106].

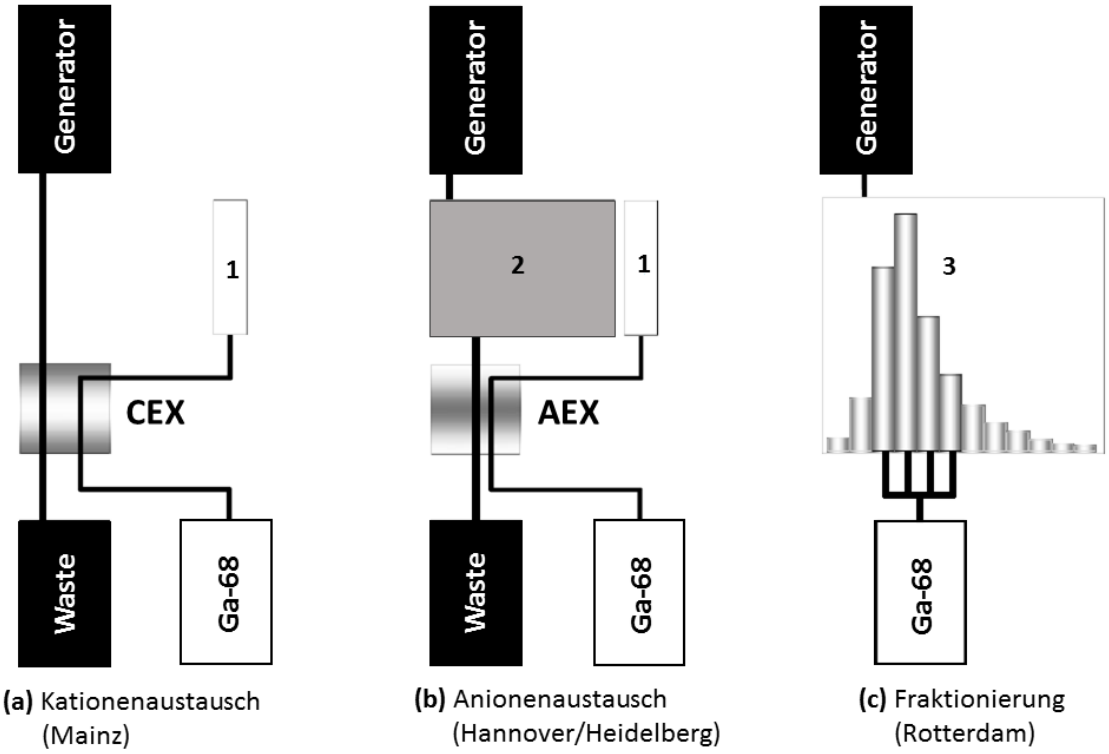

Abbildung 9: Schematische Darstellung der drei Methoden zur Gewinnung von ^{68}Ga mittels ^{68}Ge/^{68}Ga-Generatoren; CEX = cation exchange cartridge (Kationenaustauscher), AEX = anion exchange cartridge (Anionenaustauscher), 1: Elutionslösung des ^{68}Ga für CEX/AEX, 2: HCl-Reservoir (5-6 N HCl), 3: einfache Eluatfraktionen [104]

1.3.2 Zirkonium-89

Zirkonium ist ein Element der 4. Gruppe des Periodensystems und liegt überwiegend in der Oxidationsstufe +IV in wässrigen Lösungen vor. Durch sein hohes Ladungs-Radius-Verhältnis wird das Zr^{4+} als starke Lewis-Säure eingestuft und bildet, ähnlich zum Ga^{3+}, stabile Komplexe mit Sauerstoffdonoren aus, jedoch mit einer Koordinationszahl von 8 [92].

Die stabilen Isotope (^{90}Zr, ^{91}Zr, ^{92}Zr und ^{94}Zr) finden in Form des Zirkonoxid (ZrO_2) Anwendung als Keramiken für die Industrie und Prothesen im medizinischen Bereich. Aber auch im chemischen Bereich wird das Zirkonium für organometallische Katalysen eingesetzt [92,107]. Im Hinblick auf die nuklearmedizinische Anwendung hat das ^{89}Zr in den letzten Jahren große Aufmerksamkeit erhalten. Es kann, ausgehend von ^{89}Y, durch eine (p,n)- sowie eine (d,2n)-Kernreaktion am Zyklotron erzeugt werden, wobei erstere die am häufigsten verwendete Methode ist. Mit einer Halbwertszeit von 78,4 h zerfällt das ^{89}Zr zunächst zum metastabilen ^{89m}Y. Hierbei kann das Zirkonium über 2 konkurrierende Zerfallskanäle stabilisiert werden: Unter Aussendung eines Positrons (395,5 keV, 22,3 %) oder durch Elektroneneinfang (76,6 %). Das metastabile ^{89m}Y zerfällt anschließend mit einer Halbwertszeit von 15,6 s unter Aussendung eines 909 keV-Gamma-Quants zum stabilen ^{89}Y.

Die Kombination aus niederenergetischer Positronenemission und einer Halbwertszeit von mehr als 3

Tagen macht das ^{89}Zr zu einem attraktiven Radionuklid für die antikörperbasierte ImmunoPET [70,92,108,109].

1.3.3 Positronenemissionstomographie (PET)

Die PET beruht auf der Verwendung protonenreicher Kerne, die sich durch Umwandlung eines Protons in ein Neutron stabilisieren. Während dieses Umwandlungsprozesses emittiert der Kern ein Positron β^+ und ein Elektron-Neutrino ν_e (u. a. aufgrund des Spinerhalts). Der allgemeine Zerfall ist in nachfolgender Gleichung dargestellt:

$$ {}^{A}_{Z}X_N \rightarrow {}_{Z-1}{}^{A}Y_{N+1} + \beta^+ + \nu_e + Q \qquad (9) $$

Hierbei entspricht X dem Ausgangsnuklid, Y dem Zerfallsprodukt, β^+ dem Positron, ν_e dem Elektron-Neutrino, Z der Ordnungszahl, N der Neutronenzahl und Q der Zerfallsenergie. Die für jedes Nuklid charakteristische Zerfallsenergie Q verteilt sich als kinetische Energie sowohl auf das Zerfallsprodukt als auch auf die emittierten Teilchen (β^+ und ν_e). Das emittierte Positron wechselwirkt mit der umgebenden Materie und verliert dadurch an kinetischer Energie, bis es im thermischen Bereich mit einem Elektron aus der Umgebung direkt annihiliert oder unter Bildung eines Positroniums rekombiniert, welches dann annihiliert wird [110]. Man differenziert zwischen *ortho*-Positronium (*o*-Ps) und dem *para*-Positronium (*p*-Ps), welche sich in der Lage der Spins sowie der mittleren freien Lebensdauer τ_s^0. Das *p*-Ps besitzt eine antiparallele Spinanordnung, welche in einer Annihilation unter Emittierung von 2 γ-Quanten mit einer Energie von 511 keV und einem Emissionswinkel von 180° resultiert. Dieser Prozess kommt mit einer höheren Wahrscheinlichkeit vor als die Annihilation des *o*-Ps vor, sodass eine Messung der beiden γ-Quanten mit einem ringförmigen Detektorsystem in Koinzidenz möglich ist. Da nicht der Entstehungsort des Positroniums, sondern der Ort der Annihilation detektiert wird, besteht eine Ortsunschärfe von einigen Millimetern – je nach Energie des applizierten β^+-Emitters. Die verwendeten Detektoren bestehen meist aus Bismuth-Germaniumoxid (BGO), Cerium-dotiertem Lutetium-Oxyorthosilikat oder Gadolinium-Ortho-silikat [111].

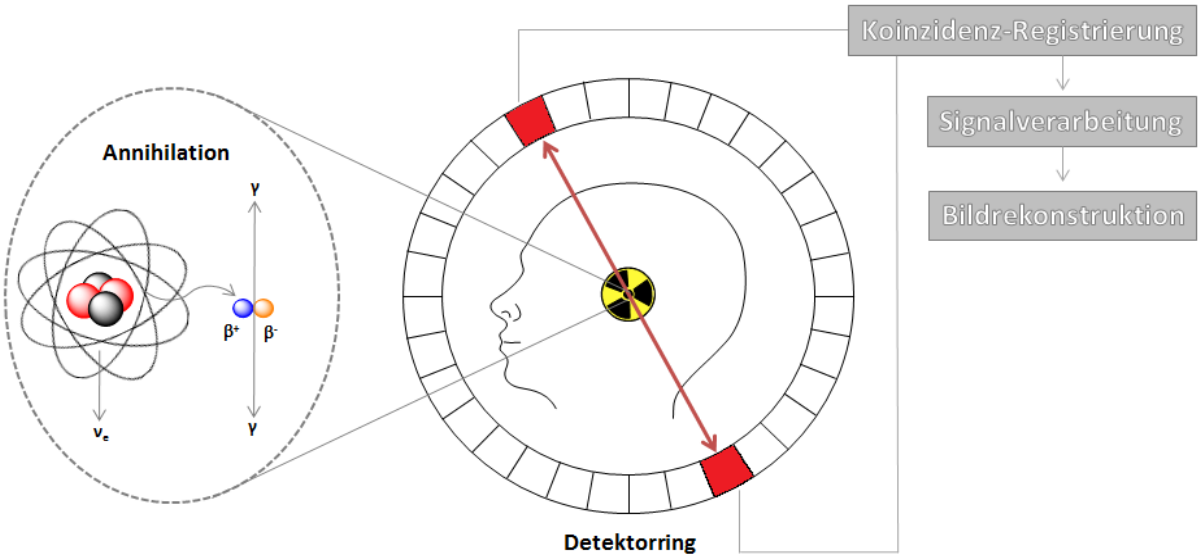

Abbildung 10: Prinzip der Positronenemissionstomographie (PET)

Der Detektorring besteht aus bis zu 32 einzelnen Detektorringen, die nochmals durch Bleiabschirmungen voneinander getrennt werden, um zufällige oder gestreute Koinzidenz minimieren. Der Ring hat einen Durchmesser von etwa 1 m und ist mit bis zu 1151 Detektoren pro Einzelring ausgestattet, um in kurzer Zeit viele Schnittbilder mit einer hohen Nachweiswahrscheinlichkeit zu erhalten [112]. Dank neuartiger Hybridsysteme aus PET und CT bzw. MRT sind Korrelationen der physiologischen Vorgänge mit der Anatomie möglich, welche in der routinemäßigen Anwendung eine hohe Sensitivität garantieren [113].

1.4 Radiometalle für die Therapie

Neben Nukliden für die Diagnostik erhalten immer mehr Radioisotope das Interesse für nuklearmedizinische Therapieverfahren. Die sogenannte Radionuklidtherapie, oder auch Endoradiotherapie, basiert auf der Applikation eines Radiopharmakons, welches das für die Therapie relevante Nuklid bindet. Es handelt sich hierbei um Isotope, welche ionisierende Strahlung wie z. B. β^-- oder α-Partikel emittieren. Wichtigste Grundlage für eine effektive Therapie ist eine hohe und spezifische Anreicherung des Radiopharmakons, um kollaterale Schäden von umliegendem, gesundem Gewebe sowie die Dosisleistung für den Patienten möglichst gering zu halten. Wichtige Bereiche sind neuroendokrine Tumore, Prostatakarzinome sowie die palliative Therapie von Knochenmetastasen [114–117].

1.4.1 Lutetium-177

Das in dieser Arbeit verwendete ^{177}Lu hat in den letzten Jahren aufgrund seiner kernchemischen Eigenschaften ein immer größer werdendes Interesse gewonnen. Mit einer Halbwertszeit von 6,71 Tagen und einer $E_{\beta,max}$ von 497 keV ist es ein für die Radionuklidtherapie attraktives Isotop [118]. ^{177}Lu kann durch Bestrahlung von natürlichem Lu_2O_3 (2,6 % ^{176}Lu) oder angereichertem Lu_2O_3 (60,6 % ^{176}Lu) mit thermischen Neutronen und einem Neutronenfluss von $3 \cdot 10^{13}$ n/cm^2/s gewonnen werden. Eine weitere Produktionsmethode ist die Bestrahlung von angereichertem ^{176}Yb mit thermischen Neutronen. Als Intermediat entsteht zunächst das ^{177}Yb ($t_{1/2}$=1,9 h), welches unter Aussenden von β^--Partikeln zum ^{177}Lu zerfällt. Zwar handelt es sich bei der zweiten Produktionsroute um eine no carrier added (n.c.a.)-Herstellung des ^{177}Lu, jedoch ist die Abtrennung des ^{176}Yb schwierig und sorgt aufgrund seiner ähnlichen radiochemischen Eigenschaften für eine kompetitive Markierung mit den verwendeten Radiopharmaka. Lebedev *et al.* entwickelten eine Separationsmethode, die eine Abtrennung des radioaktiven ^{177}Lu vom Ytterbium ermöglicht [119]. Nachfolgend sind beide Produktionsrouten angegeben.

$$^{176}\text{Lu}\ (n,\gamma)\ ^{177}\text{Lu} \qquad\qquad ^{177}\text{Lu} \xrightarrow{\beta^-} {}^{177}\text{Hf} + \beta^- + \nu_e + Q \tag{10}$$

$$^{176}\text{Yb}\ (n,\gamma,\beta^-)\ ^{177}\text{Lu} \qquad\qquad ^{177}\text{Yb} \xrightarrow{\beta^-} {}^{177}\text{Lu} \xrightarrow{\beta^-} {}^{177}\text{Hf} + \beta^- + \nu_e + Q \tag{11}$$

Das dreiwertige Lutetium wird aufgrund seiner undefinierten Elektronenorbitalstruktur nach dem HSAB-Konzept als „ionisch“ eingestuft. Daraus folgen Koordinationszahlen zwischen 6 und 12 [120]. Der für das ^{177}Lu prominenteste Chelator ist das DOTA, welches durch seine 8 Ligationsatome eine quadratisch-antiprismatische Koordinationsgeometrie verursacht [121].

1.5 Targetingvektoren

Als Targetingvektor (TV) bezeichnet man Biomoleküle, die Radiopharmaka gezielt zum malignen/tumorösen Gewebe führen. Hierbei nutzt man das Schlüssel-Schloss-Prinzip aus: der Vektor weist eine hohe Affinität und vor allem eine erhöhte Spezifizität gegenüber einem Rezeptor oder Bindemotiv (Target) auf, welches auf der Oberfläche von Tumorzellen überexprimiert vorliegt. Verknüpft man nun einen solchen Targetingvektor mit einem bifunktionellen Chelator, so kann gezielt ein Radionuklid zu diagnostischen oder therapeutischen Zwecken am Zielgewebe angereichert werden. In den nachfolgenden Kapiteln sollen für diese Arbeit relevante Systeme von Targets und Targetingvektoren beschrieben werden.

1.5.1 Somatostatin-Rezeptoren - Octreotide

1972 entdeckten Brazeau *et al.* durch Zufall das Polypeptid Somatostatin (SST, SST-28), welches als Antagonist für das Wachstumshormon Somatropin agiert [122,123]. Zwei Jahrzehnte später identifizierten Yamada *et al.* die Rezeptorstruktur für das Somatostatin und konnten zeigen, dass es sich hauptsächlich um fünf membrangebundene, G-Protein-gekoppelte Rezeptoren (sstr 1-5) handelt [124,125]. Aufgrund geringer Blutzirkulationszeit sowie enzymatischen Abbaus des SST-28 wurden infolgedessen kleinere und stabilere Derivate hergestellt. Hierbei zeigte sich, dass Octapeptide des Somatostatins eine hohe *in vivo*-Stabilität kombiniert mit einer hohen Affinität gegenüber den Rezeptoren aufwiesen [125]. Vor allem das Octreotid SMS201-995 ([DPhe^{1}][Tyr^{3}]-Octreotid (TOC)) zeigte eine hohe Affinität zu den Rezeptoren 2, 3 und 5 sowie eine erhöhte biologische Halbwertszeit [126]. Basierend auf diesem Grundgerüst wurden weitere Octapeptide für die nuklearmedizinische Anwendung mit Chelatoren wie DOTA gekoppelt und bzgl. ihrer Affinitäten gegenüber den Rezeptoren 1-5 evaluiert [127]. Zwei wichtige Chelator-Konjugate, das DOTA-TOC und das DOTA-TATE, sind in Abbildung 11 dargestellt. Ersteres erhielt als ^{68}Ga-Verbindung im Jahr 2014 den *orphan drugs status* durch die amerikanische *Food and Drug Administration* und findet seither in die nuklearmedizinischen Diagnostik neuroendokriner Tumore Verwendung [128]. Seit 2017 ist ^{177}Lu-DOTA-TATE (LUTATHERA®) als therapeutische Radiopharmakon durch die Firma Advanced Accelerator Applications (AAA) verfügbar [129].

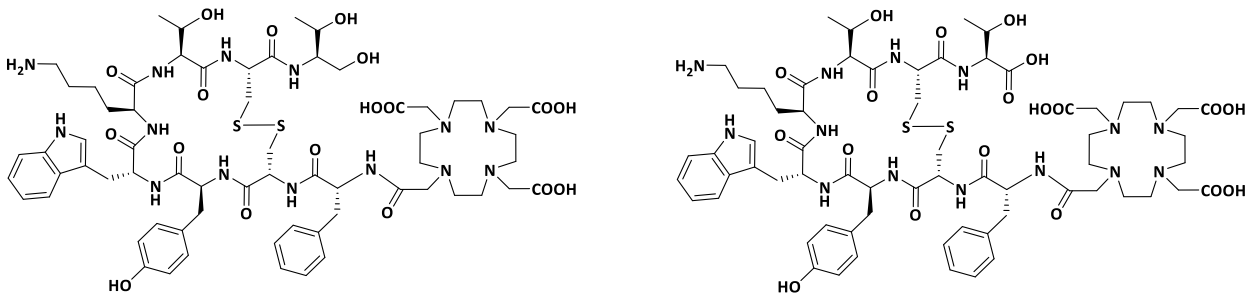

Abbildung 11: Struktur der Chelator-konjugierten Somatostatin-Analoga DOTA-TOC (links) und DOTA-TATE (rechts)

In Tabelle 2 sind die wichtigsten Vertreter und deren Affinitätsprofile gegenüber den humanen Somatostatin-Rezeptoren 1 bis 5 (hsst 1-5) aufgeführt. Das native Somatostatin SST-28 weist gegenüber allen Rezeptoren eine hohe Affinität im nanomolaren Bereich auf.

Tabelle 2: Affinitätsprofile (IC_{50}) verschiedener Somatostatinanaloga gegenüber humanen sst-Rezeptoren [127]

Peptid	hsst 1	hsst 2	hsst 3	hsst 4	hsst 5
SST-28	5,2±0,3 (19)	2,7±0,3 (19)	7,7±0,9 (15)	5,6±0,4 (19)	4,0±0,3 (19)
Octreotid	> 10.000 (5)	2,0±0,7 (5)	187±55 (3)	> 1.000 (4)	22±6 (5)
DOTA-OC	> 10.000 (3)	14±3 (4)	27±9 (4)	> 1.000 (4)	103±39 (3)
DOTA-TOC	> 10.000 (7)	14±2,6 (6)	880±324 (4)	> 1.000 (6)	393±84 (6)
DOTA-TATE	> 10.000 (3)	1,5±0,4 (3)	> 1.000 (3)	453±176 (3)	547±160 (3)
DOTA-VAP	> 10.000 (3)	29±7	419±104 (4)	743±190 (3)	80±19 (4)
DOTA-LAN	> 10.000 (7)	26±3,4 (6)	771±229 (6)	> 10.000 (4)	73±12 (6)
[^{nat}Ga]Ga-DOTA-TOC	> 10.000 (6)	2,5±0,5 (7)	613±140 (7)	> 1.000 (6)	73±21 (6)
[^{nat}Ga]Ga-DOTA-TATE	> 10.000 (3)	0,2±0,04 (3)	> 1.000 (3)	300±140 (3)	377±18 (3)

Im Vergleich hierzu zeigt das Analogon Octreotid eine verbesserte Affinität am hsst 2-Rezeptor, allerdings einen um bis zu Faktor 10 erhöhten IC_{50}-Wert (mittlere inhibitorische Konzentration; siehe 1.5.2) für die Rezeptoren 3 und 5. Alle weiteren Derivate, gekoppelt mit dem Chelator DOTA, weisen geringere Affinitäten gegenüber den Rezeptoren 1 und 4 auf. Zieht man einen Vergleich der Affinitäten bezüglich des Rezeptors 2, welcher überwiegend auf neuroendokrinen Tumoren überexprimiert ist, wird für alle Derivate deutlich, dass die Derivate [^{nat}Ga]Ga-DOTA-TATE bzw. [^{nat}Ga]Ga-DOTA-TATE die potentesten sind [127].

1.5.2 Bestimmung der mittleren inhibitorischen Konzentration IC_{50}

Um die antagonistische Wirkung des Somatostatins und seiner Analoga zu verstehen, muss man die Rezeptor-Substrat-Wechselwirkung und ihre Geschwindigkeit betrachten. 1913 schlugen Leonor Michaelis und Maud Menten ein einfaches Modell zur Erklärung dieser kinetischen Eigenschaft zwischen Substraten und Rezeptoren/Enzymen vor [130]. Hierbei wird die Bildung eines Enzym-Substrat- bzw. Rezeptor-Substrat-Komplexes als Zwischenprodukt berücksichtigt (Gleichung (12)).

$$[E] + [S] \underset{k_{-1}}{\overset{k_1}{\rightleftharpoons}} [ES] \overset{k_2}{\rightleftharpoons} [E] + [P] \quad \text{bzw.} \quad [R] + [S] \underset{k_{-1}}{\overset{k_1}{\rightleftharpoons}} [RS] \overset{k_2}{\rightleftharpoons} [RS]_{int} \tag{12}$$

mit den Konzentrationen des Enzyms [E], des Rezeptors [R], des Substrats [S], des Produkts [P], des Enzym-Substrat- bzw. Rezeptor-Substrat-Komplex [ES] bzw. [RS] sowie der Konzentration des interna-

lisierten Rezeptor-Substrat-Komplexes $[RS]_{int}$. 1924 schlugen George Briggs und John Haldane die Annahme eines Fließgleichgewichtes (*steady state*) vor, sodass die Bildung und der Zerfall von [ES] bzw. [RS] gleichgesetzt werden können [130]. Es gilt

$$k_1[E][S] = (k_{-1} - k_2)[ES] \tag{13}$$

wobei $[ES] = k_1[E][S]$ die Bildungsgeschwindigkeit und $[ES] = (k_{-1} - k_2)[ES]$ die Zerfallsgeschwindigkeit des Komplexes darstellen. Stellt man Gleichung (13) um, so erhält man den Faktor $\frac{[E][S]}{[ES]} = K_M$, welcher als Michaelis-Konstante bezeichnet wird.

$$K_M = \frac{[E][S]}{[ES]} = \frac{(k_{-1} - k_2)}{k_1} \tag{14}$$

Diese Konstante ist ein wichtiges Charakteristikum für die Enzym-Substrat-Wechselwirkungen und ist unabhängig von den Konzentrationen des Enzyms und des Substrats.
Betrachtet man nun kompetitive Hemmungen, wie sie für das Somatostatin bzw. der Analoga vorliegen, muss man folgende Dissoziationskonstante berücksichtigen:

$$K_i = \frac{[E][I]}{[EI]} \tag{15}$$

Je kleiner die Konstante K_i, desto stärker ist die Hemmung (Inhibition) durch den verwendeten Inhibitor I. Durch ausreichende Konzentration des Substrats kann die kompetitive Hemmung zwar überwunden werden, jedoch führt die Inhibition gleichzeitig zur Erhöhung des K_M-Wertes. Der neue K_M-Wert, auch K_M^{app} genannt (*apparent*, „auftretend“), wird durch folgende Gleichung beschrieben:

$$K_M^{app} = K_M \left(1 + \frac{[I]}{K_i}\right) \tag{16}$$

mit der Konzentration des Inhibitors [I] und der Dissoziationskonstanten K_i des Enzym-Inhibitor- bzw. Rezeptor-Inhibitor-Enzym-Komplexes. Bei gegebenem K_M-Wert kann hiermit die Dissoziationskonstante K_i bestimmt werden, welche ein Absolutwert ist und, wie in (15) beschrieben, Substrat-unabhängig ist. Cheng/Prusoff untersuchten 1973 den Zusammenhang zwischen dem K_i und dem IC_{50}-Wert von Inhibitoren, welcher die mittlere, inhibitorische Konzentration angibt [131]. Die Cheng-Prusoff-Gleichung gilt einen direkten Zusammenhang zwischen K_i und IC_{50} an

$$K_i = \frac{IC_{50}}{1 + \frac{[S]}{K_M}} \tag{17}$$

Es gilt, dass $K_i \approx IC_{50}$ für $[S] << K_M$, d. h. bei geringen Substratkonzentrationen entspricht die Dissoziationskonstante des Enzym-Inhibitor-Komplexes der mittleren inhibitorischen Konzentration.

1.6 Antigen - Antikörper

Monoklonale Antikörper (mAk) sind Serumproteine mit einem durchschnittlichen Molekulargewicht von 150 kDa. Sie entwickeln sich als Immunantwort auf Infektionen ausgehend von Bakterien oder Viren aus Plasmazellen. Als unlöslicher Anteil der Globulinfraktion der Serumproteine werden Antikörper zur sprachlichen Abgrenzung auch Immunoglobuline (Ig) genannt [132]. Man unterscheidet die fünf Antikörperklassen IgG, IgM, IgA, IgD und IgE, wobei sich der generelle Y-förmige Aufbau in zwei unterschiedliche Abschnitte unterteilen lässt (Abbildung 12): Die beiden identischen schweren Ketten (heavy chains; 50-70 kDa) sowie die beiden identischen leichten Ketten (light chains; 25 kDa), welche mittels kovalenter Disulfidbrücken zur Antikörper-typischen Y-Form verknüpft sind. Das antigenbindende Fragment (fragment antigene binding; Fab), bestehend aus den antigenbindenden Regionen (complementarity determing regions (CDR)), wird durch den heterogenen Bereich aus dem variablen Teil der schweren Kette (V_H), dem variablen Teil der leichten Kette (V_L) und dem konstanten Teil der leichten Kette (C_L) sowie einem Teil der schweren Kette (C_H1) gebildet.

Durch enzymatisch vermittelte Spaltung können Antikörper, abhängig vom Enzym, in bis zu drei Fragmente aufgetrennt werden. So spaltet das Enzym Papain einen IgG-Antikörper in 3 Fragmente: zwei identische Fab-Fragmente sowie das Fc-Fragment (fragment crystallizable), welches mehrere konstante Teile der schweren Kette (C_H2/C_H3) umfasst und bei intaktem Antikörper die Aktivierung des Komplementsystems bewirkt. Das Enzym Pepsin hingegen spaltet einen IgG-Antikörper in 2 Fragmente: das antigenbindene F(ab´)2- sowie das Fc-Fragment, welches durch die Behandlung in mehrere Bruchstücke zerfällt [132].

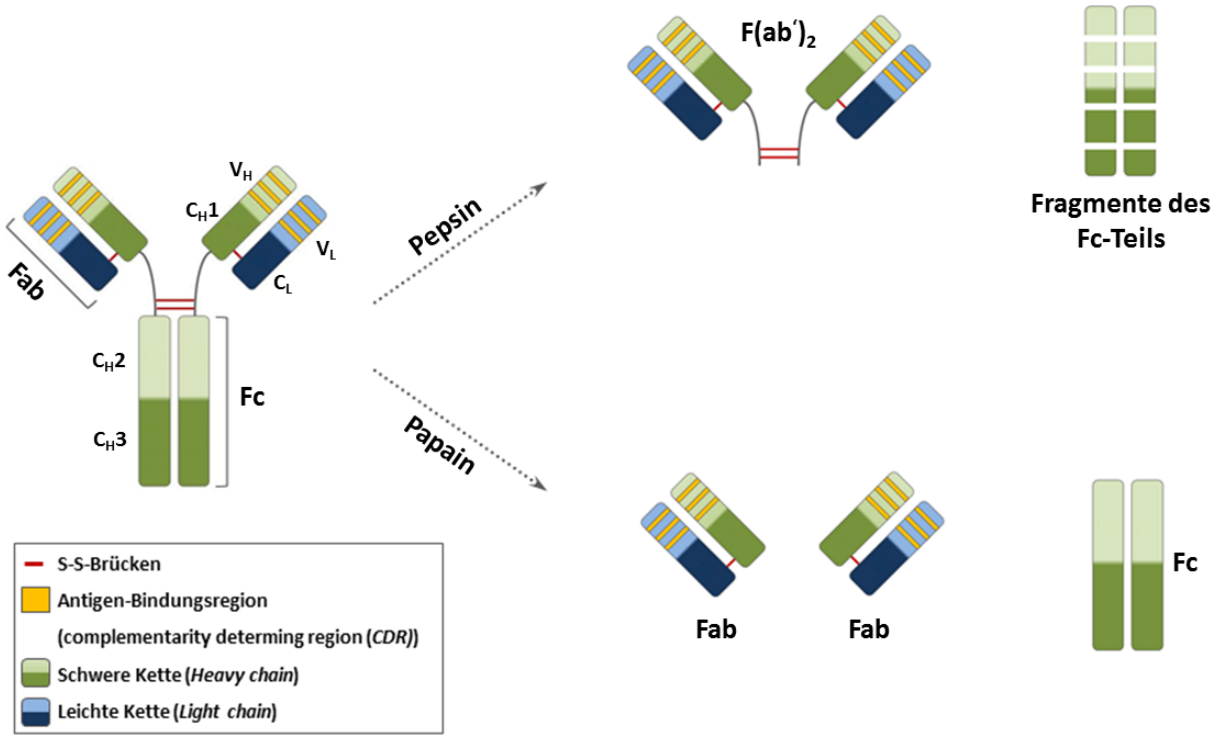

Abbildung 12: Schematischer Aufbau eines IgG-Antikörpers sowie dessen enzymatischer Abbau durch Pepsin (oben) und Papain (unten); V_L/V_H: variabler Teil der leichten bzw. schweren Kette, $C_L/C_H1/C_H2/C_H3$: konstanter Teil der leichten bzw. schweren Kette;

Aufgrund der langsamen Pharmakokinetik, welche ihre Ursache in der Größe, Form und Affinität eines Antikörpers besitzt, muss für die nuklearmedizinische Anwendung von Antikörpern ein Radionuklid mit einer der Kinetik angepassten Halbwertszeit gewählt werden. Geeignete Nuklide sind z. B. ^{124}I ($t_{1/2}$=4,18 d) und ^{89}Zr ($t_{1/2}$=78,4 h) für die PET-Diagnostik sowie ^{90}Y ($t_{1/2}$=64,1 h), ^{131}I ($t_{1/2}$=8,02 d) und ^{177}Lu ($t_{1/2}$=6,71 d) für den therapeutischen Ansatz. Sowohl die kommerzielle Verfügbarkeit des ^{89}Zr als auch die geringe *in vivo*-Stabilität Iod-markierter Derivate [133] sorgte in den letzten Jahren für einen erhöhten Fokus auf Immunokonjugaten für die Radiomarkierung mit Zirkonium [134–136]. Durch Knüpfung des Antikörpers mit einem Chelator wird eine Komplexierung des verwendeten Radiometalls ermöglicht (Abbildung 13). Von Bedeutung für die Komplexierungschemie ist eine Durchführung unter milden Bedingungen (37 °C, pH 8-9, wässrige Lösung), um eine Denaturierung als auch Agglomeration des Antikörpers zu verhindern. Des Weiteren ist eine Präkomplexierung des Radionuklids durch einen Puffer wie Citrat oder HEPES (*N*-2-hydroxyethylpiperazin-*N*'-2-ethansulfonsäure) von enormer Bedeutung, da der mAk durch seine Vielzahl an Donoratomen wie Stickstoff, Sauerstoff und Schwefel schwache Metall-Antikörper-Bindungen ausbilden kann, welche jedoch *in vivo* durch Serumproteine dekomplexiert werden [137].

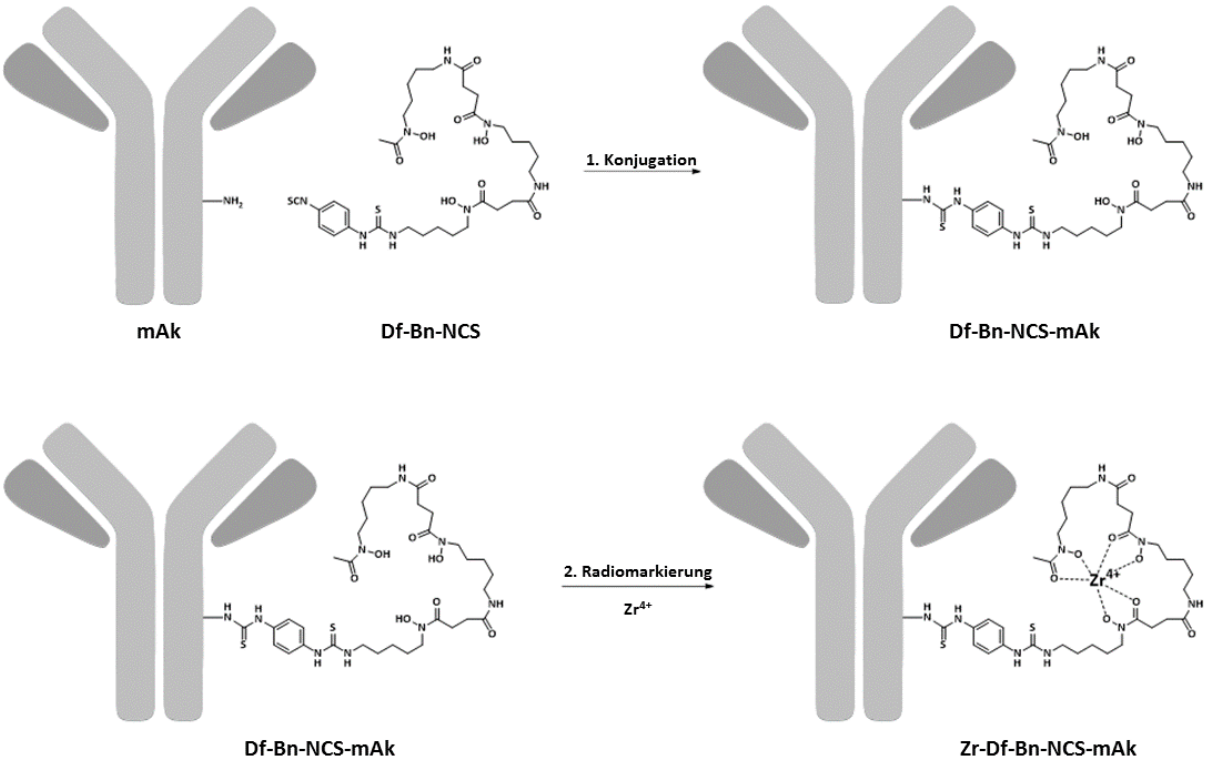

Abbildung 13: Schematische Darstellung der Konjugation zwischen einem monoklonalen Antikörper (mAk) und dem bifunktionellen Chelator Desferrioxamin-Benzyl-NCS (Df-Bz-NCS) für die Radiomarkierung mit dem tetravalenten Zirkonium

Wichtig für den Erhalt der Immunoreaktivität ist das Verhältnis zwischen Chelator und Antikörper innerhalb eines Konjugats. Zwar ist eine höhere spezifische Aktivität mit steigendem Chelator-zu-Antikörper-Verhältnis zu erwarten [138], jedoch kann gleichzeitig die Affinität und damit die Immunoreaktivität des Antikörper-Chelator-Konjugats sinken [139].

Ein wichtiges Antigen für viele Antikörper ist das membranassoziierte Glykoprotein Mucin 1 (MUC1), welches auf der Oberfläche von Epithelzellen zu finden ist [140]. Das MUC1 besteht aus einem Aminosäurenrückgrat, welches mit Oligosacchariden aus bis zu 20 Zuckereinheiten glykosyliert ist. Aufgrund einer sich wiederholenden Aminosäuresequenz (G**ST**APPAHGV**TS**APD**T**RPAP; tandem repeat sequence) mit einem hohen Anteil an Threonin (**T**; 15 %) und Serin (**S**; 10 %) ist eine hohe Glykosylierung möglich [141]. Das MUC1 sorgt einerseits für adhäsive Wechselwirkung gegenüber Selectin-ähnlichen Molekülen aufgrund des hohen Kohlenwasserstoff-Anteils, was die Ausstreuung von Metastasen begünstigt [142–145]. Andererseits agiert das MUC1 als anti-adhäsives Protein wegen der großen, umfangreichen Konformation, sodass die Zell-Zell-Wechselwirkung blockiert und somit eine Destabilisierung der Zell-Zell- bzw. Zell-Matrix-Wechselwirkungen verursacht wird [146–148]. Die für den Bereich der Nuklearmedizin wichtigste Funktion des tumorassoziierten MUC1 (TA-MUC1) ist sein hohes Überexpressionslevel in Karzinomen und Metastasen, was das TA-MUC1 zu einer hervorragenden Zielstruktur für diagnostische und therapeutische Fragestellungen macht [149].

1.6.1 Antikörper GGSK-1/30

Der in dieser Arbeit verwendete monoklonale Antikörper (GGSK-1/30) wurde durch Vakzinierung von Wildtyp-Balb/c-Mäusen mittels eines synthetisch hergestellten Vakzins gegen TA-MUC1 gewonnen. Der mAk wies in ersten *in vitro*-Studien eine hohe Affinität gegenüber den humanen Brusttumorzellen MCF-7 und T47D auf [150–152]. Die Synthese des verwendeten Vakzins basiert auf der erwähnten tandem repeat sequence, welche Teil der Antigeneinheit des Antikörpers darstellen soll, synthetisch hergestellt, mit einer Sialyl-T_N-Seitenkette gekoppelt und an Tetanus-Toxoid (TTox) gebunden wird (Abbildung 14) [151]. Das Glykopeptid soll hierbei das TA-MUC1 imitieren, wohingegen das TTox eine immunstimulierende Wirkung besitzt. Wird nun dieses Vakzin der Maus verabreicht, sorgt dies für eine Immunantwort, wodurch es zur Ausbildung von Antikörpern gegen das Glykopeptid, dem Antigen kommt.

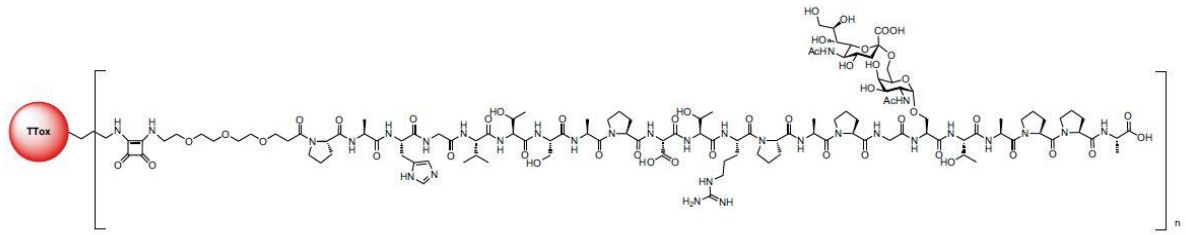

Abbildung 14: Antitumor-Vakzine aus einem an Ser17 glykosylierten MUC1-Glycopeptid und Tetanus-Toxoid [151]

1.7 Knochenmetastasen - Bisphosphonate

Knochenmetastasen sind ein optimales Target für Bisphosphonate (BP). Die Grundlage für den heutigen Einsatz von Bisphosphonaten erforschten Fleisch *et al*. mit ihren Studien zu anorganischen Pyrophosphaten, welche eine charakteristische P-O-P-Brückenbindung besitzen. In ihren *in vitro*-Studien zeigten sie, dass die Phosphatklasse neben hohen Affinitäten gegenüber Calciumphosphat auch inhibierende Wirkung sowohl auf die Bildung als auch auf die Resorption der Calciumphosphatkristalle besaß. Innerhalb von *in vivo*-Studien wiesen sie hingegen keinerlei Wirkung auf. Diese Beobachtung wurde durch die Hydrolyse der Pyrophosphate erklärt, was zur Entwicklung einer neue Klassen von Bisphosphonaten führte, welche eine P-C-P-Brückenbindung besitzen [153,154]. Die wichtigsten Vertreter der einfachen sowie stickstoffhaltigen Bisphosphonate (N-BP) sind in Abbildung 15 zu sehen.

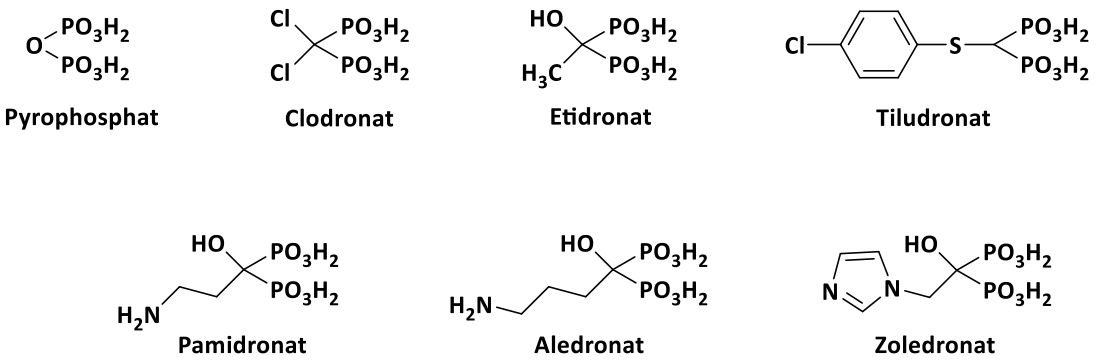

Abbildung 15: Strukturen der wichtigsten Vertreter der einfachen Bisphosphonate (obere Reihe) sowie der stickstoffhaltigen Bisphosphonate (untere Reihe)

Die therapeutische Wirksamkeit der BP beruht zunächst auf der hohen Affinität der BP gegenüber dem Hydroxyapaptit der Knochensubstanz. Die BP reichern sich auf der Knochenoberfläche an und werden von Osteoklasten, welche für die Resorption des Apatits verantwortlich sind, endozytotisch ins Zellinnere aufgenommen. Der darauf folgende Wirkungsmechanismus der einfachen BP unterscheidet sich von dem der stickstoffhaltigen BP. Die „einfachen“ BP werden innerhalb der Biosynthese des Energieträgers Adenosintriphosphat (ATP) eingebaut und bilden nicht-hydrolysierbare Metaboliten. Dies führt zur Hemmung der intrazellulären Energieversorgung und schlussendlich zum Zelltod [155,156]. Die stickstoffhaltigen BP inhibieren das Enzym Farnesylpyrophosphat-Synthase (FPS) [157–160], was dazu führt, dass die Synthese essentieller Sterole wie dem Cholesterin unterbunden wird. Der Mangel dieser Sterole im Cytosol der Osteoklasten führt auch hier zu einer Unterversorgung mit Nähr- und Signalstoffen, sodass die Zellapoptose die Folge ist [161,162].

Die hohe Affinität der BP nutzt die Nuklearmedizin seit Jahrzehnten für diagnostische und therapeutisch-palliative Anwendung [163–165]. Hierbei wird die komplexierende Eigenschaft der BP genutzt, um die Radionuklide im stabilen Komplex innerhalb der Knochenmetastasen anzureichern. In den letzten Jahren sind es vor allem DOTA- und NOTA-basierte BP, welche in präklinischen und klinischen Studien vielversprechende Ergebnisse für den Einsatz dieser Radiopharmaka liefern [166–168].

2. Problemstellung und Zielsetzung

Im Rahmen dieser Arbeit wurden verschiedene Teilprojekte (A bis E) bearbeitet, welche die Radiomarkierung verschiedener Chelator-basierter Systeme umfasste (siehe Abbildung 16). Hierbei wurden die positronenemittierenden Radiometalle ^{68}Ga und ^{89}Zr für die PET-Diagnostik sowie das β^--emittierende Radionuklid ^{177}Lu für die therapeutische Anwendung eingesetzt. Für die Teilprojekte A bis D wurden, basierend auf den Chelatoren DATA^m und AAZTA, bifunktionelle Derivate (DATA^{5m} und AAZTA^5) entwickelt.

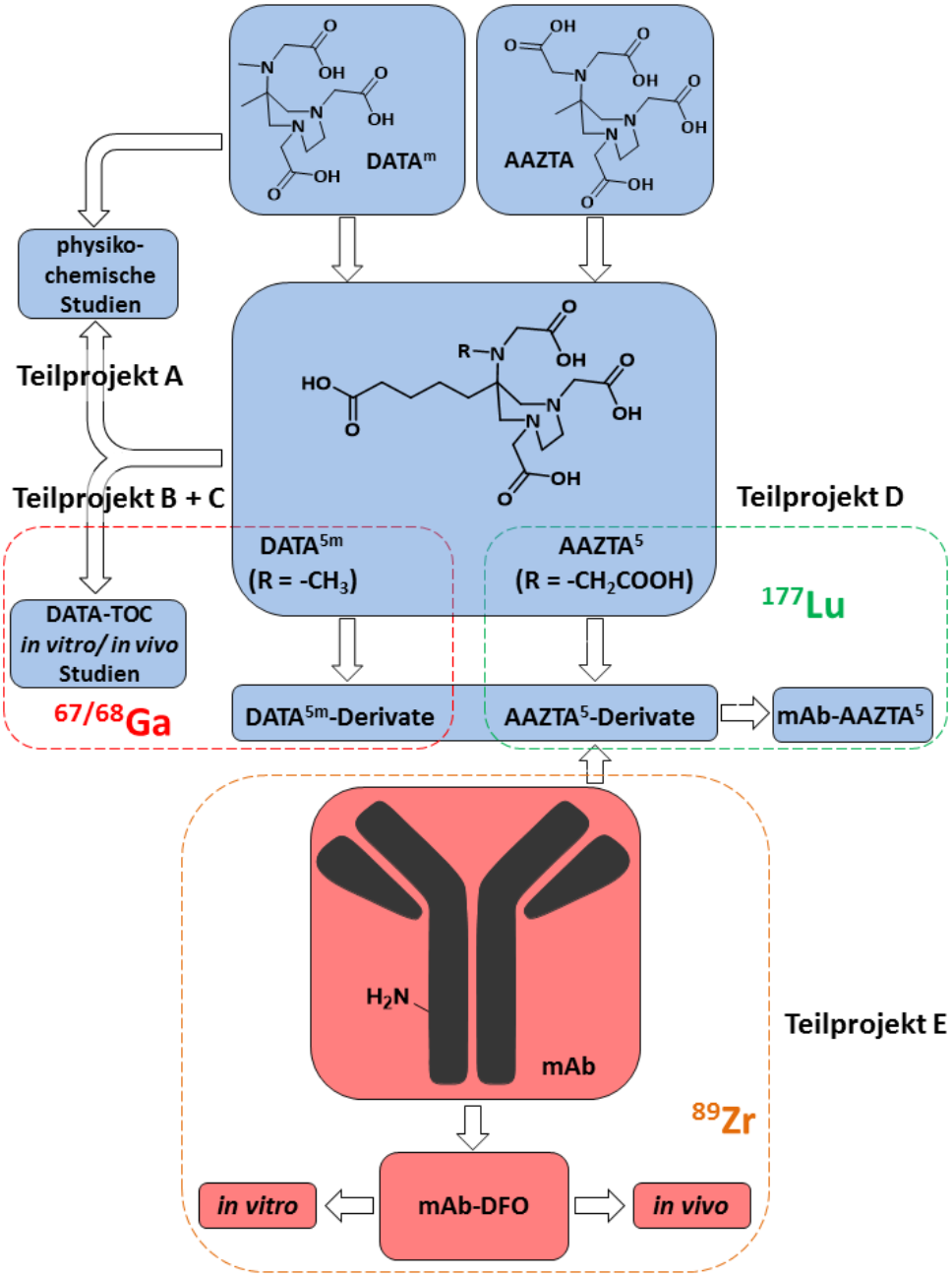

Abbildung 16: Übersicht der Teilprojekte im Hinblick auf ihre Anwendung für die jeweiligen Radionuklide

Das Teilprojekt E umschließt die Kopplung eines neuartigen Antikörpers mit dem Chelator Desferrioxamin (Df) für die Radiomarkierung mit ^{89}Zr.
Nachfolgend sollen alle Teilprojekte sowie deren Zielsetzungen kurz erläutert werden.

Teilprojekt A:

Studien im Hinblick auf kinetische, thermodynamische und strukturelle Eigenschaften von Ga^{3+}- und M^{2+}-Komplexen der Chelatoren $DATA^{m}$ und $DATA^{5m}$

Innerhalb dieses Projektes sollten die Stabilitätskonstanten des [^{nat}Ga]Ga-$DATA^{m}$ sowie [^{nat}Ga]Ga-$DATA^{5m}$ ermittelt werden. Es wurde hierbei der Vergleich zwischen beiden Chelatoren gezogen, um den Einfluss des n-Valeriansäure-Linkers am $DATA^{5m}$ auf die Komplexierungseigenschaften zu untersuchen. Mittels pH-Potentiometrie, NMR-Spektroskopie sowie UV/Vis-Spektrometrie wurden die Stabilitäten der Ga-Komplexe sowie verschiedener divalenter Metall-Komplexe untersucht. Des Weiteren wurden kinetische Studien durchgeführt, um die Halbwertszeit der Transchelatisierung der Ga-Komplexe gegen Transferrin zu untersuchen.

Teilprojekt B:

In vitro-Evaluierung von [^{nat}Ga]Ga-DATA-TOC sowie erste präklinische und klinische Studien von [^{67}Ga]/[^{68}Ga]Ga-DATA-TOC

Hier sollten Affinitätsprofile des [^{nat}Ga]Ga-DATA-TOCs hinsichtlich der Rezeptorinhibierung an den humanen Somatostatinrezeptoren (hsstr) 2, 3 und 5 untersucht und mit dem literaturbekannten [^{nat}Ga]Ga-DOTA-TOC verglichen werden. Des Weiteren wurde das [^{67}Ga]/[^{68}Ga]Ga-DATA-TOC innerhalb von *in vivo*-Studien an gesunden als auch tumortragenden Tieren durchgeführt, um Aufschluss über die Bioverteilung und -stabilität zu erhalten. Zudem wurden erste Humanstudien des [^{68}Ga]Ga-DATA-TOC im Vergleich mit [^{68}Ga]Ga-DOTA-TOC, welches seit 2014 den *orphan drug status* durch die FDA erhielt, durchgeführt [128].

Teilprojekt C:

Synthese und Radiomarkierung bifunktioneller DATA-Derivate mit ^{68}Ga für die Kopplung an Targetingvektoren unter milden Bedingungen

Um das Anwendungsgebiet des bifunktionellen Chelators $DATA^{5m}$ zu erweitern, wurden drei verschiedene Derivate ($DATA^{5m}$-Bz-NCS, $DATA^{5m}$-en-QS, $DATA^{5m}$-TEG-N_3) synthetisiert. Diese ermöglichen eine direkte Kopplung des Chelators an makromolekulare Systeme wie Peptide, Antikörperfragmente und funktionalisierte Polymere oder Nanopartikel unter milden Bedingungen. Ein Vorteil dieser Derivate liegt innerhalb der Kopplungschemie, welche die Abtrennung des Chelators vom Chelator-Biomolekül-Konjugat erleichtern soll. Alle drei Derivate wurden mit ^{68}Ga markiert und innerhalb erster *in vitro*-

Studien auf ihre Stabilität hin untersucht. Als *proof-of-concept* wurde zudem ein Bisphosphonat-Derivat (Pamidronat) am DATA^{5m}-en-QS gekoppelt, aufgereinigt und radiomarkiert.

Teilprojekt D:

Synthese und Radiomarkierung bifunktioneller AAZTA-Derivate mit ^{177}Lu für die Kopplung an Targetingvektoren unter milden Bedingungen

Um das Anwendungsgebiet des bifunktionellen Chelators AAZTA^5 zu erweitern, wurden drei verschiedene Derivate (AAZTA^5-Bz-NCS, AAZTA^5-en-QS, AAZTA^5-TEG-N_3) synthetisiert. Diese ermöglichen, wie auch im ***Teilprojekt C***, eine direkte Kopplung des Chelators an makromolekulare Systeme wie Peptide, Antikörper und funktionalisierte Polymere oder Nanopartikel unter milden Bedingungen. Alle drei Derivate wurden in ersten Studien mit ^{177}Lu markiert und im Hinblick auf ihre *in vitro*-Stabilität evaluiert. Als *proof-of-concept* wurde zusätzlich das AAZTA^5-Bz-NCS mit einem monoklonalen Antikörper GGSK-1/30 (siehe ***Teilprojekt E***) gekoppelt, radiomarkiert und hinsichtlich seiner *in vitro*-Stabilität untersucht.

Teilprojekt E:

Radiomarkierung, in vitro und in vivo-Evaluierung eines neuartigen Antikörpers für die ImmunoPET mit ^{89}Zr

Der neuartige, durch Vakzinierung generierte Antikörper GGSK-1/30 wurde mit dem bifunktionellen Chelator Desferrioxamin-Benzylisothiocyanat modifiziert (Df-Bz-NCs-mAb) und erstmals mit dem Positronenemitter ^{89}Zr radiomarkiert. Ziel dieses Projekts war es, die bis dato vorliegenden Daten zur Spezifität des mAk aus histologischen und immunologischen Untersuchungen innerhalb von *in vitro*- und *in vivo*-Studien zu bestätigen. Hierbei wurde die Immunoreaktivität des radiomarkierten Konjugats ([^{89}Zr]Zr-Df-Bz-NCS-mAb) gegenüber gesunden als auch tumorösen Epithelzellen überprüft. Zur Verifizierung wurden zudem Bioverteilungen als auch PET-Messungen an transgenen MUC1-Mäusen mit Mammakarzinomen durchgeführt.

3. Referenzen

1. Ferlay J., Soerjomataram I., Dikshit R., Eser S., Mathers C., Rebelo M., Parkin D.M., Forman D., Bray F. Cancer incidence and mortality worldwide: Sources, methods and major patterns in GLOBOCAN 2012. Int. J. Cancer. 2015; 136(5): E359–86.
2. Stewart B., Wild C.P. World Cancer Report 2014. World Cancer Rep. 2014;
3. Divino J.J., Ferlay J., Mortara I., Pisani P., Réamonn P. Global action against cancer - Updated version 2005. World Health. 2005;
4. GEKID Z. für K. Krebs in Deutschland 2009/2010, 9. Ausgabe. 2013.
5. Torre L.A., Bray F., Siegel R.L., Ferlay J., Lortet-tieulent J., Jemal A. Global Cancer Statistics, 2012. CA Cancer J. Clin. 2015; 65(2): 87–108.
6. Fischer B., Lassen U., Mortensen J., Larsen S., Loft A., Bertelsen A., Ravn J., Clementsen P., Hogholm A., Larsen K., Rasmussen T., Keiding S., Dirksen A., Gerke O., Skov B., Steffensen I., Hansen H., Vilmann P., Jacobsen G., et al. Preoperative staging of lung cancer with combined PET-CT. N Engl J Med. 2009; 361(1): 32–9.
7. Lardinois D., Weder W., Hany T.F., Kamel E.M., Korom S., Seifert B., von Schulthess G.K., Steinert H.C. Staging of Non–Small-Cell Lung Cancer with Integrated Positron Emission Tomography and Computed Tomography. N. Engl. J. Med. 2003; 348(25): 2500–7.
8. Beheshti M., Imamovic L., Broinger G., Vali R., Waldenberger P., Stoiber F., Nager M., Gruy B., Janetschek G., Langsteger W. F-18 Choline PET/CT in the Preoperative Staging of Prostate Cancer in Patients with Intermediate or High Risk of Extracapsular Disease: A Prospective Study of 130 Patients. Radiology 2010. 254AD; 3.
9. Shim S.S., Lee K.S., Kim B.-T., Chung M.J., Lee E.J., Han J., Choi J.Y., Kwon J., Shim Y.M., Kim S. Non–Small Cell Lung Cancer: Prospective Comparison of Integrated FDG PET/CT and CT Alone for Preoperative Staging. Radiology. 2005; 236(3).
10. Antoch G., Stattaus J., Nemat A.T., Marnitz S., Beyer T., Kuehl H., Bockisch A., Debatin J.F., Freudenberg L.S. Non–Small Cell Lung Cancer: Dual-Modality PET/CT in Preoperative Staging. Radiology. 2003; 229(2).
11. Baum R.P., Söldner J., Schmücking M., Niesen A. Peptidrezeptorvermittelte Radiotherapie (PRRT) neuroendokriner Tumoren: Klinische Indikationen und Erfahrung mit Yttrium-90-markierten Somatostatinanaloga. Onkologe. 2004; 10(10): 1098–110.
12. Behr T.M., Kann P.H., Gotthardt M., Béhé M., Arnold R. Nuklearmedizinische Diagnostik und Therapie neuroendokriner Tumoren des Gastrointestinaltraktes einschließlich des Karzinoides. Nuklermediziner. 2003; 26(2): 121–33.
13. Esser J.P., Krenning E.P., Teunissen J.J.M., Kooij P.P.M., Van Gameren A., Bakker W.H.,

Kwekkeboom D.J. Comparison of Lu-177-[DOTA^0,Tyr^3]octreotate and Lu-177-[DOTA^0,Tyr^3]octreotide: Which peptide is preferable for PRRT? Eur. J. Nucl. Med. Mol. Imaging. 2006; 33(11): 1346–51.

14. Zovato S., Kumanova A., Demattè S., Sansovini M., Bodei L., Di Sarra D., Casagranda E., Severi S., Ambrosetti A., Schiavi F., Opocher G., Paganelli G. Peptide receptor radionuclide therapy (PRRT) with Lu-177-DOTATATE in individuals with neck or mediastinal paraganglioma (PGL). Horm. Metab. Res. 2012; 44(5): 411–4.

15. Cwikla J.B., Sankowski A., Seklecka N., Buscombe J.R., Nasierowska-Guttmejer A., Jeziorski K.G., Mikolajczak R., Pawlak D., Stepien K., Walecki J. Efficacy of radionuclide treatment DOTATATE Y-90 in patients with progressive metastatic gastroenteropancreatic neuroendocrine carcinomas (GEP-NETs): A phase II study. Ann. Oncol. 2009; 21(4): 787–94.

16. Bergsma H., van Vliet E.I., Teunissen J.J.M., Kam B.L.R., de Herder W.W., Peeters R.P., Krenning E.P., Kewkkeboom D.J. Peptide receptor radionuclide therapy (PRRT) for GEP-NETs. Best Pract. Res. Clin. Gastroenterol. 2012; 26: 867–81.

17. Eder M., Schäfer M., Bauder-Wüst U., Hull W.E., Wängler C., Mier W., Haberkorn U., Eisenhut M. Ga-68-complex lipophilicity and the targeting property of a urea-based PSMA inhibitor for PET imaging. Bioconjug. Chem. 2012; 23(4): 688–97.

18. Eder M., Neels O., Müller M., Bauder-Wüst U., Remde Y., Schäfer M., Hennrich U., Eisenhut M., Afshar-Oromieh A., Haberkorn U., Kopka K. Novel preclinical and radiopharmaceutical aspects of Ga-68-PSMA-HBED-CC: A new PET tracer for imaging of prostate cancer. Pharmaceuticals. 2014; 7(7): 779–96.

19. Breeman W.A.P., De Jong M., De Blois E., Bernard B.F., Konijnenberg M., Krenning E.P. Radiolabelling DOTA-peptides with Ga-68. Eur. J. Nucl. Med. Mol. Imaging. 2005; 32(4): 478–85.

20. de Blois E., Sze Chan H., Naidoo C., Prince D., Krenning E.P., Breeman W.A.P. Characteristics of SnO_2-based Ge-68/Ga-68 generator and aspects of radiolabelling DOTA-peptides. Appl. Radiat. Isot. 2011; 69(2): 308–15.

21. Notni J., Pohle K., Wester H.J. Comparative gallium-68 labeling of TRAP-, NOTA-, and DOTA-peptides: practical consequences for the future of gallium-68-PET. EJNMMI Res. 2012; 2(1): 1–28.

22. Jodal A., Lankat-Buttgereit B., Brom M., Schibli R., Béhé M. A comparison of three Ga-67/68-labelled exendin-4 derivatives for β-cell imaging on the GLP-1 receptor: the influence of the conjugation site of NODAGA as chelator. EJNMMI Res. 2014; 4(1): 31.

23. Perk L.R., Visser O.J., Stigter-Van Walsum M., Vosjan M.J.W.D., Visser G.W.M., Zijlstra J.M., Huijgens P.C., Van Dongen G.A.M.S. Preparation and evaluation of Zr-89-Zevalin for monitoring of Y-90-Zevalin biodistribution with positron emission tomography. Eur. J. Nucl. Med. Mol. Imaging. 2006; 33(11): 1337–45.

24. Vugts D.J., Klaver C., Sewing C., Poot A.J., Adamzek K., Huegli S., Mari C., Visser G.W.M., Valverde I.E., Gasser G., Mindt T.L., van Dongen G.A.M.S. Comparison of the octadentate bifunctional chelator DFO*-pPhe-NCS and the clinically used hexadentate bifunctional chelator DFO-pPhe-NCS for Zr-89-immuno-PET. Eur. J. Nucl. Med. Mol. Imaging. 2016;

25. Xing Y., Zhao J., Shi X., Conti P.S., Chen K. Recent Development of Radiolabeled Nanoparticles for PET Imaging. Austin J. Nanomedicine Nanotechnol. 2014; 2(2): 1016.

26. Seo J.W., Mahakian L.M., Kheirolomoom A., Zhang H., Meares C.F., Ferdani R., Anderson C.J., Ferrara K.W. Liposomal Cu-64 labeling method using bifunctional chelators: Poly(ethylene glycol) spacer and chelator effects. Bioconjug. Chem. 2010; 21(7): 1206–15.

27. Valeur E., Bradley M. Amide bond formation: beyond the myth of coupling reagents. Chem. Soc. Rev. 2009; 38(2): 606–31.

28. Roberts M.J., Bentley M.D., Harris J.M. Chemistry for peptide and protein PEGylation. Adv. Drug Deliv. Rev. 2012; 64: 116–27.

29. Lockett M.R., Phillips M.F., Jarecki J.L., Peelen D., Smith L.M. A Tetrafluorophenyl Activated Ester Self-Assembled Monolayer for the Immobilization of Amine-Modified Oligonucleotides. Langmuir. 2009; 24(1): 69–75.

30. Tietze L.F., Arlt M., Beller M., Glüsenkamp K.-H., Jähde E., Rajewsky M.F. Anticancer Agents, 15. Squaric Acid Diethyl Ester: A New Coupling Reagent for the Formation of Drug Biopolymer Conjugates. Synthesis of Squaric Acid Ester Amides and Diamides. Chem. Ber. 1991; 124(5): 1215–21.

31. Brechbiel M.W., Gansow O.A., Atcher R.W., Schlom J., Esteban J., Simpson D.E., Colcher D. Synthesis of 1-(p-isothiocyanatobenzyl) derivatives of DTPA and EDTA. Antibody labeling and tumor-imaging studies. Inorg. Chem. 1986; 25(16): 2772–81.

32. Esteban J.M., Schlom J., Gansow O.A., Atcher R.W., Brechbiel M.W., Simpson D.E., Colcher D. New Method for the Chelation of Indium-111 to Monoclonal Antibodies : Biodistnbution and Imaging of Athymic Mice Bearing Human Colon Carcinoma Xenografts. J. Nucl. Med. 1987; 28(5): 861–71.

33. Halime Z., Frindel M., Camus N., Orain P.-Y., Lacombe M., Cherel M., Gestin J.-F., Faivre-Chauvet A., Tripier R. New synthesis of phenyl-isothiocyanate C-functionalised cyclams. Bioconjugation and Cu-64 phenotypic PET imaging studies of multiple myeloma with the te2a derivative. Org. Biomol. Chem. 2015; 13(46): 11302–14.

34. Meares C.F., McCall M.J., Reardan D.T., Goodwin D.A., Diamanti C.I., McTigue M. Conjugation of antibodies with bifunctional chelating agents: Isothiocyanate and bromoacetamide reagents, methods of analysis, and subsequent addition of metal ions. Anal. Biochem. 1984; 142(1): 68–78.

35. Jewett J.C., Bertozzi C.R. Cu-free click cycloaddition reactions in chemical biology. Chem. Soc.

Rev. 2010; 39(4): 1272–9.

36. McKay C.S., Finn M.G. Click chemistry in complex mixtures: Bioorthogonal bioconjugation. Chem. Biol. 2014; 21(9): 1075–101.

37. Baskin J.M., Prescher J.A., Laughlin S.T., Agard N.J., Chang P. V., Miller I.A., Lo A., Codelli J.A., Bertozzi C.R. Copper-free click chemistry for dynamic in vivo imaging. Proc. Natl. Acad. Sci. U. S. A. 2007; 104(43): 16793–7.

38. Taylor M.T., Blackman M.L., Dmitrenko O., Fox J.M. Design and Synthesis of Highly Reactive Dienophiles for the Tetrazine-trans-Cyclooctene Ligation. J. Am. Chem. Soc. 2011; 133(25): 9646–9.

39. Laughlin S.T., Baskin J.M., Amacher S.L., Carolyn R. In vivo Imaging of Membrane-associated Glycans in Developing Zebrafish. Sci. (New York, NY). 2008; 320(5876): 664–7.

40. Blackman M.L., Royzen M., Fox J.M. Tetrazine ligation: Fast bioconjugation based on inverse-electron-demand Diels-Alder reactivity. J. Am. Chem. Soc. 2008; 130(41): 13518–9.

41. Zeglis B.M., Sevak K.K., Reiner T., Mohindra P., Carlin S.D., Zanzonico P., Weissleder R., Lewis J.S. A pretargeted PET imaging strategy based on bioorthogonal Diels-Alder click chemistry. J. Nucl. Med. 2012; 54(8): 1389–96.

42. Meyer J.-P., Houghton J.L., Kozlowski P., Abdel-Atti D., Reiner T., Pillarsetty N.V.K., Scholz W.W., Zeglis B.M., Lewis J.S. F-18-Based Pretargeted PET Imaging Based on Bioorthogonal Diels-Alder Click Chemistry. Bioconjug. Chem. 2016; 27(2): 298–301.

43. Velikyan I., Sundberg Å.L., Lindhe Ö., Höglund A.U., Eriksson O., Werner E., Carlsoon J., Bergström M., Langström B., Tolmachev V. Preparation and Evaluation of Ga-68-DOTA-hEGF for Visualization of EGFR Expression in Malignant Tumors. J. Nucl. Med. 2005; 46(13): 1881–8.

44. Tóth I., Brücher E. Stability constants of the lanthanide(III)-1,4,7,10-tetraazacyclododecane-N,N',N'',N'''-tetraacetate complexes. Inorganica Chim. Acta. 1994; 221: 165–7.

45. Filosofov D. V., Loktionova N.S., Rösch F. A Ti-44/Sc-44 radionuclide generator for potential application of Sc-44-based PET-radiopharmaceuticals. Radiochim. Acta. 2010; 98(3): 149–56.

46. Eigner S., Vera D.R.B., Fellner M., Loktionova N.S., Piel M., Lebeda O., Rösch F., Roß T.L., Henke K.E. Imaging of protein synthesis: in vitro and in vivo evaluation of Sc-44-DOTA-puromycin. Mol. Imaging Biol. 2013; 15(1): 79–86.

47. Decristoforo C., Hernandez G.I., Carlsen J., Rupprich M., Huisman M., Virgolini I., Wester H.J., Haubner R. Ga-68- and In-111-labelled DOTA-RGD peptides for imaging of αvβ3 integrin expression. Eur. J. Nucl. Med. Mol. Imaging. 2008; 35(8): 1507–15.

48. Breeman W.A.P., De Jong M., Visser T.J., Erion J.L., Krenning E.P. Optimising conditions for radiolabelling of DOTA-peptides with Y-90, In-111 and Lu-177 at high specific activities. Eur. J. Nucl. Med. Mol. Imaging. 2003; 30(6): 917–20.

49. McDevitt M.R., Ma D., Simon J., Frank R.K., Scheinberg D.A. Design and synthesis of Ac-225 radioimmunopharmaceuticals. Appl. Radiat. Isot. 2002; 57: 841–7.

50. Ballangrud Å.M., Yang W.H., Palm S., Enmon R., Borchardt P.E., Pellegrini V.A., McDevitt M.R., Scheinberg D.A., Sgouros G. Alpha-particle emitting atomic generator (actinium-225)-labeled trastuzumab (Herceptin) targeting of breast cancer spheroids: Efficacy versus HER2/neu expression. Clin. Cancer Res. 2004; 10(13): 4489–97.

51. Bevilacqua A., Gelb R.I., Hebard W.B., Zompa L.J. Equilibrium and thermodynamic study of the aqueous complexation of 1,4,7-Triazacyclononane-N,N',N''-triacetic acid with protons, alkaline-earth-metal cations and copper(II). Inorg. Chem. 1987; 26(16): 2699–706.

52. Sun Y., Anderson C.J., Pajeau T.S., Reichert D.E., Hancock R.D., Motekaitis R.J., Martell A.E., Welch M.J. Indium(III) and gallium(III) complexes of bis(aminoethanethiol) ligands with different denticities: Stabilities, molecular modeling, and in vivo behavior. J. Med. Chem. 1996; 39(2): 458–70.

53. Velikyan I., Mäcke H.R., Langstrom B. Convenient Preparation of Temperature Ga-Based PET-Radiopharmaceuticals at Room. Bioconjug. Chem. 2008; 19: 569–73.

54. McMurry T.J., Brechbiel M.W. Synthesis of 2-(p-thiocyanatobenzyl)-1, 4, 7-triazacyclononane-1, 4, 7-triacetic acid: application of the 4-methoxy-2, 3, 6-trimethylbenzenesulfonamide protecting. Bioconjug. Chem. 1993; 4(14): 236–45.

55. Zhang Y., Hong H., Engle J.W., Bean J., Yang Y., Leigh B.R., Barnhart T.E., Cai W. Positron emission tomography imaging of CD105 expression with a Cu-64-labeled monoclonal antibody: NOTA is superior to DOTA. PLoS One. 2011; 6(12): 2–8.

56. Eisenwiener K.P., Prata M.I.M., Buschmann I., Zhang H.W., Santos A.C., Wenger S., Reubi J.C., Mäcke H.R. NODAGATOC, a new chelator-coupled somatostatin analogue labeled with Ga-67/68 and In-111 for SPECT, PET, and targeted therapeutic applications of somatostatin receptor (hsst2) expressing tumors. Bioconjug. Chem. 2002; 13(3): 530–41.

57. Price E.W., Orvig C. Matching chelators to radiometals for radiopharmaceuticals. Chem. Soc. Rev. 2014; 43(1): 260–90.

58. Notni J., Simecek J., Hermann P., Wester H.J. TRAP, a powerful and versatile framework for gallium-68 radiopharmaceuticals. Chem. - A Eur. J. 2011; 17(52): 14718–22.

59. Simecek J., Schulz M., Notni J., Plutnar J., Kubíček V., Havlícková J., Hermann P. Complexation of metal ions with TRAP (1,4,7-triazacyclononane phosphinic acid) ligands and 1,4,7-triazacyclononane-1,4,7-triacetic acid: Phosphinate-containing ligands as unique chelators for trivalent gallium. Inorg. Chem. 2012; 51(1): 577–90.

60. Notni J., Pohle K., Wester H.J. Be spoilt for choice with radiolabelled RGD peptides: Preclinical evaluation of Ga-68-TRAP(RGD)3. Nucl. Med. Biol. 2013; 40(1): 33–41.

61. Olsen J.O., Pozderac R. V., Hinkle G., Hill T., O'Dorisio T.M., Schirmer W.J., Ellison E.C., O'Dorisio M.S. Somatostatin receptor imaging of neuroendocrine tumors with indium-111 pentetreotide (Octreoscan). Semin. Nucl. Med. 1995; 25(3): 251–61.

62. Seifert J.K., Görges R., Bockisch A., Junginger T. Indium-111-DTPA-Octreotid-Szintigraphie bei kolorektalen Lebermetastasen. Langenbecks Arch. Chir. 1997; 382: 332–6.

63. Rowlinson G., Snook D., Stewart S. Intravenous EDTA to reduce bone uptake of Y-90 following Y-90-labeled antibody administration. Brit. J. Cancer. 1989; 59(322).

64. Jowsey J., Rowland E.E., Marshall J.H. The deposition of the rare earths in bone. Radiat. Res. 1958; 8(6): 490–501.

65. Kojima S., Jay M. Comparisons of labeling efficiency , biological activity and biodistribution among I-125, Ga-68-DTPA- and Ga-67-DFO-lectins. Eur. J. Nucl. Med. 1987; 13: 366–70.

66. Evers A., Hancock R.D., Martell A.E., Matekaitis R.J. Metal Ion Recognition in Ligands ith Negatively Charged Oxygen Donor Groups. Complexation of Fe(III), Ga(III), In(III), Al(III), and other Highly Charged Metal Ions. Inorg. Chem. 1989; 28: 2189–95.

67. Börjesson P.K.E., Jauw Y.W.S., Boellaard R., De Bree R., Comans E.F.I., Roos J.C., Castelijns J.A., Vosjan M.J.W.D., Kummer J.A., Leemans C.R., Lammertsma A.A., Van Dongen G.A.M.S. Performance of immuno - positron emission tomography with zirconium-89-labeled chimeric monoclonal antibody U36 in the detection of lymph node metastases in head and neck cancer patients. Clin. Cancer Res. 2006; 12(7 I): 2133–40.

68. Nagengast W.B., de Vries E.G., Hospers G.A., Mulder N.H., De Jong J.R., Hollema H., Brouwers A.H., Van Dongen G.A.M.S., Perk L.R., Lub-de Hooge M.N. In vivo VEGF imaging with radiolabeled bevacizumab in a human ovarian tumor xenograft. J. Nucl. Med. 2007; 48(8): 1313–9.

69. Perk L.R., Vosjan M.J.W.D., Visser G.W.M., Budde M., Jurek P., Kiefer G.E., Van Dongen G.A.M.S. P-Isothiocyanatobenzyl-desferrioxamine: A new bifunctional chelate for facile radiolabeling of monoclonal antibodies with zirconium-89 for immuno-PET imaging. Eur. J. Nucl. Med. Mol. Imaging. 2010; 37(2): 250–9.

70. Holland J.P., Divilov V., Bander N.H., Smith-Jones P.M., Larson S.M., Lewis J.S. Zr-89-DFO-J591 for ImmunoPET of Prostate-Specific Membrane Antigen Expression In Vivo. J. Nucl. Med. 2010; 51(8): 1293–300.

71. Patra M., Bauman A., Mari C., Fischer C.A., Blacque O., Häussinger D., Gasser G., Mindt T.L. An octadentate bifunctional chelating agent for the development of stable zirconium-89 based molecular imaging probes. Chem. Commun. 2014; 50(78): 11523–5.

72. Boros E., Ferreira C.L., Cawthray J.F., Price E.W., Patrick B.O., Wester D.W., Adam M.J., Orvig C. Acyclic chelate with ideal properties for Ga-68 PET imaging agent elaboration. J. Am. Chem. Soc. 2010; 132(44): 15726–33.

73. Eder M., Krivoshein A. V., Backer M., Backer J.M., Haberkorn U., Eisenhut M. ScVEGF-PEG-HBED-CC and scVEGF-PEG-NOTA conjugates: comparison of easy-to-label recombinant proteins for Ga-68-PET imaging of VEGF receptors in angiogenic vasculature. Nucl. Med. Biol. 2010; 37(4): 405–12.

74. Eder M., Wängler B., Knackmuss S., LeGall F., Little M., Haberkorn U., Mier W., Eisenhut M. Tetrafluorophenolate of HBED-CC: A versatile conjugation agent for Ga-68-labeled small recombinant antibodies. Eur. J. Nucl. Med. Mol. Imaging. 2008; 35(10): 1878–86.

75. Berry D.J., Ma Y., Ballinger J.R., Tavaré R., Koers A., Sunassee K., Zhou T., Nawaz S., Mullen G.E.D., Hider R.C., Blower P.J. Efficient bifunctional gallium-68 chelators for positron emission tomography: tris(hydroxypyridinone) ligands. Chem. Commun. (Camb). 2011; 47(25): 7068–70.

76. Baranyai Z., Uggeri F., Maiocchi A., Giovenzana G.B., Cavallotti C., Takács A., Tóth I., Bányai I., Bényei A., Brucher E., Aime S. Equilibrium, Kinetic and Structural Studies of AAZTA Complexes with Ga3+, In3+ and Cu2+. Eur. J. Inorg. Chem. 2013; (1): 147–62.

77. Nagy G., Szikra D., Trencsényi G., Fekete A., Garai I., Giani A.M., Negri R., Masciocchi N., Maiocchi A., Uggeri F., Tóth I., Aime S., Giovenzana G.B., Baranyai Z. AAZTA: An Ideal Chelating Agent for the Development of Sc-44 PET Imaging Agents. Angew. Chemie Int. Ed. 2017; 2118–22.

78. Aime S., Calabi L., Cavallotti C., Gianolio E., Giovenzana G.B., Losi P., Maiocchi A., Palmisano G., Sisti M. [Gd-AAZTA]-: A new structural entry for an improved generation of MRI contrast agents. Inorg. Chem. 2004; 43(24): 7588–90.

79. Baranyai Z., Uggeri F., Giovenzana G.B., Bényei A., Brücher E., Aime S. Equilibrium and kinetic properties of the lanthanoids(III) and various divalent metal complexes of the heptadentate ligand AAZTA. Chem. - A Eur. J. 2009; 15(7): 1696–705.

80. Waldron B.P., Parker D., Burchardt C., Yufit D.S., Zimny M., Rösch F. Structure and stability of hexadentate complexes of ligands based on AAZTA for efficient PET labelling with gallium-68. Chem. Commun. 2013; 49: 579–81.

81. Seemann J., Eppard E., Waldron B.P., Ross T.L., Rösch F. Cation exchange-based post-processing of Ga-68-eluate: A comparison of three solvent systems for labelling of DOTATOC, NO2APBP and DATAm. Appl. Radiat. Isot. 2015; 98: 54–9.

82. Parker D., Waldron B.P., Yufit D.S. Crystallographic and solution NMR structural analyses of four hexacoordinated gallium(III) complexes based on ligands derived from 6-amino-perhydro-1,4-diazepine. Dalton Trans. 2013; 42: 8001–8.

83. Seemann J., Waldron B.P., Rösch F., Parker D. Approaching “kit-type” labelling with Ga-68: The DATA chelators. ChemMedChem. 2015; 10(6): 1019–26.

84. Seemann J., Waldron B.P., Parker D., Rösch F. DATATOC: a novel conjugate for kit-type Ga-68 labelling of TOC at ambient temperature. EJNMMI Radiopharm. Chem. 2016; 1(1): 4.

85. Martell A.E., Motekaitis R.J. Determination and Use of Stability Constants. 1988.

86. Pehrsson L., Ingman F., Johansson A. Acid-base titrations by stepwise additions of equal volumes of titrant with special reference to automatic titrations-I. Theory, discussion of the gran functions, the hofstee method and two proposed methods for calculating equivalence volumes. Talanta. 1976; 23(11–12): 769–80.

87. Beck M.T., Nagypal I. Chemistry of complex equilibria. 1990.

88. Submeier J.L., Reilley C.N. Nuclear Magnetic Resonance Studies of Protonation of Polyamine and Aminocarboxylate Compounds in Aqueous Solution. Anal. Chem. 1964; 36(9): 1698–706.

89. Hevesy G. The Absorption and Translocation of Lead by Plants A Contribution to the Application of the Method of Radioactive Indicators in the Investigation of the Change of Substance in Plants. Biochem J. 1923; 17(4–5): 439–445.

90. Zhernosekov K.P., Filosofov D. V., Baum R.P., Aschoff P., Bihl H., Razbash A., Jahn M., Jennewein M., Rösch F. Processing of generator-produced Ga-68 for medical application. J. Nucl. Med. 2007; 48(10): 1741–8.

91. Banerjee S., Pillai M.R.A., Ramamoorthy N. Evolution of Tc-99m in diagnostic radiopharmaceuticals. Semin. Nucl. Med. 2001; 31(4): 260–77.

92. Deri M.A., Zeglis B.M., Francesconi L.C., Lewis J.S. PET Imaging with Zr-89: From Radiochemistry to the Clinic. Nucl. Med. Biol. 2013; 40(1): 3–14.

93. Radchenko V., Hauser H., Eisenhut M., Vugts D.J., Van Dongen G.A.M.S., Rösch F. Nb-90 - A potential PET nuclide: Production and labeling of monoclonal antibodies. Radiochim. Acta. 2012; 100(11): 857–63.

94. Vereshchagin Y.I., Markovskii D. V., Pavshuk V.A., Udovenko A.N., Khvostionov V.E., Chuvilin D.Y., Rice J., Tome L. Sr-89 Production in a reactor with solution fuel. At. Energy. 2006; 100(5): 350–8.

95. Walker L.A. Radioactive Yttrium-90: a Review of Its Properties, Biological Behavior, and Clinical Uses. Acta Radiol. Ther. Phys. Biol. 1964; 2(November): 302–14.

96. Boll R.A., Malkemus D., Mirzadeh S. Production of actinium-225 for alpha particle mediated radioimmunotherapy. Appl. Radiat. Isot. 2005; 62(5): 667–79.

97. Little F.E., Lagunas-Solar M.C. Cyclotron production of Ga-67. Cross sections and thick-target yields for the Zn-67 (p,n) and Zn-67 (p,2n) reactions. Int. J. Appl. Radiat. Isot. 1983; 34(3): 631–7.

98. Finlay I.G., Mason M.D., Shelley M. Radioisotopes for the palliation of metastatic bone cancer: a systematic review. Lancet Oncol. 2005; 6(6): 392–400.

99. Imam S.K. Advancements in cancer therapy with alpha-emitters: A review. Int. J. Radiat. Oncol.

Biol. Phys. 2001; 51(1): 271–8.

100. Hollemann A.F., Wiberg N. Lehrbuch der Anorganischen Chemie. 1995.

101. Wadas T.J., Wong E.H., Weisman G.R., Anderson C.J. Coordinating radiometals of copper, gallium, indium, yttrium, and zirconium for PET and SPECT imaging of disease. Chem. Rev. 2010; 110(5): 2858–902.

102. Rösch F., Riss P.J. The renaissance of the Ge-68/Ga-68 radionuclide generator initiates new developments in Ga-68 radiopharmaceutical chemistry. Curr. Top. Med. Chem. 2010; 10(16): 1633–68.

103. Rösch F., Filosofov D. V., John K.D., Mausner J.L., Ruth T.J., Samanta S.K., Knapp F.F., Mirzadeh S.J., Garland M., Ponsard B., Kuznetsov R. Production of Long Lived Parent Radionuclides for Generators : Ge-68, Sr-82, Sr-90 and W-188. IAEA Radioisot. Radiopharm. Ser. Publ. 2010.

104. Rösch F. Maturation of a key resource - the germanium-68/gallium-68 generator: development and new insights. Curr. Radiopharm. 2012; 5(3): 202–11.

105. Meyer G.-J., Mäcke H.R., Schuhmacher J., Knapp W.H., Hofmann M. Ga-68-labelled DOTA-derivatised peptide ligands. Eur. J. Nucl. Med. Mol. Imaging. 2004; 31(8): 1097–104.

106. Müller D., Klette I., Baum R.P., Gottschaldt M., Schultz M.K., Breeman W.A.P. Simplified NaCl based Ga-68 concentration and labeling procedure for rapid synthesis of Ga-68 radiopharmaceuticals in high radiochemical purity. Bioconjug. Chem. 2012; 23(8): 1712–7.

107. Nomura M., Kogure K., Okamoto M. Isotopic abundance ratios and atomic weight of zirconium. Int. J. Mass Spectrom. Ion Phys. 1983; 50(1–2): 219–27.

108. Ma M.T., Meszaros L.K., Paterson B.M., Berry D.J., Cooper M.S., Ma Y., Hider R.C., Blower P.J. Tripodal tris(hydroxypyridinone) ligands for immunoconjugate PET imaging with ^{89}Zr(4+): comparison with desferrioxamine-B. Dalton Trans. 2015; 4884–900.

109. Vosjan M.J.W.D., Perk L.R., Visser G.W.M., Budde M., Jurek P., Kiefer G.E., Van Dongen G.A.M.S. Conjugation and radiolabeling of monoclonal antibodies with zirconium-89 for PET imaging using the bifunctional chelate p-isothiocyanatobenzyl- desferrioxamine. Nat. Protoc. 2010; 5(4): 739–43.

110. Ache H.J. Chemistry of the Positron and of Positronium. Angew. Chemie Int. Ed. English. 1972; 11(3): 179–99.

111. Monike W., Hör G., Hertel A., Schelbert H. PET/CT-Atlas. PET/CT-Atlas. 2006.

112. Saha G.B. Basics of PET Imaging. Imaging. 2005.

113. Judenhofer M.S., Cherry S.R. Applications for preclinical PET/MRI. Semin. Nucl. Med. 2013; 43(1): 19–29.

114. Zoller F., Eisenhut M., Haberkorn U., Mier W. Endoradiotherapy in cancer treatment - Basic

concepts and future trends. Eur. J. Pharmacol. 2009; 625(1–3): 55–62.

115. Torres Martin De Rosales R., Finucane C., Foster J., Mather S.J., Blower P.J. Re-188-(CO)3-dipicolylamine-alendronate: A new bisphosphonate conjugate for the radiotherapy of bone metastases. Bioconjug. Chem. 2010; 21(5): 811–5.

116. Baum R.P., Kulkarni H.R., Schuchardt C., Singh A., Wirtz M., Wiessalla S., Schottelius M., Mueller D., Klette I., Wester H.J. Lu-177-Labeled Prostate-Specific Membrane Antigen Radioligand Therapy of Metastatic Castration-Resistant Prostate Cancer: Safety and Efficacy. J. Nucl. Med. 2016; 57(7): 1006–13.

117. Weineisen M., Schottelius M., Simecek J., Baum R.P., Yildiz A., Beykan S., Kulkarni H.R., Lassmann M., Klette I., Eiber M., Schwaiger M., Wester H.J. Ga-68- and Lu-177-Labeled PSMA I&T: Optimization of a PSMA-Targeted Theranostic Concept and First Proof-of-Concept Human Studies. J. Nucl. Med. 2015; 56(8): 1169–76.

118. Pillai M.R.A., Chakraborty S., Das T., Venkatesh M., Ramamoorthy N. Production logistics of Lu-177 for radionuclide therapy. Appl. Radiat. Isot. 2003; 59(2–3): 109–18.

119. Lebedev N.A., Novgorodov A., Misiak R., Brockmann J., Rösch F. Radiochemical separation of no-carrier-added Lu-177 as produced via the Yb-176 (n ,γ) Yb-177 → 177 Lu process. Appl. Radiat. Isot. 2000; 53: 421–5.

120. Speer T.W. Targeted Radionuclide Therapy. 2010.

121. Aime S., Barge A., Botta M., Fasano M., Danilo Ayala J., Bombieri G. Crystal structure and solution dynamics of the lutetium(III) chelate of DOTA. Inorganica Chim. Acta. 1996; 246(1–2): 423–9.

122. Brazeau P., Vale W., Burgus R., Ling N., Butcher M., Rivier J., Guillemin R. Hypothalamic polypeptide that inhibits the secretion of immunoreactive pituitary growth hormone. Science (New York, NY). 1973; 179(68): 77–9.

123. Burgus R., Ling N., Butcher M., Guillemin R. Primary structure of somatostatin, a hypothalamic peptide that inhibits the secretion of pituitary growth hormone. Proc. Natl. Acad. Sci. USA. 1973; 70(3): 684–8.

124. Yamada Y., Post S.R., Wang K., Tager H.S., Bell G.I., Seino S. Cloning and functional characterization of a family of human and mouse somatostatin receptors expressed in brain, gastrointestinal tract, and kidney. Proc. Natl. Acad. Sci. U. S. A. 1992; 89(1): 251–5.

125. Patel Y.C. Somatostatin and its receptor family. Front. Neuroendocrinol. 1999; 20(3): 157–98.

126. Modlin I.M., Pavel M., Kidd M., Gustafsson B.I. Review article: Somatostatin analogues in the treatment of gastroenteropancreatic neuroendocrine (carcinoid) tumours. Aliment. Pharmacol. Ther. 2010; 31(2): 169–88.

127. Reubi J.C., Schär J.C., Waser B., Wenger S., Heppeler A., Schmitt J.S., Mäcke H.R. Affinity profiles for human somatostatin receptor subtypes SST1-SST5 of somatostatin radiotracers selected for

scintigraphic and radiotherapeutic use. Eur. J. Nucl. Med. 2000; 27(3): 273–82.

128. Graham M., Mailman J. FDA Grants Orphan Drug Designation for Ga-68-DOTATOC. J. Nucl. Med. 2014; 55(1): 2014.

129. Investigational Candidates in Clinical Development. 2017.

130. Stryer L. Stryer - Biochemie. 1995.

131. Cheng Y.-C., Prusoff W.H. Relationship between the inhibition constant (KI) and the concentration of inhibitor which causes 50 per cent inhibition (I50) of an enzymatic reaction. Biochem. Pharmacol. 1973; 22(23): 3099–108.

132. Kaufmann S.H.E. Basiswissen Immunologie. 2014.

133. Mendler C.T., Friedrich L., Laitinen I., Schlapschy M., Schwaiger M., Wester H.J., Skerra A. High contrast tumor imaging with radio-labeled antibody Fab fragments tailored for optimized pharmacokinetics via PASylation. MAbs. 2015; 7(1): 96–109.

134. Van De Watering F.C.J., Rijpkema M., Perk L., Brinkmann U., Oyen W.J.G., Boerman O.C. Zirconium-89 labeled antibodies: A new tool for molecular imaging in cancer patients. Biomed Res. Int. 2014; 2014.

135. Fissers J., Waldron A.M., De Vijlder T., Van Broeck B., Pemberton D.J., Mercken M., Van Der Veken P., Joossens J., Augustyns K., Dedeurwaerdere S., Stroobants S., Staelens S., Wyffels L. Synthesis and Evaluation of a Zr-89-Labeled Monoclonal Antibody for Immuno-PET Imaging of Amyloid-beta Deposition in the Brain. Mol. Imaging Biol. 2016; 18(4): 598–605.

136. Van Dongen G.A.M.S., Visser G.W.M., Lub-de Hooge M.N., de Vries E.G., Perk L.R. Immuno-PET: A Navigator in Monoclonal Antibody Development and Applications. Oncologist. 2007; 12(12): 1379–89.

137. Meares C.F. Chelating agents for the binding of metal ions to antibodies. Int. J. Radiat. Appl. Instrumentation. 1986; 13(4): 311–8.

138. Al-Ejeh F., Darby J.M., Thierry B., Brown M.P. A simplified suite of methods to evaluate chelator conjugation of antibodies: effects on hydrodynamic radius and biodistribution. Nucl. Med. Biol. 2009; 36(4): 395–402.

139. Kukis D.L., DeNardo G.L., DeNardo S.J., Mirick G.R., Miers L.A., Greiner D.P., Meares C.F. Effect of the Extent of Chelate Substitution on the Immunoreactivity and Biodistribution of 2IT-BAT-Lym-1 Immunoconjugates. Cancer Res. 1995; 55(4): 878–84.

140. Singh R., Bandyopadhyay D. A target molecule for cancer therapy. Cancer Biol. Ther. 2007; 6(4): 481–6.

141. Gendler S.J., Spicer A.P. Epithelial mucin genes. Annu. Rev. Physiol. 1995; 57(Table 1): 607–34.

142. Aruffo A., Dietsch M.. T., Wan H., Hellstrom K.E., Hellstrom I. Granule membrane protein 140

(GMP140) binds to carcinomas and carcinoma- derived cell lines. Proc Natl Acad Sci U S A. 1992; 89(6): 2292–6.

143. Baeckström D., Hansson G.C., Nilsson O., Johansson C., Gendler S.J., Lindholm L. Purification and characterization of a membrane-bound and a secreted mucin-type glycoprotein carrying the carcinoma-associated sialyl-Lea epitope on distinct core proteins. J. Biol. Chem. 1991; 266(32): 21537–47.

144. Hanski C., Drechsler K., Hanisch F.-G., Sheehan J., Manske M., Ogorek D., Klussmann E., Hanski M.-L., Blank M., Xing P.-X., McKenzie I.F.C., Devine P.L., Riecken E.-O. Altered Glycosylation of the MUC-1 Protein Core Contributes to the Colon Carcinoma-associated Increase of Mucin-bound Sialyl-Lewisx Expression. Cancer Res. 1993; 53(17): 4082–8.

145. Rice G.E., Bevilacqua M.P. An inducible endothelial cell surface glycoprotein mediates melanoma adhesion. Science (New York, NY). 1989; 246(4935): 1303–6.

146. Braga V.M.M., Pemberton L.F., Dufflg T., Gendler S.J. Spatial and temporal expression of an epithelial mucin, Muc-1, during mouse development. Development. 1992; 115: 427–37.

147. Hilkens J., Ligtenberg M.J.L., Vos H.L., Litvinov S. V. Cell membrane-associated mucins and their adhesion-modulating property. Trends Biochem. Sci. 1992; 17(9): 359–63.

148. Ligtenberg M.J.L., Buijs F., Vos H.L., Hilkens J. Suppression of Cellular Aggregation by High Levels of Episialin. Cancer Res. 1992; 52(8): 2318–24.

149. Fontenot J.D., Tjandra N., Bu D., Ho C., Montelaro R.C., Finn O.J. Biophysical Characterization of One-, Two-, and Three-Tandem Repeats of Human Mucin (MUC1) Protein Core. Cancer Res. 1993; 53(22): 5386–94.

150. Palitzsch B., Hartmann S., Stergiou N., Glaffig M., Schmitt E., Kunz H. A fully synthetic four-component antitumor vaccine consisting of a mucin glycopeptide antigen combined with three different T-helper-cell epitopes. Angew. Chemie - Int. Ed. 2014; 53(51): 14245–9.

151. Kunz H., Hartmann S., Palitzsch B. Impfung gegen Tumore? Labor&More. 2012; 6: 16–25.

152. Gaidzik N., Westerlind U., Kunz H. The development of synthetic antitumour vaccines from mucin glycopeptide antigens. Chem. Soc. Rev. 2013; 42(10): 4421–42.

153. Fleisch H., Russell R.G.G., Straumann F. Effecto of Pyrophosphate on Hydroxyapatite and its Implications in Calcium Homeostasis. Nature. 1966; 212: 901–3.

154. Fleisch H., Russell R.G.G., Bisaz S., Casey P.A., Mühlbauer R.C. The influence of pyrophosphate analogues (diphosphonates) on the precipitation and dissolution of calcium phosphate in vitro and in vivo. Calcif. Tissue Res. 1968; 2: 10.

155. Flanagan A.M., Chambers T.J. Dichloromethylenebisphosphonate (Cl2MBP) inhibits bone resorption through injury to osteoclasts that resorb Cl2MBP-coated bone. Bone Miner. 1989; 6(1): 33–43.

156. Hughes D.E., Wright K.R., Uy H.L., Sasaki A., Yoneda T., Roodman D.G., Mundy G.R., Boyce B.F. Bisphosphonates promote apoptosis in murine osteoclasts in vitro and in vivo. J. Bone Mier Res. 1995; 10(10): 1478–87.

157. van Beek E., Pieterman E., Cohen L., Löwik C., Papapoulos S. Farnesyl Pyrophosphate Synthase Is the Molecular Target of Nitrogen-Containing Bisphosphonates. Biochem. Biophys. Res. Commun. 1999; 264(1): 108–11.

158. Dunford J.E., Thompson K., Coxon F.P., Luckman S.P., Hahn F.M., Poulter C.D., Ebetino F.H., Rogers M.J. Structure-Activity Relationships for Inhibition of Farnesyl Diphosphate Synthase in Vitro and Inhibition of Bone Resorption in Vivo by Nitrogen-Containing Bisphosphonates. J. Pharmacol. Exp. Ther. 2001; 296(2): 235–42.

159. Bergstrom J.D., Bostedor R.G., Masarachia P.J., Reszka A.A., Rodan G. Alendronate Is a Specific, Nanomolar Inhibitor of Farnesyl Diphosphate Synthase. Arch. Biochem. Biophys. 2000; 373(1): 231–41.

160. Fleisch H. Molekulare Wirkmechanismen der Bisphosphonate. Pharm. Unserer Zeit. 2001; 6(30): 500–4.

161. Amin D., Cornell S.A., Perrone M.H., Bilder G.E. 1-Hydroxy-3-(methylpentylamino)-propylidene-1,1-bisphosphonic acid as a potent inhibitor of squalene synthase. Arzneimittelforschung. 1996; 46(8): 759–62.

162. Amin D., Cornell S.A., Gustafson S.K., Needle S.J., Ullrich J.W., Bilder G.E., Perrone M.H. Bisphosphonates used for the treatment of bone disorders inhibit squalene synthase and cholesterol biosynthesis. J. Lipid Res. 1992; 33(11): 1657–63.

163. Rutty Solla G.A., Argüelles M.G., Bottazzini D.L., Furnari J.C., Parada I.G., Rojo A., Vera Ruiz H. Lutetium-177-EDTMP for bone pain palliation. Preparation, biodistribution and pre-clinical studies. Radiochim. Acta. 2000; 88(3–4): 157–61.

164. Ketring A.R. Sm-153-EDTMP and Re-186-HEDP as bone therapeutic radiopharmaceuticals. Int. J. Radiat. Appl. Instrumentation. 1987; 14(3): 223–32.

165. Littlefield J.L., Rudd T.G. Tc-99m hydroxymethylene diphosphonate and Tc-99m methylene diphosphonate: biological and clinical comparison: concise communication. J. Nucl. Med. 1983; 24(6): 463–6.

166. Vitha T., Kubíček V., Hermann P., Kolar Z.I., Wolterbeek H.T., Peters J.A., Lukeš I. Complexes of DOTA - Bisphosphonate conjugates: Probes for determination of adsorption capacity and affinity constants of hydroxyapatite. Langmuir. 2008; 24(5): 1952–8.

167. Ogawa K., Kawashima H., Shiba K., Washiyama K., Yoshimoto M., Kiyono Y., Ueda M., Mori H., Saji H. Development of Y-90-DOTA-conjugated bisphosphonate for treatment of painful bone metastases. Nucl. Med. Biol. 2009; 36(2): 129–35.

168. Pfannkuchen N., Meckel M., Kubíček V., Hermann P., Bergmann R., Steinbach J., Pietzsch J., Bal C.S., Kulkarni H.R., Mohnike W., Baum R.P., Rösch F. Ga-68- und Lu-177-markierte Bisphosphonate als Knochenmetastasen-Theranostika. TumorDiagn. u. Ther. 2015; 36(6): 349–54.

169. Tei L., Gugliotta G., Fekete M., Kálmán F.K., Botta M. Mn(II) complexes of novel hexadentate AAZTA-like chelators: a solution thermodynamics and relaxometric study. Dalton Trans. 2011; 40(9): 2025–32.

170. Barcza L., Mihályi K. Dimerization of lower fatty acids in aqueous solutions. Zeitschrift für Phys. Chemie. 1977; 104: 199–212.

171. Parker D., Waldron B.P. Conformational analysis and synthetic approaches to polydentate perhydro-diazepine ligands for the complexation of gallium(III). Org. Biomol. Chem. 2013; 11(17): 2827.

172. Smith D.L., Breeman W.A.P., Sims-Mourtada J. The untapped potential of Gallium-68-PET: The next wave of Ga-68-agents. Appl. Radiat. Isot. 2013; 76: 14–23.

173. Eppard E., Wuttke M., Nicodemus P.L., Rosch F. Ethanol-Based Post-processing of Generator-Derived Ga-68 Toward Kit-Type Preparation of Ga-68-Radiopharmaceuticals. J. Nucl. Med. 2014; 55(6): 1023–8.

174. Reubi J.C., Waser B., Schaer J.C., Laissue J.A. Somatostatin receptor sst1-sst5 expression in normal and neoplastic human tissues using receptor autoradiography with subtype-selective ligands. Eur. J. Nucl. Med. 2001; 28(7): 836–46.

175. Zolle I. Technetium-99m Pharmaceuticals. 2007.

176. Krenning E.P., Kooij P.P.M., Bakker W.H., Breeman W.A.P., Postema P.T.E., Kwekkeboom D.J., Oei H.Y., De Jong M., Visser T.J., Reijs A.E.M., Lamberts S.W.J. Radiotherapy with a radiolabeled somatostatin analogue, In-111-DTPA-[D-Phe1]-Octreotide. A case history. Ann. N. Y. Acad. Sci. 1994; 733: 496–506.

177. Valkema R., De Jong M., Bakker W.H., Breeman W.A.P., Kooij P.P.M., Lugtenburg P.J., De Jong F.H., Christiansen A., Kam B.L.R., De Herder W.W., Stridsberg M., Lindemans J., Ensing G., Krenning E.P. Phase I Study of Peptide Receptor Radionuclide Therapy With In-111-DTPA-Octreotide: The Rotterdam Experience. Semin. Nucl. Med. 2002; 32(2): 110–22.

178. Kwekkeboom D.J., Müller-Brand J., Paganelli G., Anthony L.B., Pauwels S., Kvols L.K., O'dorisio T.M., Valkema R., Bodei L., Chinol M., Mäcke H.R., Krenning E.P. Overview of results of peptide receptor radionuclide therapy with 3 radiolabeled somatostatin analogs. J Nucl Med. 2005; 46(1): 62S–66S.

179. De Jong M., Bernard B.F., De Bruin E., Van Gameren A., Bakker W.H., Visser T.J., Mäcke H.R., Krenning E.P. Internalization of radiolabelled [DTPA^0]octreotide and [DOTA^0,Try^3]octreotide: Peptides for somatostatin receptor-trageted scintigraphy and radionuclide therapy. Nucl. Med.

Commun. 1998; 19: 283–8.

180. Mausner L.F., Srivastava S.C. Selection of radionuclides for radioimmunotherapy. Med. Phys. 1993; 20(2): 503–9.

181. Goeckeler W.F., Edwards B., Volkert W.A., Holmes R.A., Simon J., Wilson D. Skeletal localization of samarium-153 chelates: potential therapeutic bone agents. J. Nucl. Med. 1987; 28(4): 495–504.

182. Ma D., Ketring A., Ehrhardt G., Jia W. Production of radiolanthanides and radiotherapy research at MURR. J. Radioanal. Nucl. Chem. 1996; (206): 119–26.

183. Das T., Banerjee S., Samuel G., Sarma H.D., Ramamoorthy N., Pillai M.R.A. Re-188-ethylene dicysteine: A novel agent for possible use in endovascular radiation therapy. Nucl. Med. Commun. 2000; 21(10): 939–45.

184. Wu A.M., Senter P.D. Arming antibodies: prospects and challenges for immunoconjugates. Nat. Biotechnol. 2005; 23(9): 1137–46.

185. Parker D. Tumour targeting with radiolabelled macrocycle-antibody conjugates. Chem. Soc. Rev. 1990; 19(3): 271–91.

186. Verel I., Visser G.W.M., Boerman O.C., van Eerd J.E.M., Finn R., Boellaard R., Vosjan M.J.W.D., Stigter-van Walsum M., Snow G.B., Van Dongen G.A.M.S. Long-lived positron emitters zirconium-89 and iodine-124 for scouting of therapeutic radioimmunoconjugates with PET. Cancer Biother. Radiopharm. 2003; 18(4): 655–61.

187. Philpott G.W., Schwarz S.W., Anderson C.J., Dehdashti F., Connett J.M., Zinn K.R., Meares C.F., Cutler P.D., Welch M.J., Siegel B.A. RadioimmunoPET: detection of colorectal carcinoma with positron-emitting copper-64-labeled monoclonal antibody. J. Nucl. Med. 1995; 36(10): 1818

188. Jurek P., Corbett R.J. Bifunctional hydroxamix acid ligands and method of synthesis. 2008. p. 26.

189. Hanisch F.G. O-glycosylation of the mucin type. Biol. Chem. 2001; 382(2): 143–9.

190. Taylor-Papadimitriou J., Burchell J., Miles D.W., Dalziel M. MUC1 and cancer. Biochim. Biophys. Acta - Mol. Basis Dis. 1999; 1455(2–3): 301–13.

191. Brockhausen I., Yang J.-M., Burchell J., Whitehouse C., Taylor-Papadimitriou J. Mechanisms Underlying Aberrant Glycosylation of MUC1 Mucin in Breast Cancer Cells. Eur. J. Biochem. 1995; 233(2): 607–17.

4. Manuskripte

Die vorliegende Arbeit basiert auf folgenden Manuskripten:

i. E. Farkas, J. Nagel, B. P. Waldron, D. Parker, I. Tóth, E. Brücher, F. Rösch, Z. Baranyai.
Equilibrium, kinetic and structural properties of gallium(III)- and some divalent metal complexes formed with the new DATA^{m} and DATA^{5m} ligands; accepted in *Chemistry – A European Journal* (DOI: 10.1002/chem.201701508)

ii. J.-P. Sinnes, J. Nagel, B. P. Waldron, T. Maina, B. A. Nock, R. Bergmann, M. Ullrich, M. Bachmann, R. P. Baum, F. Rösch.
Instant kit-preparation of ^{68}Ga-radiopharmaceuticals via the chimeric chelator DATA: Proof-of-principle with ^{68}Ga-DATA-TOC; in preparation

iii. B. A. Nock, A. Kaloudi, J. Nagel, J.-P. Sinnes, F. Rösch, T. Maina.
Novel bifunctional DATA chelator for quick access to site-directed PET ^{68}Ga-radiotracers: Preclinical proof-of-principle with [Tyr^{3}]octreotide; accepted in *Dalton Transactions* (DOI: 10.1039/C7DT01684K)

iv. J. Nagel, N. Engelbogen, P. Spang, F. Rösch.
Synthesis and radiolabelling of new DATA-derivatives with ^{68}Ga for mild coupling with targeting vectors; in preparation

v. J. Nagel, J. P. Sinnes, F. Rösch.
Synthesis and radiolabelling of new AAZTA-derivatives with ^{177}Lu for mild coupling with targeting vectors; in preparation

vi. N. Stergiou, J. Nagel, S. Pektor, M. Miederer H. Kunz, F. Rösch, E. Schmitt.
Radiolabelling, in vitro and in vivo evaluation of a novel ^{89}Zr-MUC1- antibody for ImmunoPET;
in preparation

4.1 Equilibrium, kinetic and structural properties of gallium(III)- and some divalent metal complexes formed with the new $DATA^{m}$ and $DATA^{5m}$ ligands

Equilibrium, kinetic and structural properties of gallium(III)- and some divalent metal complexes formed with the new DATA^{m} and DATA^{5m} ligands

E. Farkas,[1] J. Nagel,[2] B. P. Waldron,[3] D. Parker,[1] I. Tóth,[1] E. Brücher,[1] F. Rösch,[2] Z. Baranyai[1]

[1] Department of Inorganic and Analytical Chemistry, University of Debrecen, H-4032, Debrecen, Egyetem tér 1., Hungary
[2] Institute of Nuclear Chemistry, Johannes Gutenberg-University of Mainz, Germany
[3] Department of Chemistry, Durham University, South Road, Durham, DH1 3LE, UK

ABSTRACT

The development of $^{68}Ge/^{68}Ga$ generators has made the positron emitting ^{68}Ga isotope widely accessible, raising interest in new chelate complexes of Ga^{3+}. The hexadentate 1,4-di(acetate)-6-methyl-(amino(methyl)-acetate)-perhydro-1,4-diazepane ($DATA^{m}$) ligand and its bifunctional analogue, 1,4-di(acetate)-6-pentanoic acid-(amino(methyl)-acetate)-perhydro-1,4-diazepane ($DATA^{5m}$), rapidly form complexes with ^{68}Ga in high radiochemical yield. The stability constants of $DATA^{m}$ and $DATA^{5m}$ complexes formed with Ga^{3+}, Zn^{2+}, Cu^{2+}, Mn^{2+} and Ca^{2+} have been determined by pH-potentiometry, spectrophotometry (Cu^{2+}) and ^{1}H- and ^{71}Ga-NMR spectroscopy (Ga^{3+}). The stability constants of $Ga(DATA^{m})$ and $Ga(DATA^{5m})$ complexes are slightly higher than those of the Ga(AAZTA). The species distribution calculations indicate the predominance of Ga(L)OH mixed hydroxo complexes at physiological pH. The ^{1}H- and ^{71}Ga-NMR studies provided information about the coordinated functional groups of ligands and on the kinetics of exchange between the Ga(L) and Ga(L)OH complexes. The transmetallation reactions between the Ga(L) complexes and Cu^{2+}-citrate ($6<pH<8.5$) occur through both spontaneous and OH^{-}-assisted dissociation of the Ga(L)OH species. At pH=7.4 and 25 °C, the half lifes of the dissociation of $Ga(DATA^{m})$, $Ga(DATA^{5m})$ and Ga(AAZTA) are 11 h, 44 h and 24 h, respectively. Similar half lifes have been obtained for the ligand exchange reactions between the Ga(L)OH complexes and transferrin. The equilibrium and kinetic data indicate that the $Ga(DATA^{5m})$ complex is a good candidate as a ^{68}Ga-based radiodiagnostic.

Keywords: Ligands, Gallium, Molecular Imaging, Thermodynamic, Kinetics, Reaction mechanisms, NMR

INTRODUCTION

The visualization of biological processes at the molecular level and their qualitative and quantitative assessment is the domain of Molecular Imaging (MI). The established diagnostic power of the Positron Emission Tomography (PET) technique in MI and the increasing availability of new biological targeting vectors have led to the design and testing of a large number of radiopharmaceuticals in oncology, cardiology, neurology, and infectious diseases [1]. The introduction of radionuclides like ^{3}H, ^{11}C or ^{18}F to biological targeting vectors needs time consuming synthesis. Taking the half life of these nuclides into account, this is the main disadvantage for these radioisotopes in means of preparation and examination of their derivatives. Radiometal ions, instead, can be complexed in a single step to yield the desired product. These probes can be used for diagnosis via PET or SPECT imaging [2]. The major concern for most radionuclides is their availability and their means of production. Therefore, the use of generator produced isotopes has become of great interest over the last few years [3]. The widespread clinical application of ^{68}Ge-based radioisotope generators ($t_{1/2}(^{68}Ge)$=270.8 days) for the production of the PET isotope ^{68}Ga ($t_{1/2}$=67.71 min, $E_{\beta+,max}$=1.89 MeV, 89 % decays through positron emission), together with its favourable properties, i.e. half life sufficient for production and application of tracers with relatively low radiation dose to the patient, has gained the research activity for the development of effective, specific and safe ^{68}Ga-based radiopharmaceuticals [4–7]. Because of the similar properties of Ga^{3+} and Fe^{3+} ions, the ^{68}Ga-based radiopharmaceutical consists of a thermodynamically stable and kinetically inert Ga^{III}-complex linked to a specific vector, most often represented by peptides or pseudo-peptides. The Ga^{3+} ion is known to form stable complexes with carboxylate (e.g. TTHA, NOTA, DOTA) [8–12], picolinate (e.g. DEDPA, p-SCN-Bn-H_2dedpa) [13,14], hydroxamate (e.g. DFO, FSC) [15,16], phenolate (e.g. HBED, SHBED) [17,18], but will also bind well to “softer” thiolate groups (e.g. EDDA-SS, TACN-TM) [19,20]. The coordination of Ga^{3+} with several different ligands has been thoroughly investigated, starting from the screening work of Martell [8,9] and followed, in the last two decades, by the design and development of novel and improved Ga^{III}-complexes in order to prevent the transmetallation reaction with endogeneous metal ions (Cu^{2+}, Zn^{2+}, Ca^{2+}) or transchelation reactions with proteins such as transferrin [21,22]. It is well established that macrocyclic chelators such as 1,4,7,10-tetraazacyclododecane-1,4,7,10-tetraacetic acid (DOTA) and 1,4,7-triazacyclo-nonane-1,4,7-triacetic acid (NOTA), either free or conjugated to peptides, form thermodynamically stable and kinetically inert complexes with ^{68}Ga [21–27]. However, the efficient labeling of DOTA and NOTA ligands with ^{68}Ga isotope requires a large excess of ligand (>1000 fold) and high temperature (95 °C) which tend to denaturate the biologically active proteins. In this context, there is intensive search for highly Ga^{3+} specific chelators for efficient ^{68}Ga-labeling at room temperature [26,27].

The heptadentate ligand AAZTA (scheme 1) is easily prepared [28,29]. Its coordination properties towards a wide array of metal ions have been reported, showing its remarkable affinities to lanthanides

and transition metal ions [30–33]. The ready availability of AAZTA and recent descriptions of its lipophilic derivatives for targeting high density lipoproteins (HDL) [34], cell membranes [35], the synthesis of bifunctional compounds for conjugation purposes [29], and the fast formation of complexes prompted us to explore the possibility of employing the AAZTA platform for developing useful complexes for targeted PET applications [36]. Based on the 6-amino-1,4-diazapine (DATA) scaffold new hexadentate chelators were developed by Waldron *et al*. that shows favourable complexation behaviour [37–39].

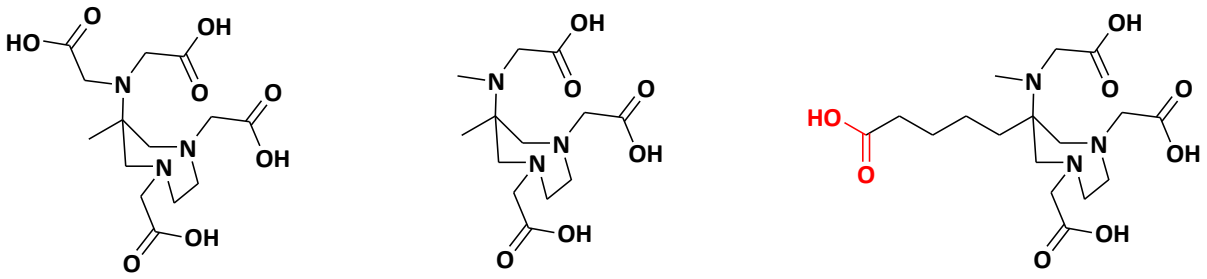

Scheme 1: Structure of AAZTA, DATA^{m} and DATA^{5m} ligands

Radiolabelling experiments with ^{68}Ga of these ligands showed high radiochemical yields after 1 minute and high stability in the first *in vitro* and *in vivo* studies [40,41]. In this study we synthesized the DATA^{m} and DATA^{5m} ligands via a new synthesis route and evaluated their protonation behaviour and complex-forming properties with various alkaline earth, transition metal and Ga^{3+} ions. The kinetic inertness of Ga(DATA^{m}) and Ga(DATA^{5m}) complexes was investigated via the exchange reactions with Cu^{2+} and transferrin under near physiological conditions. The solution structures and dynamics of the Ga(DATA^{m}) and Ga(DATA^{5m}) complexes have also been investigated by ^{1}H-NMR spectroscopy.

RESULTS AND DISCUSSION

The H_3DATA^m and H_4DATA^{5m} ligands is a derivative of H_4AAZTA in which one of the carboxylate groups is substituted by a methyl group in the imino-diacetate (IMDA) moiety (scheme 1). In the complexes of AAZTA, three N- and four carboxylate O-atoms can simultaneously bind the metal ion [19–25]. Removing one carboxylate group will evidently affect the equilibrium, kinetic and structural properties of the metal complexes formed with $DATA^m$ and $DATA^{5m}$ ligands. Indeed, the $DATA^m$ ligand has been shown to form a well-defined octahedral Ga^{III}-complex by X-ray crystallography [38,39]. Moreover, the presence of the n-valeric acid pendant used for the conjugation of $DATA^{5m}$ to biologically active molecules may influence the physicochemical properties of the metal-complexes (for bioconjugation reactions, the orthogonal protected $DATA^{5m}$ is used with the base labile methyl ester of the n-valeric acid pendant and the *t*-butyl ester of the carboxylate groups) [35]. Taking into account these considerations, the behaviour of $DATA^m$ and $DATA^{5m}$ has been compared in detail.

Solution equilibria of the $DATA^m$ and $DATA^{5m}$ ligands and its complexes

Protonation equilibria of the H_3DATA^m and H_4DATA^{5m} ligands:

The protonation constants of the ligands, defined by eq. (1), have been determined by pH-potentiometry and the $\log K_i^H$ values are listed in table 1. (standard deviations are shown in parentheses). The charges of the ligands and complexes will be used only when it is really necessary.

$$K_i^H = \frac{[H_iL]}{[H_iL][H^+]} \qquad (1)$$

where i=1, 2,…5.

Table 1: Protonation constants of $DATA^m$, $DATA^{5m}$ and AAZTA ligand (0.15 M NaCl, 25°C);(MeAAZ3A=$DATA^m$, a: The protonation constant of n-valeric acid is not considered (due to the negligible role in metal binding).

	$DATA^m$	**MeAAZ3A [42]**	**$DATA^{5m}$**	**AAZTA [31]**
$\log K_1^H$	11.27 (1)	10.90	11.39 (1)	10.06
$\log K_2^H$	5.15 (2)	5.14	5.30 (2)	6.50
$\log K_3^H$	3.49 (1)	3.71	4.35 (2) -COOH	3.77
$\log K_4^H$	2.08 (2)	2.17	3.45 (2)	2.33
$\log K_5^H$	–	–	2.28 (4)	1.51
$\Sigma \log K_i^H$	21.99	21.92	26.77 / 22.42 [a]	24.17

The protonation sequence of the AAZTA ligand was determined by a study of the pH-dependence of the ^{1}H-NMR chemical shifts of non-labile protons [30]. The first protonation takes place at the nitrogen atoms of the ring and the pendant arm (the protonation occurs partially at a ring N- and at the imino-diacetate N-atom). The second protonation occurs at the ring nitrogen, whereas the first proton is transferred to the nitrogen of the IMDA group, because of the electrostatic repulsion between the protonated ring and the exocyclic nitrogen. Further protonations occur at one of the ring-carboxylate groups and non-protonated ring nitrogen atom and/or the carboxylate pendant arms, respectively. According to the $\Delta\delta_H$ values of the non-labile protons of the DATA^m ligand published by Waldron *et al*. [37] the protonation scheme of DATA^m and DATA^{5m} ligands is very similar to that of AAZTA. A comparison of the protonation constants (table 1) indicates that logK_1^H and logK_2^H values of DATA^{5m} are slightly higher, whereas the logK_3^H value for DATA^{5m} is 0.7 logK unit higher than for DATA^m. The higher logK_1^H and logK_2^H values of DATA^{5m} can be explained by differential solvation of the protonated ligand following introduction of the n-valeric acid moiety.

By considering the protonation constant of n-valeric acid (logK_1^H=4.69) [43], it is reasonable to assume that the third protonation of DATA^{5m} involves the carboxylate group of the n-valeric acid pendant. Finally, the logK_3^H and logK_4^H values of DATA^m and logK_4^H and logK_5^H values of DATA^{5m}, corresponding to the protonation of the ring-carboxylate and non-protonated ring nitrogen or carboxylate groups, are very similar. It is worth noting that the logK_1^H value of DATA^m and DATA^{5m} is significantly higher than that of the AAZTA ligand, which can be explained by the formation of Na(AAZTA)$^{3-}$ complex competing with the first protonation process. The lower affinity of DATA^m and DATA^{5m} towards Na^+ may be related to the absence of one acetate arm results in the lower overall charge of the fully deprotonated ligands.

Complexation properties with M^{2+} cations:

The stability and protonation constants of the metal complexes are defined by eqs. (2) and (3).

$$K_{ML} = \frac{[ML]}{[M][L]} \tag{2}$$

$$K_{MH_i L} = \frac{[MH_i L]}{[MH_{i-1}L][L]} \tag{3}$$

where i=1-3. The protonation and stability constants of the DATA^m and DATA^{5m} complexes have been calculated from the titration curves obtained at 1:1 metal to ligand concentration ratios. The best fitting was obtained by using a model which includes the formation of *ML*, *MHL*, *MH_2L* and *MH_3L* species in equilibrium. The titration data of the DATA^m and DATA^{5m} in the presence of Zn^{2+} and Cu^{2+} indicate base consuming processes at pH>9. These processes can be interpreted by assuming the hydrolysis of

the metal ion; the coordination of OH^- ion results in the formation of M(L)OH species. The protonation of the M(L)OH species can be characterized by the equilibrium constant K_{MLH-1} (eq. (4)).

$$M(L)OH^- + H^+ \rightleftarrows ML + H_2O \tag{4}$$

$$K_{MH_i L} = \frac{[MH_i L]}{[MH_{i-1}L][L]}$$

Because of the high stability of the Cu(DATA^m) and Cu(DATA^{5m}) complex, the determination of the stability constants cannot be carried out by direct pH-potentiometry. However, it is possible by spectrophotometry. The stability constant has been determined by studying the equilibrium in the Cu^{2+}-DATA^m-H^+ and Cu^{2+}-DATA^{5m}-H^+ systems with UV/Vis spectrophotometry. The competition reaction (eq. (5)) has been studied in the $[H^+]$ range 0.01-1.0 M, where the species Cu^{2+}, $Cu(H_3L)$, $Cu(H_2L)$ and Cu(HL) are present in the equilibria.

$$Cu^{2+} + H_xL \rightleftarrows Cu(H_yL) + (x-y)\,H^+ \tag{5}$$

where x=3-4 and y=1-2 for DATA^m and x=4-5 and y=2-3 for DATA^{5m}. Some characteristic absorption spectra obtained for the Cu^{2+}-DATA^m-H^+ and Cu^{2+}-DATA^{5m}-H^+systems are shown in figure 1. The stability constants obtained by pH-potentiometric titration and by UV/Vis spectrophotometric technique for the Cu^{2+} are presented in table 2. The stability constants of Ca^{II}-, Mn^{II}- and Cu^{II}-complexes formed with DATA^m and DATA^{5m} ligands are lower by 2-3 logK units than those of the corresponding AAZTA complexes. Interestingly, the stability constants of Zn(DATA^m) and Zn(DATA^{5m}) complexes are higher than that of Zn(AAZTA). A comparison of the $logK_{ML}$ values of metal complexes formed with DATA^m and DATA^{5m} indicates that the stability constants of the DATA^{5m} complexes (table 2) are generally higher by 0.2-0.5 logK units than those of the corresponding complexes of DATA^m.

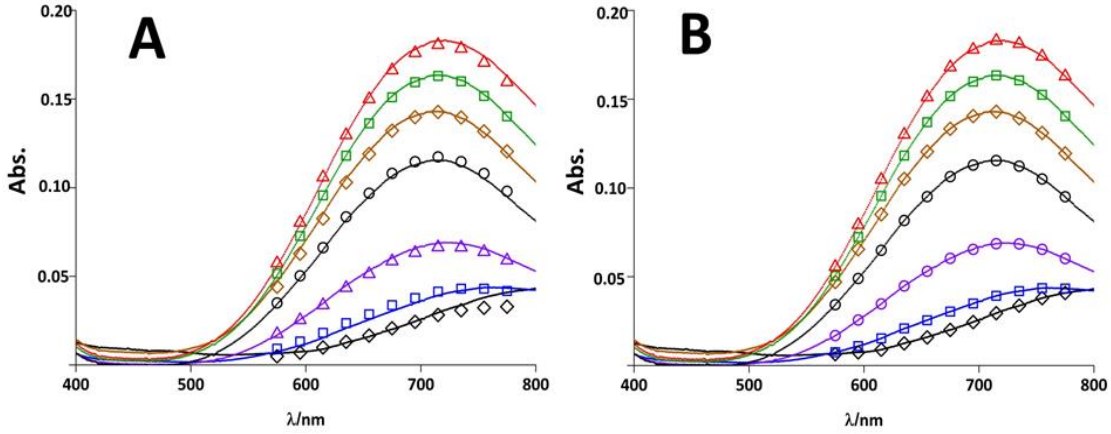

Figure 1: The absorption spectra of the Cu^{2+}-$DATA^{m}$-H^{+} (A) and Cu^{2+}-$DATA^{5m}$-H^{+} (B) systems as a function of $[H^{+}]$. The curves and the open symbols represent the experimental and the calculated absorbance values, respectively. ($[H^{+}]$=1.0 (◇), 0.60 (□), 0.32 (△), 0.10 (○), 0.05 (◇), 0.025 (□) and 0.01 M (△); $[Cu^{2+}]=[DATA^{m}]=[DATA^{5m}]$=0.002 M, $[H^{+}]\leq$0.15 M→$[Na^{+}]+[H^{+}]$=0.15 M, 25°C, I=1 cm).

Table 2: Stability and protonation constants of $DATA^{m}$, $DATA^{5m}$ and AAZTA complexes formed with Ca^{2+}, Mn^{2+}, Zn^{2+} and Cu^{2+} ions (0.15 M NaCl, 25°C); *a:* Spectrophotometry, $[H^{+}]$=0.01-1.0 M, I=$[H^{+}]+[Na^{+}]$=0.15 M in samples at [H+]<0.15 M

	$DATA^{m}$	**$DATA^{5m}$**	**AAZTA[31]**
CaL	8.70 (2)	9.09 (2)	11.75 (1)
CaHL	5.49 (4)	5.64 (5)	3.41 (3)
CaH_2L	–	4.71 (5)	–
MnL	11.43 [42]	11.63 (2)	14.19 [42]
MnHL	3.36 [42]	4.86 (1)	2.61 [a]
MnH_2L	–	3.53 (4)	–
ZnL	16.54 (2)	16.91 (2)	16.02 (1)
ZnHL	1.76 (5)	4.77 (1)	3.95 (1)
ZnH_2L	–	1.77 (5)	2.53 (1)
Zn(L)OH	11.94 (4)	12.00 (5)	11.36 (2)
CuL[c]	18.36 (4)	18.97 (2)	20.60 (4)
CuHL	3.56 (2)	4.58 (1)	3.86 (1)
CuH_2L	1.52 (2)	3.35 (1)	2.43 (1)
CuH_3L	–	1.34 (2)	1.37 (3)
Cu(L)OH	10.88 (1)	11.10 (4)	10.62 (2)

The complexes formed with the $DATA^{m}$ and $DATA^{5m}$**,** similarly to those of AAZTA, can be protonated at lower pH values and the protonation constants have been determined by pH-potentiometry (table 2). The $logK_{MHL}$ value of Mn^{II}, Zn^{II}- and Cu^{II}-, and the $logK_{MH2L}$ value of Ca^{II}-complexes formed with $DATA^{5m}$ are very similar to the $logK_3^{H}$ value of the free ligand, $DATA^{5m}$. These findings clearly indicate that the n-valeric acid fragment of $DATA^{5m}$ does not participate in the coordination of metal ions, so it can protonate/deprotonate independently. For the complexes formed with Zn^{2+} and Cu^{2+} ions one and two

lower protonation constants could be determined, respectively. In these complexes there exists probably one weakly-coordinated donor atoms (a carboxylate-O), which can be protonated in the pH range 2-5.

Equilibrium properties of Ga^{3+}-$DATA^{m}$ and Ga^{3+}-$DATA^{5m}$ systems:

The stability and protonation constants of $Ga(DATA^{m})$ and $Ga(DATA^{5m})$, defined by eqs. (2) and (3), were determined by pH-potentiometric titration of solutions from basic to acidic conditions by following the competition between the OH^- ions and the $DATA^{m}$ or $DATA^{5m}$ ligands for Ga^{3+} at high pH values (pH>8), as described in eq. (6). For the calculations the hydrolysis constants of the free Ga^{3+}-ion ($\log K_{[Ga(OH)]2+}$= -2.97, $\log K_{[Ga(OH)2]+}$=-5.92, $\log K_{[Ga(OH)3]}$ =-8.2 and $\log K_{[Ga(OH)4]^-}$=-17.3) were also used [44–46].

$$GaL + 4\ OH^- \rightleftarrows [Ga(OH)_4]^- + H_xL \qquad (6)$$

The protonation constants of $Ga(DATA^{m})$ and $Ga(DATA^{5m})$ have been calculated from the titration curves obtained at 1:1 metal to ligand concentration ratios by titrating the preformed complex with standardized HCl solution. The titration data obtained for $Ga(DATA^{m})$ and $Ga(DATA^{5m})$ at 8>pH>5 indicated the occurrence of an extra acid consuming process. This process can be interpreted by the reaction of a H^+ ion with the [Ga(L)OH] species. The formation and protonation of mixed hydroxo [Ga(L)OH] complexes could be characterized by eqs. (4) and (7):

$$Ga^{3+} + L + OH^- \rightleftarrows Ga(L)OH^- \qquad (7)$$

$$\beta_{GaLH_{-1}} = \frac{[Ga(L)OH]}{[Ga^{3+}][L^-][OH^-]}$$

The Ga^{3+}-$DATA^{m}$ and Ga^{3+}-$DATA^{5m}$ equilibrium systems have also been investigated by ^{1}H- and ^{71}Ga-NMR spectroscopy. The ^{1}H- and ^{71}Ga-NMR spectra of the Ga^{3+}-$DATA^{m}$ and Ga^{3+}-$DATA^{5m}$ systems obtained in the pH range 1.7-12 are presented in figures 2 and 3, S1 and S2, respectively.

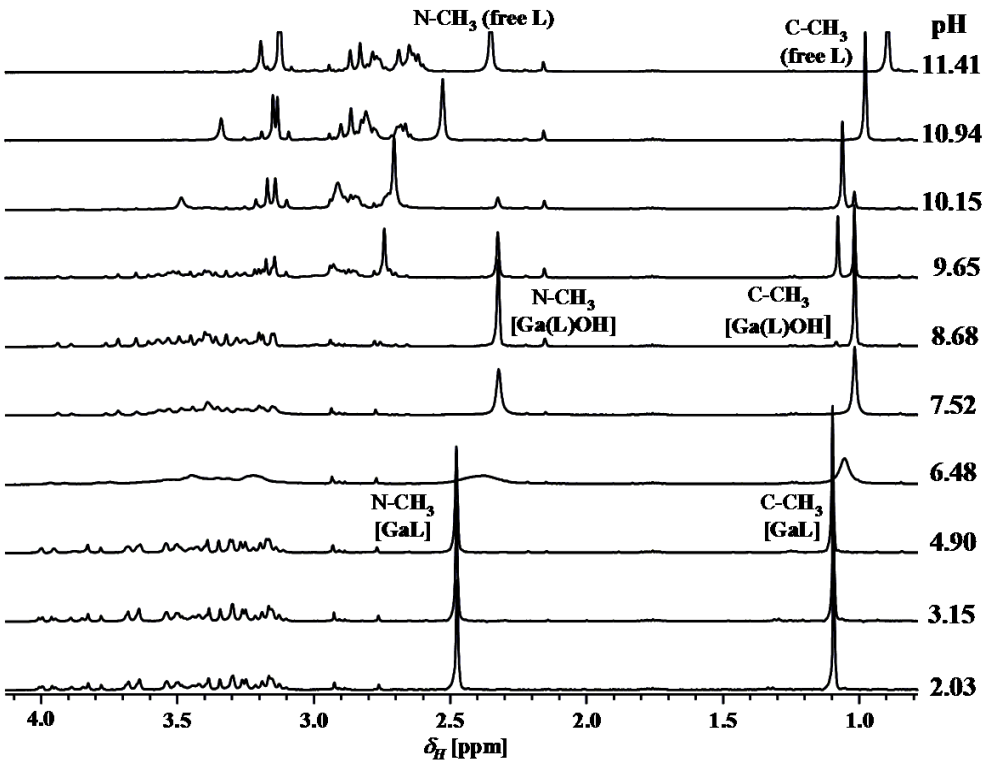

Figure 2: 400 MHz ^{1}H-NMR spectra of the Ga^{3+}-$DATA^{m}$ system ([Ga^{3+}]=8.15 mM, [$DATA^{m}$]=8.30 mM, 0.15 M NaCl, 298K)

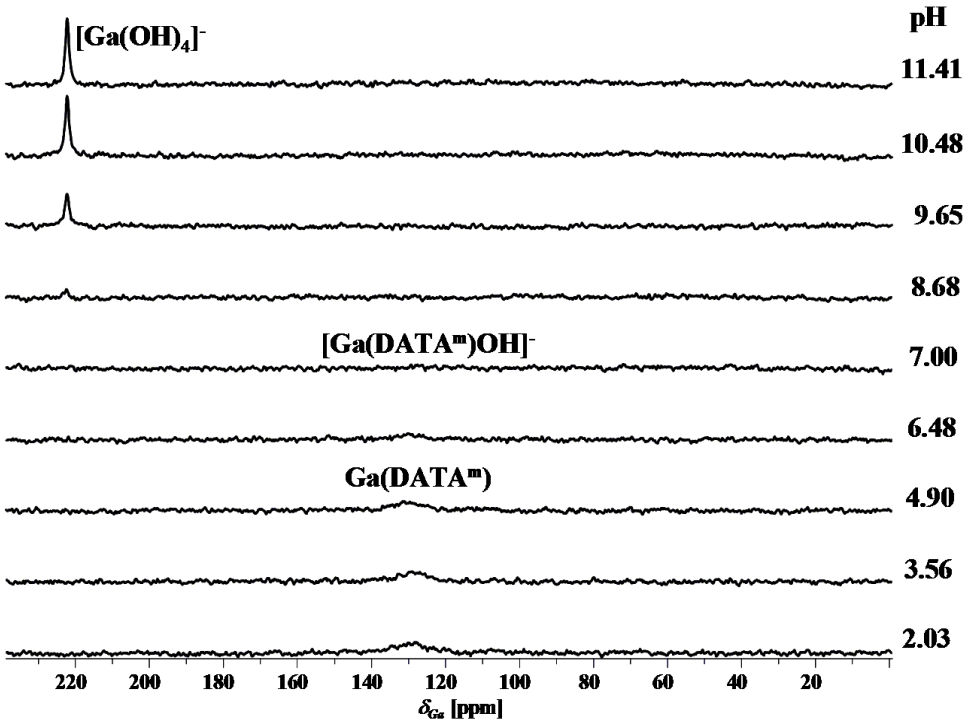

Figure 3: 122 MHz ^{71}Ga-NMR spectra of the Ga^{3+}-$DATA^{m}$ system ([Ga^{3+}]=8.15 mM, [$DATA^{m}$]=8.30 mM, 0.15 M NaCl, 298 K)

The ^{1}H- and ^{71}Ga-NMR data have also been used to calculate the stability and protonation constants of Ga(DATA^{m}) and Ga(DATA^{5m}) complexes by taking into account the integrals of the ^{1}H- (Ga(DATA^{m}): C**H$_3$**-C- (1.0 ppm), C**H$_3$**-N- (2.3 ppm), see figure 2; Ga(DATA^{5m}): C**H$_3$**-N- (2.35 ppm), see figure S1; and ^{71}Ga-NMR signals of ([Ga(OH)$_4$]$^{-}$ (223 ppm), see figures 3 and S2). Moreover, the protonation constant of the n-valeric acid fragment in the Ga(DATA^{5m}) complex has also been calculated from the chemical shift variation of the triplet resonance, -C**H$_2$**-COO^{-}, (2.2 ppm), (see figure S1) as a function of pH. The stability and protonation constants of Ga(DATA^{m}) and Ga(DATA^{5m}) complexes obtained by pH-potentiometry, ^{1}H- and ^{71}Ga-NMR spectroscopy are listed and compared with those of Ga(AAZTA) in table 3.

Table 3: Stability and protonation constants of Ga(DATA^{m}), Ga(DATA5^{m}) and Ga(AAZTA) complexes (0.15 M NaCl, 25°*C)*

	Ga(DATA^{m})		**Ga(DATA^{5m})**		**Ga(AAZTA)[31]**
method	pH-pot.	^{1}H/^{71}Ga-NMR	pH-pot.	^{1}H/^{71}Ga-NMR	pH-pot.
	pH=12-1.7				pH=1.7-12
logK_{GaL}	21.54 (2)	21.80 (4)	21.41 (2)	21.60 (5)	21.15
logK_{GaHL}	2.42 (2)	2.25 (9)	4.44 (3) -COOH	4.40 (4) -COOH	3.14
logK_{GaH2L}	–	–	2.05 (5)	–	1.14
logK_{GaLH-1}	6.25 (2)	6.38 (4)	6.31 (4)	6.20 (4)	4.60
logβ_{GaLH-1}	15.29 (2)	15.42 (4)	15.07 (4)	15.40 (5)	16.57

The stability constants of Ga(DATA^{m}) and Ga(DATA^{5m}) complexes are slightly higher than those of Ga(AAZTA). Since the total basicity (ΣlogK_i^H) of AAZTA is significantly higher than those of DATA^{m} and DATA^{5m} (table 1), the higher logK_{GaL} values of Ga(DATA^{m}) and Ga(DATA^{5m}) can be explained by considering the structural properties of these complexes. In Ga(DATA^{m}), the Ga^{3+} ion is coordinated by three amine-N and three carboxylate-O donor atoms (two ring- and one exocyclic-carboxylate-O) in a slightly distorted octahedral fashion [37–39]. However, in Ga(AAZTA) the Ga^{3+} ion is coordinated by 3 amine-N and 3 carboxylate-O donor atoms (two exocyclic- and one ring-carboxylate-O, whereas one of the ring-carboxylate-O does not coordinate) with a more distorted octahedral geometry, that results in a less favourable coordination environment for the Ga^{3+} ion and the lower stability of Ga(AAZTA) [31]. By taking into account these assumptions and presuming similar coordination geometry for the Ga^{III}- and Zn^{II} complexes, the higher stability of the Zn(DATA^{m}) and Zn(DATA^{5m}) by comparing with that of Zn(AAZTA) might also be explained by the less favourable coordination environment of the Zn^{II} ion in the more distorted Zn(AAZTA) complex. Owing to the higher stability of the Ga(DATA^{m}) and Ga(DATA^{5m}), the formation of [Ga(DATA^{m})OH]$^{-}$ and [Ga(DATA^{5m})OH]$^{2-}$ (logK_{GaLH-1}, table 3) takes place at higher pH values than that of [Ga(AAZTA)OH]$^{2-}$. However, [Ga(DATA^{m})OH]$^{-}$ and [Ga(DATA^{5m})OH]$^{2-}$ species still predominate under physiological conditions (figures 4 and S3) and are characterized by significantly lower stabilities than that of [Ga(AAZTA)OH]$^{2-}$ (logβ_{GaLH-1}, table 3), in accord with the different

constitution of $[Ga(DATA^{m})OH]^{-}$, $[Ga(DATA^{5m})OH]^{2-}$ and $[Ga(AAZTA)OH]^{2-}$. The equilibrium data, obtained by pH-potentiometric titration, allowed a calculation of the species distribution diagram for the Ga^{3+}-$DATA^{m}$ and Ga^{3+}-$DATA^{5m}$ systems, (see figures 4 and S3.)

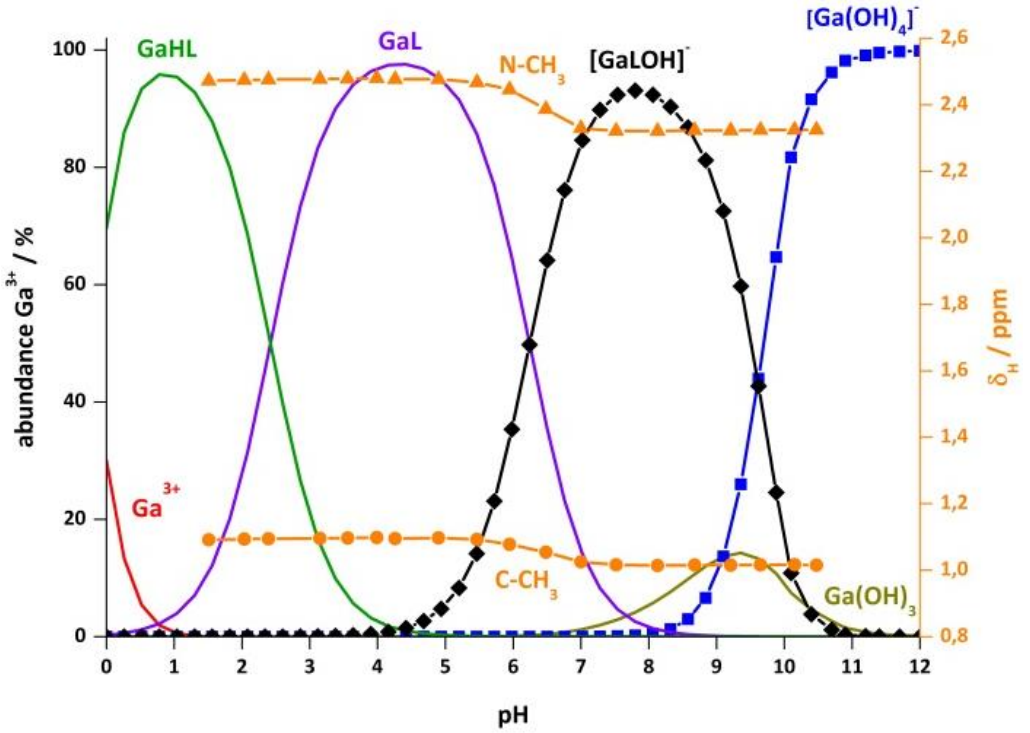

Figure 4: The species distribution (red, green, purple, black, brown and blue solid lines) in the Ga^{3+}-$DATA^{m}$ system calculated from pH-potentiometric data (table 3). ($[Ga^{3+}]=[DATA^{m}]=8.2$ mM, 0.15 M NaCl, 25 °C). The percentage of the $[Ga(DATA^{m})OH]^{-}$ (◆) and $[Ga(OH)_4]^{-}$ (■) species were calculated from the ^{1}H- and ^{71}Ga-NMR spectra of the Ga^{3+}-$DATA^{m}$ system. Chemical shifts of the N-CH_3 (▲) and C-CH_3 (●) protons of $Ga(DATA^{m})$ complex against pH

In the species distribution diagrams (figures 4 and S3), the ^{1}H- and ^{71}Ga-NMR data (figures 2, 3, S1 and S2) indicate that the competition reaction between $DATA^{m}$ and $DATA^{5m}$ ligands and OH^{-} ions for the Ga^{3+} ion with the formation of $[Ga(DATA^{m})OH]^{-}$ and $[Ga(DATA^{5m})OH]^{2-}$ is complete at about pH<8. In the ^{1}H-NMR spectrum, the changes in the intensity and the chemical shifts of the free $DATA^{m}$ and $DATA^{5m}$ signals indicate the formation of $[Ga(DATA^{m})OH]^{-}$ and $[Ga(DATA^{5m})OH]^{2-}$ species and the protonation of free $DATA^{m}$ and $DATA^{5m}$ ligands in the pH range 8-1.4. The ^{71}Ga-NMR signal is relatively sharp for the highly symmetric $[Ga(OH^{-})_4]^{-}$ species (figures 3 and S2, δ_{Ga}=223 ppm, $\nu_{½}$=88 Hz) at pH>11. The intensity of the ^{71}Ga-NMR signal of the $[Ga(OH^{-})_4]^{-}$ species decreases by decreasing pH due to the formation of $[Ga(DATA^{m})OH]^{-}$ and $[Ga(DATA^{5m})OH]^{2-}$ complexes in the pH range 11.4-8. In the pH range 7-8, the $[Ga(DATA^{m})OH]^{-}$ and $[Ga(DATA^{5m})OH]^{2-}$ complexes predominate. At pH<7, the protonation of $[Ga(DATA^{m})OH]^{-}$ and $[Ga(DATA^{5m})OH]^{2-}$ complexes by the formation of $Ga(DATA^{m})$ and $Ga(DATA^{5m})^{-}$ result in shifts to higher frequency of all the signals in the ^{1}H-NMR spectrum (figures 2 and S1). The ^{71}Ga-NMR signal of the $Ga(DATA^{m})$ and $Ga(DATA^{5m})^{-}$ is broad (figures 3 and S2, $Ga(DATA^{m})$: δ_{Ga}=129 ppm, $\nu_{½}$=1000 Hz; $Ga(DATA^{5m})$: δ_{Ga}=129 ppm, $\nu_{½}$=1100 Hz, pH=4.5). However, the ^{71}Ga-NMR

signal of the Ga(AAZTA)$^-$ is even broader (δ_{Ga}=118 ppm, $\nu_{½}$=2218 Hz, pH=4.0) as a result of the more asymmetric coordination geometry of AAZTA [31]. In the pH range 3-5, the protonation of the n-valeric acid side chain of Ga(DATA^{5m})$^-$ takes place with a shift to higher frequency of the -C**H$_2$**-COO$^-$ signal (triplet at 2.3 ppm, figure S1). The protonation constant of n-valeric acid entity of Ga(DATA^{5m})$^-$ (logK_{GaHL}=4.40, table 3) is very similar to that of the free DATA^{5m} (logK_3^H=4.35, table 1), which indicates, that the carboxylate group of n-valeric acid arm in DATA^{5m} does not coordinate to the Ga^{3+} ion, so it can protonate/deprotonate independently. In the pH range 1.7-3.5, the formation of Ga(HDATA^m)$^+$ and Ga(H$_2$DATA^{5m})$^+$ results in a small shift of all signals in the range of 3-4 ppm (figures 2 and S1), which indicates that this process takes place at the weakly-coordinated ring-carboxylate groups of ligands. The stability constant of Ga(DATA^m) and Ga(DATA^{5m})$^-$ obtained by the pH-potentiometry and multinuclear NMR spectroscopy) are in very good agreement (see table 3).

Dynamic NMR study of chemical exchange processes

The chemical exchange processes between Ga(DATA^m) and [Ga(DATA^m)OH]$^-$, and Ga(DATA^{5m})$^-$ and [Ga(DATA^{5m})OH]$^{2-}$ complexes have been investigated by ^{1}H-NMR spectroscopy in D$_2$O solution (see figures 5 and S4). The solution structure of Ga(DATA^{5m})$^-$ is expected to be similar to that of the corresponding Ga(DATA^m), investigated in the solid state by X-ray diffraction [37]. Crystallographic data of Ga(DATA^m) reveal, that the coordination geometry around each Ga^{3+} ion can be described as a slightly distorted octahedral geometry, where one of the ring N, the exocyclic N, one of the ring carboxylate O and the exocyclic carboxylate O donor atoms are coordinated in a square planar fashion in equatorial positions. The other ring N and ring carboxylate O donor atoms complete the coordination sphere of the Ga^{3+} ion in axial positions [37].

In the ^{1}H-NMR spectra (273 K and pH=6.4), signals of the C**H$_3$**-N and C**H$_3$**-C in Ga(DATA^m) and the C**H$_3$**-N in Ga(DATA^{5m}) give rise to two singlets. By increasing the temperature, the singlets broaden, coalesce (Ga(DATA^m): C**H$_3$**-C, T=283 K; C**H$_3$**-N, T=298 K; Ga(DATA^{5m}): C**H$_3$**-N, T=298 K) and then merge into a single resonance (figures 5 and S4).

$$GaL + OH^- \rightleftarrows Ga(L)OH \qquad (8)$$

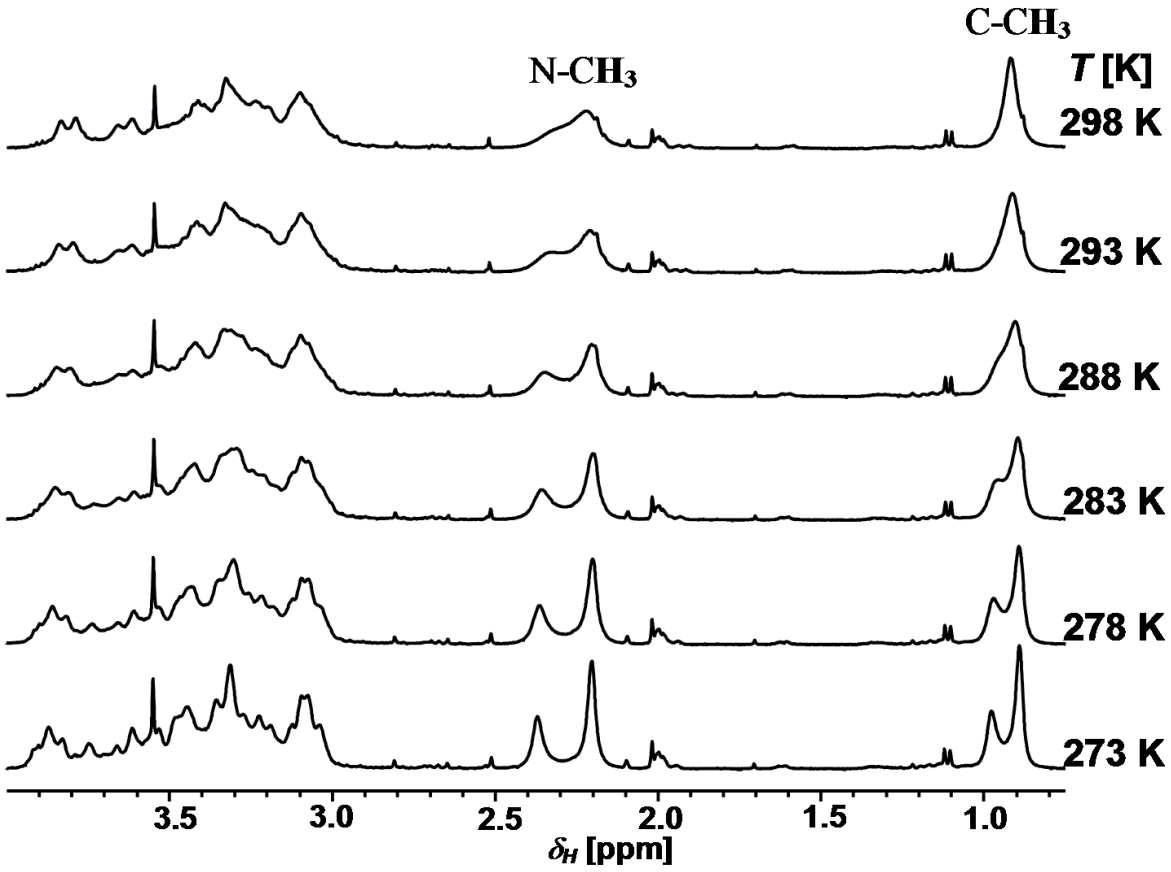

Figure 5: VT-400 MHz ^{1}H-NMR study of Ga(DATA^m)-Ga(DATA^m)OH system ([GaL]=15 mM, D_2O, pD=6.8 (pD=pH + 0.41))

Since at pH=6.4 the Ga(DATA^m) and Ga(DATA^{5m})$^-$ complexes are present in the form of GaL and Ga(L)OH species (the ratio of the GaL and Ga(L)OH species is about 2 to 3), this behaviour can be attributed to a chemical exchange process between GaL and Ga(L)OH species via the replacement of one ring carboxylate-O donor atom with an OH^- ion in the inner sphere of the Ga(DATA^m) and Ga(DATA^{5m}) complexes (eq. (8)). Interestingly, the signal of the C**H$_3$**-C protons in the ^{1}H-NMR spectra of Ga(AAZTA)$^-$ obtained at 273 K and pH=4.6 (the ratio of GaL and Ga(L)OH species is about 1 to 1) has not been split to two singlets indicating the differing structures and exchange processes of Ga(AAZTA)$^-$ and [Ga(AAZTA)OH]$^{2-}$ complexes (figure S5). A complete line-shape analysis allows the extraction of kinetic parameters for the exchange process (figures S6 and S7). The proton NMR spectral data were measured at eight different temperatures, in the range 273-298 K (figures 5 and S4). The limiting value of the transverse relaxation time (T_2) has been calculated from the line width of the singlet at 3.55 ppm (figure 5) (T_2=0.07 s), because of its temperature independence below 298 K. The chemical shift differences ($\Delta\delta_H$, between the C**H$_3$**-C and C**H$_3$**-N protons of Ga(DATA^m) and [Ga(DATA^m)OH]$^-$ complexes are 35 and 67 Hz, whereas the $\Delta\delta$ value for the C**H$_3$**-N protons in Ga(DATA^{5m})$^-$ and [Ga(DATA^{5m})OH]$^{2-}$ complexes is 66 Hz.

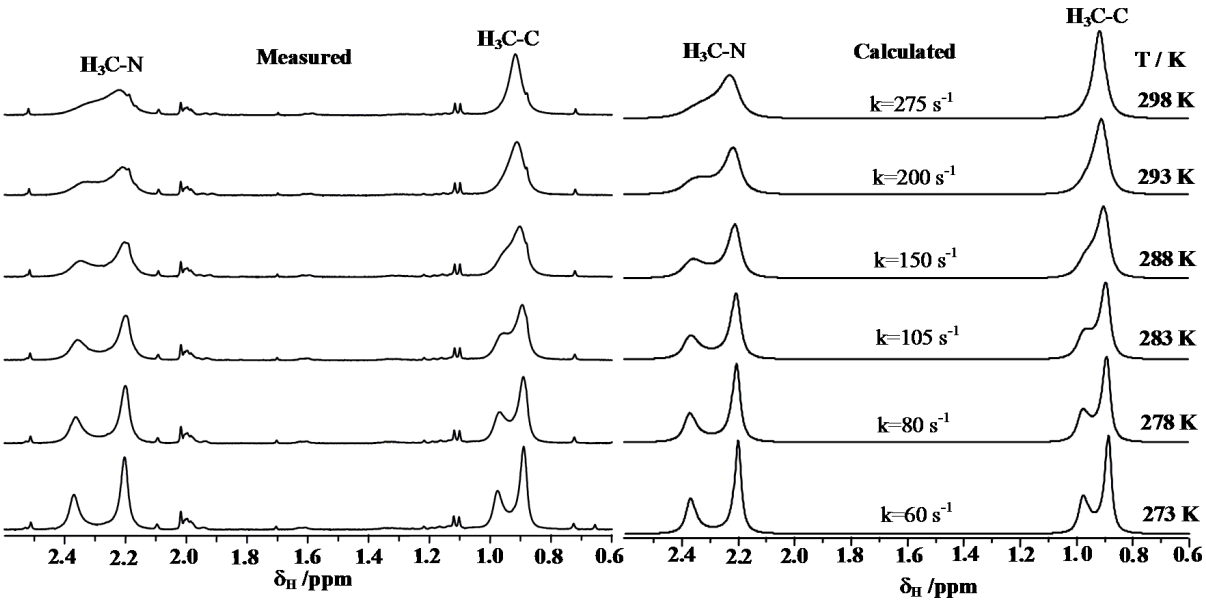

Figure 6. Experimental and calculated ^{1}H-NMR spectra (400 MHz) of the N-CH_3 and C-CH_3 protons in Ga(DATA^{m}) – Ga(DATA^{m})OH systems as a function of temperature.

The activation parameters were assessed from the temperature dependence of the calculated rate constants (k_{ex}=1/τ) using the *Eyring* equation (figure S8). The activation parameters for the exchange reaction between GaL and Ga(L)OH species of Ga(DATA^{m}) and Ga(DATA^{5m}) complexes are listed in table 4. The band shape analysis provides very similar free energy ($\Delta G^{\ddagger}_{298}$), activation enthalpy ($\Delta H^{\ddagger}$) and activation entropy ($\Delta S^{\ddagger}$) values for the exchange reactions between GaL and Ga(L)OH species for the Ga(DATA^{m}) and Ga(DATA^{5m}) complexes. In fact, the same exchange processes for Ga(DATA^{m}) and Ga(DATA^{5m}) complexes take place with similar activation parameters, which is clearly indicated by the similar exchange rates (k_{ex}^{298}) (table 4), and the similar slopes and the intercepts obtained from the *Eyring* plots (figure S8). The formation of Ga(L)OH species from both Ga(DATA^{m}) and Ga(DATA^{5m}) complexes requires the decoordination of a ring carboxylate O donor atom and the coordination of OH^{-} ion. It results in the weakening of the bonds formed between the Ga^{3+} ion and the nitrogen donor atoms of the ring. Since the exchange between GaL and Ga(L)OH species for Ga(AAZTA)$^{-}$ takes place more rapidly even at low temperature, (figure S5) it can be assumed that the formation of Ga(L)OH species occurs by the (relatively slow) structural rearrangement of the Ga(DATA^{m}) and Ga(DATA^{5m}) complexes, as characterized by relatively high $\Delta G^{\ddagger}_{298}$ values.

Table 4: Rate constant and activation parameters for the exchange reaction between GaL and Ga(L)OH species of Ga(DATA^{m}) and Ga(DATA^{5m}) complexes obtained from the line-shape analysis of the ^{1}H-NMR spectra.

	Ga(DATA^{m})	Ga(DATA^{5m})
$\Delta H^{\ddagger}$ /kJ·mol^{-1}	39 (1)	32.7 (8)
$\Delta S^{\ddagger}$ /J·mol^{-1}K^{-1}	-67 (4)	-89 (3)
$\Delta G^{\ddagger}_{298}$ /kJ·mol^{-1}	59.0 (1)	59.3 (1)
k^{298} /s^{-1}	280	250

Dissociation kinetics

In order to apply the Ga(DATA^{m}) and Ga(DATA^{5m}) complexes as ^{68}Ga based radiodiagnostics *in vivo*, their kinetic stability with respect to metal dissociation must be evaluated. Nowadays, it is generally accepted that the kinetic inertness of metal complexes *in vivo* is more important than the thermodynamic stability, especially for shorter-lived radioisotope complexes. The inertness can avoid a rapid loss of the metal ion and the loss of radioactivity from the targeted agent. The dissociation rate of the metal ion from a Ga^{III} complex is typically measured in strong acidic ([H^{+}]>1.0 M) and/or strong basic conditions ([OH^{-}]>0.1 M) [12,23]. These conditions differ considerably from the physiological ones and limiting the value of the data to predict the behaviour of metal complexes in body fluids for *in vivo* experiments. The intravenously administered Ga^{III} complex may interact with the endogenous ions (Cu^{2+}, Zn^{2+} and Ca^{2+}) or serum proteins such as transferrin that results in the release of the Ga^{3+} ion. In order to assess the kinetic inertness, the transmetallation and trans-chelation reactions of Ga(DATA^{m}) and Ga(DATA^{5m}) complexes with Cu^{2+} and transferrin have been studied by spectrophotometry.

Transmetallation reactions:

The transmetallation reactions occurring between the Ga^{III}-chelates and Cu^{2+} ions have been studied by spectrophotometry examining the absorption band of the resulting Cu^{II} complexes in the presence of excess citrate, to prevent the hydrolysis of Ga^{3+} and Cu^{2+} ions over the pH range 6.0-9.0. Under such conditions Cu^{2+} is predominantly present as Cu(Cit)H$_{-1}$ species, whereas the Ga^{3+} ion forms Ga(Cit)H$_{-1}$- and Ga(Cit)$_2$ complexes [31]. The absorption spectra of the Ga(DATA^{m})$^{-}$- and Cu^{2+}-citrate as well as the Ga(DATA^{5m})$^{-}$ and Cu^{2+} citrate reacting systems are presented in figures 6 and S9. The transmetallation reactions can be described as follows:

$$GaL + Cu^{2+} \rightleftarrows CuL + Ga^{3+} \quad (9)$$

The rates of the transmetallation reactions have been studied in the presence of excess of GaL complexes ([GaL]$_{tot}$/[Cu^{2+}]$_{tot}$=10 and 20), when a pseudo-first order kinetic model can be applied and the rates of reaction can be expressed by eq. (10):

$$-\frac{d[GaL]_t}{dt} = \frac{d[CuL]_t}{dt} = k_d[GaL]_t \quad (10)$$

where k_d is a pseudo-first-order rate constant, $[GaL]_t$ and $[CuL]_t$ are the total concentration of complexes (e.g. GaL, Ga(L)OH, CuL) at the time *t*, respectively. During the course of transmetallation reactions, the concentration of Cu(DATA^m) and Cu(DATA^{5m}) complexes increase, while that of Cu(Cit)H$_{-1}$ decreases.

By the use of 1.0 cm cells, the first-order rate constant, k_d can be calculated by eq. (11):

$$k_d = \frac{\Delta Abs}{\Delta t} \cdot \frac{1}{\varepsilon_{CuL} - \varepsilon_{Cu(Cit)H_{-1}}} \cdot \frac{1}{[GaL]_t} \qquad (11)$$

In eq. (11) $\Delta Abs/\Delta t$ values (the increase of the absorbance during the time Δt) are calculated from the slope of the kinetic curves. $\varepsilon_{Cu(Cit)H-1}$ and ε_{CuL} are the molar absorptivities of the Cu(Cit)H$_{-1}$ (921 M^{-1}cm^{-1}), Cu(DATA^m) (1406 M^{-1}cm^{-1}) and Cu(DATA^{5m}) (2146 M^{-1}cm^{-1}) complexes at 300 nm (the absorption of Ga^{3+} containing species at 300 nm can be neglected). The pseudo-first-order rate constants obtained for the reactions of Ga(DATA^m) and Ga(DATA^{5m}) with Cu^{2+} at different pH-values in the presence of citrate are shown in figure 7.

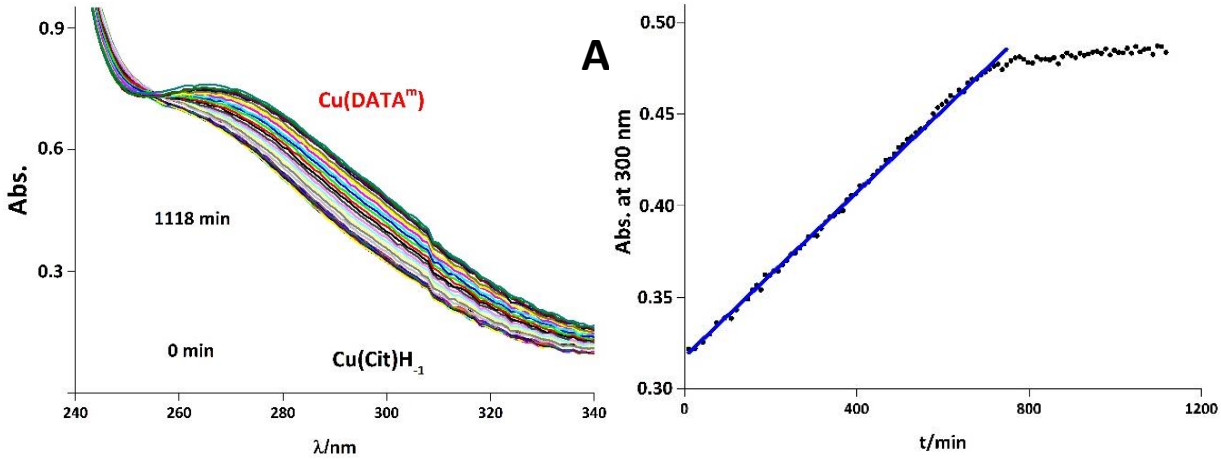

Figure 7: Absorption spectra (A) and absorbance values measured at 300 nm (B) for the Ga(DATA^m) – Cu^{2+} reacting system in the presence of citrate. The blue line represents the slope of the kinetic curve ($\Delta Abs/\Delta t$) used for the calculation of k_d values. ([GaL]=2.0 mM, [Cu^{2+}]=0.2 mM, [Cit]=2.0 mM, [MES]=0.01 M, pH=6.0, 0.15 M NaCl, 298 K, l=1 cm)

The k_d values presented in figure 7 are independent of the concentration of Cu^{2+} and Cu(Cit)H$_{-1}$, indicating that the rate determining step of the exchange reactions is the dissociation of the Ga^{III} complexes. Since the rate data have been obtained in the pH range 6-8.5, and according to the species distribution plots (figures 4 and S3) at pH=6 approximately 40 % of the Ga^{3+} is present in the form of Ga(L)OH and with increasing pH the concentration of these species increases and at pH=7.5 it is about 90 %, it can be assumed that the dissociable complex is the Ga(L)OH. (In the ternary Ga(L)OH complexes the DATA^m and DATA^{5m} ligands are coordinated by 5 donor atoms only and the electrostatic repulsion between the donor atoms and the OH^- ion is also stronger than in the GaL parent complexes. Therefore, the spontaneous dissociation of the Ga(L)OH species is more probable. Since the k_d values (see

figure 7) are directly proportional to the OH^- concentration and the straight line shows a non-zero intercept, we assume that the dissociation of Ga(L)OH complexes may occur spontaneously and with the assistance of OH^- ions, as indicated by equations (12) and (13).

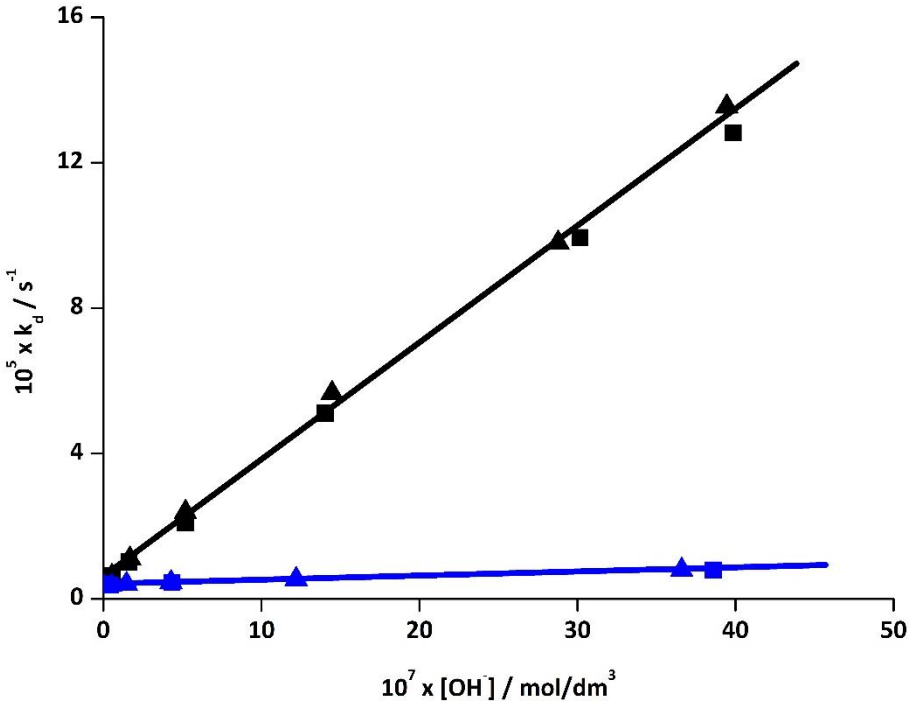

Figure 8: k_d values vs. $[OH^-]$ for the reaction of Ga(DATA^m) and Ga(DATA^{5m}) with Cu^{2+}. ([Ga(DATA^m)]=[Ga(DATA^{5m})]=2.0 mM, $[Cu^{2+}]$=0.1 (■, ■) and 0.2 mM (▲, ▲) [Cit]=2.0 mM, [MES]=[HEPES]=0.01 M, 0.15 M NaCl, 25°C)

$$[Ga(L)OH] + OH^- \xrightarrow{k_{OH^2}} Ga^{3+} + H_xL + 2\ OH^- \qquad (13)$$

The rate determining dissociation of complexes is followed by the rapid reaction of free ligands with the Cu^{2+} ions. By taking into account the two pathways, the rate of the dissociation of Ga(DATA^m) and Ga(DATA^{5m}) can be expressed by eq. (14).

$$-\frac{d[GaL]_t}{dt} = k_{OH}\,[Ga(L)OH] + k_{OH^2}\,[Ga(L)OH][OH^-] \qquad (14)$$

Considering the total concentration of the complex ($[GaL]_{tot}$= [GaL]+[Ga(L)OH]) and the protonation constant of Ga(L)OH species (K_{GaLH-1}, eq. (4)), the pseudo-first-order rate constants (k_d, (eq. 10)) can be expressed as follows:

$$k_d = \frac{(k_{OH}\,[OH^-] + k_{OH^2}\,[OH^-]^2)\,(K_w K_{GaLH-1})^{-1}}{1+[OH^-]\,(K_w K_{GaLH-1})^{-1}} \qquad (15)$$

where K_W is the ionic product of water (pK_w=13.85, 0.15 M NaCl, 25°C), whereas k_{OH} and k_{OH}^2 rate constants characterizing the spontaneous and OH^- assisted dissociation of Ga(DATA^m)OH and Ga(DATA^{5m})OH, respectively. The rate and equilibrium constants characterizing the transmetallation reaction of Ga(DATA^m) and Ga(DATA^{5m}) were calculated by fitting the k_d values presented in figure 7 to the eq. (15) and the values obtained are shown and compared with those of Ga(AAZTA)$^-$ in table 5. The "deprotonation" constants (logK_{GaLH-1}) obtained by pH-potentiometry (table 3) and from kinetic data are in good agreement. The k_{OH} and the k_{OH}^2 rate constants characterizing the spontaneous and OH^--assisted dissociation of Ga(DATA^m)OH are somewhat higher than the corresponding rate constants of Ga(AAZTA)OH. Interestingly, the k_{OH}^2 rate constant characterizing the OH^--assisted dissociation of Ga(DATA^{5m})OH is about 8 times lower than the corresponding rate constant of Ga(AAZTA)OH. The spontaneous dissociation of Ga(DATA^m)OH, Ga(DATA^{5m})OH and Ga(AAZTA)OH likely proceeds through the intramolecular rearrangement of the Ga^{III}-complexes that results in a cascade-like de-coordination of each donor atom, with the consequent release of the Ga^{3+} ion. The more rapid spontaneous dissociation of Ga(DATA^m)OH and Ga(DATA^{5m})OH can be interpreted in terms of the distorted coordination around the Ga^{3+} ion, that causes the faster intramolecular rearrangement of the Ga(L)OH species. With the use of the rate and equilibrium constants presented in table 5, the half lifes ($t_{1/2}$=ln2/k_d) of the dissociation reactions of Ga(DATA^m) and Ga(DATA^{5m}) at pH=7.4 have been calculated and compared with that of Ga(AAZTA). The $t_{1/2}$ values of Ga(DATA^m), Ga(DATA^{5m}) and Ga(AAZTA)$^-$ are 11, 44 and 21 h, respectively, consistent with the higher kinetic inertness of Ga(DATA^{5m}) due to the slower OH^--assisted dissociation of the [Ga(DATA^{5m})OH] species.

Table 5: Rate and equilibrium constants and half lifes ($t_{1/2}$=ln2/k_d) for the transmetallation reactions of Ga(DATA^m), Ga(DATA^{5m}) and Ga(AAZTA) complexes (0.15 M NaCl, 25 °C); a: Ionic product of water determined by pH-potentiometry (0.15 M NaCl, 25 °C)

	Ga(DATA^m)	**Ga(DATA^{5m})**	**Ga(AAZTA) [31]**
k_{OH}/s^{-1}	$(8.0 \pm 0.2)\cdot10^{-6}$	$(4.2 \pm 0.1)\cdot10^{-6}$	$3.0\cdot10^{-6}$
k_{OH^2}/M^{-1}s^{-1}	31 ± 1	1.2 ± 0.1	10
K_{GaLH-1}	$(1.6 \pm 0.1)\cdot10^{6}$	$(1.7 \pm 0.2)\cdot10^{6}$	$1.4\cdot10^{9}$
pK_w [a]		13.85	
logK_{GaLH-1}	6.20 (2)	6.25 (4)	4.72
k_d / s^{-1} (pH=7.4)	$1.7\cdot10^{-5}$	$4.3\cdot10^{-6}$	$9.2\cdot10^{-6}$
$t_{1/2}$ / h (pH=7.4)	11	44	21

Exchange reactions with transferrin:

Because of the relatively high concentration of transferrin in human plasma [47,48] and the strong affinity of Ga^{3+} to transferrin (Ga^{3+}-transferrin: $\log K_{GaTf}$=18.9, $\log K_{Ga2Tf}$=17.7) [49] this protein may compete with $DATA^{m}$ and $DATA^{5m}$ for the Ga^{3+} ion leading to the dissociation of $Ga(DATA^{m})$ and $Ga(DATA^{5m})$. In order to determine the extent of trans-chelation between $Ga(DATA^{m})$, $Ga(DATA^{5m})$ and transferrin, the ligand exchange reactions between Ga^{III}-complexes and human serum transferrin (sTr) were studied by spectrophotometry at the absorption band of the Ga^{3+}-sTf complex in the 240-250 nm range (figures 8 and S10). The absorbance values of the $Ga(DATA^{m})$-sTf and $Ga(DATA^{5m})$-sTf reacting systems obtained at [GaL]=0.2 and 0.3 mM are shown in figures S11 and S12. The ligand exchange reaction between $Ga(DATA^{m})$, $Ga(DATA^{5m})$ and human sTf is expressed by eq. (16):

$$Ga(L) + sTf \rightleftarrows Ga(sTf) + L \qquad (16)$$

The rates of the ligand exchange reaction were studied in the presence of high excess of $Ga(DATA^{m})$ and $Ga(DATA^{5m})$ ([GaL]=0.2 and 0.3 mM, [sTf]=10 μM). Under such conditions, the ligand exchange reaction can be treated as a pseudo-first-order process and the rate of the reaction can be expressed by equation (10). By taking into account the molar absorptivity of Ga(sTf) (ε_{246}=13800 $cm^{-1}M^{-1}$) [31], the rate constants (k_d) were calculated from the slope of the kinetic curves ($\Delta Abs/\Delta t$, figures S11 and S12) with equation (11) (the middle term in equation (11) has been replaced by $1/\varepsilon_{Ga(sTf)}$).

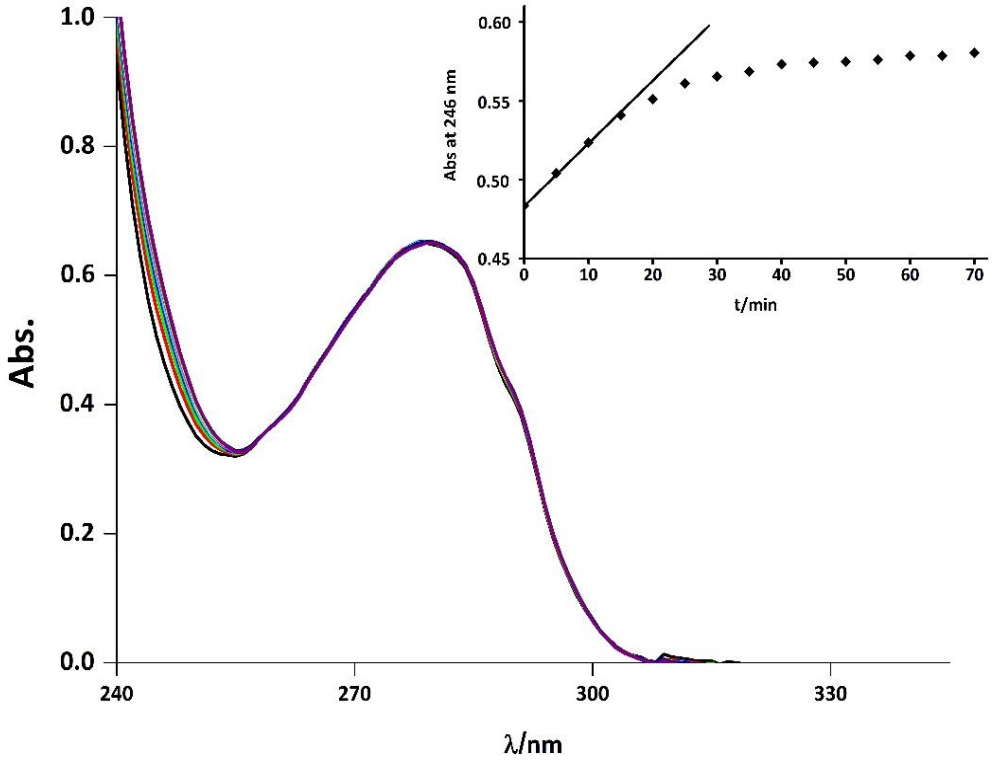

Figure 9: Absorption spectra of the $Ga(DATA^{m})$-transferrin system. Inserted figure shows the absorbance values of the reacting system at 246 nm as a function of time ([GaL]=0.2 mM, [Trf]=10 μM, [$NaHCO_3$]=25 mM, pH=7.4, 0.15 M NaCl, 25 °C)

The slope of the kinetic curves were considered up to 30 % conversion, in order to be sure of the Ga(sTf)-complex formation. The rate constant (k_d) and half life ($t_{1/2}=\ln 2/k_d$) values obtained for the trans-chelation reactions are shown and compared with that of Ga(AAZTA) in table 6.

Table 6: Rate constants (k_d) and half lifes ($t_{1/2}=\ln 2/k_d$) characterizing the trans-chelation reactions of Ga(DATA^m), Ga(DATA^{5m}) and Ga(AAZTA) complexes with transferrin (0.15 M NaCl, 25°C, pH=7.4)

	Ga(DATA^m)	**Ga(DATA^{5m})**	**Ga(AAZTA)[17]**
k_d **/ s^{-1}**	$(21\pm0.1)\times10^{-6}$	$(4.2\pm0.2)\times10^{-6}$	8.0×10^{-6}
$t_{½}$ **/ h**	9.4	46	24

The k_d rate constants obtained for the ligand exchange reaction of Ga(DATA^m) and Ga(DATA^{5m}) with sTf (table 6) and the metal exchange reactions of Ga(DATA^m) and Ga(DATA^{5m}) with Cu^{2+} in the presence of citrate (table 5) are essentially equal. These findings suggest that human transferrin has no effect on the rate of dissociation, which practically takes place through the spontaneous and hydroxide assisted dissociation of Ga(L)OH species followed by the fast reaction between the released Ga^{3+} ion and human sTf. The dissociation half life values of Ga(DATA^m)OH calculated from the transmetallation studies ($t_{1/2}$=11 h) and from the ligand exchange reactions ($t_{1/2}$=9.4 h) indicates that the kinetic inertness of Ga(DATA^m)OH is lower than that of Ga(AAZTA)OH. However, the dissociation half-life of Ga(DATA^{5m})OH is about four and two times higher than that of Ga(DATA^m)OH and Ga(AAZTA)OH, respectively. On the basis of these results ligands based on Ga(DATA^{5m}) represent good candidates for the development of the Ga^{3+}-based radiodiagnostics, in accord with the excellent PET images obtained in recent ^{68}Ga radiolabelling experiments on peptide conjugates [40,41].

CONCLUSION

The complexation properties of the AAZTA derivative hexadentate DATA^{m} and DATA^{5m} ligands have been studied by by pH-potentiometry, spectrophotometry and ^{1}H- and ^{71}Ga-NMR spectroscopy. The complex forming ability of the new derivatives with Ga^{3+} and Zn^{2+} is higher than that of heptadentate AAZTA, while the stabilities of Ca^{II}-, Mn^{II}- and Cu^{II}-(AAZTA) complexes are higher than those of the DATA^{m} and DATA^{5m} ligands. Owing to the strong affinity of OH^{-} ions to Ga^{3+}, at physiological pH the monohydroxo Ga(L)OH-complexes predominate.

The rates of exchange reaction between the Ga(L) and Ga(L)OH complexes were studied by ^{1}H-NMR spectroscopy in the temperature range 273-293 K. The transmetallation reactions between the Ga(DATA^{m}) and Ga(DATA^{5m}) complexes and Cu^{2+} citrate and the ligand exchange reactions between the Ga^{III}-complexes and the serum protein transferrin in the pH range of 6-8.5 occur through the same mechanism. The metal and ligand exchange reactions take place through the spontaneous and OH^{-}-assisted dissociation of the Ga(L)OH complexes. The half lifes of the dissociation of Ga(DATA^{m}), Ga(DATA^{5m}) and Ga(AAZTA) are 11 h, 44 h and 24 h, respectively. Based on the equilibrium and kinetic properties the ^{68}Ga(DATA^{5m}) complex and its derivatives constitute a promising family of candidates as radiopharmaceutical agents for the use in PET diagnostics.

ACKNOWLEDGEMENT

The research was supported by the EU and co-financed by the European Regional Development Fund under the project GINOP-2.3.2.-15-2016-00008. E.F., I.T. and E.B. gratefully acknowledge the financial support for this research by the National Science Fund, Hungary (K109029, K120224).

SUPPORTING INFORMATION

General

New compounds were characterized by ^{1}H, ^{13}C, ^{1}H-^{1}H-COSY, HSQC, HMBC, MS, and HRMS. ^{1}H (400 MHz) and ^{13}C NMR (100 MHz) spectra were obtained with with Bruker Avance III HD 400 (9.4 T) by the use of TMS as internal standard. Column chromatography was performed on silica gel (MERCK silica gel 60). Purification via HPLC was performed on a column from Phenomenex (Luna 10 u (C18) 100 Å (250x10.00 mm 10 micron)). As mobile phase a system of water (0.1 %TFA; **A**) and acetonitrile (0.1 % TFA; **B**) was used.

Materials

$Ga(NO_3)_3$ was prepared by dissolving Ga_2O_3 (99.9%, Fluka) in 6M HNO_3 and evaporating of the excess acid. The solid $Ga(NO_3)_3$ was dissolved in 0.1 M HNO_3 solution. The concentration of the $Ga(NO_3)_3$ solution was determined by using the standardized Na_2H_2EDTA in excess. The excess of the Na_2H_2EDTA was measured with standardized $ZnCl_2$ solution and xylenol orange as indicator. The concentration $CaCl_2$ (Sigma), $MnCl_2$ (Sigma), $ZnCl_2$ (Sigma) and $CuCl_2$ (Sigma) solutions were determined by complexometric titration with standardized Na_2H_2EDTA and xylenol orange ($ZnCl_2$), murexide ($CuCl_2$) *Patton & Reeder* ($CaCl_2$) and eriochrome black T ($MnCl_2$) as indicator. The H^+ concentration of the $Ga(NO_3)_3$ solution was determined by pH potentiometric titration in the presence of excess Na_2H_2EDTA. The concentration of H_3DATA^m, H_4DATA^{5m} and H_4AAZTA (provided by Prof. Giovanni Battista Giovenzana, Dipartimento di Scienze del Farmaco, Università del Piemonte Orientale, Novara, Italy) stock solutions was determined by pH-potentiometric titrations in the presence and absence of a 40-fold excess of Ca^{2+}. The citrate solution was prepared from H_3Citrate (Sigma) and its concentration was determined by pH-potentiometry. The pH-potentiometric titrations were made with standardized 0.2 M NaOH.

Synthesis of $DATA^m$:

*N,N'-Dibenzyl-N,N'-di-(tert-butylacetate)-ethylendiamine (**1**)*:

N,N´-dibenzylethylenediamine (3.00 g; 12.48 mmol) and Na_2CO_3 (5.12 g; 48.67 mmol) were stirred at room temperature in dry acetonitrile (50 mL) for 30 min. *Tert*-butylbromoacetate (4.64 g; 23.72 mmol), dissolved in dry acetonitrile (10 mL), was added at room temperature over period of 30 min. After completion the suspension was heated over night at 90 °C, filtrated and the filtrate was concentrated under vacuum. After purification via column chromatography (H/EA; 6:1; R_f=0.25) the product was obtained as colourless solid (5.56 g; 11.9 mmol; 95 %).

^{1}H-NMR ($CDCl_3$, 400 MHz, δ [ppm]): 7.34-7.21 (m, 10 H); 3.78 (s, 4 H); 3.26 (s, 4H); 2.82 (s, 4 H); 1.44 (s, 18 H); ^{13}C-NMR ($CDCl_3$, 100 MHz, δ [ppm]): 171.03 (s); 139,18 (s); 129.05 (s); 128.30 (s); 127.10 (s); 80.86 (s); 58.39 (s); 55.27 (s); 51.73 (s); 28.24 (s)

MS (ESI^+): 469.28, 470.31, 471.33 ($M+H^+$)

*1,4-Di(tert-butylacetate)-6-methyl-6-nitroperhydro-1,4-diazepane (**2**)*:

1 (0.29 g; 0.92 mmol) was dissolved in 5 mL abs. ethanol and formic acid (69 µL; 1.84 mmol). To this solution Pd/C (0.06 g; 16 wt%) was added and the solution was saturated and kept overnight with hydrogen. After completion the Pd/C was filtrated over celite, the filtrate was concentrated and dried. The crude product 2a (0.29 g; 0.89 mmol; 96 %) was used without further purification. Nitroethane (89 µL; 1.25 mmol) and 2a (0.29 g; 0.89 mmol) was dissolved in dry methanol (5 mL) and heated overnight. The solution was concentrated under vacuum and purified via column chromatography (H/EA, 5:1; R_f=0.24). The product was obtained as yellowish oil (0.18 g; 0.46mmol; 52 %).

^{1}H-NMR ($CDCl_3$, 400 MHz, δ [ppm]): 3.66 (d, J=14.9 Hz, 2 H); 3.49 (d, J=17.5 Hz, 2 H); 3.38 (d, J=17.5 Hz, 2 H); 3.13 (d, J=14.9 Hz, 2 H); 2.89 (m, 4 H); 1.46 (s, 21 H); ^{13}C-NMR ($CDCl_3$, 100 MHz, δ [ppm]): 170.83 (s); 91.80 (s); 81.42 (s); 77.48 (s); 77.16 (s); 76.84 (s); 62.38 (s); 60.85 (s); 56.52 (s); 28.36 (s); 24.07 (s)

MS (ESI^+): 388.14, 389.18, 390.20 ($M+H^+$)

*1,4-Di(tert-butylacetate)-6-methyl-6-(amino-tert-butylacetate)-perhydro-1,4-diazepane (**3**)*:

2 (0.16 g; 0.41 mmol) was dissolved in abs. ethanol (2.5 mL), combined with RaneyNickel 2800® (0.1 g) (washed 4 times with ethanol) and the suspension was saturated with hydrogen and stirred at 40 °C for 6 h. After completion the RaneyNickel was filtrated over Celite/sand, the filtrate was concentrated and dried under vacuum. The product 3a (0.09 g; 0.28 mmol) was dissolved with diisopropylethylamine (49 µL; 0.28 mmol) in dry acetonitrile and stirred under nitrogen for 30 minutes at room temperature. *Tert*-butylbromoacetate (0.05 g; 0.25 mmol) was added dropwise to the solution and stirred at room temperature overnight. The solution was concentrated under vacuum and purified via column chromatorgraphy (H/EA, 2:1; R_f=0.39). The product **3** was obtained as yellow oil (0.06 g; 0.13 mmol; 45 %).

^{1}H-NMR ($CDCl_3$, 400 MHz, δ [ppm]): 3.30 (s, 2 H); 3.26 (s, 2 H); 2.79 (m, 4 H); 2.67 (m, 4 H); 1.45 (s, 9 H); 1.43 (s, 18 H) 0.92 (s, 3 H) ; ^{13}C-NMR ($CDCl_3$, 100 MHz, δ [ppm]): 171.94 (s); 80.95 (s); 64.72 (s); 61.95 (s); 57.29 (s); 56.02 (s); 45.08 (s); 28.34 (s); 28.26 (s); 22.76 (s)

MS (ESI^+): 472.31, 473.13, 474.35 ($M+H^+$).

*1,4-Di(tert-butylacetate)-6-methyl-6-(amino(methyl)-tert-butylacetate)-perhydro-1,4-diazepane (**4**)*:

3 (0.21 g, 0.46 mmol) was dissolved in acetonitrile (5 mL), formalin solution (379 µL, 4.56 mmol, 37 wt%) and acetic acid (77 µL, 1.35 mmol) and stirred for 30 min at room temperature. To this solution sodium borohydride (0.05 g, 1.35 mmol) was added portion wise and stirred for 1 h at room temperature. After completion the mixture was quenched with water (10 mL), extracted with chloroform and concentrated under vacuum. The residue was purified via column chromatography (H/EA, 1:1; R_f=0.12). The product **4** was obtained as yellowish oil (0.16 g, 0.32 mmol; 70 %).

^{1}H-NMR ($CDCl_3$, 400 MHz, δ [ppm]): 3.44 (s, 2 H); 3.27 (s, 4 H); 2.94 (d, 2 H, J=14.1 Hz); 2.82-2.67 (m, 4 H); 2.57 (d, 2 H, J=14.1 Hz); 2.32 (s, 3 H), 1.45 (s, 27 H); 1.08 (s, 3 H); ^{13}C-NMR ($CDCl_3$, 100 MHz, δ [ppm]): 172.00 (s); 171.03 (s); 80.97 (s); 80.58 (s); 63.41 (s); 62.45 (s); 61.02 (s); 59.06 (s); 54.42 (s); 37.47 (s); 28.36 (s); 28.28 (s); 23.79 (s)

MS (ESI^+): 486.30, 487.33, 488.37 ($M+H^+$)

*1,4-Di(acetate)-6-methyl-6-(amino(methyl)-acetate)-perhydro-1,4-diazepane (**5**)*:

4 (0.12 g; 0.25 mmol) was dissolved in dichlormethane (2 mL) and trifluoracetic acid (0.7 mL) and stirred for 19 h at room temperature. After completion of the reaction the solution was concentrated under vacuum. The residue was dissolved in acetonitrile (1 mL), ice cold diethylether was added and the product was precipitated as colourless solid (23.8 mg; 0.08 mmol; 30 %; t_R=7.0 min (0 % to 30 % **B** in 20 min)). ^{1}H-NMR ($CDCl_3$, 400 MHz, δ [ppm]): 3.45 (s, 2 H); 3.27 (s, 4 H); 2.94 (d, 2 H, J=14.1 Hz); 2.78 (m, 2 H); 2.57 (d, 2 H, J=14.1 Hz); 2.33 (s, 3 H), 1.45 (s, 27 H); 1.08 (s, 3 H); ^{13}C-NMR ($CDCl_3$, 100 MHz, δ [ppm]): 174.42 (s); 170.27 (s); 59.87 (s); 55.81 (s); 55.14 (s); 54.65 (s); 43.77 (s); 37.39 (s); 13.15 (s)

HR-MS (ESI^+): 340.1476, 341.1537, 342.1546 ($M+H^+$)

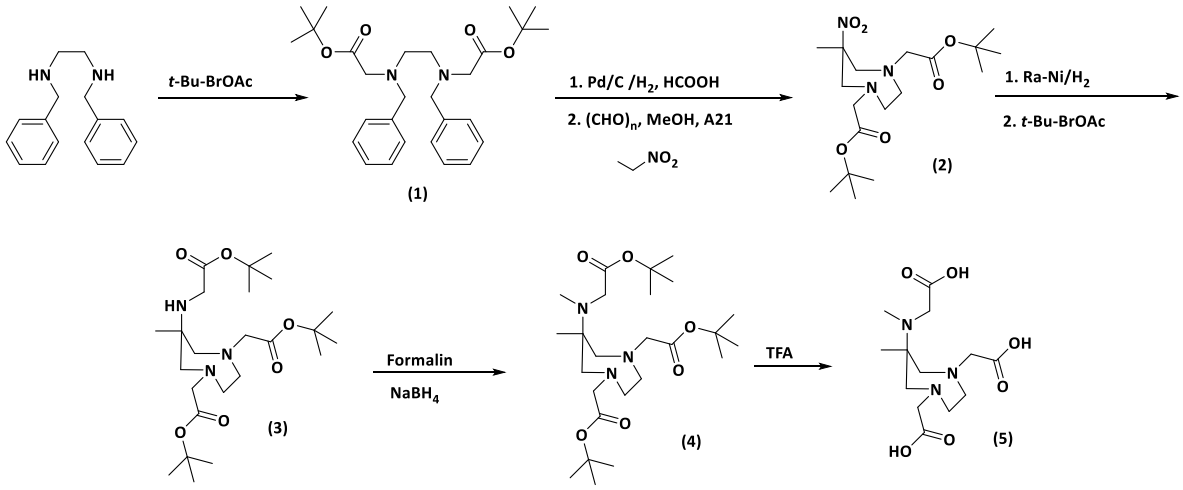

Synthesis of DATA^{5m}:

*N,N'-Dibenzyl-N,N'-di-(tert-butylacetate)-ethylendiamine (**1**)*:

N,N´-dibenzylethylenediamine (3.00 g; 12.48 mmol) and Na_2CO_3 (5.12 g; 48.67 mmol) were stirred at room temperature in dry acetonitrile (50 mL) for 30 min. *Tert*-butylbromoacetate (4.64 g; 23.72 mmol), dissolved in dry acetonitrile (10 mL), was added at room temperature over period of 30 min. After completion the suspension was heated over night at 90 °C, filtrated and the filtrate was concentrated under vacuum. After purification via column chromatography (H/EA; 6:1; R_f=0.25) the product was obtained as colourless solid (5.56 g; 11.87 mmol; 95 %).

^{1}H-NMR ($CDCl_3$, 400 MHz, δ [ppm]): 7.34-7.21 (m, 10 H); 3.78 (s, 4 H); 3.26 (s, 4H); 2.82 (s, 4 H); 1.44 (s, 18 H); ^{13}C-NMR ($CDCl_3$, 100 MHz, δ [ppm]): 171.03 (s); 139,18 (s); 129.05 (s); 128.30 (s); 127.10 (s); 80.86 (s); 58.39 (s); 55.27 (s); 51.73 (s); 28.24 (s)

MS (ESI$^+$): 469.28, 470.31, 471.33 (M+H$^+$)

*1,4-Di(tert-butylacetate)-6-methylpentonate-6-nitroperhydro-1,4-diazepane (**2**)*:

1 (3.89 g; 8.32 mmol) was dissolved in 20 mL abs. ethanol and formic acid (627.8 µL; 16.64 mmol). To this solution Pd/C (0.62 g; 16 wt%) was added and the solution was saturated and kept overnight with hydrogen. After completion the Pd/C was filtrated over celite, the filtrate was concentrated and dried. The crude product **2a** (2.29 g; 8.12 mmol; 98 %) was used without further purification.

A solution of 2-nitrocyclohexanone (1.16 g; 8.12 mmol) and amberylst A21 (2 mass-eq) in dry methanol (30 mL) was heated for 1 h. Then product **2a** (2.29 g; 8.12 mmol) and paraformaldehyde (0.88 g; 29.23 mmol) was added and the suspension was heated overnight under reflux. The suspension was filtrated, the filtrate was concentrated under vacuum and purified via column chromatography (H/EA, 2:1; R_f=0.43). The product **2** was obtained as yellowish oil (2.66 g; 5.50 mmol; 67 %).

^{1}H-NMR ($CDCl_3$, 400 MHz, δ [ppm]): 3.65 (s, 3 H); 3.60 (d, J=14.6 Hz, 2 H); 3.45 (d, J=17.3 Hz, 2 H); 3.30 (d, J=17.3 Hz, 2 H); 3.12 (d, J=14.6 Hz, 2 H); 2.84 (m, 4 H); 2.27 (t, 3 H); 1.83 (m, 2 H), 1.57 (m, 2 H); 1.46 (s, 18 H); 1.18 (m, 2 H); ^{13}C-NMR ($CDCl_3$, 100 MHz, δ [ppm]): 173.73 (s); 170.92 (s); 95.12 (s); 81.31 (s); 61.57 (s); 61.18 (s); 56.87 (s); 51.68 (s); 37.27 (s); 33.71 (s); 28.35 (s); 24.82 (s); 22.99 (s)

MS (ESI$^+$): 488.27, 489.29, 490.31 (M+H$^+$)

*1,4-Di(tert-butylacetate)-6-methylpentonate-6-amino-tert-butylacetate-perhydro-1,4-diazepane (**3**)*:

2 (1.59 g; 3.27 mmol) was dissolved in absolute ethanol (15 mL), combined with RaneyNickel 2800® (0.5 g) (washed 4 times with ethanol) and the suspension was saturated with hydrogen and stirred at 40 °C for 6 h. After completion the RaneyNickel was filtrated over Celite/sand, the filtrate was concentrated and dried under vacuum. The product **3a** (1.08 g; 2.36 mmol) was dissolved with diisopropylethylamine (419 µL; 2.36 mmol) in dry acetonitrile and stirred under nitrogen for 30 minutes at room temperature. *Tert*-butylbromoacetate (0.61 g; 3.12 mmol) was added dropwise to the solution

and stirred at room temperature overnight. The solution was concentrated under vacuum and purified via column chromatorgraphy (H/EA, 3:1; R_f=0.32). The product **3** was obtained as yellow oil (0.66 g; 1.17 mmol; 49 %).

^{1}H-NMR ($CDCl_3$, 400 MHz, δ [ppm]): 3.64 (s, 3 H); 3.28 (s, 4 H); 3.21 (s, 2 H); 2.77 (m, 4 H); 2.67 (m, 4 H); 2.30 (t, 3 H); 1.59(m, 2 H); 1.45 (s, 9 H); 1.44 (s, 18 H); 1.28 (m, 4 H); ^{13}C-NMR ($CDCl_3$, 100 MHz, δ [ppm]): 174.25 (s), 171.97 (s), 171.09 (s), 81.05 (s), 80.96 (s), 63.58 (s), 62.12 (s), 58.10 (s), 57.46 (s), 51.58 (s), 44.78 (s), 35.34 (s), 34.18 (s), 28.36 (s), 28.27 (s), 25.86 (s), 22.73 (s)

MS (ESI$^+$): 572.34, 573.38, 574.41 (M+H$^+$)

*1,4-Di(tert-butylacetate)-6-methylpentonate-6-(amino(methyl)-tert-butylacetate)-perhydro-1,4-diazepane (**4**)*:

3 (0,60 g; 1.05 mmol) was dissolved in acetonitrile (5 mL) and formaline solution (293 µL; 10.50 mmol) and acidified with acetic acid (180 µL; 3.15 mmol). The solution was stirred for 15 minutes and sodium borohydride (0.12 g; 3.15 mmol) was added portionwise. After completion the solution was quenched with water, extracted with chloroform (3 x 10 mL) and the organic fractions were dried over sodium sulfate, filtrated and concentrated under vaccum. The crude product was purified via column chromatography (H/EA, 1:1; R_f=0.20). The product **4** was obtained as yellowish oil (0.50 g; 0.86 mmol; 82 %).

^{1}H-NMR ($CDCl_3$, 400 MHz, δ [ppm]):3.64 (s, 3 H); 3.46 (s, 2 H); 3.25 (m, 4 H); 2.94 (d, 2 H); 2.84-2.65 (m, 6 H); 2.31 (t, 2 H); 1.57 (m, 4 H); 1.45 (s, 18 H); 1.44 (s, 9 H); 1.35 (s, 2 H); ^{13}C-NMR ($CDCl_3$, 100 MHz, δ [ppm]): 174.23 (s), 172.17 (s), 170.72 (s), 80.90 (s), 80.35 (s), 77.34 (s), 62.52 (s), 62.34 (s), 58.80 (s), 53.99 (s), 51.42 (s), 37.34 (s), 36.61 (s), 34.09 (s), 28.22 (s), 28.12 (s), 25.73 (s), 21.91 (s)

MS (ESI$^+$): 586.34, 587.39, 588.43 (M+H$^+$)

*1,4-Di(acetate)-6-pentanoic acid-6-(amino(methyl)-acetate)-perhydro-1,4-diazepane (**5**)*:

4 (0.43 g; 0.72 mmol) was dissolved in 1,4-dioxane (10 mL), treated with 1M LiOH solution (3.8 mL; 3.80 mmol) and heated at 40 °C for 6 h. After completion the solution was concentrated, the residue was dissolved in a mixture of acetonitrile (0.5 mL), methanol (0.5 mL) and water (0.5 mL). The solution was treated with ice cold diethylether and the colourless precipitate was filtrated and purified via HPLC. The product **5** was obtained as colourless solid (58.0 mg; 0.14 mmol; 20 %; t_R=10.6 min (0 % to 30 % **B** in 20 min)).

^{1}H-NMR (D_2O, 400 MHz, δ [ppm]): 3.15 (s, 2 H); 3.10 (s, 4 H); 2.87-2.83 (d, J=14.5 Hz, 2 H); 2.85-2.79 (m, 2 H); 2.71-2.68 (d, J=14.8 Hz, 2 H); 2.58-2.52 (m, 2 H); 2.17 (s, 3 H); 2.13 (t, 2 H); 1.48-1.41 (m, 2H); 1.31-1.16 (m, 4 H); ^{13}C-NMR (D_2O, 100 MHz, δ [ppm]): 182.53 (s); 180.32 (s); 66.68 (s); 64.94 (s); 62.24 (s); 56.19 (s); 38.75 (s); 36.58 (s); 31.53 (s); 28.61 (s); 25.29 (s); 24.04 (s); 15.24 (s)

MS (ESI$^+$): 404.2014, 405.2098, 406.2268 (M+H$^+$)

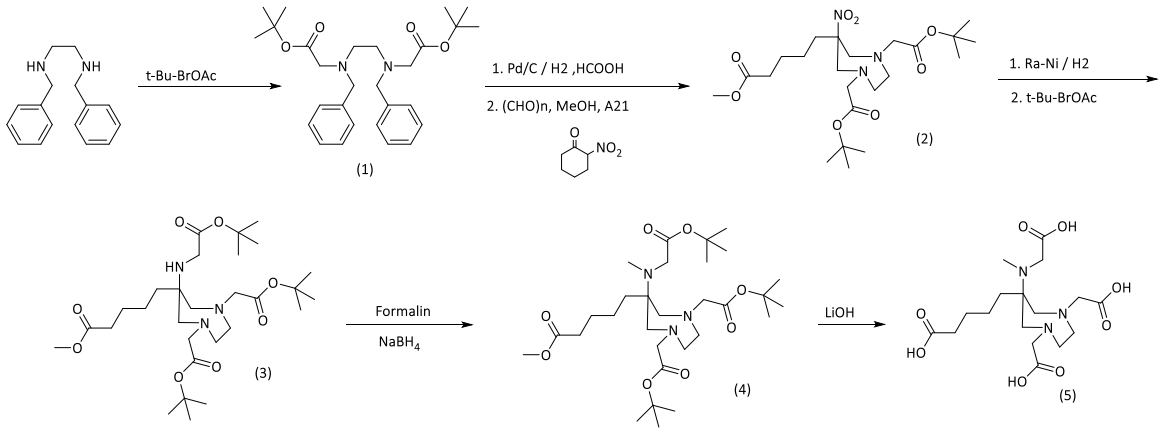

5. Equilibrium measurements

The protonation constants of $DATA^{m}$ and $DATA^{5m}$ ligands, the stability and protonation constants of Ca^{II}-, Mn^{II}- and Zn^{II}-complexes formed with $DATA^{m}$ and $DATA^{5m}$ ligands were determined by pH-potentiometric titration from acidic to basic pH range. The metal-to-ligand concentration ratios were 1:1 (the concentration of the ligands were generally 0.002 M). The stability and protonation constants of the "cold" Ga^{III}-complexes of $DATA^{m}$ and $DATA^{5m}$ were calculated from the pH-potentiometric titration of the Ga^{3+}-L systems obtained from basic to acidic pH range by studying the competition reaction between $DATA^{m}$ or $DATA^{5m}$ and OH^{-} for Ga^{3+} ([L]=[Ga^{3+}]=3×10^{-3} M). The protonation constants of $Cu(DATA^{m})^{-}$ and $Cu(DATA^{5m})^{2-}$ were determined by pH-potentiometric titrations of CuL complex in the pH range of 1.7-11.7

([CuL]=2×10^{-3} M). For pH measurements and pH-potentiometric titrations, a Metrohm 785 DMP Titrino titration workstation and a Metrohm-6.0233.100 combined electrode were used. The pH potentiometric titrations were performed at constant ionic strength (0.15 M NaCl) in 6 ml samples at 25 °C. The solutions were stirred, and N_2 was bubbled through them. The titrations were made in the pH range of 1.7-11.7. KH-phthalate (pH=4.005) and borax (pH=9.177) buffers were used to calibrate the pH meter. For the calculation of [H^{+}] from the measured pH values, the method proposed by Irving *et al.* was used. A 0.01 M HCl solution was titrated with the standardized NaOH solution in the presence of 0.15 M NaCl ionic strength. The differences between the measured (pH_{read}) and calculated pH (-log[H^{+}]) values were used to obtain the equilibrium H^{+} concentration from the pH values, measured in the titration experiments. The ionic product of water (pK_w) at 25 °C in 0.15 M NaCl was found to be 13.85 [50]. The stability constant of $Cu(DATA^{m})^{-}$ and $Cu(DATA^{5m})^{2-}$ was determined by spectrophotometry in the [H^{+}] range of 0.01-1.0 M ([L]=[Cu^{2+}]=2×10^{-3} M). Seven samples were prepared and the H^{+} concentration ([H^{+}]=0.010, 0.025, 0.050, 0.10, 0.32, 0.60 and 1.0 M) in the samples was adjusted with the addition of calculated amounts of 2.0 M HCl. The samples were kept at 25 °C for 7 days in order to

attain the equilibrium (the time needed to reach the equilibrium was determined by spectrophotometry). The absorbance values of the samples were measured at 11 wavelengths (575, 595, 615, 635, 655, 675, 695, 715, 735, 755 and 775 nm). The ionic strength of samples with $[H^+]$=0.32, 0.60 and 1.0 M was not constant (the ionic strength of samples with $[H^+]$=0.010, 0.025, 0.050, 0.10 M was $[H^+]+[Na^+]$=0.15 M). For the equilibrium calculations, the molar absorptivities of the Cu^{2+}, CuL, CuHL, CuH_2L and CuH_3L species were used. The molar absorptivities of Cu^{2+}, $Cu(DATA^m)^-$ and $Cu(DATA^{5m})^{2-}$ complexes were determined by recording the VIS spectra (λ=400-800 nm) of 1.0×10^{-4}, 2.0×10^{-4}, 3.0×10^{-4} and 4.0×10^{-4} M solutions in the pH range 1.7-7.0 (0.15 M NaCl, 25 °C). The pH was adjusted by stepwise addition of concentrated NaOH or HCl. The spectrophotometric measurements were made with the use of a Cary 1E spectrophotometer at 25 °C, using 1.0 cm cells. The protonation and stability constants were calculated with the PSEQUAD program [51].

6. NMR experiments

^{1}H- and ^{71}Ga-NMR measurement were performed with a Bruker DRX 400 (9.4 T) equipped with a Bruker VT-1000 thermocontroller and a BB inverse z gradient probe (5 mm). The formation and protonation/ deprotonation processes of the $Ga(DATA^m)$ and $Ga(DATA^{5m})^-$ were followed from basic to acidic pH range at 298 K in 0.15 M NaCl. For these experiments, 0.008 M solution of the $Ga(DATA^m)$ and $Ga(DATA^{5m})$ in H_2O was prepared (a capillary with D_2O was used for lock). The pH was adjusted with the addition of concentrated solution of NaOH and HCl. Because of the metal exchange between the $Ga(DATA^m)OH$ or $Ga(DATA^{5m})OH$ and $[Ga(OH)_4]^-$ was in the "slow exchange regime" on the actual NMR timescale, the calculation of the $\log\beta_{GaLH-1}$ value of $Ga(DATA^m)OH$ and $Ga(DATA^{5m})OH$ was performed by using the integrals of the ^{71}Ga-NMR signal of $[Ga(OH)_4]^-$-complex. The molar integral values of ^{71}Ga-NMR signal of $[Ga(OH)_4]^-$-complex were determined by recording the ^{71}Ga NMR spectra of 0.01, 0.015, 0.02 and 0.025 M solutions of $[Ga(OH)_4]^-$ complex (pH=12.5, 0.15 M NaCl, 25 °C). Calculation of the the $\log\beta_{GaLH-1}$ value was performed by the fitting of the integral-pH data pairs with the computer program *Micromath Scientist*, version 2.0 (Salt Lake City, UT, USA).

The structural behavior and the dynamic processes of the $Ga(DATA^m)$, $Ga(DATA^{5m})^-$- and $Ga(AAZTA)^-$-complexes were followed by ^{1}H-NMR spectroscopy. The $Ga(DATA^m)$-, $Ga(DATA^{5m})^-$- and $Ga(AAZTA)^-$-complexes were prepared in D_2O ($[Ga(DATA^m)]$=0.015 M, ($[Ga(DATA^{5m})]$=0.008 M and ($[Ga(AAZTA)]$=0.010 M). The pH of samples was adjusted by stepwise addition of NaOH and/or HCl. The chemical shifts are reported in ppm, with respect to DSS (4,4-dimethyl-4-silapentane-1-sulfonic acid) an external standard (0 ppm for the methyl protons of DSS).

7. Transmetallation kinetics

The rates of the exchange reactions taking place between $Ga(DATA^m)$ or $Ga(DATA^{5m})$ and Cu^{2+} in the presence of citrate were studied by spectrophotometry, following the formation of the $Cu(DATA^m)$ or

Cu(DATA^{5m}) complexes at 300 nm, with the use of 1.0 cm cells and a Cary 1E spectrophotometer. The concentration of Cu^{2+} was 0.1 and 0.2 mM, while that of Ga^{III}-complexes were 10 and 20 times higher, in order to ensure pseudo-first-order conditions. In order to prevent the hydrolysis of Ga^{3+} and Cu^{2+} ions, the transmetallation reactions were studied in the presence of citrate excess ($[Cit]_t$=2.0 mM). The exchange rates were studied in the pH range about 6.0-9.0. For keeping the pH values constant, MES (pH range 6.0-7.0), HEPES (pH range 7.0-8.5) and piperazine (pH range 8.5-9.0) buffers (0.01 M) were used. The temperature was maintained at 25 °C and the ionic strength of the solutions was kept constant (0.15 M NaCl). The pseudo-first-order rate constants (k_d) were calculated from the tangent to the absorbance vs. time curves ($\Delta Abs/\Delta t$) with eq. (12). For the calculations, the molar absorptivities of Cu(DATA^m), Cu(DATA^{5m}) and Cu(Cit)H_{-1} were used, which were determined at 300 nm by recording the spectra of 1.0×10^{-4}, 2.0×10^{-4}, 3.0×10^{-4} and 4.0×10^{-4} M solutions in the pH range 5-10 (0.15 M KCl, 25°C). The calculations were performed with the use of the computer program *Micromath Scientist*, version 2.0 (Salt Lake City, UT, USA).

8. Ligand-exchange kinetics with transferrin

The ligand exchange reaction between Ga(DATA^m) or Ga(DATA^{5m}) and human serum transferrin (Sigma, partially Fe^{3+} saturated) have been studied by spectrophotometry, following the formation of Ga(sTf) complex at 246 nm and pH=7.4 with the use of 1.0 cm cells and Cary 1E spectrophotometer. The concentration of the human serum transferrin solution was determined from the absorbance at 280 nm using the molar absorptivity ε_{280}=91200 $cm^{-1}M^{-1}$ [52]. In order to ensure the pseudo-first-order condition, the rate of the ligand exchange reactions were studied in the presence of high excess of Ga^{III}-complexes ([Ga(DATA^m)]= [Ga(DATA^{5m})]=0.2 and 0.3 mM, [sTf]=10 μM)). The temperature was maintained at 25 °C, the ionic strength and the hydrogen-carbonate concentration of the samples were kept constant; 0.15 M for NaCl and 0.025 M for $NaHCO_3$, respectively.

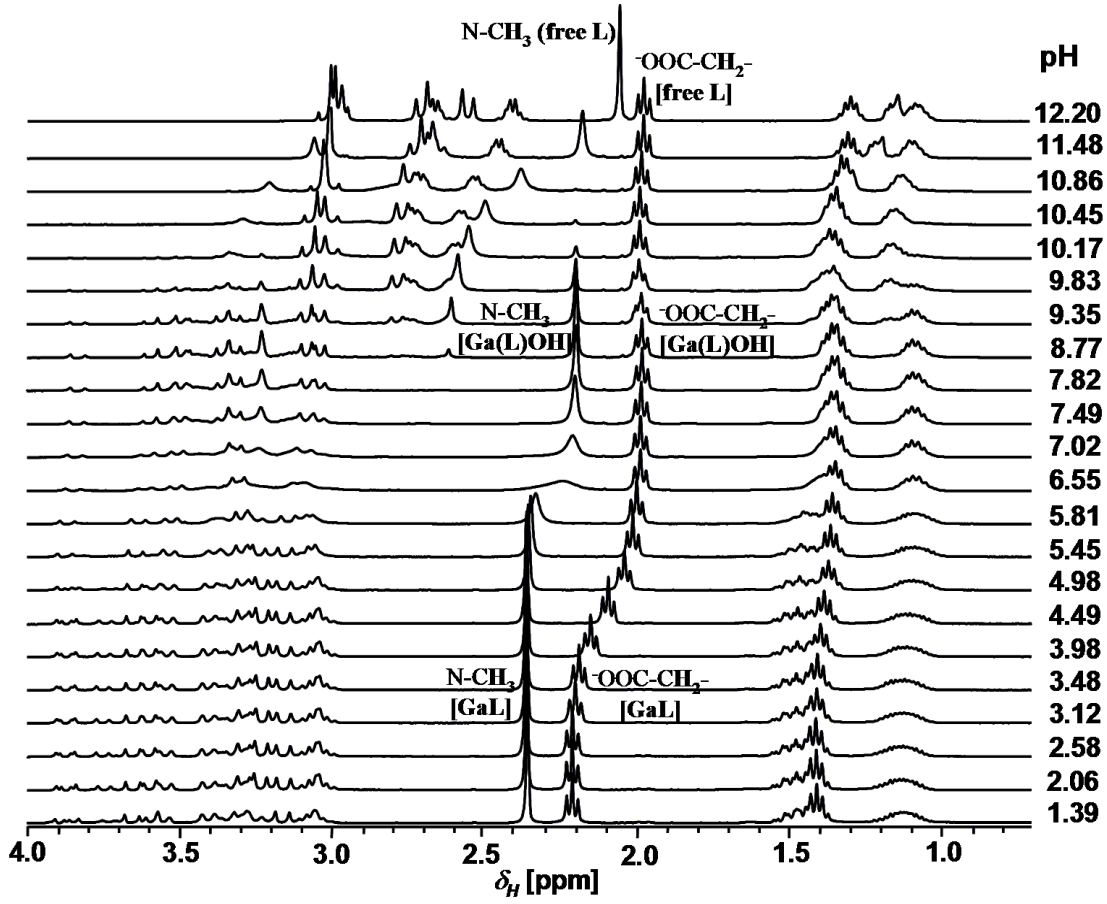

Figure S 1: 400 MHz ^{1}H-NMR spectra of the Ga^{3+}-$DATA^{5m}$ system ([Ga^{3+}]=7.93 mM, [$DATA5^{m}$]=7.95 mM, D_2O, 0.15 M NaCl, 298 K)

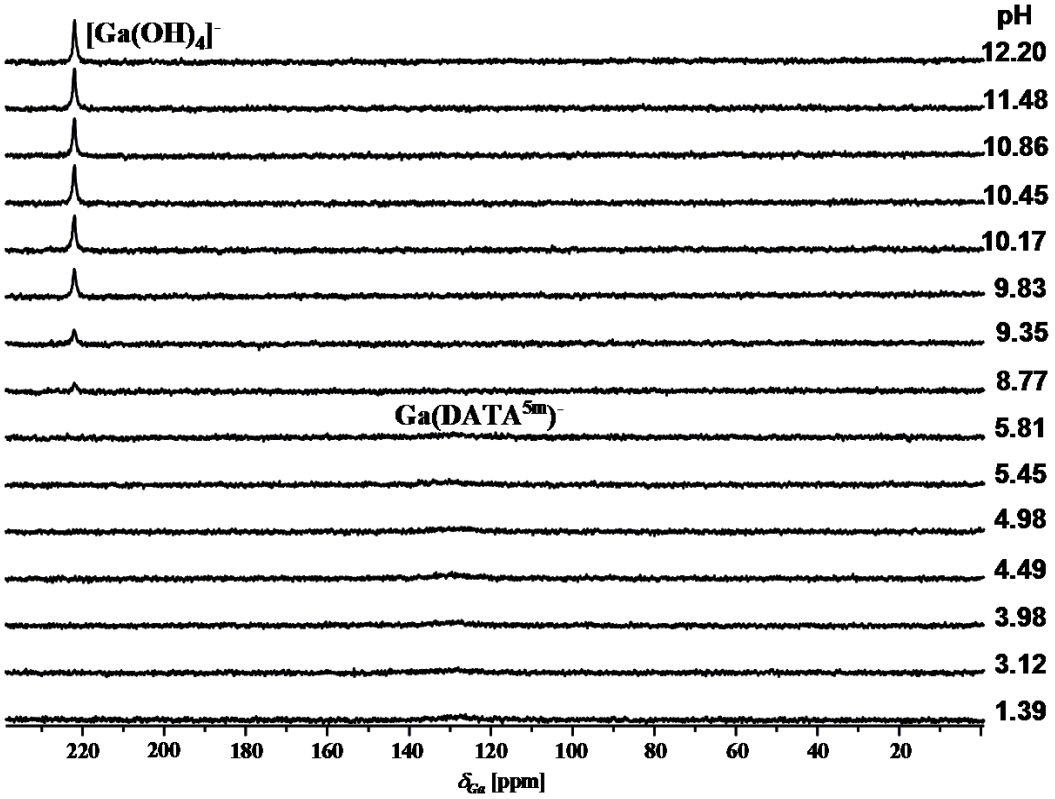

Figure S 2: 122 MHz ^{71}Ga-NMR spectra of the Ga^{3+}-$DATA^{5m}$ system ([Ga^{3+}]=7.93 mM, [$DATA^{5m}$]=7.95, H_2O, 0.15 M NaCl, 298 K)

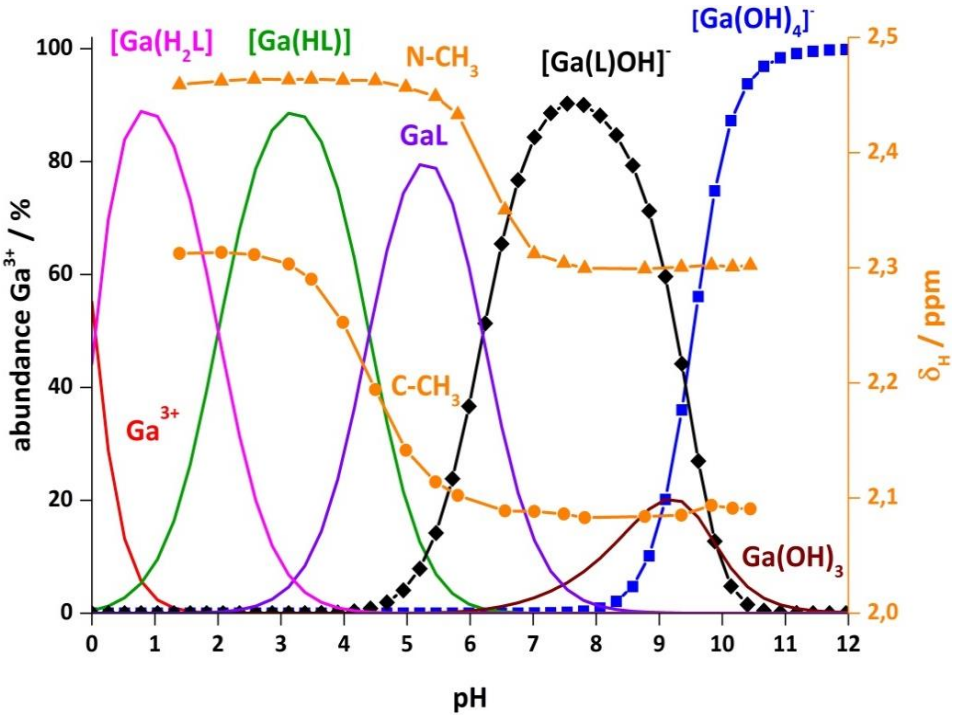

Figure S 3: The species distribution (red, pink, green, purple, black, brown and blue solid lines) in the Ga^{3+}-$DATA^{5m}$ calculated from pH-potentiometric data (table 3). ([Ga^{3+}]=[$DATA^{5m}$]=7.9 mM, 0.15 M NaCl, 25 °C). The percentage of the $[Ga(DATA^{5m})OH]^-$ (◆) and $[Ga(OH)_4]^-$ (■) species calculated from the ^{1}H- and ^{71}Ga-NMR spectra of the Ga^{3+}-$DATA^{5m}$ system. Chemical shifts of the N-CH_3 (▲) and HOOC-CH_2- (●) protons of $Ga(DATA^{5m})$ complex against pH

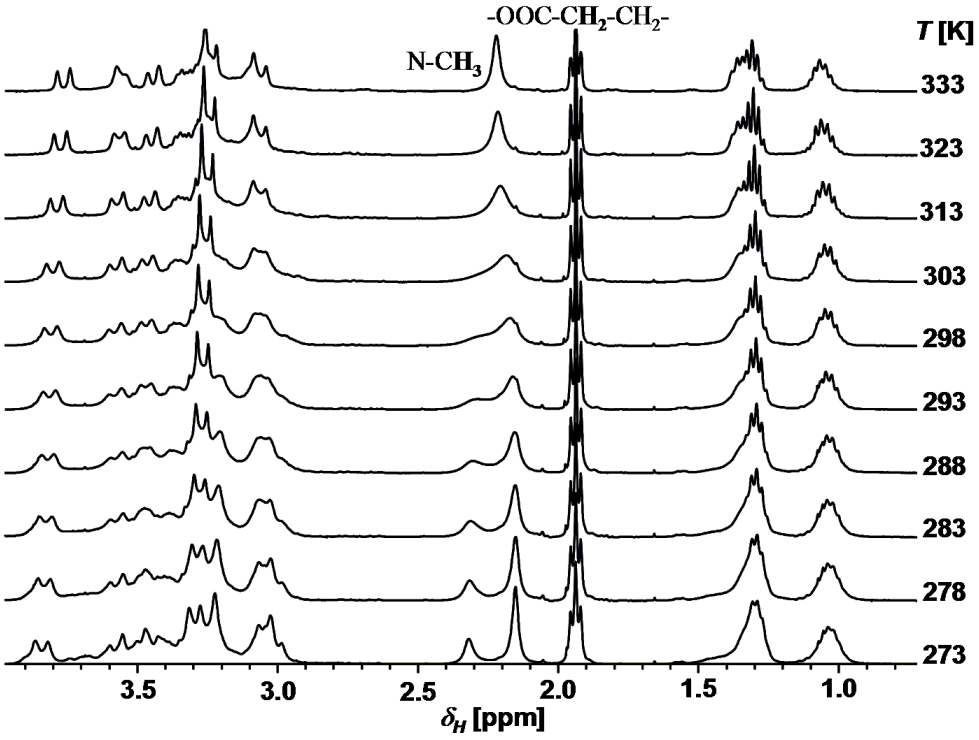

Figure S 4: VT-400 MHz ^{1}H-NMR studies of $Ga(DATA^{5m})$ – $Ga(DATA^{5m})OH$ systems ([GaL]=7.9 mM, D_2O, pD=6.91 (pD=pH + 0.41)) VT-400 MHz ^{1}H-NMR studies of $Ga(DATA^{5m})$ – $Ga(DATA^{5m})OH$ systems ([GaL]=7.9 mM, D_2O, pD=6.91 (pD=pH + 0.41))

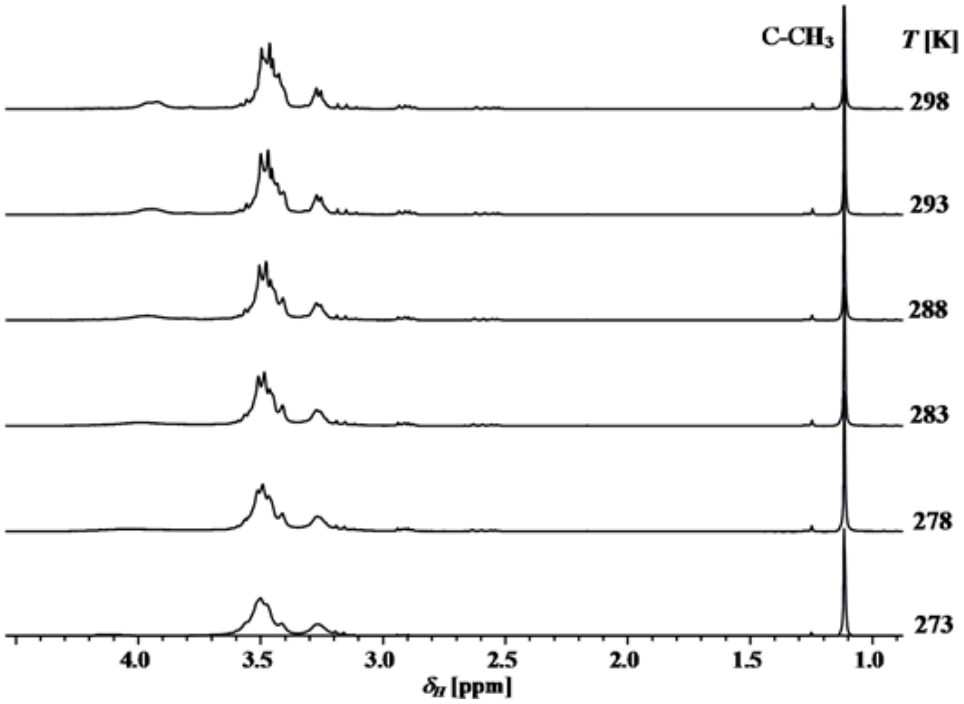

Figure S 5: VT-400 MHz ^{1}H-NMR studies of Ga(AAZTA)$^-$ - [Ga(AAZTA)OH]$^-$ systems ([GaL]=10 mM, D_2O, pD=5.0 (pD=pH + 0.41)

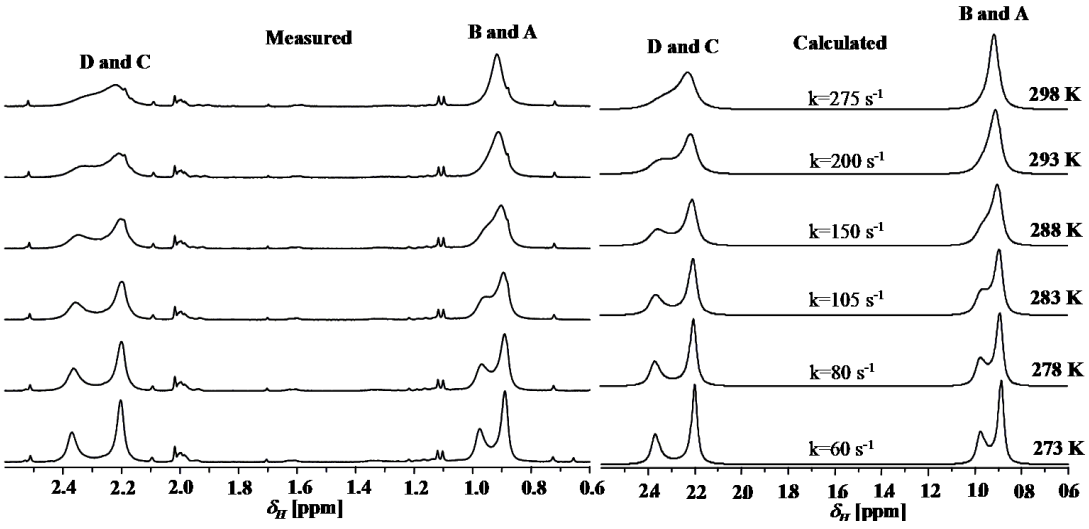

Figure S 6: Experimental and calculated ^{1}H-NMR spectra (400 MHz) of the N-CH_3 and C-CH_3 protons in Ga(DATA^m) -Ga(DATA^m)OH systems as a function of temperature.

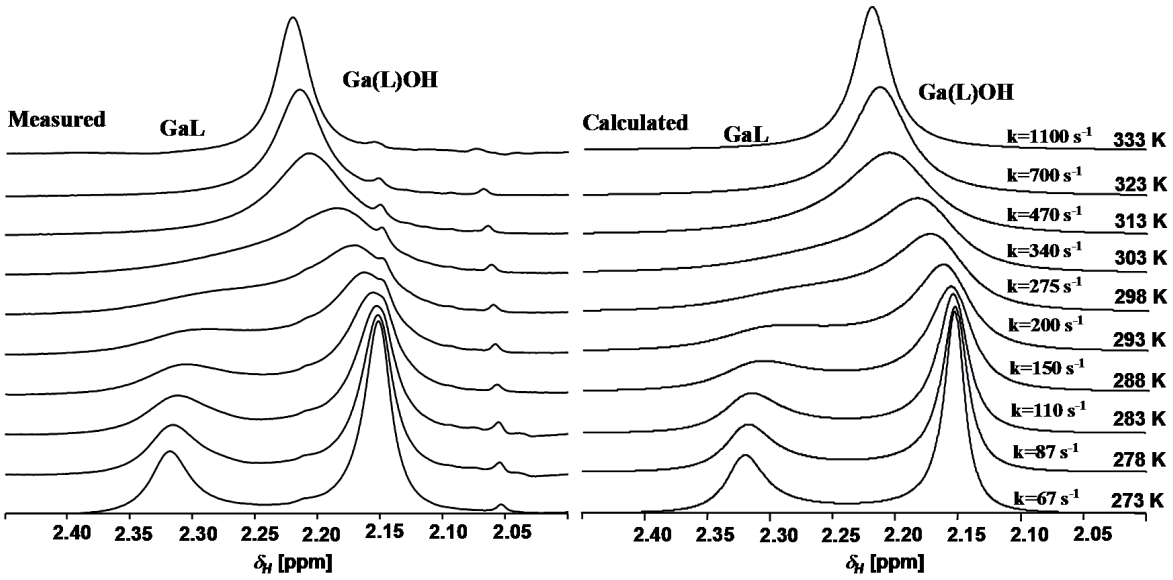

Figure S 7: Experimental and calculated ^{1}H-NMR spectra (400 MHz) of the N-CH_3 protons in $Ga(DATA^{5m})^{-}$ – $[Ga(DATA^{5m})OH]^{2-}$ systems as a function of temperature.

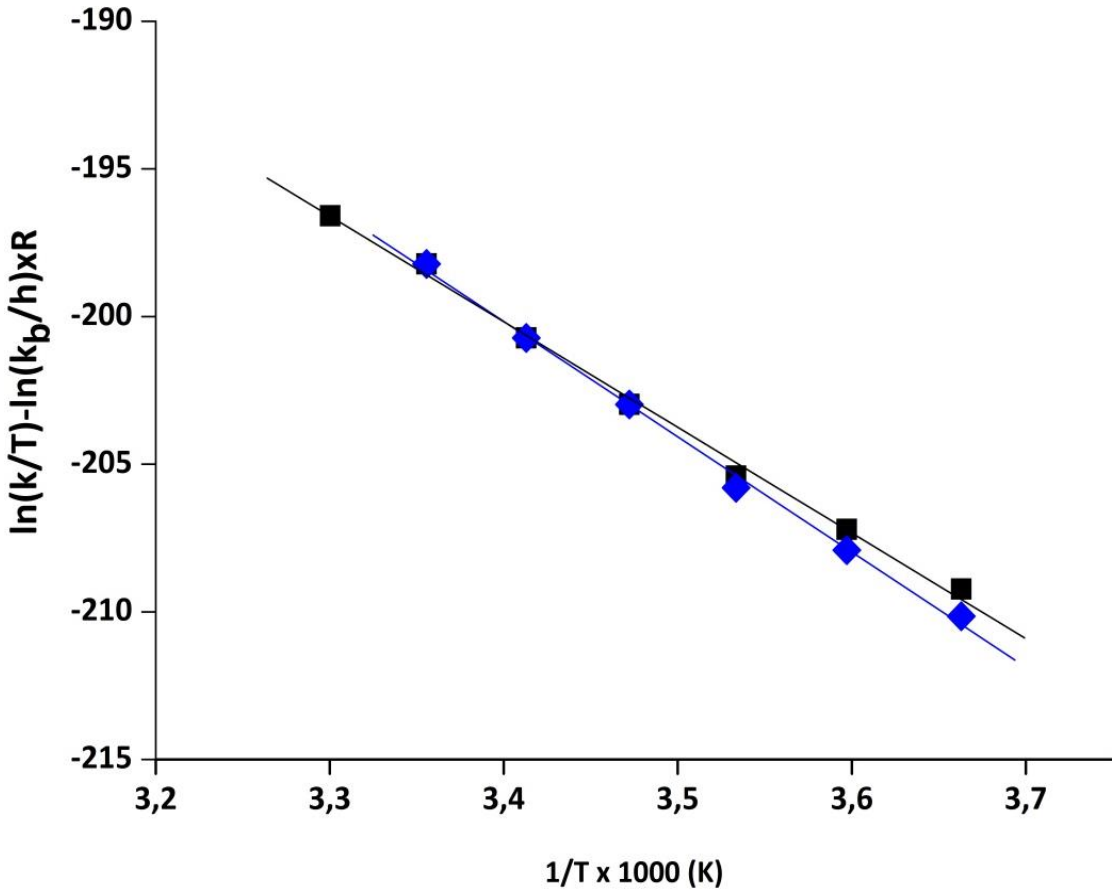

Figure S 8: Eyring plot for for determining the activation parameters characterising the exchange reactions between GaL and Ga(L)OH species of $Ga(DATA^{m})$ and $Ga(DATA^{5m})^{-}$ complexes

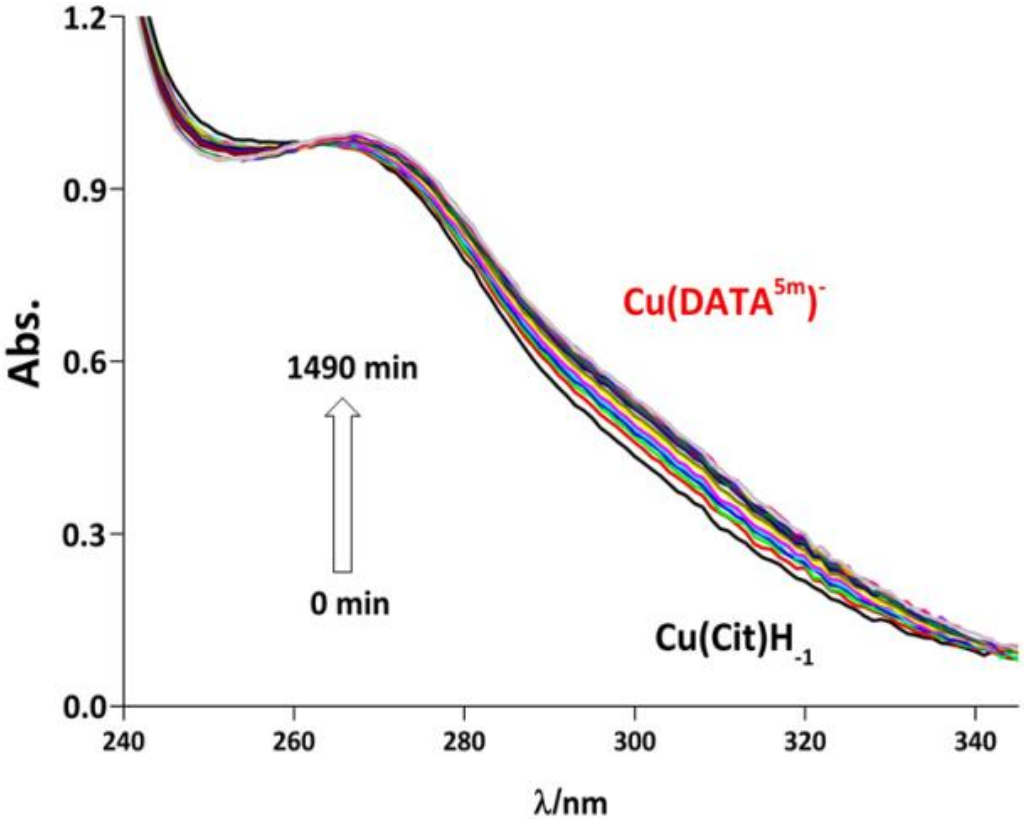

Figure S 9: . Absoprtion spectra of the $Ga(DATA^{5m})^-$ – Cu^{2+} reacting system in the presence of citrate ([GaL]=2.0 mM, [Cu^{2+}]=0.2 mM, [Cit]=2.0 mM, [MES]=0.01 M, pH=6.0, 0.15 M NaCl, 298 K, l=1 cm

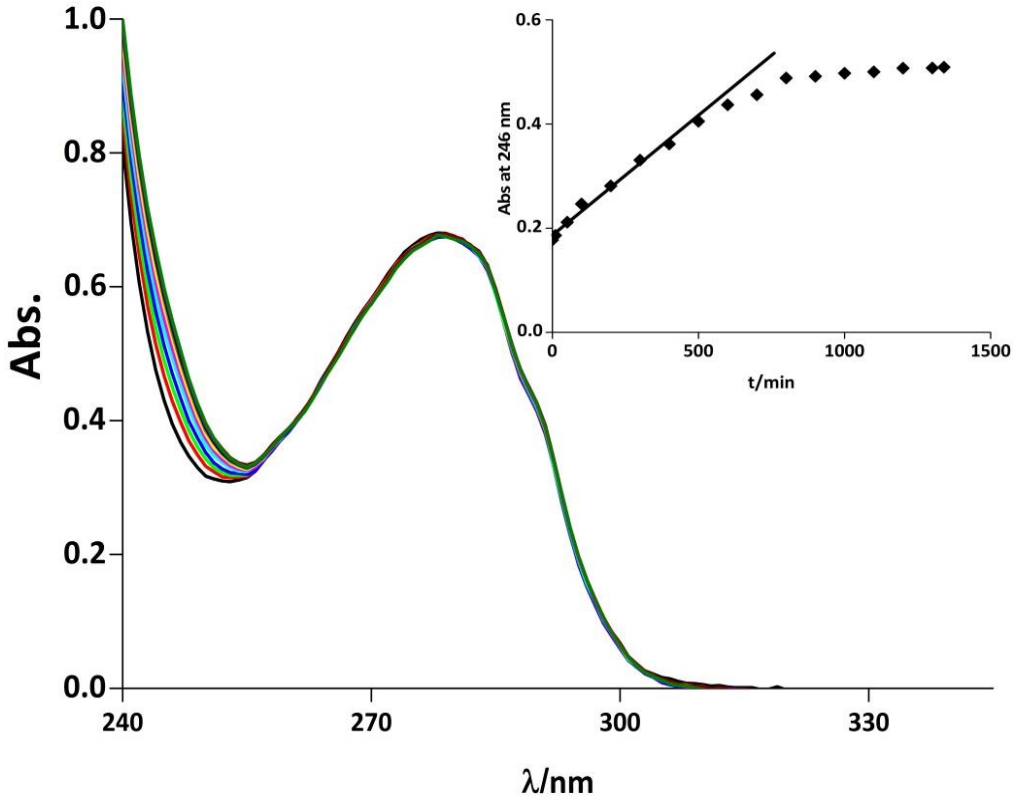

Figure S 10: Absorption spectra of the $Ga(DATA^{5m})$-transferrin system. Inserted figure shows the absorbance values of the reacting system at 246 nm as a function of time ([GaL]=0.1 mM, [Trf]=10 μM, [$NaHCO_3$]=25 mM, pH=7.4, 0.15 M NaCl, 25°C, l=1 cm)

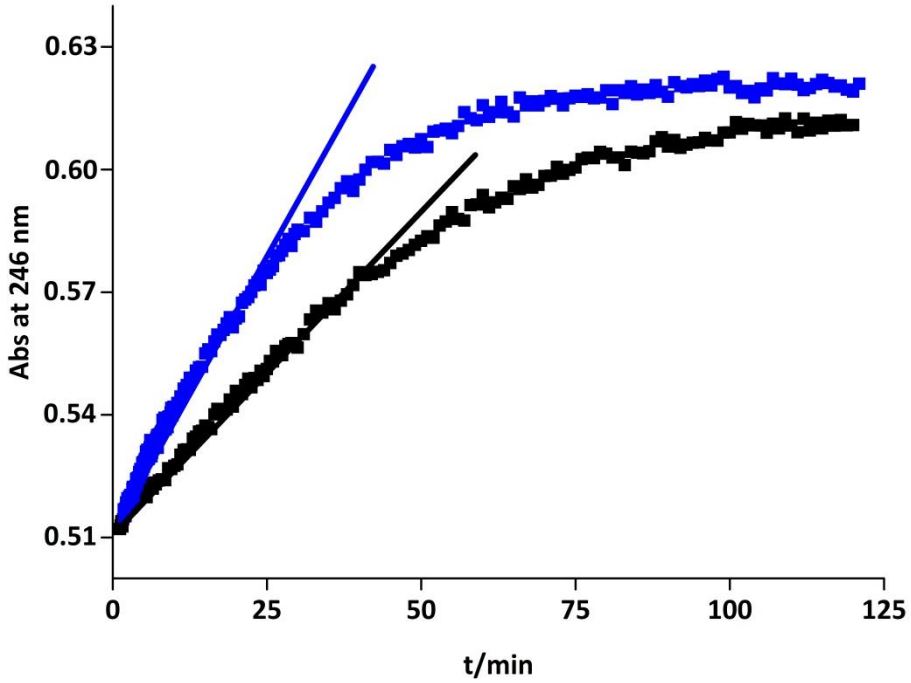

Figure S 11: Absorbance of the Ga(DATA^{m})-sTf systems at 246 nm, ([Ga(DATA^{m}]=2.0×10^{-4} M (◆) and 3.0×10^{-4} M (■), [sTf]=1.0×10^{-5} M, pH=7.4, 0.025 M $NaHCO_3$, 0.15 M NaCl, 25°C, l=1 cm)

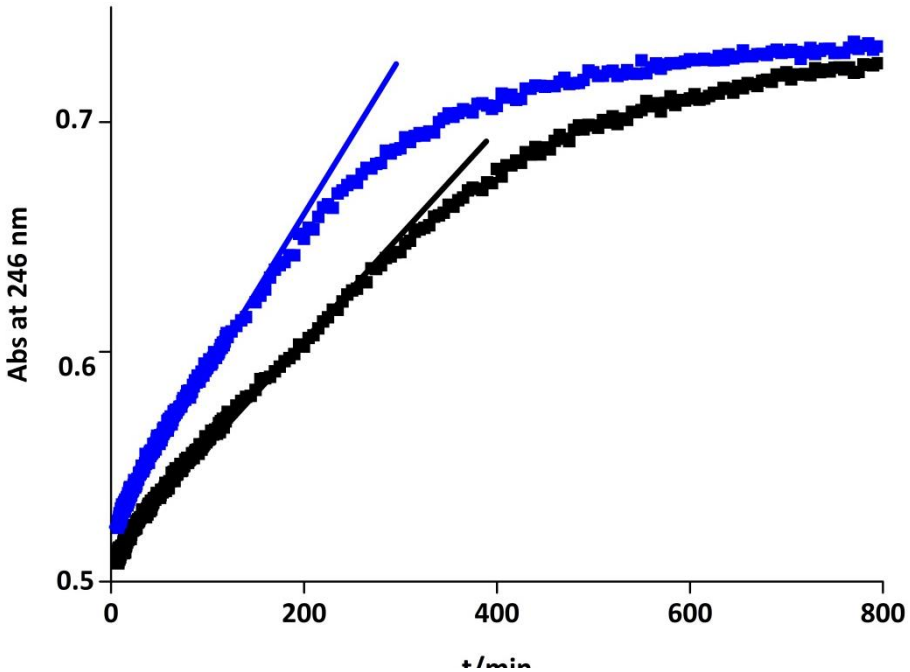

Figure S 12: Absorbance of the Ga(DATA^{5m})-sTf systems at 246 nm. ([Ga(DATA^{5m}]=2.0×10^{-4} M (◆) and 3.0×10^{-4} M (■), [sTf]=1.0×10^{-5} M, pH=7.4, 0.025 M $NaHCO_3$, 0.15 M NaCl, 25°C, l=1 cm)

REFERENCES

1. Velikyana I. Continued rapid growth in Ga-68 applications: Update 2013 to June 2014. J. Label. Compd. Radiopharm. 2015; 58(3): 99–121.

2. Fani M., André J.P., Mäcke H.R. Ga-68-PET: a powerful generator-based alternative to cyclotron-based PET radiopharmaceuticals. Contrast Media Mol. Imaging. 2008; 3(2): 53–60.

3. Vértes A., Nagy S., Klencsár Z., Rezsó G.L., Rösch F. Radionuclide Generators. 2 nd. Handb. Nucl. Chem. 2011.

4. Velikyan I. Ga-68-based radiopharmaceuticals: Production and application relationship. Molecules. 2015; 20(7): 12913-12943.

5. Velikyan I. Prospective of Ga-68-Radiopharmaceutical development. Theranostics. 2014; 4(1): 47–80.

6. Wadas T.J., Wong E.H., Weisman G.R., Anderson C.J. Coordinating radiometals of copper, gallium, indium, yttrium, and zirconium for PET and SPECT imaging of disease. Chem. Rev. 2010; 110(5): 2858–902.

7. Rösch F. Past, present and future of Ge-68/Ga-68 generators. Appl. Radiat. Isot. 2013; 76: 24–30.

8. Harris W.R., Martell A.E. Aqueous complexes of gallium(III). Inorg. Chem. 1976; 15(3): 713–20.

9. Motekaitis R.J., Martell A.E. Gallium complexes of multidentate ligands in aqueous solution. Inorg. Chem. 1980; 19(6): 1646–51.

10. Clarke E.T., Martell A.E. Stabilities of the Fe(III), Ga(III) and In(III) chelates of N,N´,N´´-triazacyclononanetriacetic acid. Inorganica Chim. Acta. 1991; 181(2): 273–80.

11. Clarke E.T., Martell A.E. Stabilities of trivalent metal ion complexes of the tetraacetate derivatives of 12-, 13- and 14-membered tetraazamacrocycles. Inorganica Chim. Acta. 1991; 190(1): 37–46.

12. Kubíček V., Havlícková J., Kotek J., Tircsó G., Hermann P., Tóth É., Lukes I. Gallium(III) complexes of DOTA and DOTA-Monoamide: Kinetic and thermodynamic studies. Inorg. Chem. 2010; 49(23): 10960–9.

13. Boros E., Ferreira C.L., Cawthray J.F., Price E.W., Patrick B.O., Wester D.W., Adam M.J., Orvig C. Acyclic chelate with ideal properties for ^{68}Ga PET imaging agent elaboration. J. Am. Chem. Soc. 2010; 132(44): 15726–33.

14. Boros E., Ferreira C.L., Yapp D.T.T., Gill R.K., Price E.W., Adam M.J., Orvig C. RGD conjugates of the H_2dedpa scaffold: Synthesis, labeling and imaging with Ga-68. Nucl. Med. Biol. 2012; 39(6): 785–94.

15. Evers A., Hancock R.D., Martell A.E., Matekaitis R.J. Metal Ion Recognition in Ligands ith Negatively Charged Oxygen Donor Groups. Complexation of Fe(III), Ga(III), In(III), Al(III), and other Highly Charged Metal Ions. Inorg. Chem. 1989; 28: 2189–95.

16. Knetsch P.A., Zhai C., Rangger C., Blatzer M., Haas H., Kaeopookum P., Haubner R., Decristoforo C. Ga-68-FSC-(RGD)3 a trimeric RGD peptide for imaging αvβ3 integrin expression based on a novel siderophore derived chelating scaffold-synthesis and evaluation. Nucl. Med. Biol. 2015; 42(2): 115–22.

17. Ma R., Motekaitis R.J., Martell A.E. Stability of metal ion complexes of N,N'-bis(2-N'-diacetic acid). Inorganica Chim. Acta. 1994; 224: 151–5.

18. Motekaitis R.J., Martell A.E., Welch M.J. Stabilities of trivalent metal complexes of phenolic ligands related to N,N'-bis(2-hydroxybenzyl)ethylenediamine-N,N'-diacetic acid (HBED). Inorg. Chem. 1990; 29(8): 1463–7.

19. Sun Y., Anderson C.J., Pajeau T.S., Reichert D.E., Hancock R.D., Motekaitis R.J., Martell A.E., Welch M.J. Indium(III) and gallium(III) complexes of bis(aminoethanethiol) ligands with different denticities: Stabilities, molecular modeling, and in vivo behavior. J. Med. Chem. 1996; 39(2): 458–70.

20. Ma R., Welch M.J., Martell A.E. Stability of metal ion complexes of 1, 4, 7-tris(2-mercaptoethyl)-1, 4, 7-triazacyclononane(TACN-TM) and molecular structure. Inorganica Chim. Acta. 1995; 236: 75–82.

21. Price E.W., Orvig C. Matching chelators to radiometals for radiopharmaceuticals. Chem. Soc. Rev. 2014; 43(1): 260–90.

22. Craig A.S., Parker D., Adams H., Bailey N.A. Stability, Ga-71 NMR, and Crystal Structure of a Neutral Gallium(lll) Complex of 1,4,7-Triazacyclononanetriacetate: a Potential Radiopharmaceutical? J. Chem. Soc. Chem. Commun. 1989; (1): 1793–4.

23. Notni J., Hermann P., Havlíčková J., Kotek J., Kubíček V., Plutnar J., Loktionova N., Riss P.J., Rösch F., Lukeš I. A triazacyclononane-based bifunctional phosphinate ligand for the preparation of multimeric Ga-68 tracers for positron emission tomography. Chem.-A Eur. J. 2010; 16(24): 7174–85.

24. Notni J., Simecek J., Hermann P., Wester H.J. TRAP, a powerful and versatile framework for gallium-68 radiopharmaceuticals. Chem.-A Eur. J. 2011; 17(52): 14718–22.

25. Simecek J., Schulz M., Notni J., Plutnar J., Kubíček V., Havlícková J., Hermann P. Complexation of metal ions with TRAP (1,4,7-triazacyclononane phosphinic acid) ligands and 1,4,7-triazacyclononane-1,4,7-triacetic acid: Phosphinate-containing ligands as unique chelators for trivalent gallium. Inorg. Chem. 2012; 51(1): 577–90.

26. Velikyan I., Mäcke H.R., Langstrom B. Convenient Preparation of Temperature Ga-Based PET-Radiopharmaceuticals at Room. Bioconjug. Chem. 2008; 19: 569–73.

27. Berry D.J., Ma Y., Ballinger J.R., Tavaré R., Koers A., Sunassee K., Zhou T., Nawaz S., Mullen G.E.D., Hider R.C., Blower P.J. Efficient bifunctional gallium-68 chelators for positron emission tomography: tris(hydroxypyridinone) ligands. Chem. Commun. (Camb). 2011; 47(25): 7068–70.

28. Aime S., Calabi L., Cavallotti C., Gianolio E., Giovenzana G.B., Losi P., Maiocchi A., Palmisano G., Sisti M. [Gd-AAZTA]-: A new structural entry for an improved generation of MRI contrast agents. Inorg. Chem. 2004; 43(24): 7588–90.

29. Gugliotta G., Botta M., Giovenzana G.B., Tei L. Fast and easy access to efficient bifunctional chelators for MRI applications. Bioorganic Med. Chem. Lett. 2009; 19(13): 3442–4.

30. Baranyai Z., Uggeri F., Giovenzana G.B., Bényei A., Brücher E., Aime S. Equilibrium and kinetic properties of the lanthanoids(III) and various divalent metal complexes of the heptadentate ligand AAZTA. Chem.-A Eur. J. 2009;15(7):1696–705.

31. Baranyai Z., Uggeri F., Maiocchi A., Giovenzana G.B., Cavallotti C., Takács A., Tóth I., Bányai I., Bényei A., Brucher E., Aime S. Equilibrium, Kinetic and Structural Studies of AAZTA Complexes with Ga3+, In3+ and Cu2+. Eur. J. Inorg. Chem. 2013; 1: 147–62.

32. Nagy G., Szikra D., Trencsényi G., Fekete A., Garai I., Giani A.M., Negri R., Masciocchi N., Maiocchi A., Uggeri F., Tóth I., Aime S., Giovenzana G.B., Baranyai Z. AAZTA: An Ideal Chelating Agent for the Development of Sc-44 PET Imaging Agents. Angew. Chemie Int. Ed. 2017; 2118

33. Vágner A., D'Alessandria C., Gambino G., Schwaiger M., Aime S., Maiocchi A., Tóth I., Baranyai Z., Tei L. A rigidified AAZTA-like ligand as efficient chelator for Ga-68 radiopharmaceuticals. ChemistrySelect. 2016; 1(2): 163–71.

34. Briley-Saebo K.C., Geninatti-Crich S., Cormode D.P., Barazza A., Mulder W.J.M., Chen W., Giovenzana G.B., Fisher E.A., Aime S., Fayad Z.A. High-Relaxivity Gadolinium-Modified High-Density Lipoproteins as Magnetic Resonance Imaging Contrast Agents. J. Phys. Chem. B. 2009; 113(18): 6283–9.

35. Gianolio E., Giovenzana G.B., Ciampa A., Lanzardo S., Imperio D., Aime S. A novel method of cellular labeling: Anchoring MR-imaging reporter particles on the outer cell surface. ChemMedChem. 2008; 3(1): 60–2.

36. Manzoni L., Belvisi L., Arosio D., Bartolomeo M.P., Bianchi A., Brioschi C., Buonsanti F., Cabella C., Casagrande C., Civera M., De Matteo M., Fugazza L., Lattuada L., Maisano F., Miragoli L., Neira C., Pilkington-Miksa M., Scolastico C. Synthesis of Gd and Ga-68 Complexes in Conjugation with a Conformationally Optimized RGD Sequence as Potential MRI and PET Tumor-Imaging Probes. ChemMedChem. 2012; 7(6): 1084–93.

37. Waldron B.P., Parker D., Burchardt C., Yufit D.S., Zimny M., Rösch F. Structure and stability of hexadentate complexes of ligands based on AAZTA for efficient PET labelling with gallium-68. Chem. Commun. 2013; 49(6): 579–81.

38. Parker D., Waldron B.P. Conformational analysis and synthetic approaches to polydentate

perhydro-diazepine ligands for the complexation of gallium(III). Org. Biomol. Chem. 2013; 11(17): 2827.

39. Parker D., Waldron B.P., Yufit D.S. Crystallographic and solution NMR structural analyses of four hexacoordinated gallium(III) complexes based on ligands derived from 6-amino-perhydro-1,4-diazepine. Dalton Trans. 2013; 42: 8001–8.

40. Seemann J., Waldron B.P., Rösch F., Parker D. Approaching “kit-type” labelling with Ga-68: The DATA chelators. ChemMedChem. 2015; 10(6): 1019–26.

41. Seemann J., Waldron B.P., Parker D., Rösch F. DATATOC: a novel conjugate for kit-type Ga-68 labelling of TOC at ambient temperature. EJNMMI Radiopharm. Chem. 2016; 1(1): 4.

42. Tei L., Gugliotta G., Fekete M., Kálmán F.K., Botta M. Mn(II) complexes of novel hexadentate AAZTA-like chelators: a solution thermodynamics and relaxometric study. Dalton Trans. 2011; 40(9): 2025–32.

43. Barcza L., Mihályi K. Dimerization of lower fatty acids in aqueous solutions. Zeitschrift für Phys. Chemie. 1977; 104: 199–212.

44. Akitt J.W., Kettle D. Ga-71 nuclear magnetic resonance investigation of aqueous gallium(III) and its hydrolysis. Magn. Reson. Chem. 1989; 27: 377–9.

45. Tóth I., Zékány L., Brücher E. Equilibrium study of the systems of aluminium(III), gallium(III) and indium(III) with mercaptoacetate, 3-mercaptopropionate and 2-mercaptobenzoate. Polyhedron. 1984; 3(7): 871–7.

46. Baes C.F., Mesmer R.E. The hydrolysis of cations. Wiley, New York. 1976;

47. Jackson G.E., Byrne M.J. Metal ion speciation in blood plasma: gallium-67-citrate and MRI contrast agents. J. Nucl. Med. 1996; 37: 379–86.

48. May P.M., Linder P.W., Williams D.R. Computer Simulation of Metal-ion Equilibria in Biofluids : Models for low-molecular-weight complex distribution of calcium(II), magnesium(II), manganese(II), iron(III), copper(II), zinc(II) and lead(II) ions in human blood plasma. J. Chem. Soc. 1977; 2(6): 588–95.

49. Harris W.R., Pecoraro V.L. Thermodynamic binding constants for gallium transferrin. Biochemistry. 1983; 22(2): 292–9.

50. Irving H.M., Miles M.G., Pettit L.D. A study of some problems in determining the stoicheiometric proton dissociation constants of complexes by potentiometric titrations using a glass electrode. Anal. Chim. Acta. 1967; 38: 475–88.

51. Zékány L., Nagypal I. Computational Method for Determination of Formation Constants. 1985.

52. Oe H., Takahashi N., Doi E., Hirose M. Effects of Anion Binding on the Conformations of the Two Domains of Ovotransferrin. J. Biochem. 1989; 106(5): 858–63.

4.2 Instant kit-preparation of ^{68}Ga-radiopharmaceuticals via the chimeric chelator DATA: Proof-of-principle with ^{68}Ga-DATA-TOC

Instant kit-preparation of ^{68}Ga-radiopharmaceuticals via the chimeric chelator DATA: Proof-of-principle with ^{68}Ga-DATA-TOC

J.-P. Sinnes[1], J. Nagel[1], B. P. Waldron[1], T. Maina[2], B. A. Nock[2], R. Bergmann[3], M. Ullrich[3], M. Bachmann[3,6], R. P. Baum[4], F. Rösch[1]

[1]Johannes Gutenberg-University Mainz, Institute of Nuclear Chemistry, Germany

[2]NCSR "Demokritos", Molecular Radiopharmacy, INRASTES, Athens, Greece

[3]Helmholtz-Zentrum Dresden-Rossendorf, Institute of Radiopharmaceutical Cancer Research, Dresden, Germany

[4]Zentralklinik Bad Berka GmbH, Clinic for Molecular Radiotherapy, Bad Berka, Germany

[5]Technische University Dresden, Uniklinikum 'Carl Gustav Carus', UCC, Tumorimmunology, Dresden, Germany

[6]National Center for Tumor Diseases, 'Carl Gustav Carus' Technical University Dresden, Dresden, Germany

ABSTRACT

The widespread use of ^{68}Ga for positron emission tomography (PET) depends on our ability to develop radiopharmaceuticals that can be prepared in a simple, quick and convenient manner. The DATA (6-Amino-1,4-diazapine-triacetate) scaffold represents a novel hybrid chelator type possessing both cyclic and acyclic character, that may allow for facile access to ^{68}Ga-radiotracers in the clinic. We report the first bifunctional DATA chelator conjugated to [Tyr^3]octreotide (TOC), a somatostatin subtype 2 receptor (sst_2)-targeting vector for neuroendocrine tumors (NETs).

The DATA chelator was synthesized in a 5-step synthesis and coupled to TOC to afford DATA-TOC. Competition binding assays with [^{nat}Ga]Ga-DATA-TOC and [^{nat}Ga]Ga-DOTA-TOC against [^{125}I-Tyr^{25}]LTT-28 were conducted in HEK293-$hsst_2$ cell membranes. First *in vivo* studies were performed in female SCID/beige mice bearing sst_2+ MPC-EGFP-Luc cells to determine the *in vivo* sst_2-targeting and pharmacokinetics. Eventually, a direct comparison of [^{68}Ga]Ga-DATA-TOC with the well-established PET radiotracer [^{68}Ga]Ga-DATA-TOC was performed in a 46-year-old male patient with a well-differentiated NET.

DATA-TOC was labelled with ^{68}Ga in a yield >95 % in less than 10 min at ambient temperature. The $hsst_2$-affinities of [^{nat}Ga]Ga-DATA-TOC and [^{nat}Ga]Ga-DOTA-TOC were found very comparable (IC_{50}=1.03 ±0.08 nM and 0.21±0.01 nM, respectively). In mice, [^{68}Ga]Ga-DATA-TOC was able to visualize various tumor lesions, previously detected in luciferase imaging, showing comparable SUVs to [^{68}Ga]Ga-DOTA-TOC. Direct comparison of the two PET-tracers in a NET patient revealed comparable tumor uptake with better tumor-to-liver contrast for [^{68}Ga]Ga-DATA-TOC.

[^{68}Ga]Ga-DATA-TOC performed comparably well to [^{68}Ga]Ga-DOTA-TOC in all preclinical tests and achieved higher tumor-to-liver contrast in a NET-patient, illustrating the potential of the DATA-chelator for easy access to ^{68}Ga-radiotracers in a routine clinical environment.

Keywords: Gallium-68, DATA-TOC, neuroendocrine tumor, somatostatin, PET

INTRODUCTION

There has been a surge in the development of ^{68}Ga-radiopharmaceuticals over last decade initiated by the clinical success of [^{68}Ga]Ga-DOTA-TOC (TOC: DPhe-c[Cys-Tyr-DTrp-Lys-Thr-Cys]-Thr-ol) and [^{68}Ga]Ga-DOTA-TATE (TATE: DPhe-c[Cys-Tyr-DTrp-Lys-Thr-Cys]-Thr-OH), as well as by significant improvements in the provision of ^{68}Ga eluate now fulfilling pharmaceutical standards [1–6].

As a result, [^{68}Ga]Ga-DOTA-TOC and [^{68}Ga]Ga-DOTA-TATE are currently being used in clinical settings for the diagnosis of neuroendocrine tumors (NETs). Furthermore, last year [^{68}Ga]Ga-DOTA-TATE acquired FDA approval as a diagnostic PET-radiopharmaceutical for the visualization of NET lesions [7]. Despite the availability of ^{68}Ga via commercial ^{68}Ge/^{68}Ga-generators and its favorable emission characteristics for PET imaging (β^+=89 %, $E_{\beta,max}$=1.9 MeV), other radionuclides and modalities compete for routine application in the clinic [1,8–11]. Hence, the easy and fast *in-situ* access to ^{68}Ga-radiopharmaceuticals will boost the use of ^{68}Ga in PET centers. A key step in this direction is related to labelling protocols which essentially depend on the type of the bifunctional chelator (BFC) attached to the vector of interest. Hitherto established BFCs for ^{68}Ga require relatively harsh conditions (high temperatures and/or low pH) for full incorporation of the metal [2,12]. This inherently limits the portfolio of ^{68}Ga-radiopharmaceuticals because several biomolecules promising for application in nuclear oncology are temperature and/or pH sensitive [13].

It should be noted, that the dominance of ^{99m}Tc radiopharmaceuticals in diagnostic nuclear medicine in the ´70's has been actually based on their simple, convenient and standardized kit-type labelling along with the commercial availability of the ^{99}Mo/^{99m}Tc-generator [14]. Nowadays however nuclear medicine has evolved beyond the realm of perfusion imaging agents towards radiolabelled molecular vectors able to elucidate complex pathological processes with a high specificity. Accordingly, labelling of such often temperature-vulnerable molecules imposes new stringent requirements on the BFC, i.e. >95 % labelling efficiency at ambient temperatures in high specific activities in view of the easy saturability of target biomolecular systems. In addition, in the case of short-lived radionuclides, like ^{68}Ga ($t_{1/2}$= 67.7 min), short labelling times are highly desirable as well as formation of a high quality radiolabelled product not requiring further purification prior to use. The development of such labelling protocols would be of excellent added-value to the aforementioned advantages of ^{68}Ga, but presents significant challenges, especially in the design of suitable BFCs [15].

In general, chelators can be distinguished as predominantly cyclic (DOTA, NOTA, TRAP – associated with high thermodynamic and kinetic stability) or acyclic (DFO, DTPA and more recently THP – linked to fast, mild and high labelling efficiency) (figure 1) [12,16–20].

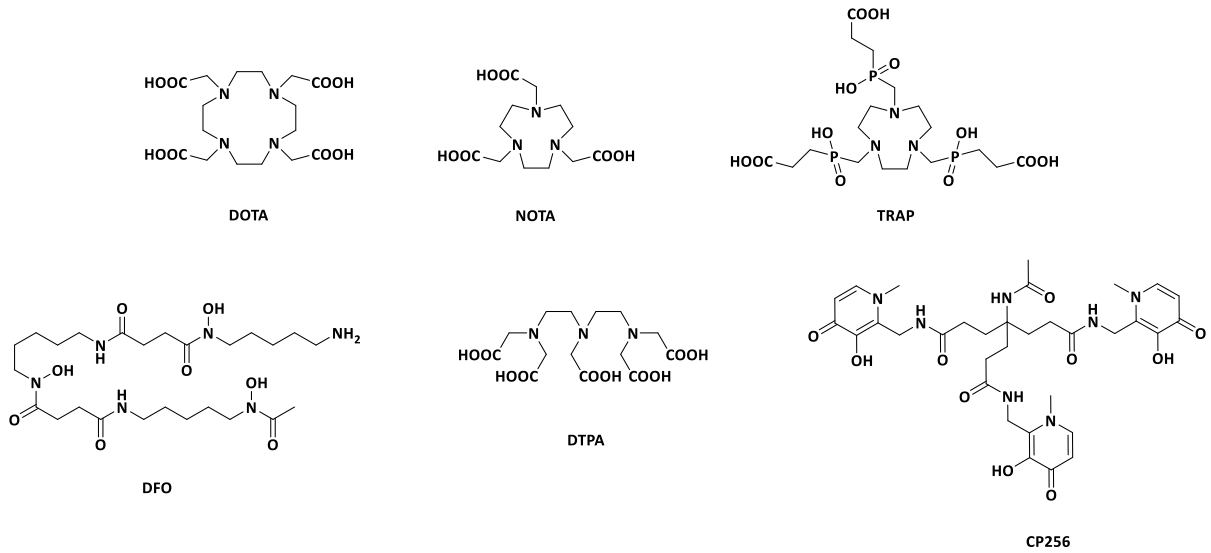

Figure 1: Chemical structure of relevant cyclic chelators like DOTA, NOTA and TRAP and acyclic chelators like DFO, DTPA and CP256

In contrast, the new DATA-scaffold represents a novel approach to chelator design in that chelators are essentially hybrids, possessing both cyclic and acyclic character. It is assumed that flexibility of the acyclic portion facilitates rapid complexation, whilst the preorganised cyclic portion minimizes the energy-barrier to complexation and inhibits decomplexation processes [21,22]. The favorable radiolabelling kinetics of the DATA-chelators along with the stability of the forming ^{68}Ga-chelates motivated us to develop a bifunctional version of DATA suitable for coupling to vectors of clinical interest. We recently reported on the synthesis and ^{68}Ga-radiolabelling of the first DATA peptide conjugate, DATA-TOC (figure 2) [23].

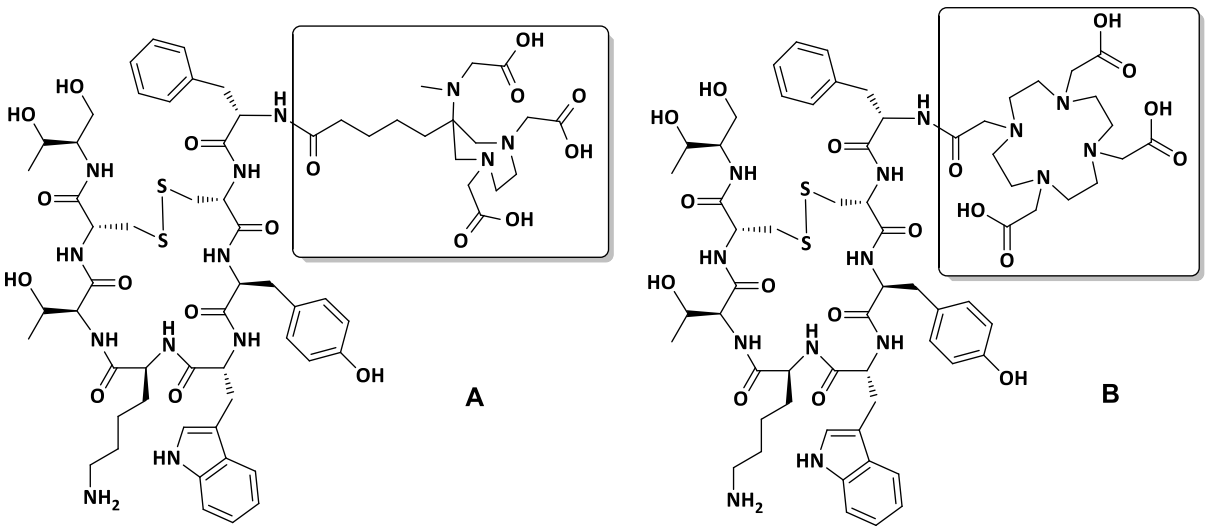

Figure 2: Structures of [Tyr^3]octreotide coupled with (**A**) DATA and (**B**) DOTA; chelator structures are highlighted

For the first time in a kit-type procedure, the DATA-TOC radiotracer-precursor in form of a lyophilised solid could be radiolabelled with ^{68}Ga in less than 10 min at ambient temperature in a >95 % yield. The speed, reliability, flexibility and simplicity with which [^{68}Ga]Ga-DATA-TOC could be obtained, opens the

possibility of introducing a kit-type labelling to routine ^{68}Ga-PET by means of DATA-based BFCs.

In the present work, we were interested to evaluate the suitability of DATA-based ^{68}Ga-radiolabelling of contemporary molecular vectors, using ^{68}Ga-DATA-TOC as our first paradigm. Specifically, we compared [^{68}Ga]Ga-DATA-TOC with the clinically established reference [^{68}Ga]Ga-DOTA-TOC in a series of biological *in vitro* and *in vivo* models expressing the human sst_2, namely: (i) competition binding assays in $hsst_2$-positive cell membranes, (ii) biodistribution and small animal PET imaging in a preclinical pheochromocytoma (PHEO) mouse model, and (iii) clinical studies in a NET-patient.

RESULTS AND DISCUSSION

Affinity of [^{nat}Ga]Ga-DATA-TOC and [^{nat}Ga]Ga-DOTA-TOC for the hsst$_{2/3/5}$

The metalated peptide-conjugates [^{nat}Ga]Ga-DATA-TOC and [^{nat}Ga]Ga-DOTA-TOC were tested for their ability to displace the pansomatostatin radioligand [^{125}I-Tyr^{25}]LTT-28 from hsst$_{2/3/5}$-binding sites in HEK293-hsst$_{2/3/5}$ cell membranes using the pansomatostatin ligand LTT-SS-28 as reference [24–26]. As shown in figure 3, both octapeptide analogs exhibited high affinity for the hsst$_2$, which was very comparable to LTT-SS28 [27].

Based on IC_{50} values thus determined the analogs can be ranked as follows: LTT-SS28 (IC_{50} = 0.05±0.01 nM) ≤ [^{nat}Ga]Ga-DOTA-TOC (IC_{50} = 0.21±0.01 nM) ≤ [^{nat}Ga]Ga-DATA-TOC (IC_{50} = 1.03± 0.08 nM).

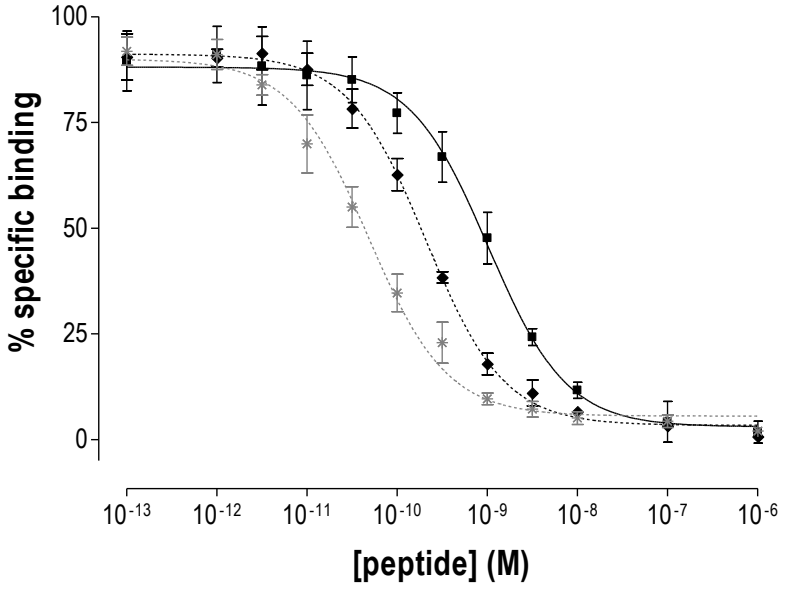

Figure 3: Displacement of [^{125}I-Tyr^{25}]LTT-SS-28 from hsst$_2$ binding sites in HEK293-hsst$_2$ cell membranes by increasing concentrations of: ■ [^{nat}Ga]Ga-DATA-TOC (IC_{50}=1.03±0.08 nM, n=3); ◆ [^{nat}Ga]Ga-DOTA-TOC (IC_{50}=0.21±0.01 nM, n=2); control: ✳ LTT-SS-28 (IC_{50}=0.05±0.01 nM, n=3). Results represent the average IC_{50} values±sd of independent experiments performed in triplicate.

Small animal PET and Biodistribution

In exemplary PET studies with NMRI nu/nu mice bearing the allogenic subcutaneous MPC-mCherry tumor was it clearly visible with both radiotracers (figure 4), and the uptake could be nearly complete blocked by simultaneous injection of the potent somatostatin analogue (100 µg/mouse) [Nal^3]-Octreotide acetate. The kinetic tumor to blood ratios of [^{68}Ga]Ga-DATA-TOC and [^{68}Ga]Ga-DOTA-TOC (figure 5) showed a similar linear shape and values (figure 6). The tumor-to-blood ratios (standard uptake ratio, SUR) of the control and blocking experiments with both compounds reached at two hours after

injection similar levels between of 31.6±16.0 (n=9), 28.1±1.3 (n=3) and 3.6±0.0 (n=2), 0.7±0.3 (n=2) for [^{68}Ga]Ga-DATA-TOC, [^{68}Ga]Ga-DOTA-TOC in control and blocking, respectively.

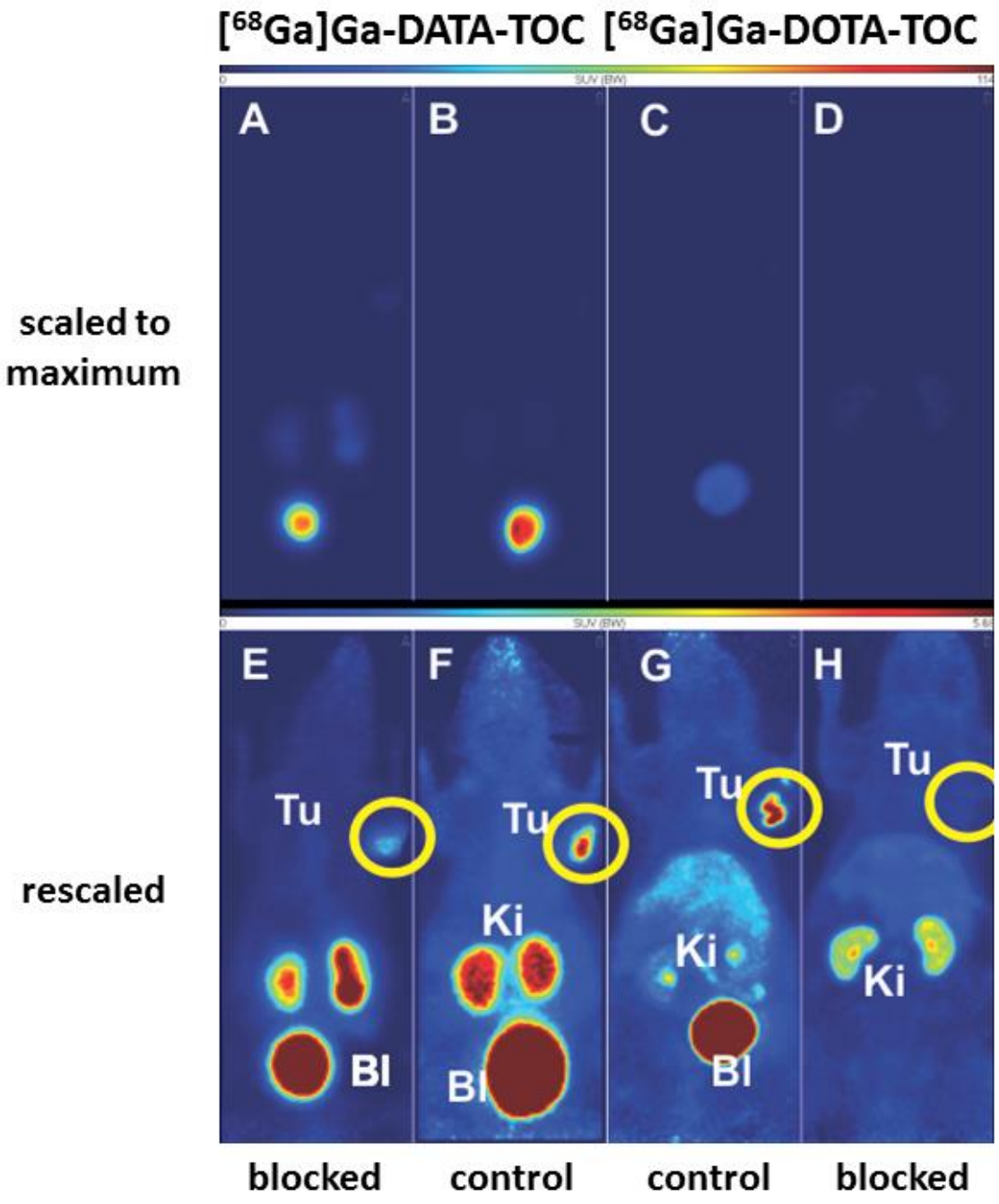

Figure 4: Maximum intensity projections of PET images of [^{68}Ga]Ga-DOTA-TOC (A, B, E, F) and [^{68}Ga]Ga-DATA-TOC (C, D, G, H) measurements from 1 to 2 h (midframe time 90 min) after single intravenous injection in MPC-mCherry tumor-bearing NMRI nu/nu mice as control and blocked by 100 µg/mouse [Nal^{3}]Octreotide acetate. The images A–D are scaled to the maximum SUV in the image, and images E-F are individually scaled to visualize the tumors (yellow circle) (Bl-bladder, Ki-kidney, Tu-tumor).

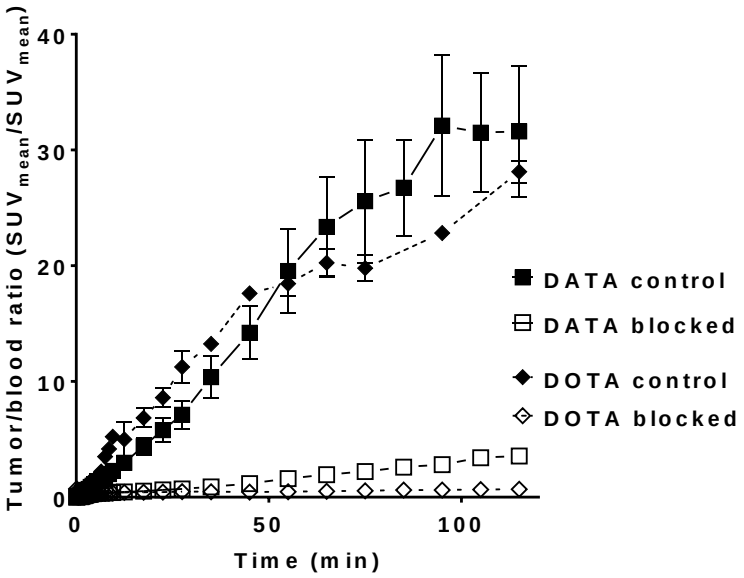

Figure 5 Tumor-to-blood and tumor-to-muscle ratios of [^{68}Ga]Ga-DATA-TOC control (DATA control, n=7), [^{68}Ga]Ga-DATA-TOC blocked with Octreotide (DATA blocked, n=5), and [^{68}Ga]Ga-DOTA-TOC control (DOTA control, n=3) and blocked with Octreotide (DOTA blocked, n=3) calculated from dynamic PET studies (values are mean±SEM)

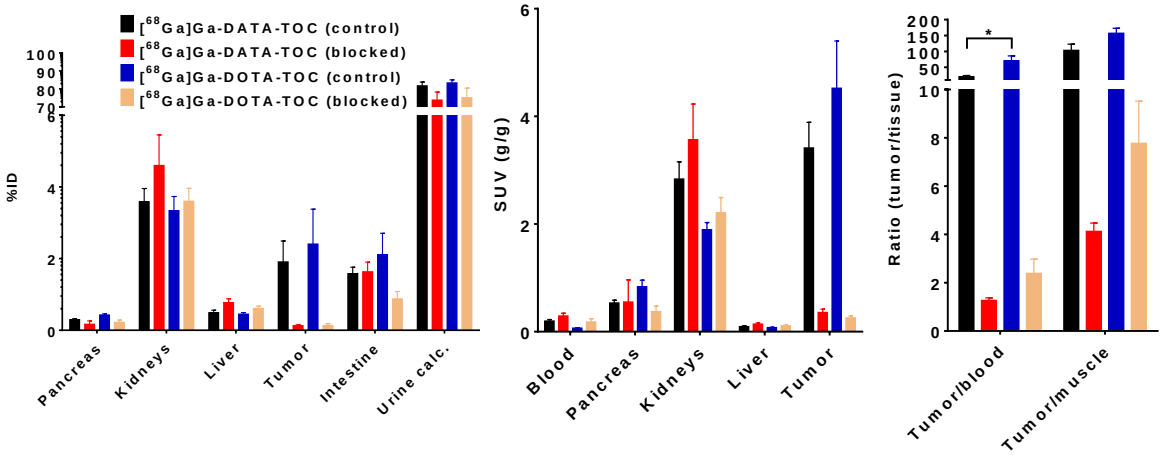

Figure 6: Biodistribution of [^{68}Ga]Ga-DATA-TOC and [^{68}Ga]Ga-DOTA-TOC in selected organs and tissues (**A**) activity amounts (%ID), activity concentrations (**B**) and tumor-totissue ratios (SUV/SUV) (**C**) 60 min after single intravenous injection of [^{68}Ga]Ga-DATA-TOC (control 9 animals, blocked 8 animals) and [^{68}Ga]Ga-DATA-TOC (control 5 animals, blocked 7 animals) in MPC-mCherry NMRI nu/nu tumor-bearing mice in control and blocked (100 µg/mouse [Nal^{3}]Octreotide acetate) experiments.

Biodistribution

Biodistribution studies over 1 h p.i. of the [^{68}Ga]Ga-DATA-TOC and [^{68}Ga]Ga-DOTA-TOC in s.c. tumor-bearing mice were carried out for quantitative comparison of tumor accumulation, distribution and elimination in control and blocked state (figure 6). The tumor uptake of both [^{68}Ga]Ga-DATA-TOC and [^{68}Ga]Ga-DOTA-TOC at 1 h after injection was in the same range with SUV's of 3.41±1.43 and 4.52±1,96 (P=0.2838), respectively. The higher blood concentration of the [^{68}Ga]Ga-DATA-TOC (0.19±0.08 SUV) in comparison to [^{68}Ga]Ga-DOTA-TOC (0.06±0.01 SUV; P<0.01) resulted in a lower tumor-to-blood ratio

20.2±11.9 SUV versus 70.5±34.3 SUV; P<0.01. However, the tumor to muscle ratios for both radiotracers were not different with 103.0±57.2 for [^{68}Ga]Ga-DATA-TOC and 157.0±34.6 for [^{68}Ga]Ga-DOTA-TOC (P=0.1027). A significant difference was the higher uptake of [^{68}Ga]Ga-DOTA-TOC in the pancreas with 0.836±0.267 to [^{68}Ga]Ga-DATA-TOC with 0.534±0.152, P<0.05. The simultaneous injection of 100 µg/mouse [Nal^{3}]Octreotide acetate blocked the tumor accumulation distinctly of both radiotracers. The resulting activity concentrations were not different between both with 0.358±0.169 SUV [^{68}Ga]Ga-DATA-TOC and 0.256±0.094 SUV [^{68}Ga]Ga-DOTA-TOC, P=0.2145. The [Nal^{3}]-Octreotide acetate injection decreased also the accumulation of the [^{68}Ga]Ga-DOTA-TOC in the pancreas from 0.836±0.267 SUV to 0.374±0.268, P<0.05. On the other site was the uptake of [^{68}Ga]Ga-DATA-TOC increased in the spleen and of the [^{68}Ga]Ga-DOTA-TOC in the brain by application of the Octreotide. Both radiotracers were predominantly excreted via the kidneys in comparable amounts with 85.3 %ID of the [^{68}Ga]Ga-DATA-TOC and 86.6 %ID of the [^{68}Ga]Ga-DOTA-TOC. The hepatobiliary excretion of both radiotracers was small and comparably with 2.07±0.72 %ID ([^{68}Ga]Ga-DATA-TOC), and 2.76±1.15 %ID ([^{68}Ga]Ga-DOTA-TOC) for both radiotracers. The elimination via the liver of [^{68}Ga]Ga-DOTA-TOC was decreased by the Octreotide injection to 1.36±0.63 %ID

Patients

Compared with [^{68}Ga]Ga-DOTA-TOC PET/CT before PRRT, post-PRRT [^{68}Ga]Ga-DOTA-TOC PET/CT demonstrated partial disease remission according to molecular imaging criteria (65 % decrease of uptake in the primary pancreatic tumor based on the target-to-pituitary ratio). PET/CT with [^{68}Ga]Ga-DATA-TOC, performed 24 h later at the same time post tracer injection, demonstrated a similar, very intense $hsst_2$-expression in the primary pancreatic tumor (figure 7), but relatively lower uptake in normal liver (table 1). If confirmed in a larger series of patients, the lower hepatic uptake of [^{68}Ga]Ga-DATA-TOC will allow for more sensitive detection of small liver metastases.

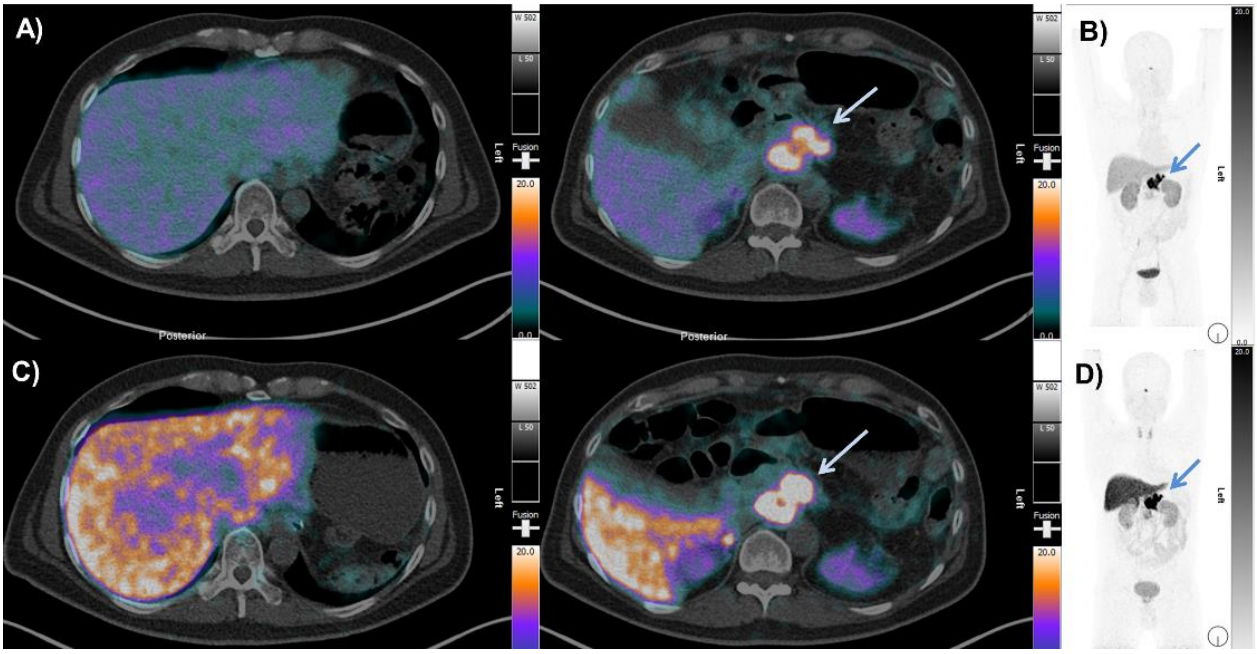

Figure 7: [^{68}Ga]Ga-DATA-TOC PET/CT images - **A**) transverse PET/CT fusion, **B**) PET MIP. [^{68}Ga]Ga-DOTA-TOC PET/CT images - **C**) transverse PET/CT fusion, **D**) PET MIP. Arrows demonstrate high uptake in the primary pancreatic NET. The [^{68}Ga]Ga-DATA-TOC PET/CT images show slightly higher physiological uptake in the kidneys as compared to the [^{68}Ga]Ga-DOTA-TOC PET/CT study in the same patient. There is significantly higher uptake in normal liver after injection of [^{68}Ga]Ga-DOTA-TOC in comparison with PET/CT images obtained after using [^{68}Ga]Ga-DATA-TOC

Table 1: Comparison of SUVs between [^{68}Ga]Ga-DATA-TOC and [^{68}Ga]Ga-DOTA-TOC in 46-year-old male patient with a well-differentiated NET in the body and tail of the pancreas

location	SUV	
	[^{68}Ga]Ga-DATA-TOC	[^{68}Ga]Ga -DOTA-TOC
target lesion	46.9	71.1
liver	9.11	23.09
ratio (target-to-liver)	5.15	3.08
Pituitary gland	14.57	23.69
ratio (target-to-pituitary gland)	3.22	3.00

The newly presented bifunctional DATA-chelator and its conjugate to TOC, DATA-TOC, showed the potential to establish a kit-type labelling routine for ^{68}Ga [23,28]. To show that the DATA chelator does not negatively affect the receptor affinity and the *in vivo* performance of the targeting vector, [$^{68/nat}$Ga]Ga-DATA-TOC was evaluated in a series of *in vitro*- and *in vivo*-studies and directly compared with [$^{68/nat}$Ga]Ga-DOTA-TOC.

Summarizing these results the newly presented bifunctional DATA-chelator and its conjugate to TOC, DATA-TOC, showed the potential to establish an instant kit-type labelling routine for ^{68}Ga [23,31]. To show that the DATA chelator does not negatively affect the receptor affinity and the *in vivo* performance of the targeting vector, [$^{68/nat}$Ga]Ga-DATA-TOC was evaluated in a series of *in vitro*- and *in vivo*-studies and directly compared with [$^{68/nat}$Ga]Ga-DOTA-TOC.

Radiolabeling with ^{68}Ga for animal studies was completed at 25 °C for DATA-TOC, whereas for DOTA-TOC was a higher temperature required achieving comparable labeling efficiency. This finding corroborates previously reported radiochemical data for convenient kit-type labelling of DATA-TOC with ^{68}Ga [23]. It should be stressed that upscaling the radiolabeling from animal to patient synthesis levels was successful without applying higher than 25 °C temperatures, but by optimizing the amount of DATA-TOC and buffer used.

The $hsst_2$-affinities of [^{nat}Ga]Ga-DATA-TOC and [^{nat}Ga]Ga-DOTA-TOC were found very comparable with almost equivalent IC_{50} values (figure 3), revealing the suitability of DATA-chelator as a means for convenient and successful labelling of TOC with ^{68}Ga.

Furthermore, first animal studies comparing [^{68}Ga]Ga-DATA-TOC to [^{68}Ga]Ga-DOTA-TOC showed similar biodistribution and kinetic profiles. The uptake in the tumors was specific, reaching comparable values and following similar kinetics. The almost linear tumor to blood curves (SUR) of both radiotracers seemed to be like the ^{18}FDG-kinetics an result of a nearly irreversible trapping and could be described by a irreversible two tissue compartment model [33,34]. The tumor accumulation of both radiotracers was blocked by [NaI^3]-Octreotide acetate to all about the same activity concentration in the tumors. The pancreatic [^{68}Ga]Ga-DOTA-TOC uptake in the mice was also blocked by the Octreotide injection supporting the detection of natural expressing $mSSTR_2$. The baseline uptake of the [^{68}Ga]Ga-DATA-TOC in the pancreas was lower and showed therefore no significant difference between the control and blocking experiments.

The tumor-to-tissue ratios during biodistribution or small animal PET. The observed tumor-to-tissue ratios were in good agreement with $hsst_2$-affinities of the two analogs. Similarly, the first comparison of [^{68}Ga]Ga-DATA-TOC and [^{68}Ga]Ga-DOTA-TOC in a 46-year old NET patient showed comparable uptake in the tumor lesions. Although [^{68}Ga]Ga-DATA-TOC resulted in a lower overall tumor uptake (SUV: 46.9), a significantly better tumor-to-liver ratio of 5.15 (compared to 3.08 for [^{68}Ga]Ga-DOTA-TOC) could be achieved, facilitating the visualization of liver metastases.

CONCLUSION

In conclusion, the [$^{68/nat}$Ga]Ga-DATA-TOC achieved similar or improved results in affinity and imaging studies, maintaining the considerable advantage of fast mild radiolabelling (pH 4.5-6 and 25 °C) over the [^{68}Ga]Ga-DOTA-TOC. This advantage reveals the DATA chelator as an elegant tool towards establishing radiolabeling with ^{68}Ga for sensitive target vectors, which can´t be assessed with the DOTA chelator due to degradation under radiolabeling conditions (pH 3-4 and > 90 °C).

ACKNOWLEDGEMENT

The authors greatly acknowledge the excellent technical assistance of Andrea Suhr, Regina Herrlich, and Sebastian Meister. MPC 4/30PRR cells were kindly provided by Prof. Arthur Tischler.

SUPPORTING INFORMATION

Synthetic part

The DATA-TOC chelator was synthesized in a 8 step synthesis starting from 2-nitrocyclohexanone, where the ready for coupling TOC was purchased from ABX GmbH (Radeberg, Germany). The final product was purified by HPLC (24 % B isocratic on a Luna 10 µm (C18) 100 A (250 mm×21.23 mm, 10 µm); eluent A: 0.1 % (v/v) TFA in H_2O; eluent B: 0.1 % (v/v) TFA in MeCN). The cold complexes [^{nat}Ga]Ga-DATA-TOC and [^{nat}Ga]Ga-DOTA-TOC were synthesized after treatment of the respective peptide conjugates with excess $^{nat}GaCl_3$ and were purified by HPLC (Luna 10 µm (C18) 100 A (250 mm×10 mm, 10 µm); A: H_2O, B: MeCN). The retention time of [^{nat}Ga]Ga-DOTA-TOC was 18.6 min and 19.9 for [^{nat}Ga]Ga-DATA-TOC (gradient: 5 % B to 50 % B in 20 min). LTT-SS28 (H-Ser-Ala-Asn-Ser-Asn-Pro-Ala-Leu-Ala-Pro-Arg-Glu-Arg-Lys-Ala-Gly-c[Cys-Lys-Asn-Phe-Phe-DTrp-Lys-Thr-Tyr-Thr-Ser-Cys]-OH) was purchased from Bachem. DOTA-TOC was purchased by ABX GmbH (Radeberg, Germany).

Radiolabelling

^{68}Ga was eluted from a ^{68}Ge/^{68}Ga-generator (iThemba Labs, or IDB Holland) with 1 M HCl or water. The final HCl-concentration in the eluates from both generators was approximately 1 M. The pH of the fractionated ^{68}Ga-eluate (300 µL) was adjusted to pH 4.0–4.5 using 2 M NH_4OAc. A solution of $^{68}Ga(OAc)_3$ in acetate buffer was added to 20 nmol of each peptide. The reaction mixture was shaken for 15 min at 80 °C to afford [^{68}Ga]Ga-DOTA-TOC or at 25 °C to afford [^{68}Ga]Ga-DATA-TOC. Reaction mixtures were analyzed by radio-HPLC.

HPLC was performed on a Series 1200 device (Agilent) equipped with the Ramona ß/γ-ray detector (Raytest). Eluent A: 0.1 % (v/v) TFA in H_2O; eluent B: 0.1 % (v/v) TFA in MeCN; HPLC system: Zorbax (Agilent) SB-C18, 300 Å, 4 µm, 250 mm×9.4 mm; gradient elution using 95 % eluent A to 95 % eluent B in 10 min, 50 °C. Radiolabelled conjugates with radiochemical purity higher than 95 % were used for subsequent biological experiments after filtering the labelling reaction mixture (45 µm pore size, RE-ZIST 13/0.45 PTFE, Schleicher & Schuell). Filtrates were diluted with electrolyte solution 0.1 mL electrolyte solution E-153 (Serumwerk Bernburg, Germany) to a final concentration of about 80 MBq/mL [29,30].

Radiotracer stability was assessed separately for trans-chelation (against apotransferrin and DTPA) and trans-metalation (against Fe^{III}) at 37 °C and pH 7 in phosphate-buffered saline (PBS), applying radio-HPLC [23].

For the preparation of [^{125}I-Tyr^{25}]LTT-28, [^{125}I]NaI was provided by PerkinElmer in dilute sodium hy-

droxide solution pH 8-11 in an activity concentration of 365.39 mCi/mL. Radioiodination was performed according to the chloramine-T method using 0.1 M D,L-methionine to quench the reaction and the radioligand was isolated by HPLC, as previously described [24–26].

Reagents and Cell Lines

The HEK293 cell line transfected to stably express the human sst_2 (HEK293-$hsst_2$) used for receptor affinity assessments was a kind gift of Prof. S. Schultz (Institute of Pharmacology and Toxicology, University Hospital, Friedrich Schiller University Jena, Germany). Cells were cultured at 37 °C and 5 % CO_2 in Dulbecco's modified eagle medium containing 10 % fetal bovine serum, 100 U/mL penicillin, 100 mg/mL streptomycin, and 500 mg/mL G418, as previously described [24,25]. All culture reagents were from Gibco BRL, Life Technologies or from Biochrom KG Seromed.

The recently established mouse MPC-mCherry cells [31] with high expressing $mSSTR_2$ ($mSSTR_2$, $\approx 10^5$ sites/cell) were derived from lentivirally gene-modified MPC cells; clone 4/30PRR, passage 32) [32], cultured and prepared for in vivo application, as previously described [31]. Shortly, mouse pheochromocytoma cells (MPC 4/30PRR) were cultured in collagen coated flasks and maintained in RPMI 1640 including HEPES (GIBCO) in a humidified 5 % CO_2/95 % (v/v) O_2 atmosphere at 37 °C. Culture medium was supplemented with 10 % (v/v) heat inactivated horse serum (GIBCO), 5% (v/v) fetal bovine serum superior (BIOCHROM) and 0.1 % (v/v) gentamicin (GIBCO) and replaced every 48-72 h. Cells were routinely passaged every 7-10 d. Before injection into animals cells at 70-80% confluence were detached using 0.05 % (w/v) Trypsin-EDTA in magnesium- and calcium-free phosphate buffered saline and adjusted to a concentration of $2 \cdot 10^6$ cells per 60 µL in 50 % (v/v) Matrigel (BD Biosciences)/phosphate buffered saline.

Competition Binding Assays

Competition binding experiments were performed for [^{nat}Ga]Ga-DATA-TOC and [^{nat}Ga]Ga-DOTA-TOC in HEK293-$hsst_{2/3/5}$ cell membranes, harvested as previously described [26]. [^{125}I-Tyr^{25}]LTT-28 served as radioligand and [LTT]SS-28 ([Leu^8,DTrp^{22},Tyr^{25}]SS-28) as reference compound [24,25,27]. In brief, radioligand (70 µL, 50 pM corresponding to ≈ 40,000 cpm), test peptide (30 µL solution of increasing concentrations, 10^{-5}-10^{-13} M) and membrane homogenates (200 µL) were added in each assay tube (total volume of 300 µL in binding solution: 50 mM HEPES pH 7.4, 1 % BSA, 5.5 mM $MgCl_2$, 35 µM bacitracin); triplicates for each concentration point were used. Samples were incubated for 60 min at 22 °C in an Incubator-Orbital Shaker unit, (MPM Instr. SrI). Ice-cold washing buffer (10 mM HEPES pH 7.4, 150 mM NaCl) was added, followed by rapid filtration over glass fiber filters (Whatman GF/B, pre-soaked for 2 h in a 1 % polyethyleneimine, PEI, aqueous solution) on a Brandel Cell Harvester (Adi Hasel Inginieur Büro) and by rinsing the filters with ice-cold washing buffer. Filters were collected and their activity

was counted in a γ-counter (automated well-type multi-sample gamma counter; NaI(Tl) 3´´ crystal, Canberra Packard Auto-Gamma 5000 series instrument). The half maximal inhibitory concentration (IC_{50}) values were calculated by nonlinear regression according to a one-site model applying the PRISM 2 program (Graph Pad Software) and represent mean IC_{50}±sd from n experiments performed in triplicate; [^{nat}Ga]Ga-DATA-TOC (n=3), [^{nat}Ga]Ga-DOTA-TOC (n=2) and LTT-SS-28 (n=3).

Animal experiment

Animal experiments were carried out at the HZDR according to the guidelines of German Regulations for Animal Welfare and have been approved by the Landesdirektion Dresden. A number of $2 \cdot 10^6$ MPC-EGFP-Luc cells (passage 13) were injected intravenously in 6 weeks old female SCID/beige mice (Harlan, Netherlands). General anesthesia was induced and maintained with inhalation of 10 % (v/v) desflurane in 30/10 (v/v) oxygen/air during imaging studies. Body weight (BW) was measured every 3-4 days. Luminescence distribution in the mice was imaged once a week.

***In vivo* biodistribution**

Four animals (body weight 36.3 ± 2.1 g) for each radiotracer were injected intravenously into a tail vein with approximately 2.3 MBq (0.06 µCi) in 0.1 mL electrolyte solution E-153 (Serumwerk Bernburg, Germany) without (control) or with simultaneous injection of 100 µg/mouse [Nal^3]Octreotide acetate (blocked). Animals were euthanized at 60 min post-injection. Blood, tumor and the major organs were collected, weighed, and counted in a cross-calibrated γ-counter (Isomed 1000, Isomed GmbH, Dresden) and Wallac WIZARD Automatic Gamma Counter (PerkinElmer, Germany). The activity of the tissue samples was decay-corrected and calibrated by comparing the counts in tissue with the counts in aliquots of the injected radiotracer that had been measured in the γ-counter at the same time. The activity in the selected organs was expressed as percent-injected dose per organ (%ID) and the activity concentration in tissues and organs as standardized uptake value (SUV in g/g). Values are quoted as mean ± standard deviation for each group of four animals.

Small animal PET

PET scans were performed using a dedicated rodent PET/CT scanner (NanoPET/CT, Mediso, Budapest). The gas anesthetized (9 % Desfluran, 30 % oxygen in air) female NMRI nu/nu mice with subcutaneous pheochromocytoma (MPC-mCherry) on the right shoulder were positioned on a heated bed along the scanner axis. The ^{68}Ga-labeled peptides (10 MBq/300 µml) were infused over one minute into a tail vein without (control) or with simultaneous injection of 100 µg/mouse [Nal^3]Octreotide acetate (blocked). Two hour dynamic scans were acquired and reconstructed into 38 frames. The following data acquisition parameters were used: 5 ns coincidence window and 250 to 750 keV energy window

in 1–5 coincidence mode. Crystal efficiency correction was applied. For rebinning was a 2D SSRB method applied, with a ring difference of 8, and the reconstruction process was a three-dimensional ordered-subsets exception maximum algorithm (Tera-Tomo-3D, subsets, 6; iterations, 4). Pixel size was 0.5 mm, and the slice thickness was 0.5 mm. Data were analyzed with ROVER (ABX GmbH, Radeberg, Germany). The ROI values were not corrected for recovery and partial volume effects. For each Nano-PET/CT scan, 3D regions of interest (ROIs) were drawn over tumor, heart, muscle, liver and kidney in decay-corrected whole-body orthogonal images.

Statistical analysis

Statistical analysis: Statistical analyses were carried out with GraphPad Prism version 6 (GraphPad Software, San Diego California USA). The data are expressed as mean ± SEM, and were submitted to one-way analysis of variance (ANOVA) followed by Bonferroni correction. Values of $p < 0.05$ were considered statistically significant and indicated by an asterisk (*).

Human studies

A direct comparison between [^{68}Ga]Ga-DATA-TOC and [^{68}Ga]Ga-DOTA-TOC was performed in a 46-year-old male patient with a well-differentiated NET in the body and tail of the pancreas as well as peritumoral lymph-node metastases, first diagnosed in November 2012. The large primary tumor involving the stomach, the spleen and the left adrenal gland was surgically resected (R2) by distal pancreatectomy, partial gastrectomy, splenectomy, left adrenalectomy and omentectomy. Despite octreotide therapy, the disease was progressing and in 2015 the patient was treated by peptide receptor radionuclide therapy (PRRT, administering 5 GBq of [^{90}Y]Y-DATA-TOC). Before the second cycle, restaging was performed (figure 7) on a Biograph mCT FLOW 64 PET/CT from the vertex until mid-thigh exactly 50 min after injection of 117 MBq of [^{68}Ga]Ga-DOTA-TOC and 120 MBq of [^{68}Ga]Ga-DATA-TOC, respectively.

REFERENCES

1. Smith D.L., Breeman W.A.P., Sims-Mourtada J. The untapped potential of Gallium 68-PET: The next wave of ^{68}Ga-agents. Appl. Radiat. Isot. 2013; 76: 14–23.

2. Boros E., Ferreira C.L., Cawthray J.F., Price E.W., Patrick B.O., Wester D.W., Adam M.J., Orvig C. Acyclic chelate with ideal properties for Ga-68 PET imaging agent elaboration. J. Am. Chem. Soc. 2010; 132(44): 15726–33.

3. Eppard E., Wuttke M., Nicodemus P.L., Rösch F. Ethanol-Based Post-processing of Generator-Derived ^{68}Ga Toward Kit-Type Preparation of ^{68}Ga-Radiopharmaceuticals. J Nucl Med. 2014; 55(6): 1023–8.

4. Mueller D., Klette I., Baum R.P., Gottschaldt M., Schultz M.K., Breeman W.A.P. Simplified NaCl based ^{68}Ga concentration and labeling procedure for rapid synthesis of ^{68}Ga radiopharmaceuticals in high radiochemical purity. Bioconjug. Chem. 2012; 23(8): 1712–7.

5. Zhernosekov K.P., Filosofov D. V, Baum R.P., Aschoff P., Bihl H., Razbash A. a, Jahn M., Jennewein M., Rösch F. Processing of generator-produced ^{68}Ga for medical application. J. Nucl. Med. 2007; 48(10): 1741–8.

6. Breeman W.A.P., De Jong M., De Blois E., Bernard B.F., Konijnenberg M., Krenning E.P. Radiolabelling DOTA-peptides with ^{68}Ga. Eur. J. Nucl. Med. Mol. Imaging. 2005. p. 478–85.

7. Graham M., Mailman J. FDA Grants Orphan Drug Designation for ^{68}Ga-DOTATOC. J. Nucl. Med. 2014; 55(1): 2014.

8. Fani M., André J.P., Maecke H.R. ^{68}Ga-PET: a powerful generator-based alternative to cyclotron-based PET radiopharmaceuticals. Contrast Media Mol. Imaging. 2008; 3(2): 53–60.

9. Buchmann I., Henze M., Engelbrecht S., Eisenhut M., Runz A., Schäfer M., Schilling T., Haufe S., Herrmann T., Haberkorn U. Comparison of Ga-68-DOTATOC PET and In-111-DTPAOC (Octreoscan) SPECT in patients with neuroendocrine tumours. Eur. J. Nucl. Med. Mol. Imaging. 2007; 34(10): 1617–26.

10. Tran K., Khan S., Taghizadehasl M., Palazzo F., Frilling A., Todd J.F., AL-Nahhas A. Gallium-68 dotatate PET/CT is superior to other imaging modalities in the detection of medullary carcinoma of the thyroid in the presence of high serum calcitonin. Hell. J. Nucl. Med. 2015; 18(1): 19–24.

11. Mukherjee A., Pandey U., Chakravarty R., Sarma H., Dash A. Single vial kit formulation for preparation of PET radiopharmaceutical: ^{68}Ga-DOTA-TOC. J Radioanal Nuc Chem. 2014; 302: 1253–8.

12. Notni J., Simecek J., Hermann P., Wester H.J. TRAP, a powerful and versatile framework for gallium-68 radiopharmaceuticals. Chem. - A Eur. J. 2011; 17(52): 14718–22.

13. Wängler C., Wängler B., Lehner S., Elsner A., Todica A., Bartenstein P., Hacker M., Schirrmacher R. A Universally Applicable ^{68}Ga-Labeling Technique for Proteins. J. Nucl. Med. 2011; 52(4): 586–91.

14. Eckelman W.C. Unparalleled Contribution of Technetium-99m to Medicine Over 5 Decades. JACC Cardiovasc. Imaging. 2009; 2(3): 364–8.

15. Rösch F. Past, present and future of ^{68}Ge/^{68}Ga generators. Appl. Radiat. Isot. 2013; 76: 24–30.

16. Fani M., Tamma M.L., Nicolas G.P., Lasri E., Median C., Raynal I., Port M., Weber W.A., Mäcke H.R. In vivo imaging of folate receptor positive tumor xenografts using novel Ga-68-NODAGA-folate conjugates. Mol Pharm. 2012; 9(5): 1136–45.

17. Simecek J., Zemek O., Hermann P., Wester H.J., Notni J. A monorective bifunctional triazacyclononane phosphinate chelator with high selectivity for Gallium-68. ChemMedChem. 2012; 7(8): 1375–8.

18. Boros E., Ferreira C.L., Yapp D.T.T., Gill R.K., Price E.W., Adam M.J., Orvig C. RGD conjugates of the H_2dedpa scaffold: Synthesis, labeling and imaging with ^{68}Ga. Nucl. Med. Biol. 2012; 39(6): 785–94.

19. Berry D.J., Ma Y., Ballinger J.R., Tavaré R., Koers A., Sunassee K., Zhou T., Nawaz S., Mullen G.E.D., Hider R.C., Blower P.J. Efficient bifunctional gallium-68 chelators for positron emission tomography: tris(hydroxypyridinone) ligands. Chem. Commun. (Camb). 2011; 47(25): 7068–70.

20. Eder M., Wängler B., Knackmuss S., LeGall F., Little M., Haberkorn U., Mier W., Eisenhut M. Tetrafluorophenolate of HBED-CC: A versatile conjugation agent for ^{68}Ga-labeled small recombinant antibodies. Eur. J. Nucl. Med. Mol. Imaging. 2008; 35(10): 1878–86.

21. Waldron B.P., Parker D., Burchardt C., Yufit D.S., Zimny M., Rösch F. Structure and stability of hexadentate complexes of ligands based on AAZTA for efficient PET labelling with gallium-68. Chem. Commun. (Camb). 2013; 49: 579–81.

22. Parker D., Waldron B.P. Conformational analysis and synthetic approaches to polydentate perhydro-diazepine ligands for the complexation of gallium(III). Org. Biomol. Chem. 2013; 11(17): 2827.

23. Seemann J., Waldron B., Parker D., Rösch F. DATATOC: a novel conjugate for kit-type ^{68}Ga labelling of TOC at ambient temperature. EJNMMI Radiopharm. Chem. 2017; 1(1): 4.

24. Maina T., Cescato R., Waser B., Tatsi A., Kaloudi A., Krenning E.P., De Jong M., Nock B.A., Reubi J.C. LTT-SS28, a first pansomatostatin radioligand for in vivo targeting of somatostatin receptor-positive tumors. J. Med. Chem. 2014; 57(15): 6564–71.

25. Tatsi A., Maina T., Cescato R., Waser B., Krenning E.P., de Jong M., Cordopatis P., Reubi J.C., Nock B. a. [^{111}In-DOTA]Somatostatin-14 analogs as potential pansomatostatin-like radiotracers - first results of a preclinical study. EJNMMI Res. 2012; 2(1): 25.

26. Maina T., Nock B., Nikolopoulou A., Sotiriou P., Loudos G., Maintas D., Cordopatis P., Chiotellis E. [^{99m}Tc]Demotate, a new ^{99m}Tc-based [Tyr3]octreotate analogue for the detection of somatostatin receptor-positive tumours: Synthesis and preclinical results. Eur. J. Nucl. Med. 2002; 29(6): 742–53.

27. Patel Y.C., Srikant C.B. Subtype selectivity of peptide analogs for all five cloned human somatostatin receptors (hsstr 1-5). Endocrinology. 1994; 135(6): 2814–7.

28. Seemann J., Waldron B.P., Rösch F., Parker D. Approaching "kit-type" labelling with ^{68}Ga: The DATA chelators. ChemMedChem. 2015; 10(6): 1019–26.

29. Kilian T.-M., Klöting N., Bergmann R., Els-Heindl S., Babilon S., Clément-Ziza M., Zhang Y., Beck-Sickinger A.G., Chollet C. Rational Design of Dual Peptides Targeting Ghrelin and Y2 Receptors to Regulate Food Intake and Body Weight. J. Med. Chem. 2015; 58(19),4180-4193.

30. Chollet C., Bergmann R., Pietzsch J., Beck-Sickinger A.G. Design, evaluation, and comparison of ghrelin receptor agonists and inverse agonists as suitable radiotracers for PET imaging. Bioconjug. Chem. 2012; 23(4): 771–84.

31. Ullrich M., Bergmann R., Peitzsch M., Cartellieri M., Qin N., Ehrhart-Bornstein M., Block N.L., Schally A. V., Pietzsch J., Eisenhofer G., Bornstein S.R., Ziegler C.G. In vivo fluorescence imaging and urinary monoamines as surrogate biomarkers of disease progression in a mouse model of pheochromocytoma. Endocrinology. 2014; 155(11): 4149–56.

32. Ullrich M., Bergmann R. Peitsch M., Zenker E. F., Cartellieri M., Bachmann M., Ehrhart-Bronstein M., Block N. L., Schally A. V., Eisenhofer G., Bornstein S. R., Pietzsch J., Ziegler C. G. Multimodol somatostatin receptor theranostics using [^{64}Cu]Cu-/[^{177}Lu]Lu-DOTA-[Tyr^{3}]octreotate and AN-238 in a mouse pheochromoxytoma model. Thernostics. 2016; 6: 650-665

33. van den Hoff J., Oehme L., Schramm G., Maus J., Lougovski A., Petr J., Beuthien-Baumann B., Hofheinz F. The PET-derived tumor-to-blood standard uptake ratio (SUR) is superior to tumor SUV as a surrogate parameter of the metabolic rate of FDG. EJNMMI Research. 2013; 3: 77

34. van den Hoff J. Principles of quantitative positron emission tomography. Amino Acids. 2005;29:341-353.

4.3 Novel bifunctional DATA chelator for quick access to site-directed PET ^{68}Ga-radio-tracers: Preclinical proof-of-concept with [Tyr^3]octreotide

Novel bifunctional DATA chelator for quick access to site-directed PET ^{68}Ga-radiotracers: Preclinical proof-of-principle with [Tyr^3]octreotide

B. A. Nock [1], A. Kaloudi[1], J. Nagel[2], J.-P. Sinnes[2], F. Rösch[2], T. Maina[1]

[1]Molecular Radiopharmacy, INRASTES, NCSR "Demokritos", GR-15310 Athens, Greece

[2]Institute of Nuclear Chemistry, Johannes Gutenberg-University of Mainz, D-55126 Mainz, Germany

ABSTRACT

Molecular imaging of tumors with the PET radionuclide ^{68}Ga has gained momentum in clinical oncology due to the expanding availability of commercial ^{68}Ge/^{68}Ga-generators in combination with state-of-the-art PET/CT and PET/MRI hybrid imaging systems. Concurrently, interesting peptide-based or small-size vectors have been developed for theranostic use in cancer patients. Owing to the short half-life of ^{68}Ga ($t_{1/2}$=67.7 min) and the sensitivity of many targeting biomolecules, labeling and kit reconstitution in mild conditions allowing for quick access to ready-for-injection PET-tracers are highly desirable. The novel DATA^{5M} ((6-pentanoic acid)-6-(amino(methyl))-1,4-diazepinetriacetate) chelator previously showing pro-mising qualities for kit type labeling, was coupled to TOC ([Tyr^3]octreotide). We herein report results from a first proof-of-principle study directly comparing of [^{67}Ga]Ga-DATA-TOC with the well-established [^{67}Ga]Ga-DOTA-TOC in a series of preclinical models. Both analogs were shown to be sst_2-preferring and specifically internalized in AR42J and HEK293-$hsst_2$ cells, with [^{67}Ga]Ga-DOTA-TOC internalizing faster in both cell lines. Similarly, after injection in mice bearing either AR42J or HEK293-$hsst_2$ tumors, both tracers efficiently and specifically localized in the implants. Whereas [^{67}Ga]Ga-DOTA-TOC exhibited higher tumor values, [^{67}Ga]Ga-DATA-TOC cleared faster from background tissues. These findings support the suitability of newly introduced bifunctional chelator DATA^{5m} as reliable, quick and convenient means for labeling of medically relevant vectors with the PET radiometal ^{68}Ga.

Keywords: Gallium-67, Octreotide, DATA-TOC, DOTA-TOC, Somatostatin,

INTRODUCTION

Recent advances in the field of nuclear medicine involve the use of peptide-based vectors radiolabelled with diagnostic (suitable for SPECT or PET imaging) or particle emitting radiometals (suitable for radionuclide therapy) in an integrated theranostic approach, allowing for personalized management of cancer patients [1–5]. Molecular imaging of tumors with the PET radionuclide ^{68}Ga has gained momentum in clinical oncology due to the expanding availability of commercial ^{68}Ge/^{68}Ga-generators in combination with state-of-the-art PET/CT and PET/MRI hybrid imaging systems [6–10]. Furthermore, functionalization of clinically relevant vectors with the universal chelator DOTA (1,4,7,10-tetraazacyclododecane-1,4,7,10-tetraacetic acid) has facilitated labeling of the same radiopharmaceutical-precursor with theranostic radiometal pairs, such as ^{68}Ga and ^{177}Lu or ^{90}Y for PET imaging and radionuclide therapy, respectively [11]. In this respect, the recent approval by FDA of [^{68}Ga/^{177}Lu]Ga/Lu-DOTA-TATE (TATE: DPhe-c[Cys-Tyr-DTrp-Lys-Thr-Cys]-Thr-OH) as a theranostic pair in the management of neuroendocrine tumors (NETs) represents a significant success.

The application of ^{68}Ga-based PET radiotracers in the clinic will be further propagated by the availability of freeze-dried formulations of the radiopharmaceutical precursor, “kits”, in analogy to the widely popular ^{99m}Tc-kits dominating diagnostic nuclear medicine in the previous decades. Owing to the short half life of ^{68}Ga ($t_{1/2}$=67.7 min) on one hand and the sensitivity of many targeting biomolecules on the other, labeling and kit reconstitution at ambient temperature to quickly provide a ready-for-injection ^{68}Ga-radiotracer are highly desirable. For such purposes, chelators other than DOTA would be preferable for ^{68}Ga-labeling, especially when taking into account a few recent findings. First, the distinct coordination chemistries of Ga and Lu with DOTA have often led to significant differences in biological responses, especially with regards to pharmacokinetics, tumor targeting efficacy and retention [11]. Then, accumulating experience has shown that diagnostic imaging and radionuclide therapy may be best served by a pair of a diagnostic and a therapeutic version of the vector, each addressing distinct application requirements [12,13].

As a result, several new chelators more appropriate for ^{68}Ga-labeling of clinically attractive vectors have been introduced over the past few years. These predominantly display either acyclic behavior, associated with better labeling kinetics (e.g. DFO, deferoxamine), or cyclic characteristics, resulting in higher thermodynamic stability of the forming metal-chelate (e.g. NOTA, 1,4,7-triazacyclononane-1,4,7-triacetic acid) [11,14–23]. In an innovative approach, chimeric-type tri-anionic chelators have been lately introduced, based on the 6-amino-1,4-diazepine-triacetic acid (DATA)-scaffold and exhibiting both cyclic and acyclic features [24–26]. The novel DATA chelators have shown promising properties for kit-type labeling of state-of-the-art ^{68}Ga-radiopharmaceuticals over existing alternatives, because they allow for fast and quantitative labeling within a wider labeling pH range at ambient temperature. Furthermore, the forming ^{68}Ga-chelates are stable towards trans-chelation (DTPA and apo-

transferrin) and trans-metalation (Fe^{III}).

In a next critical step, the first bifunctional pro-chelator DATA^{5M}-(^{t}Bu)$_3$ (5-[1,4-Bis-*tert*-butoxycarbonyl-methyl-6-(*tert*-butoxycarbonylmethylmethylamino)-[1,4]diazepan-6-yl]-pentanoic acid) was developed for convenient conjugation to selected primary amines of clinically interesting vectors. As a first paradigm, DATA^{5M}-(^{t}Bu)$_3$ was coupled to the primary amine of DPhe^1 of [Tyr^3]octreotide (TOC, DPhe-c[Cys-Tyr-DTrp-Lys-Thr-Cys]-Thr-ol) to yield DATA-TOC. Excessive study on the ^{68}Ga-labeling of DATA-TOC has shown that a high quality radiopharmaceutical can be prepared in excellent radiochemical yield from a lyophilized solid at room temperature and within a short time that does not require post-labeling purification to meet pharmacopeia standards [26,27].

In the present preclinical proof-of-principle study we aimed to further explore the suitability of the new semi-cyclic bifunctional chelator DATA for ^{68}Ga-labeling of clinically interesting vectors. For this purpose, the effects of the new coordination chemistry on the responses of the resulting radiopharmaceutical in the biological milieu were investigated for the first time using as paradigm-vector the somatostatin receptor subtype 2 (sst2)-specific TOC. Specifically, the biological profiles of [^{68}Ga]Ga-DATA-TOC and the well-established [^{68}Ga]Ga-DOTA-TOC [10,28] (figure 1) were directly compared in a series of *in vitro* and *in vivo* models using the respective surrogates labeled with longer-lived and practically more convenient ^{67}Ga ($t_{1/2}$=3.3 d).

RESUTLS AND DISSCUSION

Ligands and Radioligands

The DATA pro-chelator DATA^{5M}-3^{t}Bu was synthesized and coupled to TOC, as previously described [26,27]. The [^{67}Ga]Ga-DATA-TOC and [^{67}Ga]Ga-DOTA-TOC surrogates were used for convenience in all biological evaluations in AR42J and HEK-293-hsst$_x$ (x: 2, 3 and 5) cells and tumor-bearing mice [29], in view of the longer half life of the gamma emitter ^{67}Ga ($t_{1/2}$=3.3 d) compared to ^{68}Ga ($t_{1/2}$=67.7 min). Labeling with ^{67}Ga was quantitative after 15 min at room temperature (pH 4.0) for DATA-TOC and after 30 min at 90 ^{o}C (pH 4.0) for DOTA-TOC at a specific activity 3.7 MBq/nmol, as verified by radioanalytical HPLC. Both radiotracers were used in all subsequent biological experiments without further purification.

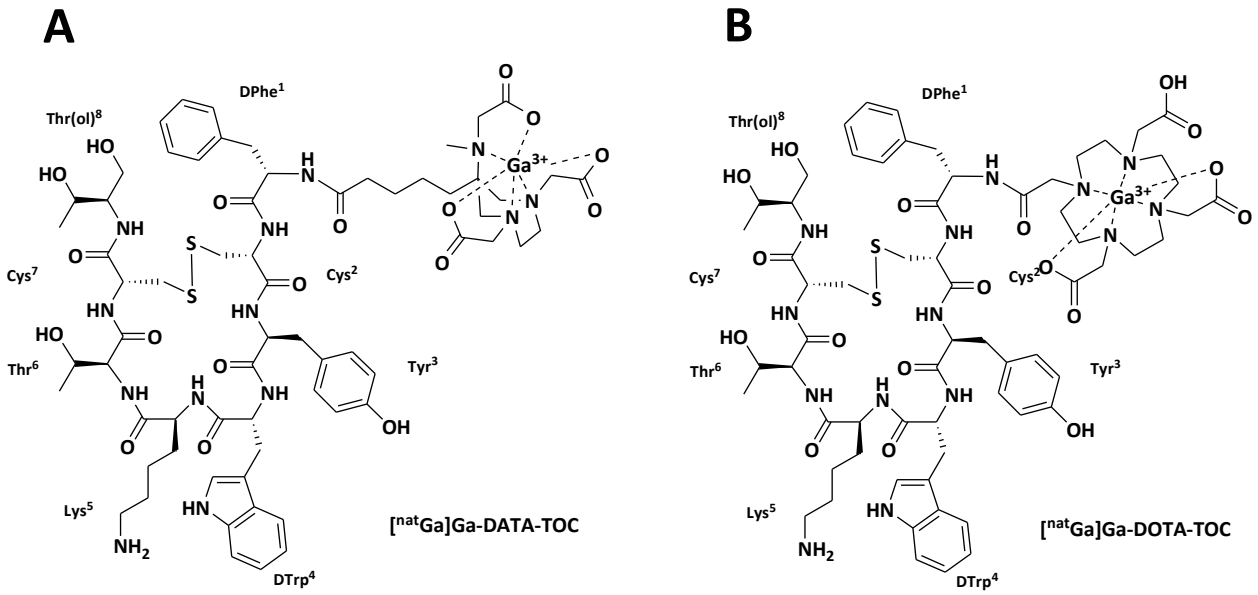

Figure 1: Chemical structure of [^{nat}Ga]Ga-DATA-TOC (**A**) and [^{nat}Ga]Ga-DOTA-TOC (**B**)

In Vitro Comparison of [^{67}Ga]Ga-DATA-TOC and [^{67}Ga]Ga-DOTA-TOC

The binding affinity of the ^{nat}Ga-peptide conjugates for the hsst$_2$ has been determined by competition binding assays against the pansomatostatin radioligand [^{125}I-Tyr^{25}]LTT-SS28 in HEK293-hsst$_2$ cell membranes using LTT-SS28 (H-Ser-Ala-Asn-Ser-Asn-Pro-Ala-Leu-Ala-Pro-Arg-Glu-Arg-Lys-Ala-Gly-c[Cys-Lys-Asn-Phe-Phe-DTrp-Lys-Thr-Tyr-Thr-Ser-Cys]-OH) as a pansomatostatin reference [30–32]. The *IC$_{50}$* values measured previously from these assays were 1.03±0.08 nM for [^{nat}Ga]Ga-DATA-TOC, 0.21±0.01 nM for [^{nat}Ga]Ga-DOTA-TOC and 0.05±0.01 nM for LTT-SS28 [33]. It should be noted that LTT-SS28 displayed sub-nM affinity also for hsst$_3$ (*IC$_{50}$*=0.09±0.01 nM) and hsst$_5$ (*IC$_{50}$*=0.17±0.03 nM), determined in HEK293-hsst$_3$ and HEK293-hsst$_5$ cell membranes. In contrast, [^{nat}Ga]Ga-DATA-TOC and [^{nat}Ga]Ga-DOTA-

TOC were found to be $hsst_2$-prefering, showing indistinguishable specific from non-specific binding in the concentration range applied.

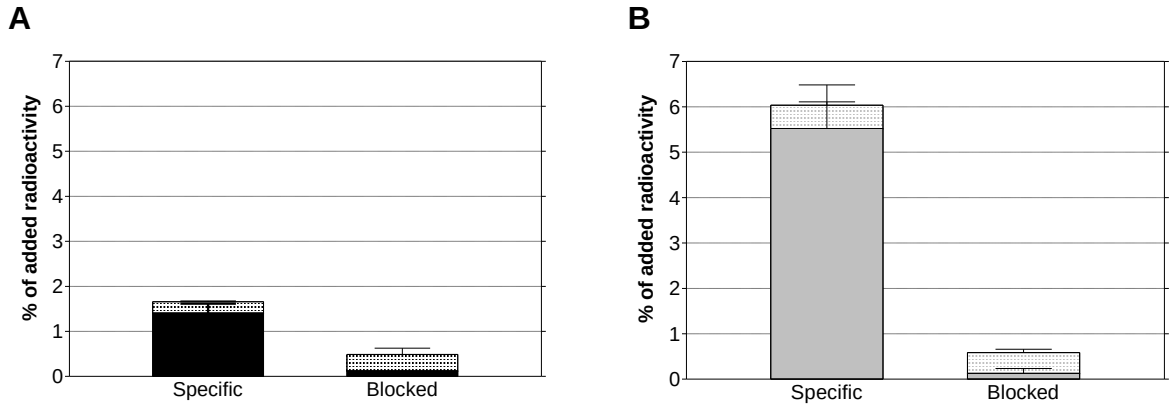

Figure 2: Percentage of cell-associated vs. total-added radioactivity, comprising internalized (solid bars) and membrane-bound fractions (checkered bars) after 1 h incubation at 37 °C of (**A**) [^{67}Ga]Ga-DATA-TOC and (**B**) [^{67}Ga]Ga-DOTA-TOC in AR42J cells; results represent average of two independent experiments performed in triplicate±sd; the first bars in each diagram represent specific values, followed by lower bars of non-specific values determined in the presence of excess TATE (1 µM).

The internalization and overall cell-binding capacity of [^{67}Ga]Ga-DATA-TOC and [^{67}Ga]Ga-DOTA-TOC were compared in AR42J cells spontaneously expressing the rat sst_2 [34] as well as in HEK293-$hsst_x$ cells (x: 2, 3 and 5) during 1 h incubation at 37 °C. As shown in figure 2, within this period the percentage of AR42J cell-bound activity reached 1.66±0.19 % for [^{67}Ga]Ga-DATA-TOC, while for [^{67}Ga]Ga-DOTA-TOC this value was 6.04±1.03 % (P<0.05). In both cases the bulk of cell-bound radioactivity was found within the cells with a small fraction still found on the cell membrane, as consistent with a receptor-agonist profile. In the presence of excess TATE in the medium cell-binding was 0.49±0.14 % and 0.59±0.17 %, respectively, suggesting an sst_2-mediated process.

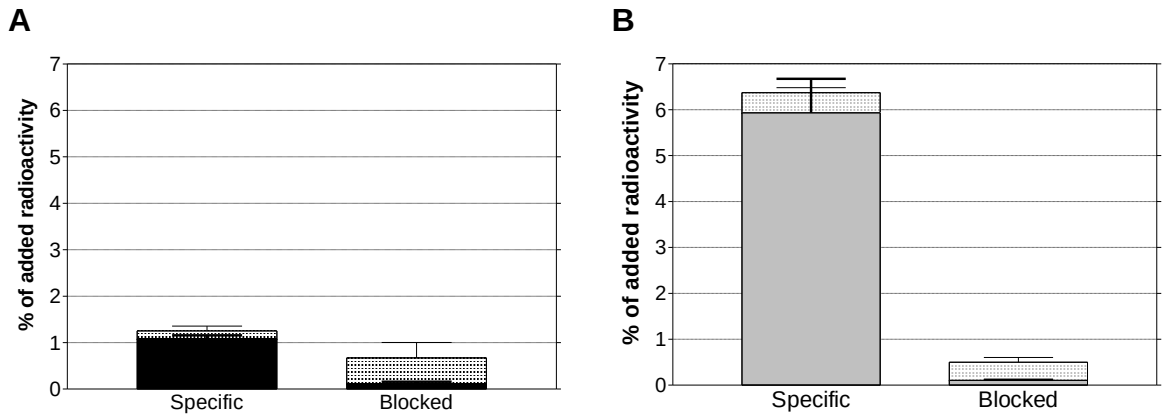

Figure 3: Percentage of cell-associated vs. total-added radioactivity, comprising internalized (solid bars) and membrane-bound fractions (checkered bars) after 1 h incubation at 37 °C of (**A**) [^{67}Ga]Ga-DATA-TOC and (**B**) [^{67}Ga]Ga-DOTA-TOC in HEK293-$hsst_2$ cells; results represent average of four independent experiments performed in triplicate±sd; the first bars in each diagram represent specific values, followed by lower bars of non-specific values determined in the presence of excess TATE (1 µM).

A very similar pattern was acquired from the same series of experiments in HEK293-$hsst_2$ cells. As shown in figure 3, the percentage of cell-associated activity of [^{67}Ga]Ga-DATA^{5M}-TOC amounted to 1.23±0.16 %, while again [^{67}Ga]Ga-DOTA-TOC well surpassed this value with 6.34±0.78 % (P<0.05). The bulk of radioactivity was found internalized in the cells, whereas overall cell-binding was banned in the presence of excess TATE in the medium. It should be noted that in the case of HEK293-$hsst_3$ or HEK293-$hsst_5$ cells, specific cell-binding was indistinguishable from non-specific (in the presence of 1 μM KE108: Tyr-c[D-diaminobutyric acid-Arg-Phe-Phe-DTrp-Lys-Thr-Phe]) [35] for either radioligand. This finding is in line with the lack of measurable binding affinity for the $hsst_3$ or $hsst_5$ of the two metalated peptide-conjugates, assessed during competition binding assays in the respective cell membranes.

Comparative Biodistribution of [^{67}Ga]Ga-DATA-TOC and [^{67}Ga]Ga-DOTA-TOC in Tumor-Bearing Mice

The tissue distribution of [^{67}Ga]Ga-DATA^{5M}-TOC and [^{67}Ga]Ga-DOTA-TOC was compared in male SCID mice bearing subcutaneous AR42J tumors or HEK293-$hsst_2$ xenografts. No further biodistribution experiments were performed in mice bearing HEK293-$hsst_3$ or HEK293-$hsst_5$ xenografts due to the lack of $hsst_3$/$hsst_5$-affinity displayed by the metalated peptide-conjugates as well as due to the inability of either ^{67}Ga-radioligand to specifically bind to HEK293-$hsst_3$ or HEK293-$hsst_5$ cells *in vitro*.

Table 1: Comparative biodistribution data of [^{67}Ga]Ga-DATA-TOC and [^{67}Ga]Ga-DOTA-TOC in AR42J tumor-bearing SCID mice at 1 h and 4 h p.i.; a: For *in vivo* sst_2-blockade 50 nmol TATE were co-injected together with the radioligand and this group included 3 animals in total; b: *in vivo* sst_2-blockade mice groups not included

%ID/g tissue±sd, n=5

Organs	[^{67}Ga]Ga-DATA-TOC			[^{67}Ga]Ga-DOTA-TOC	
	1 h	4 h	4 h+ TATE[a]	1 h	4 h[b]
Blood	1.13±0.19	0.42±0.04	0.56±0.05	0.67±0.13	0.12±0.01
Liver	0.73±0.08	0.46±0.05	0.51±0.08	0.89±0.12	0.75±0.02
Heart	0.54±0.10	0.20±0.03	0.20±0.04	0.53±0.11	0.19±0.03
Kidneys	12.62±2.72	7.21±1.83	9.38±0.70	10.83±2.39	10.97±3.30
Stomach	4.21±0.91	3.48±0.68	0.51±0.12	11.25±1.60	7.47±1.62
Intestines	2.11 ±0.16	2.62±0.40	0.65±0.09	3.66±0.34	3.57±0.54
Spleen	0.91±0.15	0.61±0.12	0.47±0.11	1.65±0.26	1.24±0.54
Muscle	0.22±0.07	0.06±0.03	0.06±0.01	0.16±0.04	0.06±0.02
Femur	0.86±0.13	0.61±0.04	0.62±0.05	0.76±0.20	0.43±0.10
Pancreas	3.50±0.79	1.00±0.17	0.27±0.05	11.92±2.79	5.61±0.83
Tumor	**22.31±1.87**	**15.10±1.98**	**0.76±0.09**	**37.10±10.37**	**33.62±7.56**

Biodistribution data in AR42J tumor-bearing mice is summarized in table 1. Thus, [^{67}Ga]Ga-DATA-TOC showed a high tumor uptake of 22.31±1.87 %ID/g at 1 h p.i., declining to 15.10±1.98 %ID/g at 4 h p.i. Tumor values dropped to as low as 0.76±0.09 %ID/g at 4 h p.i. after coinjection of 50 nmol TATE, as expected for a sst_2-specific uptake. The corresponding values for [^{67}Ga]Ga-DOTA-TOC in the AR42J tumors were higher, reaching 37.10±10.37 %ID/g at 1 h p.i. and 33.62±7.56 %ID/g at 4 h p.i. This finding

is in line with the faster internalization rate of [^{67}Ga]Ga-DOTA-TOC *vs*. [^{67}Ga]Ga-DATA-TOC in AR42J cells observed *in vitro*. Both tracers cleared rapidly from background tissues predominantly via the kidneys and the urinary tract. It should be noted that [^{67}Ga]Ga-DATA-TOC cleared more rapidly from most physiological tissues than [^{67}Ga]Ga-DOTA-TOC, showing lower radioactivity levels e.g. in the pancreas, the stomach and in the kidneys.

Table 2: Comparative biodistribution data of [^{67}Ga]Ga-DATA-TOC and [^{67}Ga]Ga-DOTA-TOC in HEK293-hsst$_2$ xenograft-bearing SCID mice at 1 h and 4 h p.i.; a: For *in vivo* sst$_2$-blockade 50 nmol TATE were co-injected together with the radioligand and this group included 3 animals in total; b: *in vivo* sst$_2$-blockade mice groups not included

%ID/g tissue±sd, n=5

Organs	[^{67}Ga]Ga-DATA-TOC			[^{67}Ga]Ga-DOTA-TOC	
	1 h	4 h	4 h+ TATE[a]	1 h	4 h[b]
Blood	1.11±0.29	0.40±0.05	0.70±0.05	0.66±0.21	0.10±0.02
Liver	0.66±0.10	0.43±0.10	0.54±0.09	0.77±0.16	0.40±0.01
Heart	0.52±0.16	0.19±0.03	0.25±0.06	0.50±0.14	0.17±0.02
Kidneys	15.45±2.71	6.35±1.39	14.11±1.91	12.47±2.76	9.73±1.82
Stomach	2.96±0.94	2.35±0.69	0.19±0.03	12.30±2.88	7.89±2.39
Intestines	1.59 ±0.28	2.12±0.60	0.99±0.15	3.08±0.69	3.68±0.44
Spleen	1.04±0.37	0.50±0.09	0.41±0.07	1.99±0.57	1.32±0.06
Muscle	0.17±0.05	0.07±0.04	0.08±0.01	0.15±0.05	0.06±0.04
Femur	0.81±0.18	0.77±0.07	0.55±0.04	1.21±0.73	1.09±0.12
Pancreas	2.42±0.64	0.63±0.10	0.21±0.02	9.89±2.21	4.45±0.22
Tumor	**18.78±5.91**	**11.79±3.04**	**0.60±0.12**	**25.69±9.38**	**20.85±5.60**

The respective biodistribution data for [^{67}Ga]Ga-DATA-TOC and [^{67}Ga]Ga-DOTA-TOC in SCID mice bearing HEK293-hsst$_2$ xenografts are included for comparison in table 2 for the 1 h and 4 h p.i. time intervals. Similarly, [^{67}Ga]Ga-DATA-TOC showed a high uptake of 18.78±5.91 %ID/g at 1 h p.i., declining to 11.79±3.04 %ID/g at 4 h p.i. in the HEK293-hsst$_2$ xenografts. This uptake dropped to as low as 0.60±0.12 %ID/g at 4 h after coinjection of 50 nmol TATE, suggesting again hsst$_2$-specific accumulation. The corresponding values for [^{67}Ga]Ga-DOTA-TOC in the HEK293-hsst$_2$ xenografts were likewise higher, reaching 25.69±9.38 %ID/g at 1 h p.i. and 20.85±5.60 %ID/g at 4 h p.i. Differences in the uptake of [^{67}Ga]Ga-DATA-TOC and [^{67}Ga]Ga-DOTA-TOC in HEK293-hsst$_2$ xenografts in mice were in line with differences observed during the *in vitro* internalization and overall cell-binding of the two radiotracers in HEK293-hsst$_2$ cells.

It should be noted that in both AR42J and HEK293-hsst$_2$ tumor models, differences of tumor uptake between [^{67}Ga]Ga-DATA-TOC and [^{67}Ga]Ga-DOTA-TOC were statistically significant despite the rather broad variation of individual values. The latter may be attributed to variations in tumor size, growth-rate and vascularization as well as to the inconsistent extent of necrotic areas across tumors. Undesirable deviations of uptake were observed as a result of tumor non-homogeneity, even though double-tumors were induced in five animals per time point for each analog. This allowed for including a total

number of 10 tumors in uptake-calculations to improve statistics. Interestingly, broad tumor uptake differences could be observed as well between tumors grown in the same animal. Of particular interest is the fact that [^{67}Ga]Ga-DATA-TOC showed considerably high and sst_2-specific uptake in both AR42J and HEK293-$hsst_2$ tumor models, although localization was found lower in comparison to [^{67}Ga]Ga-DOTA-TOC. On the other hand, [^{67}Ga]Ga-DATA-TOC consistently displayed lower accumulation in several physiological tissues, including kidneys, liver, intestines, stomach and pancreas (tables 1 and 2). These findings are in agreement with first results acquired from a NET patient of an ongoing clinical comparison of [^{68}Ga]Ga-DATA-TOC and [^{68}Ga]Ga-DOTA-TOC, revealing higher tumor-to-background ratios for [^{68}Ga]Ga-DATA-TOC during PET/CT [33]. It should be expected that introduction of suitable linkers will further improve the in vivo tumor targeting and overall pharmacokinetics of ^{68}Ga-DATA-derivatized TOC-analogs, as observed during the development of several peptide-radiopharmaceuticals.

CONCLUSION

In this proof-of-principle work, a first head-to-head preclinical comparison of the newly introduced [^{67}Ga]Ga-DATA-TOC with the well-established [^{67}Ga]Ga-DOTA-TOC in biological models was presented. First of all, quantitative labeling with ^{67}Ga was concluded faster and in milder conditions for [^{67}Ga]Ga-DATA-TOC than for [^{67}Ga]Ga-DOTA-TOC, corroborating previous reports. This finding bears significant consequences for the application of "kit"-like formulations for easy, fast and reproducible preparation of ^{68}Ga-radiopharmaceuticals in PET clinical units. Most importantly, it was demonstrated in a first paradigm application using TOC that after replacement of the DOTA chelator in DOTA-TOC by the new DATA chelator the interaction capacity of the end [^{67}Ga]Ga-DATA-TOC radiopharmaceutical with the sst_2 was highly preserved. In view of the above, it is reasonable to assume that the new DATA chelator system representing aspects of new Ga(III)-coordination chemistry can be successfully "translated" in molecular radiopharmaceutical design with attractive perspectives to promote PET imaging with ^{68}Ga in a clinical setting.

ACKNOWLEDGEMENT

This work has been partially supported by the Greek General Secretariat for Research and Technology and the European Regional Development Fund under the Action "Development Grants for Research Institutions—KRIPIS" of OPCE II (to T. M. N. and B. A. N.).

SUPPORTING INFORMATION

Ligands and Radioligands

The DATA pro-chelator DATA^{5M}-3^{t}Bu was synthesized and coupled to TOC, as previously reported [26,27]. DOTA-TOC was purchased by ABX Advanced Biochemical Compounds, GmbH, whereas LTT-SS28 and KE108 were provided by Bachem. TATE used for sst_2-blocking experiments was synthesized as previously described [32].

Lyophilized DATA^{5M}-TOC and DOTA-TOC were dissolved in HPLC-grade H_2O and 50 µL aliquots thereof were stored in Eppendorf Protein LoBind tubes at –20 °C. For labeling, $^{67}GaCl_3$ in dilute HC1 at an activity concentration of 1,100-1,500 MBq/mL was provided by IDB Holland. [^{67}Ga]Ga-DATA^{5M}-TOC and [^{67}Ga]Ga-DOTA-TOC were obtained at specific activities of ≈ 3.7 MBq/nmol peptide-conjugate. Briefly, 5 nmol of each conjugate was mixed with 17-20 MBq of $^{67}GaCl_3$; 1 M sodium acetate was used to adjust the pH of the reaction mixture to 4.0. The mixture was incubated at room temperature for 15 min for [^{67}Ga]Ga-DATA-TOC and at 90 °C for 30 min for [^{67}Ga]Ga-DOTA-TOC. Sodium EDTA (0.1 M, pH 4.0) was added to a final concentration of 1 mM to scavenge traces of "free" $^{67}Ga^{3+}$. For HPLC analysis, a Waters Chromatograph with a 600 solvent delivery system coupled to a Gabi gamma detector (Raytest RSM Analytische Instrumente GmbH) controlled by the Millennium Software was used. A Symmetry Shield RP18 (5 µm, 3.9 mm × 20 mm, Waters) cartridge column was eluted at 1 mL/min flow rate with a linear gradient of 0.1 % aqueous trifluoroacetic acid (TFA) solution and acetonitrile (MeCN), starting from 0 % MeCN with 2 % increase of MeCN/min. Under these conditions [^{67}Ga]Ga-DATA-TOC eluted with a t_r=15.1 min and [^{67}Ga]Ga-DOTA-TOC with a t_r=14.4 min.

Cell-Binding Assays with [^{67}Ga]Ga-DATA^{5M}-TOC and [^{67}Ga]Ga-DOTA-TOC

Cell Lines and Cell Culture

The rat pancreatic tumor cell line AR42J endogenously expressing the sst_2 [34] was kindly provided by S. Mather (St. Bartholomew's Hospital, London, UK) and cultured as previously described [30,32,36]. The HEK293 cell line expressing the human T7-epitope-tagged sst_2 receptor (HEK293-hsst_2) or the human sst_3 or sst_5 receptor (HEK293-hsst_3, HEK293-hsst_5) were a kind gift of S. Schultz (Jena, Germany) and were cultured as previously described [30]. All culture reagents were from Gibco BRL, Life Technologies or from Biochrom KG Seromed.

Radioligand Internalization Assays in AR42J Cells

AR42J cells were seeded in six-well plates (0.7×10^6 cells/well) and left to grow for 48 h. On the day of the experiment cells were washed twice with ice-cold internalization medium (F-12K with 1 % FBS). They were supplied with fresh medium (1.2 mL) and each of [^{67}Ga]Ga-DATA-TOC or [^{67}Ga]Ga-DOTA-TOC (150 µL, 50,000 cpm, 0.5 pmol peptide) was added per well, followed by 0.5 % BSA PBS alone (150 µL, total series) or by a 1 µM TATE solution (0.5 % BSA-PBS; 150 µL, nonspecific series). Cells were incubated at 37 °C for 60 min and incubation was interrupted by removal of the medium and rapid rinsing with ice-cold 0.5 % BSA-PBS. Cells were incubated (2x5 min) at ambient temperature in acid wash buffer (50 mM glycine in 0.1 M NaCl, pH 2.8). Supernatants were collected (membrane-bound radioligand fraction). Cells were rinsed with 0.5 % BSA-PBS, lyzed with 1 M NaOH and collected (internalized radioligand fraction). Collected fractions were measured for their radioactivity content in an automated well-type γ-counter (NaI(Tl)-3´´-crystal, Canberra Packard Auto-Gamma 5000 series model) and the percentage of internalized plus membrane-bound (specific and non-specific) fractions was calculated using the Microsoft Excel program; results represent average±sd values from 2 independent experiments conducted in triplicates.

Radioligand Internalization Assays in HEK293-sst$_{2/3/5}$ Cells

The internalization of [^{67}Ga]Ga-DATA-TOC or [^{67}Ga]Ga-DOTA-TOC was additionally studied in confluent monolayers of HEK293 cells transfected to stably express either the hsst$_2$, the hsst$_3$ or the hsst$_5$ 24 h after seeding the cells (10^6 cells/well) in poly-lysine coated six-well plates. Cells were rinsed twice with ice-cold internalization medium (DMEM Glutamax-I supplemented by 1 % (v/v) FBS). Fresh medium was added (1.2 mL) followed by ^{67}Ga-DATA-TOC or ^{67}Ga-DOTA-TOC (50,000 cpm corresponding to 0.5 pmol total peptide in 150 µL 0.5 % BSA PBS). Non-specific internalization was determined by a parallel series containing 1 µM TATE (HEK293-hsst$_2$ cells), or 1 µM KE108 (HEK293-hsst$_3$ and HEK293-hsst$_5$ cells) and the same procedure was followed as described above. Results represent average±sd values from four independent experiments conducted in triplicates.

Biodistribution Experiments in Tumor-Bearing Mice

Biodistribution in AR42J Tumor-Bearing Mice

For biodistribution experiments, SCID mice of 7 weeks of age (15-20 g) on arrival day (NCSR ‘‘Demokritos’’ Animal House) were subcutaneously injected in both flanks with a suspension of AR42J cells (150 µL inocula of 6.7×10^6 cells in normal saline). Animals were kept under aseptic conditions for 12 d until well-palpable tumors (200-800 mg) were grown at the inoculation sites. At the day of the biodistribution mice were injected in the tail vein in groups of five with [^{67}Ga]Ga-DATA-TOC or [^{67}Ga]Ga-DOTA-TOC (100 µL, 37 kBq, 10 pmol total peptide); three further animals were co-injected with excess TATE (50 nmol) together with the radioligand (blocked animals). Mice were euthanized at 1 and 4 h

p.i. and tumors and tissue samples were collected, weighed and measured for radioactivity in the γ-counter. Biodistribution data were calculated with the aid of suitable standards of the injected dose as mean %ID/g±sd using the Graph Pad Software (Prism^{TM} 2.01). For comparison of values the 2-tailed Student's *t*-test was applied and a *P* value <0.05 was considered statistically significant.

Biodistribution in HEK293-hsst$_2$ Xenograft-Bearing Mice

Inocula (150 μL) containing a suspension of freshly harvested 1.2×10^7 HEK293-hsst$_2$ cells in normal saline were subcutaneously injected in both flanks of SCID mice (17±3 g, six weeks of age on arrival day, NCSR "Demokritos" Animal House Facility). Well-palpable tumors were grown at the inoculation site (300-600 mg) after 3 weeks. On the day of the experiment [^{67}Ga]Ga-DATA^{5M}-TOC or [^{67}Ga]Ga-DOTA-TOC was injected via the tail vein as a 100 μL bolus (37 kBq, 10 pmol total peptide) and the animals were euthanized in groups of five at 1 and 4 h p.i.; for *in vivo* receptor-blockade separate 4-h animal groups of three were co-injected with excess TATE (50 nmol). Biodistribution was subsequently performed as described above.

Animal experiments were carried out in compliance with European and national regulations and were approved by national authorities.

REFERENCES

1. Öberg K. Molecular Imaging Radiotherapy: Theranostic for Personalized Patient Management of Neuroendocrine Tumors (NETs). Theranostics. 2012; 2(5): 448–58.

2. Fani M., Mäcke H.R., Okarvi S.M. Radiolabeled peptides: Valuable tools for the detection and treatment of cancer. Theranostics. 2012; 2(5): 481–501.

3. Baum R.P., Kulkarni H.R., Carreras C. Peptides and receptors in image-guided therapy: Theranostics for neuroendocrine neoplasms. Semin. Nucl. Med. 2012; 42(3): 190–207.

4. Brasse D., Nonat A. Radiometals: towards a new success story in nuclear imaging? Dalt. Trans. 2015; 44(11): 4845–58.

5. Fani M., Peitl P., Velikyan I. Current status of radiopharmaceuticals for the theranostics of neuroendocrine neoplasms. Pharmaceuticals. 2017; 10(1): 1–22.

6. Öberg K. Gallium-68 somatostatin receptor PET/CT: Is it time to replace Indium-111 DTPA octreotide for patients with neuroendocrine tumors? Endocrine. 2012; 42(1): 3–4.

7. Shetty D., Lee Y.S., Jeong J.M. Ga-68-labeled radiopharmaceuticals for positron emission tomography. Nucl. Med. Mol. Imaging (2010). 2010; 44(4): 233–40.

8. Velikyan I. Ga-68-based radiopharmaceuticals: Production and application relationship. Molecules. 2015.

9. Velikyana I. Continued rapid growth in Ga-68 applications: Update 2013 to June 2014. J. Label. Compd. Radiopharm. 2015; 58(3): 99–121.

10. Antunes P., Ginj M., Zhang H., Waser B., Baum R.P., Reubi J.C., Mäcke H. Are radiogallium-labelled DOTA-conjugated somatostatin analogues superior to those labelled with other radiometals? Eur. J. Nucl. Med. Mol. Imaging. 2007; 34(7): 982–93.

11. Cutler C.S., Hennkens H.M., Sisay N., Huclier-Markai S., Jurisson S.S. Radiometals for combined imaging and therapy. Chem. Rev. 2013; 113(2): 858–83.

12. Chatalic K.L.S., Kwekkeboom D.J., de Jong M. Radiopeptides for Imaging and Therapy: A Radiant Future. J. Nucl. Med. 2015; 56(12): 1809–12.

13. De Jong M., Breeman W.A.P., Kwekkeboom D.J., Valkema R., Krenning E.P. Tumor imaging and therapy using radiolabeled somatostatin analogues. Acc. Chem. Res. 2009; 42(7): 873–80.

14. Boros E., Ferreira C.L., Cawthray J.F., Price E.W., Patrick B.O., Wester D.W., Adam M.J., Orvig C. Acyclic chelate with ideal properties for Ga-68 PET imaging agent elaboration. J. Am. Chem. Soc. 2010; 132(44): 15726–33.

15. Price T.W., Greenman J., Stasiuk G.J. Current advances in ligand design for inorganic positron emission tomography tracers Ga-68, Cu-64, Zr-89 and Sc-44. Dalt. Trans. 2016; 45(40): 15702–24.

16. Notni J., Simecek J., Hermann P., Wester H.J. TRAP, a powerful and versatile framework for gallium-68 radiopharmaceuticals. Chem. - A Eur. J. 2011; 17(52): 14718–22.

17. Simecek J., Zemek O., Hermann P., Wester H.J., Notni J. A Monoreactive Bifunctional Triazacyclononane Phosphinate Chelator with High Selectivity for Gallium-68. ChemMedChem. 2012; 7(8): 1375–8.

18. Simecek J., Notni J., Kapp T.G., Kessler H., Wester H.J. Benefits of NOPO As Chelator in Gallium-68 Peptides, Exemplified by Preclinical Characterization of Ga-68-NOPO-c(RGDfK). Mol. Pharm. 2014; 11: 1687–95.

19. Boros E., Ferreira C.L., Yapp D.T.T., Gill R.K., Price E.W., Adam M.J., Orvig C. RGD conjugates of the H_2dedpa scaffold: Synthesis, labeling and imaging with Ga-68. Nucl. Med. Biol. 2012; 39(6): 785–94.

20. Eder M., Wängler B., Knackmuss S., LeGall F., Little M., Haberkorn U., Mier W., Eisenhut M. Tetrafluorophenolate of HBED-CC: A versatile conjugation agent for Ga-68-labeled small recombinant antibodies. Eur. J. Nucl. Med. Mol. Imaging. 2008; 35(10): 1878–86.

21. Berry D.J., Ma Y., Ballinger J.R., Tavaré R., Koers A., Sunassee K., Zhou T., Nawaz S., Mullen G.E.D., Hider R.C., Blower P.J. Efficient bifunctional gallium-68 chelators for positron emission tomography: tris(hydroxypyridinone) ligands. Chem. Commun. (Camb). 2011; 47(25): 7068–70.

22. Ma M.T., Cullinane C., Imberti C., Baguna Torres J., Terry S.Y.A., Roselt P., Hicks R.J., Blower P.J. New Tris(hydroxypyridinone) Bifunctional Chelators Containing Isothiocyanate Groups Provide a Versatile Platform for Rapid One-Step Labeling and PET Imaging with ^{68}Ga3+. Bioconjug. Chem. 2016; 27(2): 309–18.

23. Ma M.T., Cullinane C., Waldeck K., Roselt P., Hicks R.J., Blower P.J. Rapid kit-based Ga-68-labelling and PET imaging with THP-Tyr^3-octreotate: a preliminary comparison with DOTA-Tyr^3-octreotate. EJNMMI Res. 2015; 5(1): 52.

24. Waldron B.P., Parker D., Burchardt C., Yufit D.S., Zimny M., Rösch F. Structure and stability of hexadentate complexes of ligands based on AAZTA for efficient PET labelling with gallium-68. Chem. Commun. (Camb). 2013; 49: 579–81.

25. Parker D., Waldron B.P. Conformational analysis and synthetic approaches to polydentate perhydro-diazepine ligands for the complexation of gallium(III). Org. Biomol. Chem. 2013; 11(17): 2827.

26. Seemann J., Waldron B.P., Rösch F., Parker D. Approaching “kit-type” labelling with Ga-68: The DATA chelators. ChemMedChem. 2015; 10(6): 1019–26.

27. Seemann J., Waldron B.P., Parker D., Rösch F. DATATOC: a novel conjugate for kit-type Ga-68 labelling of TOC at ambient temperature. EJNMMI Radiopharm. Chem. 2016; 1(1): 4.

28. Buchmann I., Henze M., Engelbrecht S., Eisenhut M., Runz A., Schäfer M., Schilling T., Haufe S., Herrmann T., Haberkorn U. Comparison of Ga-68-DOTATOC PET and In-111-DTPAOC (Octreoscan) SPECT in patients with neuroendocrine tumours. Eur. J. Nucl. Med. Mol. Imaging. 2007; 34(10): 1617–26.

29. Nock B.A., Kaloudi A., Lymperis E., Giarika A., Kulkarni H.R., Klette I., Singh A., Krenning E.P., de Jong M., Maina T., Baum R.P. Theranostic Perspectives in Prostate Cancer with the Gastrin-Releasing Peptide Receptor Antagonist NeoBOMB1: Preclinical and First Clinical Results. J. Nucl. Med. 2017; 58: 75–80.

30. Maina T., Cescato R., Waser B., Tatsi A., Kaloudi A., Krenning E.P., De Jong M., Nock B.A., Reubi J.C. LTT-SS28, a first pansomatostatin radioligand for in vivo targeting of somatostatin receptor-positive tumors. J. Med. Chem. 2014; 57(15): 6564–71.

31. Patel Y.C., Srikant C.B. Subtype selectivity of peptide analogs for all five cloned human somatostatin receptors (hsstr 1-5). Endocrinology. 1994; 135(6): 2814–7.

32. Tatsi A., Maina T., Cescato R., Waser B., Krenning E.P., De Jong M., Cordopatis P., Reubi J.C., Nock B.A. DOTA Somatostatin-14 analogs and their In-111-radioligands: Effects of decreasing ring-size on sst1-5 profile, stability and tumor targeting. Eur. J. Med. Chem. 2014; 73: 30–7.

33. Maina T., Nock B.A., Nagel J., Sinnes J.-P., Baum R.P., Rösch F. In vitro binding affinities and initial in vivo evaluation of Ga-68-DATA-TOC. J. Nucl. Med.J. Nucl. Med. 2016; 57: 1112.

34. Coy D.H., Taylor J.E. Receptor-specific somatostatin analogs: correlations with biological activity. Metabolism. 1996; 45(8 Suppl 1): 21–3.

35. Reubi J.C., Eisenwiener K.P., Rink H., Waser B., Mäcke H.R. A new peptidic somatostatin agonist with high affinity to all five somatostatin receptors. Eur. J. Pharmacol. 2002; 456(1–3): 45–9.

36. Maina T., Nock B., Nikolopoulou A., Sotiriou P., Loudos G., Maintas D., Cordopatis P., Chiotellis E. Tc-99m-Demotate, a new Tc-99m-based [Tyr3]octreotate analogue for the detection of somatostatin receptor-positive tumours: Synthesis and preclinical results. Eur. J. Nucl. Med. 2002; 29(6): 742–53.

4.4 Synthesis and radiolabelling of new DATA-derivatives with ^{68}Ga for mild coupling with targeting vectors

Synthesis and radiolabelling of new DATA-derivatives with ^{68}Ga for mild coupling with targeting vectors

J. Nagel, N. Engelbogen, P. Spang, F. Rösch

Institute of Nuclear Chemistry, Johannes Gutenberg-University of Mainz, Germany

ABSTRACT

Bifunctional chelators have become an important tool as chelating agents in nuclear medicine. The novel chelator DATA^{5m} based on the 6-amino-1,4-diazepine-triacetate (DATA) scaffold shows a high affinity to metal ions such as Ga^{3+}. Radiolabelling of this chelator type with ^{68}Ga ($t_{1/2}$=67.7 min, β^+=89 %, $E_{\beta,max}$=1,9 MeV) can be performed quantitatively within minutes and under mild conditions. With these properties DATA facilitates a kit-type labelling of ^{68}Ga for nuclear medical application. Based on this, three new derivatives of the bifunctional DATA (DATA^{5m}) – short DATA^{5m}-Bz-NCS, DATA^{5m}-en-SA and DATA^{5m}-TEG-N_3 - have been synthesized and characterized. As proof-of-concept the DATA^{5m}-en-SA was coupled with a bisphosphonate as targeting vector. The ligands were radiolabelled at room temperature with ^{68}Ga under different conditions (pH, concentration, and buffer system). All derivatives offered quantitative radiolabelling yields (>95 %) with 2.5 nmol after 10 min. Their stabilities were tested in different media (human serum, PBS, EDTA, DTPA). All derivatives showed stabilities >88 % in human serum and >95 % in PBS. Additionally DATA^{5m} itself was evaluated regarding due to the influence of trace metals like Al^{3+}, Ca^{2+}, Mg^{2+}, Fe^{3+}, Zn^{2+}, Ti^{4+} and Sn^{4+}.

In summary the derivatives offering a fast and convenient labelling of ^{68}Ga at room temperature. The new coupling sites allow the covalent conjugation to a variety of targeting vectors, which are in particular pH and heat sensitive. This features and broadens the application field of this ligand for the radiolabelling with ^{68}Ga.

Keywords: Gallium-68, DATA, bifunctional chelator, radiolabelling, buffer

INTRODUCTION

Chelating agents have become of strong interest in the last decades for medical applications [1]. Especially for nuclear medicine these compounds (ligands) have received much attention [2]. For diagnostic and therapeutic applications several requirements have to be fulfilled by the ligands to be used *in vitro* and *in vivo*. First of all the ligand has to be bifunctional. This enables the coupling to a targeting vector for addressing the right tissue and the complexation of trivalent metal radionuclides such as ^{68}Ga and ^{177}Lu. The coupling as well as the complexation has to show high *in vivo* stability. The latter is important due to transmetallation or decomplexation by glycoproteins, enzymes or even bones [3–5]. Therefore, thermodynamic and especially kinetic stability play a key role for the application of radiometal ligands in nuclear medicine. The ligands can be divided into two categories: macrocyclic and acyclic. Macrocyclic ligands like DOTA, NOTA or their derivatives show high thermodynamic stability constants with radionuclides like ^{68}Ga, ^{111}In or ^{177}Lu, but a slow complexation reaction [6]. Acyclic ligands like DTPA, EDTA, Df or more recently the ligands HBED, DEDPA or CP256 offer a faster complexation, but also a reduced thermodynamic stability [7–12]. Another type of ligand was developed by Waldron *et al* [13]. The 6-amino-1,4-diazepine-triacetate (DATA) scaffold possesses a hybrid structure offering the advantage of macrocyclic and acyclic ligands – a fast complexation even at low temperatures with a high thermodynamic and kinetic stability. Due to the conformational flexibility of the 7-membered skeleton, a preorganized system is crucial for labelling with ^{68}Ga or other metal ions. This preorganization of the ligand depends on two factors: the pH of the buffer solution and the structure of the ligand itself. In scheme 1 both factors and their influence on the conformation of the ligand are represented.

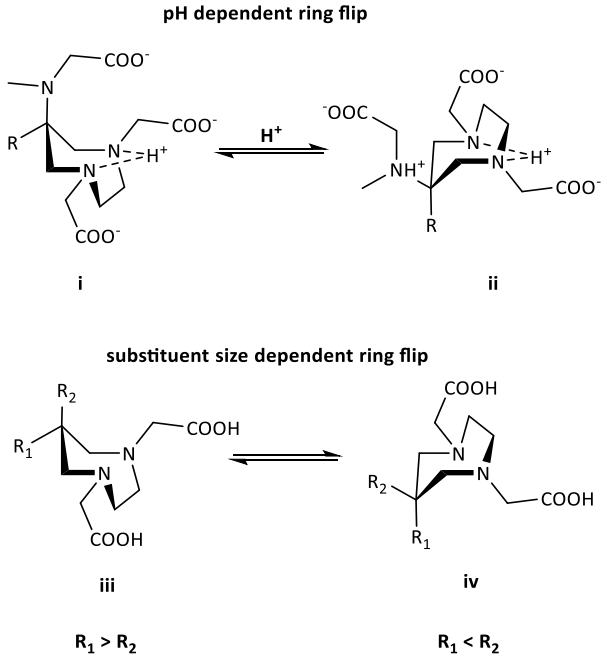

Scheme 1: Conformational flexibility of the 7-membered 1,4-diazepine ring depending on the pH and the size of the substituents on the C6-atom

The ideal conformation for complexation of metal ions is conformation **i** in scheme 1, since it creates a pseudo-octahedral N_3O_3 geometry. Because of repulsive interaction of the protons conformation **ii** is favored at low pH values. Looking at the size dependent ring flip, substituent R_1 has to be bulkier than R_2 (if R_2 is -N(Me)CH_2COOH group) to create the preferred conformation. For this effect the conformational energy (A-values) of different substituents within the ring conformation have to be considered [14,15].

Based on this knowledge the novel bifunctional chelator DATA^{5m} (scheme 2) was synthesized and evaluated in terms of its thermodynamic and kinetic stability. The results of this previous study indicate a high stability of the [^{nat}Ga]Ga-DATA^{5m} with a logK value of 21.45 and physiological half life of 46 h in NaCl (0.15 M, 25 °C) [16].

In this work we present the total synthesis of the key compound DATA^{5m} and the introduction of three new coupling sites and the attachment of a bisphosphonate (pamidronic acid) to ligand **B** as proof-of-concept (scheme 2). The versatile coupling sites enable the usage of the ligands for several fields like bisphosphonates, proteins, antibodies, nanoparticles and polymers.

The derivative **A** can be introduced via the benzyl-isothiocyanate group (-Bz-NCS) to free amines on polypeptides or antibodies/antibody fragments. This type of coupling has already been investigated with a number of different chelating agents [17–20].

Derivate **B** is functionalized with an ethylene diamine squaric acid (-en-SA) derivative. This enables amide coupling under mild conditions (pH 9, RT) [21,22].

Derivate **C** possesses a triglycol azide linker (-TEG-N_3) and can be linked to nanoparticles, polypeptides or polymers which are attached to alkynes or ring strained systems like the DBCO group. This offers a mild coupling via the [1,3] dipolar cycloaddition [23,24].

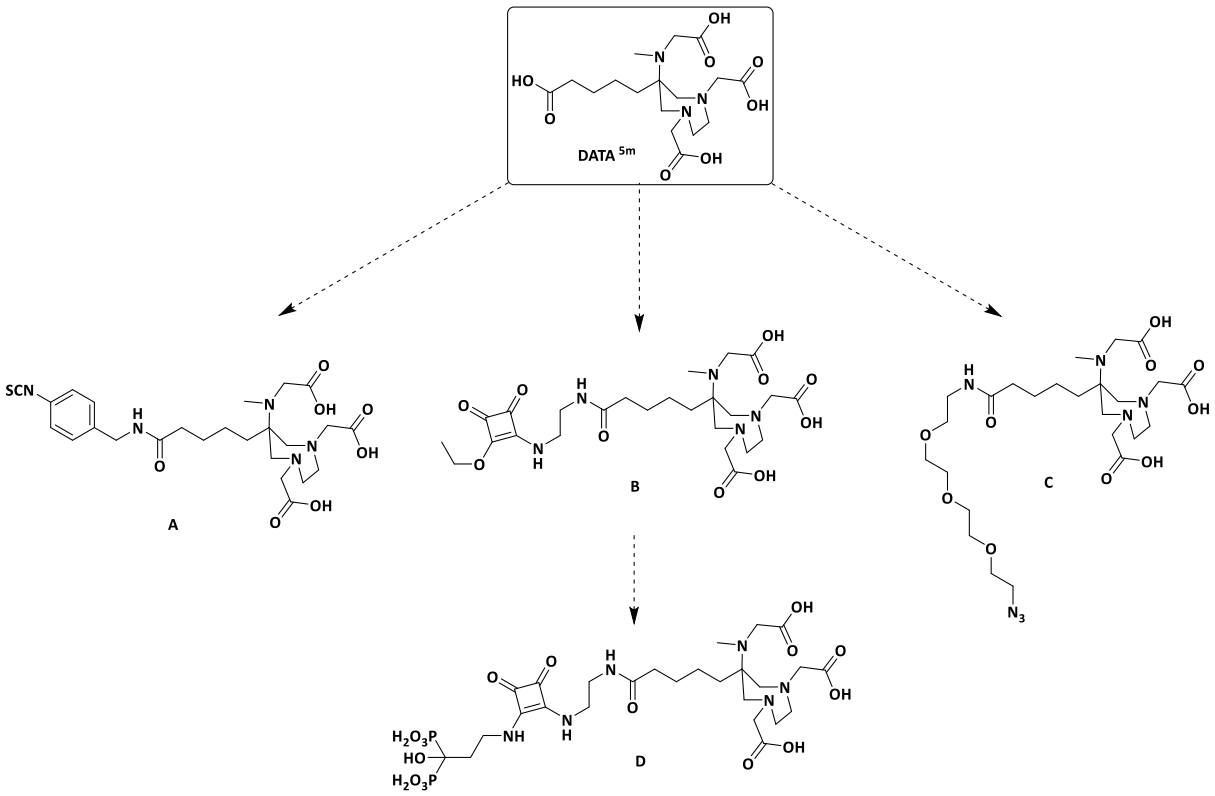

Scheme 2: DATA^{5m} and its different coupling site: DATA^{5m}-Bz-NCS (**A**), DATA^{5m}-en-SA (**B**), DATA^{5m}-TEG-N_3 (**C**) and DATA^{5m}-en-SA-PAM (**D**)

According to these coupling sites we investigated the influence on the radiolabelling (concentration, buffer system and pH) of the derivatives with ^{68}Ga. Additionally, the stabilities in different media (human serum, EDTA, DTPA, PBS) were examined for all ligands as well as the influence on the radiolabelling yields of the chelator itself by spiking the ^{68}Ga eluate with different trace metals.

RESULTS AND DISCUSSION

Organic synthesis

The synthesis was started with the alkylation of *N,N*'-dibenzylethylenediamine with *tert*-butyl bromoacetate (scheme 3**, 1**). After deprotection of the diamine the diazepine was built by a Nitro-Mannich-reaction with paraformaldehyde and 2-nitrocyclohexanone to yield product **2**. The nitro group of **2** was reduced to the corresponding amine, alkylated with *tert*-butyl bromoacetate (**3**) and methylated via reductive amination to give product **4**. The methyl ester was deprotected with LiOH to yield the derivative **5** (DATA^{5m}) ready for coupling to the linker.

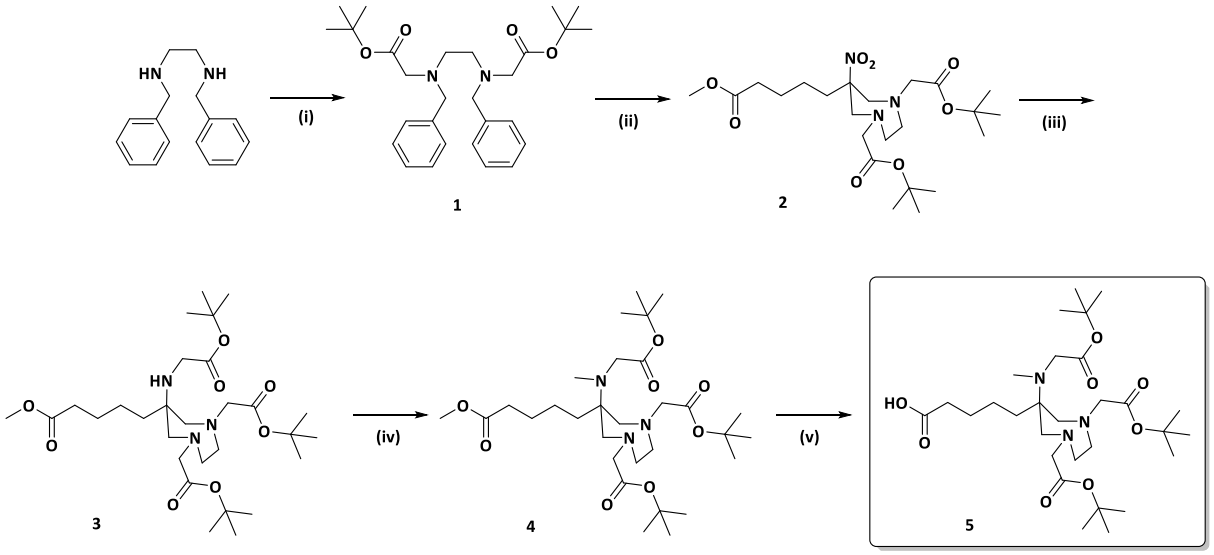

Scheme 3: Synthesis route of the DATA^{5m}: (i) *tert*-butyl bromoacetate, Na_2CO_3, ACN, 95 %; (ii) a) Pd/C, EtOH, H_2, 100 %; paraformaldehyde, 2-nitrocyclohexanone, MeOH, 67 %; (iii) a) Raney®-Nickel, EtOH, H_2, 100 %; b) *tert*-butyl bromoacetate, DIEA, ACN, 49 %; (iv) Formalin (37 %), AcOH, $NaBH_4$, ACN, 82 %; (v) LiOH, dioxane/H_2O, 91 %

Starting from DATA^{5m} the different linkers were coupled via the free carboxylic acid (scheme 3). The coupling reactions for product **6** and **7** were performed under equal conditions with HATU, DIEA and ACN at room temperature (scheme 4). For amide bond formation of product **C** HOBt and EDC·HCl were used instead. By use of HATU the amino group of the 11-azido-3,6,9-trioxaundecan-1-amine reacted to the guanidinium ion, which couldn't be separated from the product even by HPLC. An important factor for the synthesis of the squaric acid derivative **B** was the adjustment of the pH to 7. At lower pH no reaction occurred, whereas at higher pH two ligand molecules were coupled to the squaric acid ester. The latter fact is going to be used for the attachment of this derivative to free amines of polypeptide, macromolecular systems or the afore mentioned pamidronic acid [21]. The synthesis of the aniline intermediate of product **A** was carried out in different media with different catalysts. The best system was Raney®Nickel in THF. Using Pd/C as catalyst either with ethanol or THF resulted in the addition of at least one unit of a solvent molecule to the amino group. This effect is known due to the evolution of acetaldehyde and the reductive amination with the produced amine [25,26]. Regarding

the THF side product Russell *et al.* investigated the Pd-mediated addition of peroxidic THF to aromatic amines [27].

After deprotection under acidic conditions all ligands were purified by means of HPLC under isocratic conditions.

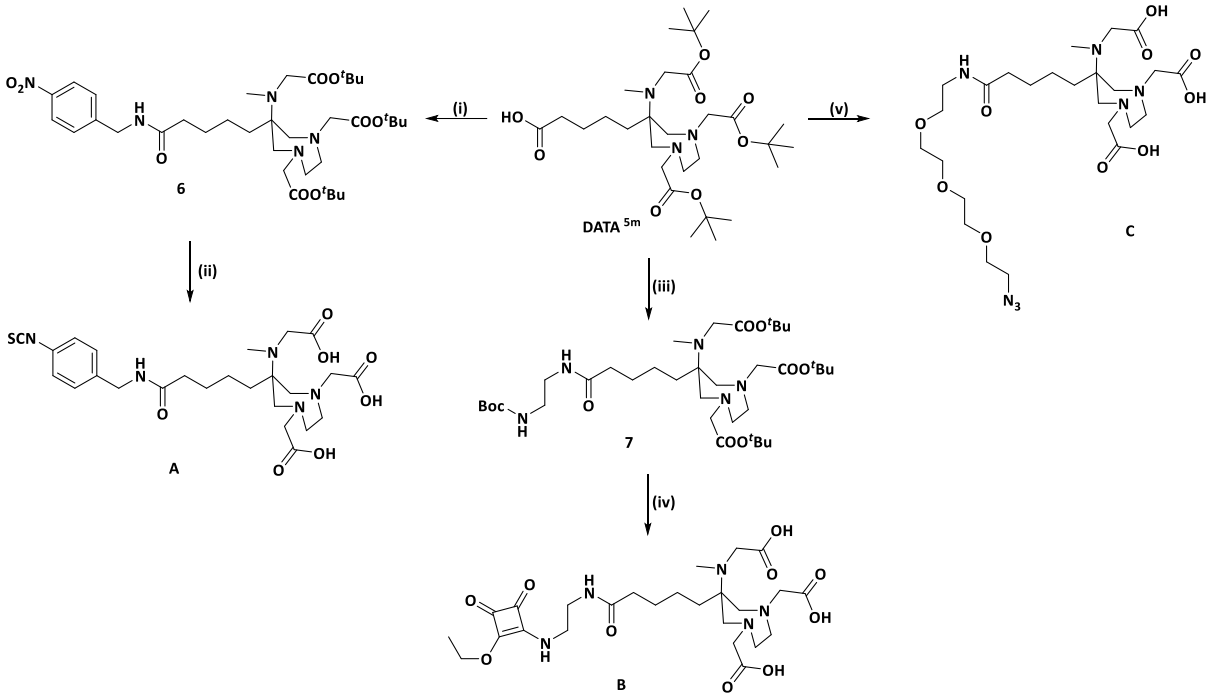

Scheme 4: Synthesis route for the derivatives DATA^{5m}-Bz-NCS (**A**), DATA^{5m}-en-SA (**B**) and DATA^{5m}-TEG-N_3 (**C**): (i) 4-nitromethylaminobenzyl hydrochloride, HATU, DIEA, ACN, 80 %; (ii) a) Raney®Nickel, H_2, EtOH; b) $SCCl_2$, TEA, $CHCl_3$; c) TFA/DCM, RT, 28 %; (iii) *tert*-butyl-*N*-(2-aminoethyl)carbamate, HATU, DIEA, ACN, 80 %; (iv) a) TFA/DCM, 100 %; b) 3,4-diethoxy-3-cyclobutene-1,2-dione, phosphate buffer (0.5 M, pH 7), 33 %; (v) a) 11-azido-3,6,9-trioxaundecan-1-amine, HOBt/EDC·HCl, DIEA, ACN; b) 4 M HCl in dioxane, RT, 33 %

As proof-of-concept, the squaric acid derivative **B** was coupled with pamidronic acid (PAM). Under alkaline conditions (pH 9) the primary amine of the pamidronic acid substitutes the ethyl ester group to give the squaramide. After HPLC purification the pure product **D** with a yield of 55 % was obtained (scheme 5).

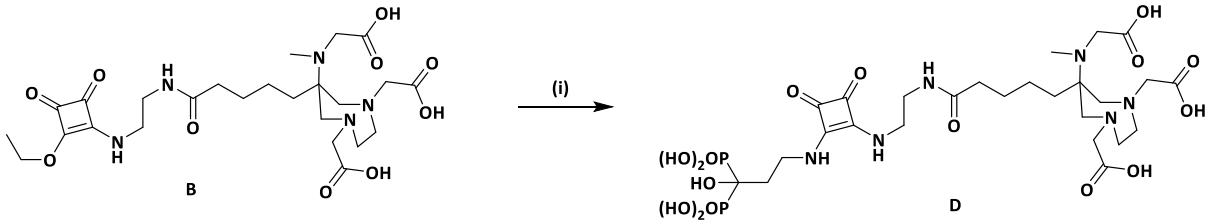

Scheme 5: Synthesis of DATA^{5m}-en-SA-PAM (**D**) – (i) Na_2HPO_4 (pH 9), pamidronic acid (PAM), 16 h, RT, 55 %

Important for this reaction is the use of metal-free buffer, since DATA is able to complex trace metals like zinc and copper [16]. These thermodynamically stable complexes would have an influence on the

radiolabelling with ^{68}Ga due to transmetalation between the trace metal-ligand complex and the gallium. The great advantage of this reaction is the easy coupling chemistry in aqueous solution at room temperature with ethanol as only side-product.

Radiolabelling (pH- and concentration-dependence)

Derivatives **A**, **B** and **C** were radiolabelled with ^{68}Ga under various conditions (concentration, pH, buffer system). The most commonly used buffer systems for ^{68}Ga labelling are sodium acetate (NaOAc), ammonium acetate (AmOAc) and *N*-2-hydroxyethyl piperazine-*N'*-2-ethanesulfonic acid (HEPES). Several studies have already demonstrated the influence on labelling efficiencies by the choice of buffer system [9,28,29]. In table 1 the radiolabelling yields for all three derivatives **A**, **B** and **C** are listed.

Table 1: Radiolabelling yields (in %) of derivatives **A, B** and **C** with various buffer systems and ligand concentrations after 10 min at 25 °C (n=3; A(^{68}Ga)=20-25 MBq (0.2-0.25 pmol))

	NaOAc (0.25 M, pH 4.5)			AmOAc (0.25 M, pH 5.5)			HEPES (0.25 M, pH 4.3)		
µM	**[^{68}Ga]Ga-A**	**[^{68}Ga]Ga-B**	**[^{68}Ga]Ga-C**	**[^{68}Ga]Ga-A**	**[^{68}Ga]Ga-B**	**[^{68}Ga]Ga-C**	**[^{68}Ga]Ga-A**	**[^{68}Ga]Ga-B**	**[^{68}Ga]Ga-C**
1	10.8 ± 8.0	78.9 ± 13.0	98.8 ± 0.3	55.0 ± 12.4	84.4 ± 1.9	96.7 ± 0.8	4.6 ± 1.8	3.7 ± 0.4	9.7 ± 2.6
2.5	96.8 ± 0.4	96.0 ± 1.2	99.4 ± 0.0	94.7 ± 1.0	97.7 ± 1.0	97.8 ± 0.6	5.1 ± 0.5	4.1 ± 0.3	8.1 ± 2.8
5	99.3 ± 0.1	97.2 ± 0.7	99.5 ± 0.0	94.5 ± 0.8	96.7 ± 0.5	97.6 ± 2.5	98.0 ± 0.2	97.4 ±0.8	99.4 ± 0.1
10	98.6 ± 0.2	98.3 ± 0.6	99.5 ± 0.1	99.8 ± 0.1	99.1 ± 0.3	99.8 ± 0.0	99.2 ± 0.0	99.7 ±0.1	99.5 ± 0.0

First reactions were carried out with 10 µM of each ligand. The labelling reactions were performed in a total volume of 1 mL resulting in concentrations of 1 µM (1 nmol) to 10 µM (10 nmol) with 20-25 MBq n.c.a. ^{68}Ga. All ligands reached radio chemical yields (RCY) > 95 % by 10 min for 5 and 10 µM, independent of the used buffer system. Also with 2.5 µM all ligands could be labelled quantitatively, but only with NaOAc and AmOAc as buffers. With HEPES buffer (0.25 M) no radiolabelling yield greater 15 % could be determined; neither with 1 µM nor with 2.5 µM. Interestingly, ligand **A** showed labelling yields in NaOAc and AmOAc lower 60 % for 1 µM amount of substance. By taking a closer look on the kinetic studies, derivative **C** comes with the fastest complexation kinetic for ^{68}Ga. According to the structure-dependent properties of the DATA skeleton (scheme 1) these results are not surprising: The bulky triglycol linker seems to have a greater effect on the pre-organization of the DATA than the benzyl- and ethylenediamine-construct. Comparing 1 µM ligand of **A** and **B** within the buffer systems NaOAc and AmOAc the latter one shows higher yields (78.9 % with NaOAc and 84.4 % with AmOAc). These results bring up two theses: First of all, AmOAc seems to be the better choice of buffer system for these ligands. The second thesis proposes, that ligand **B** possesses a faster kinetic complexation ability. Looking at the structure of ligand **B**, it can be said, that the squaramide function seems to have a positive influence on the labelling ability of **B**. The squaramide offers a dione back bone, which is able to complex transition metals and lanthanides such as copper, zinc, lanthanum or gadolinium [30,31]. A similar effect regarding enhanced labelling effects for a squaramide-chelator-system was observed

by Rudd *et al.* [22]. They labelled Df-squaramide-trastuzumab with ^{89}Zr within a shorter time period compared to the DFO-Bz-NCS conjugate. Additionally, a higher stability for the complex was determined due to the contributory complexation effect of the dione back bone of the squaramide.

In terms of the buffer systems a detailed investigation of the HEPES was evaluated. Since the radiolabelling yields for lower ligand concentrations did not show any kinetic progress, it was assumed, that the HEPES interacts with the ^{68}Ga by building a weak Ga-HEPES-complex (logK=1.99 ± 0.01), as proposed by Azab *et al.* [32]. Therefore the molarity of the HEPES was decreased from 0.25 M to 0.025 mM, to get an insight into the influence of HEPES on the labelling efficiency. Table 2 lists the RCY for 1 and 2.5 µM of each derivative after 15 min.

Table 2: Comparison of the radiolabelling yields (in %) of derivatives **A**, **B** and **C** with 0.25 M and 0.025 M HEPES buffer systems after 15 min at 25 °C (n=3; A(^{68}Ga)=20-25 MBq (0.2-0.25 pmol))

	HEPES (0.025 mM, pH 4.3)			**HEPES (0.25 M, pH 4.3)**		
µM	[^{68}Ga]Ga-**A**	[^{68}Ga]Ga-**B**	[^{68}Ga]Ga-**C**	[^{68}Ga]Ga-**A**	[^{68}Ga]Ga-**B**	[^{68}Ga]Ga-**C**
1	27.6 ± 1.1	95.9 ± 1.0	90.8 ± 1.8	4.7 ± 1.8	4.7 ± 0.4	10.4 ± 3.8
2.5	93.7 ± 5.3	95.5 ± 1.2	99.2 ± 0.2	5.2 ± 0.0	4.3 ± 0.7	7.2 ± 2.9

Similar to the findings of Martins *et al.* [33], the ratio between the concentrations of HEPES buffer and the ligand has a major impact on the labelling yields for all derivatives. Whereas the labelling reactions with 0.25 M HEPES offered no further increase of the yields after 10 min, the system with 0.025 M HEPES and lower ligand concentrations indicated a further increase in the labelling yields beyond 10 min. All derivatives (except 1 µM of ligand **A**) result in RCYs greater 90 % in 0.025 M HEPES after 15 min (or less).

Based on these results the radiolabelling efficiency of ligand **D** with ^{68}Ga was examined in the same manner as for ligands **A** to **C**. Starting with 10 µM ligand concentration in NaOAc radiolabelling yields below 50 % were obtained at 25 °C and 40 °C after 10 min. Therefore, the temperature was raised to 90 °C according to the labelling protocols of NOTA-bisphosphonates with ^{68}Ga [34,35]. Holub *et al.* have shown, that for NO2AP^{BP} and NOTAM^{BP} more forced conditions led to faster complexation and higher yields with ^{68}Ga [34]. In table 3 the radiolabelling yields for [^{68}Ga]Ga-**D** are listed for all three buffer systems.

Table 3: Comparison of the radiolabelling yields (in %) of derivative **D** with various buffer systems and ligand concentrations after 10 min at 90 °C (n=3; A(^{68}Ga)=20-25 MBq (0.2-0.25 pmol))

nmol	NaOAc (25 mM, pH 4.5)	AmOAc (25 mM, pH 5.5)	HEPES (0.025 M, pH 4.3)
1	0.0 ± 0.0	49.2 ± 3.2	55.5 ± 7.1
2.5	40.2 ± 1.5	69.1 ± 5.0	98.6 ± 0.1
5	97.6 ± 0.2	97.7 ± 0.6	97.1 ± 1.5
10	99.2 ± 0.1	98.4 ± 0.8	96.8 ± 1.0

Within all buffer systems and concentrations of 5 µM to 10 µM the bisphosphonate is labelled quantitatively after 10 min. For lower ligand amounts RCY higher 50 % could only be reached with HEPES as buffer. These findings are in good agreement with the results of the previous evaluated derivatives. In summary, all four ligands show quantitative radiolabelling yields in low micromolar concentrations at room temperature. Even 2.5 µM of each ligand resulted in quantitative radiochemical yields, especially with HEPES as buffer system. Though the information on the toxicity of HEPES is limited and the use in humans is still debated [36], HEPES has the additional advantage of acting as scavenger for radicals, which are formed by gamma radiation [37].

***In vitro* stability**

Besides quantitative labelling a ligand should possess high thermodynamic and kinetic stability. Consequently [^{68}Ga]Ga-**A**, [^{68}Ga]Ga-**B**, [^{68}Ga]Ga-**C** and [^{68}Ga]Ga-**D** were evaluated regarding their stability *in vitro* in different media. In HS as well as in PBS all complexes (except [^{68}Ga]Ga-**A** in HS) show a high stability of >98 % after 2 h. Even in the presence of DTPA and EDTA, which are competitive ligands, stabilities over 95 % for [^{68}Ga]Ga-**B**, [^{68}Ga]Ga-**C** and [^{68}Ga]Ga-**D**, and over 78 % for [^{68}Ga]Ga-**A** could be obtained. Evidently, the complexes [^{68}Ga]Ga-**C** and [^{68}Ga]Ga-**D** are the most stable and have the highest kinetic inertness. Nevertheless the other two derivatives and their Ga-complexes have shown a high potential as excellent ligands for *in vivo* application.

Table 4: Stability of [^{68}Ga]Ga-**A**, [^{68}Ga]Ga-**B**, [^{68}Ga]Ga-**C** and [^{68}Ga]Ga-**D** (in % intact complex) in human serum (HS), DTPA, EDTA and PBS after 1 h and 2 h at 37 °C

	t / h	HS	DPTA	EDTA	PBS
[^{68}Ga]Ga-A	**1**	92.0 ± 0.3	89.8 ± 0.3	88.2 ± 0.7	99.8 ± 0.1
	2	88.1 ± 0.5	86.0 ± 0.5	78.1 ± 0.5	99.7 ± 0.0
[^{68}Ga]Ga-B	**1**	99.9 ± 0.0	93.3 ± 0.8	92.7 ± 0.4	99.8 ± 0.1
	2	99.0 ± 0.3	81.4 ± 0.9	81.5 ± 0.7	99.8 ± 0.0
[^{68}Ga]Ga-C	**1**	99.8 ± 0.0	99.8 ± 0.1	98.4 ± 0.4	99.9 ± 0.0
	2	99.6 ± 0.1	99.5 ± 0.1	95.2 ± 0.4	99.8 ± 0.0
[^{68}Ga]Ga-D	**1**	98.4 ± 0.1	98.7 ± 0.2	98.8 ± 0.2	99.7 ± 0.0
	2	97.7 ± 0.6	98.0 ± 1.1	98.2 ± 0.8	99.6 ± 0.0

Aside from the radiolabelling under different conditions the purity of the ^{68}Ga solution plays an important role for the radiochemical yield. Impurities within the eluate of a ^{68}Ge/^{68}Ga generator are metals like Ge(IV), Zn(II), Sn(IV), Ti(IV), Fe(II)/(III), Al(III) and Cu(II). Fe(III), Cu(II) and Zn(II) are common trace metals, while Zn(II) is additionally formed via the decay of ^{68}Ga. Sn(IV) and Ti(IV) contaminations originate from generator matrixes and Al(III) from other generator materials. Even if the concentrations are reported to be in the sub-nanomolar range these metals, especially Zn(II) and Fe (II)/(III), have a great influence on the radiolabelling [38–40]. This influence of metal ion contaminations on the labelling of **5** (DATA^{5m}) was investigated by spiking the ^{68}Ga-eluate with these metal ions. Additionally, the influence of the divalent cations Ca(II) and Mg(II), which are present in physiological conditions, were tested.

The labelling was carried out in a 10 µM solution of **5** in NaOAc-buffer (0.2 M, pH 4.5) with 20-30 MBq ^{68}Ga which was purified via cationic post-processing. Under these conditions **5** reached RCY >95 % after 1 min. For the contamination experiments the purified ^{68}Ga-eluate was mixed with different amounts of metal ions before adding it to **5** resulting in chelator to metal ion ratios of 10:1, 1:1, 1:10 and for cases where little metal influence was observed 1:100. Labelling results for metal ion contaminations with little influence are shown in figure 1.

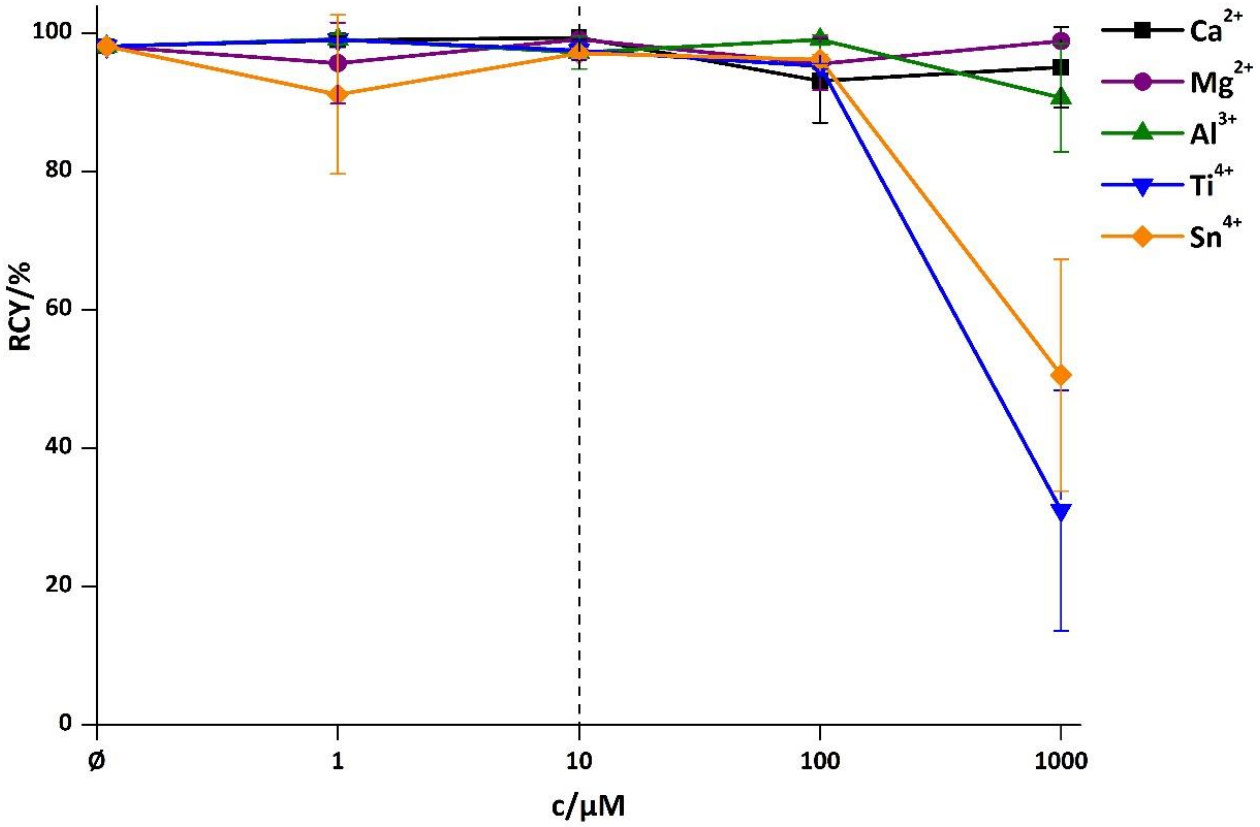

Figure 1: Incorporation of $^{68}Ga^{3+}$ by **5** as function of increasing concentrations of metal ions. Ø=no metal added. Vertical dashed line indicates equal concentrations of chelator and contaminant (10 µM).

The labelling of **5** is not influenced by the divalent cations Ca(II) or Mg(II). Al(III) also shows not influence even in high concentrations. The rapid decrease in RCY for high concentrations of Ti(IV) and Sn(IV) is caused by formation of colloids of these metals in these concentrations which can incorporate $^{68}Ga^{3+}$ and make it inaccessible for the DATA-Chelator. Ti(IV) and Sn(IV) are not competing with $^{68}Ga^{3+}$ for complexation by the chelator.

Fe(III), Cu(II) and Zn(II) have a higher influence on the labeling of **5** with ^{68}Ga (s. figure 2). When ratios of chelator to metal contaminant reach 1:1 the RCY starts to decrease.

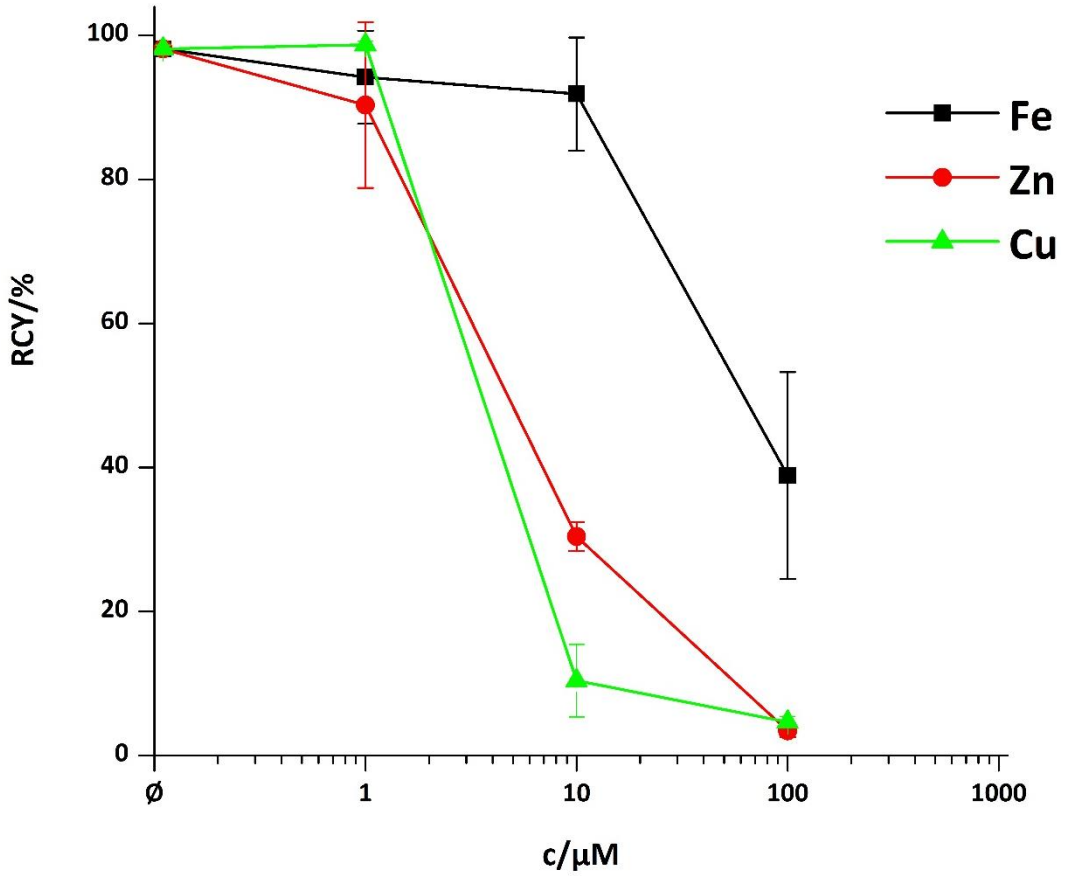

Figure 2: Incorporation of $^{68}Ga^{3+}$ by **5** as function of increasing concentrations of metal ions (Fe^{3+}, Zn^{2+} and Cu^{2+}). Ø=no metal added. Vertical dashed lines indicate equal concentrations of chelator and contaminant (10 µM).

Although the complexations of Fe^{3+} and Ga^{3+} are often described as similar, the Fe^{3+} ion seems to be less of an obstacle for the ^{68}Ga complexation by the DATA-chelator compared to the influence of divalent cations Zn^{2+} and Cu^{2+}. In general, problematic contaminant concentrations for the labelling of **5** with ^{68}Ga are not reached in usually used generator eluates [40]. Zn(II) seems to be the most concerning contaminant and might have to be considered when using small amounts of the DATA-chelator with unprocessed ^{68}Ga eluate from generators with a long standing time. The behavior of the DATA-chelator in the presence of Cu^{2+} might indicate a suitable chelator for the complexation of ^{64}Cu.

CONCLUSION

The novel chelator DATA and the reported derivatives are promising candidates for ^{68}Ga labelling. With their coupling sites the DATA derivatives expand their application field to a broad spectrum of molecular targeting vectors. Especially their coupling chemistry, which can be performed under similar conditions as the ^{68}Ga-DATA radiolabelling itself (pH 7-9, RT), creates new pathways to introduce the DATA scaffold on bisphosphonates, polypeptides, polymers, nanoparticles or antibody fragments. The fast and simple labelling setup at room temperature, which is similar to the kit-type labelling of ^{99m}Tc pharmaceuticals [41,42], magnifies the use of ^{68}Ga pharmaceuticals for the clinical use.

SUPPORTING INFORMATION

General methods:

All used chemicals were commercially available at Acros Organics, Bachem, Fluka, SigmaAldrich or VWR and were used without further purification. For radiolabelling reactions trace metal-free salts and water were used. The measurements of ^{1}H- and ^{13}C-NMR spectra were performed on a Bruker Avance III HD 400 (400 MHz) or Avance III 600 (600 MHz). Chemical shifts are given in parts per millions downfield from TMS (δ=0 ppm) referred to the solvent residual signal. Low-resolution mass spectra (LR-MS) were recorded on Agilent 6100 Series Single Quadrupole LC/MS and high-resolution mass spectra (HR-MS) were recorded on either a Micromass Quattro Micro API LC-ESI or a Finnigan MAT90-Spectrometer. Purification and analysis of the compounds was performed on a HPLC system from Merck (LaChrom; pump: Hitachi L7100; UV-detector: L7400). Following columns were used: Luna 10 u (C18) 100 Å (250x10.00 mm 10 micron) (**A**); Gemini 5 u (C18) 110 Å (250x10.00 mm 5 micron) (**B**); Luna 10 u (C18) 100 Å (250x21.23 mm 10 micron) (**C**)). As eluent H_2O (0.1 % TFA) and ACN (0.1 % TFA) were used. For radiolabelling a ^{68}Ge/^{68}Ga generator (TiO_2-based matrix, Cyclotron Co. Obninsk, Russia) was used. The eluate was purified as described in Zhernosekov *et al.* [43]. Radiolabelling reactions were performed in 1 mL total volume at 25 °C/90 °C in a heating block at 600 rpm. Radio-TLCs were performed on Merck Silica F_{254} TLC plates with citrate buffer (0.01 M, pH 4) or acetone/acetylacetone/conc. HCl (3:3:1 vol%) and analyzed with the radio detector GABI STAR from Raytest.

Experimental Section:

DATA^{5m} synthesis

*N,N'-Dibenzyl-N,N'-di-(tert-butylacetate)-ethylenediamine (**1**)*

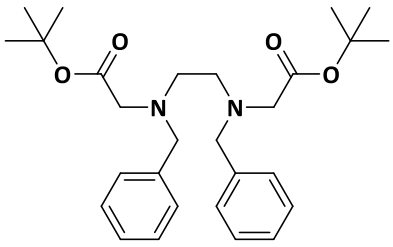

1

N,N´-dibenzylethylenediamine (3.00 g; 12.48 mmol) and Na_2CO_3 (5.12 g; 48.67 mmol) were stirred at room temperature in dry acetonitrile (50 mL) for 30 min. *Tert*-butyl bromoacetate (4.64 g; 23.72 mmol), dissolved in dry acetonitrile (10 mL), was added at room temperature over a period of 30 min. After completion the suspension was heated over night at 90 °C, filtrated and the filtrate was concentrated under vacuum. After purification via column chromatography (H/EA; 6:1; R_f=0.25) the product was obtained as colourless solid (5.56 g; 11.87 mmol; 95 %).

^{1}H-NMR ($CDCl_3$, 400 MHz, δ [ppm]): 7.34-7.21 (m, 10 H); 3.78 (s, 4 H); 3.26 (s, 4H); 2.82 (s, 4 H); 1.44 (s, 18 H); ^{13}C-NMR ($CDCl_3$, 100 MHz, δ [ppm]): 171.03 (s); 139,18 (s); 129.05 (s); 128.30 (s); 127.10 (s); 80.86 (s); 58.39 (s); 55.27 (s); 51.73 (s); 28.24 (s)

MS (ESI$^+$): m/z (%): 469.28, 470.31, 471.33 (M+H$^+$); 507.32, 508.34, 509.35 (M+K$^+$)

*1,4-Di(tert-butylacetate)-6-methylpentanoate-6-nitroperhydro-1,4-diazepane (**2**)*

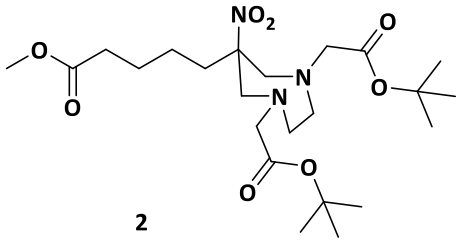

2

1 (3.89 g; 8.32 mmol) was dissolved in 20 mL abs. ethanol and formic acid (627.8 µL; 16.64 mmol). To this solution Pd/C (0.62 g; 16 wt%) was added and the solution was saturated and kept overnight with hydrogen. After completion the Pd/C was filtrated over celite, the filtrate was concentrated and dried. The crude product **2a** (2.29 g; 8.12 mmol; 98 %) was used without further purification.

A solution of 2-nitrocyclohexanone (1.16 g; 8.12 mmol) and Amberylst A21 (2 mass-eq) in dry methanol (30 mL) was heated for 1 h. Then product **2a** (2.29 g; 8.12 mmol) and paraformaldehyde (0.88 g; 29.23 mmol) were added and the suspension was heated overnight under reflux. The suspension was filtrated, the filtrate was concentrated under vacuum and purified via column chromatography (H/EA, 2:1; R_f=0.43). The product **2** was obtained as yellowish oil (2.66 g; 5.50 mmol; 67 %).

^{1}H-NMR ($CDCl_3$, 400 MHz, δ [ppm]): 3.65 (s, 3 H); 3.60 (d, J=14.6 Hz, 2 H); 3.45 (d, J=17.3 Hz, 2 H); 3.30 (d, J=17.3 Hz, 2 H); 3.12 (d, J=14.6 Hz, 2 H); 2.84 (m, 4 H); 2.27 (t, 3 H); 1.83 (m, 2 H), 1.57 (m, 2 H); 1.46 (s, 18 H); 1.18 (m, 2 H); ^{13}C-NMR ($CDCl_3$, 100 MHz, δ [ppm]): 173.73 (s); 170.92 (s); 95.12 (s); 81.31 (s); 61.57 (s); 61.18 (s); 56.87 (s); 51.68 (s); 37.27 (s); 33.71 (s); 28.35 (s); 24.82 (s); 22.99 (s)

MS (ESI$^+$): m/z (%): 388.14, 389.18, 390.20 (M+H$^+$); 410.15, 411.17, 412.18 (M+Na$^+$)

*1,4-Di(tert-butylacetate)-6-methylpentonate-6-amino-tert-butylacetate-perhydro-1,4-diazepane (**3**)*

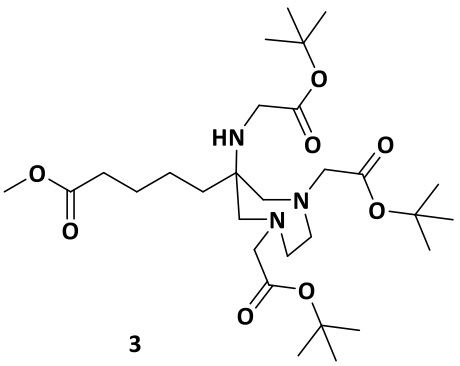

3

2 (1.59 g; 3.27 mmol) was dissolved in absolute ethanol (15 mL), combined with Raney®Nickel 2800® (0.5 g) (washed 4 times with ethanol) and the suspension was saturated with hydrogen and stirred at 40 °C for 6 h. After completion the nickel was filtrated over celite/sand, the filtrate was concentrated and dried under vacuum. The product **3a** (1.08 g; 2.36 mmol) was dissolved with *N,N*-diisopropylethylamine (419 µL; 2.36 mmol) in dry acetonitrile and stirred under nitrogen for 30 minutes at room temperature. *Tert*-butyl bromoacetate (0.61 g; 3.12 mmol) was added dropwise to the solution and stirred at room temperature overnight. The solution was concentrated under vacuum and purified via column chromatorgraphy (H/EA, 3:1; R_f=0.32). The product **3** was obtained as yellow oil (0.66 g; 1.17 mmol; 49 %).

^{1}H-NMR ($CDCl_3$, 400 MHz, δ [ppm]): 3.64 (s, 3 H); 3.28 (s, 4 H); 3.21 (s, 2 H); 2.77 (m, 4 H); 2.67 (m, 4 H);

2.30 (t, 3 H); 1.59(m, 2 H); 1.45 (s, 9 H); 1.44 (s, 18 H); 1.28 (m, 4 H); ^{13}C-NMR ($CDCl_3$, 100 MHz, δ [ppm]): 174.25 (s), 171.97 (s), 171.09 (s), 81.05 (s), 80.96 (s), 63.58 (s), 62.12 (s), 58.10 (s), 57.46 (s), 51.58 (s), 44.78 (s), 35.34 (s), 34.18 (s), 28.36 (s), 28.27 (s), 25.86 (s), 22.73 (s)

MS (ESI^+): m/z (%): 472.31, 473.13, 474.35 ($M+H^+$)

*1,4-Di(tert-butylacetate)-6-methylpentonate-6-(amino-(methyl)-tert-butylacetate)-perhydro-1,4-di-azepane (**4**)*

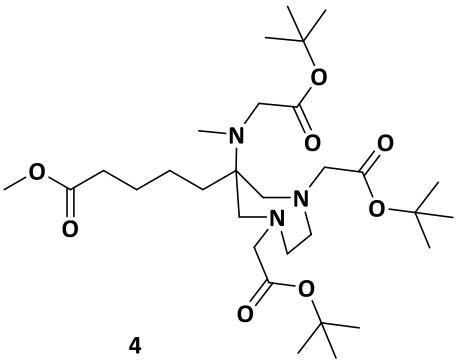

4

3 (0,60 g; 1.05 mmol) was dissolved in acetonitrile (5 mL) and formaline solution (293 µL; 10.50 mmol) and acidified with acetic acid (180 µL; 3.15 mmol). The solution was stirred for 15 minutes and sodium borohydride (0.12 g; 3.15 mmol) was added portionwise. After completion the solution was quenched with water, extracted with chloroform (3 x 10 mL) and the organic fractions were dried over sodium sulfate, filtrated and concentrated under vaccum. The crude product was purified via column chromatography (H/EA, 1:1; R_f=0.20). The product **4** was obtained as yellowish oil (0.50 g; 0.86 mmol; 82 %).

^{1}H-NMR ($CDCl_3$, 400 MHz, δ [ppm]): 3.64 (s, 3 H); 3.46 (s, 2 H); 3.25 (m, 4 H); 2.94 (d, 2 H); 2.84-2.65 (m, 6 H); 2.31 (t, 2 H); 1.57 (m, 4 H); 1.45 (s, 18 H); 1.44 (s, 9 H); 1.35 (s, 2 H); ^{13}C-NMR ($CDCl_3$, 100 MHz, δ [ppm]): 174.23, 172.17, 170.72, 80.90, 80.35, 77.34, 62.52, 62.34, 58.80, 53.99, 51.42, 37.34, 36.61, 34.09, 28.22, 28.12, 25.73, 21.91

MS (ESI^+): m/z (%): 486.30, 487.33, 488.37 ($M+H^+$); 508.33, 509.35, 510.36 ($M+Na^+$)

*1,4-Di(tert-butylacetate)-6-pentanoic acid-6-(amino(methyl)-tert-butylacetate)-perhydro-1,4-diazepane (**5**)*

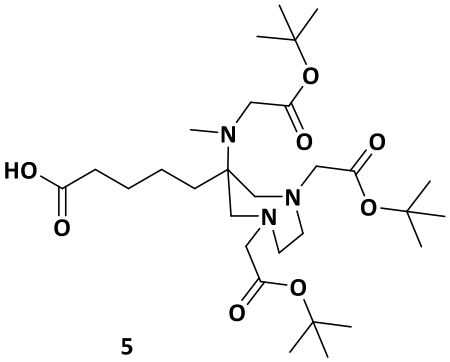

5

4 (0.96 g, 1.64 mmol) was dissolved in 1,4-dioxane/water (2:1, 15 mL), 1 M LiOH (2.87 mL, 2.87 mmol) and stirred at room temperature. After completion the solution was concentrated under vacuum and the residue was extracted with $NaHCO_3$ (1M) and chloroform. The organic layer was dried over sodium sulfate, filtrated and concentrated under vacuum. The product was obtained as yellowish oil without further purification (0.85 g, 1.49 mmol, 91 %).

^{1}H-NMR ($CDCl_3$, 400 MHz, δ [ppm]): 3.45 (s, 2 H); 3.25 (s, 4 H); 2.94 (d, J=14.0 Hz, 2 H); 2.82-2.65 (m, 4 H); 2.66 (d, J=14.0 Hz, 2 H); 2.35 (t, 2 H); 2.29 (s, 3 H); 1.58 (m, 4 H); 1.45 (s, 18 H); 1.44 (s, 9 H); 1.28

(m, 2 H); ^{13}C-NMR ($CDCl_3$, 100 MHz, δ [ppm]): 178.09 (s); 170.97 (s); 81.05 (s); 80.51 (s); 62.80 (s); 62.56 (s); 58.97 (s); 54.19 (s); 37.50 (s); 36.81 (s); 36.77 (s); 34.07 (s); 28.37 (s); 28.27 (s); 25.69 (s); 21.96 (s)

MS (ESI^+): m/z (%): 572.33, 573.38, 574.40 ($M+H^+$); 594.36, 595.38, 596.30 ($M+Na^+$)

*Pamidronic acid (**PAM**)*

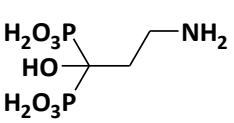

According to Kovács *et al.* [44] pamidronic acid was synthesized as follows: β-Alanine (2.2 g, 25 mmol) and phosphorous acid (4.1 g, 50 mmol) were dissolved in sulfolane (8 mL) and added dropwise to phosphor trichloride (6.9 g, 50 mmol) within 15 min. The mixture was stirred for 3 h at 75 °C. After cooling to 0 °C the mixture was quenched with water (25 mL) and stirred 12 h at 105 °C. Ethanol (20 mL) was added to the mixture and it was cooled to 0 °C. Precipitate was removed by filtration to obtain the product as colourless solid (2.1 g, 8.9 mmol, 36 %).

^{1}H-NMR (D_2O, 300 MHz, δ [ppm]): 2.20 (tt, J=6,2 Hz; J=13 Hz; 2 H); 3.27 (t, J=6,2 Hz, 2 H)

^{31}P-NMR (D_2O, 121.5 MHz, δ [ppm]): 17.5 (s, 2 P)

MS (ESI^+): m/z (%):236.0 $[M+H]^+$; 471.0 $[2M+H]^+$ ($M+H^+$)

Synthesis of derivatives DATA^{5m}-Bz-NCS (A), DATA^{5m}-en-SA (B), DATA^{5m}-TEG-N_3 (C) and DATA^{5m}-en-SA-PAM (D)

*1,4-Di(acetate)-6-((5-((4-isothiocyanatobenzyl)amino)-5-oxopentyl)-6-(amino(methyl)-acetate)-perhydro-1,4-diazepane(*DATA^{5m}-Bz-NCS (**A**)*)*

*1,4-Di(tert-butylacetate)-6-((5-((4-nitrobenzyl)-amino)-5-oxopentyl)-6-(amino(methyl)-(tert-butylacetate)-perhydro-1,4-diazepane (**6**)*

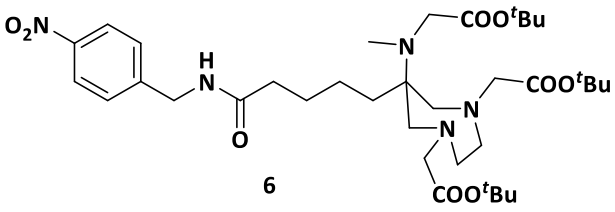

6

5 (0.17 g; 0.30 mmol) was dissolved in dry acetonitrile (1 mL), combined with HATU (0.14 g; 0.36 mmol), DIEA (157 µL; 0.90 mmol) and stirred for 15 min at room temperature. To this solution 4-nitrobenzylamine hydrochloride (0.08 g; 0.45 mmol) was added and stirred for 1 h at room temperature. After completion of the reaction the solution was concentrated under vacuum and the residue was purified via column chromatography (DCM/MeOH; 20:1; R_f=0.29). The product **6** was obtained as orange oil (0.17 g; 0.24 mmol; 80 %).

^{1}H-NMR ($CDCl_3$, 400 MHz, δ [ppm]): 8.27 (br, 1 H); 8.12 (d, J=8.48 Hz, 2 H); 7.47 (d, J=8.48 Hz, 2 H); 4.45 (d, J=5.31 Hz, 2 H); 3.89 (s, 2 H); 3.38-3.25 (m, 6 H); 2.99-2.96 (m, 6 H); 2.81 (s, 3 H); 2.34 (t, 2 H); 1.68-1.64 (m, 4 H); 1.50 (s, 9 H); 1.43 (s, 18 H); 1.37-1.31 (m, 2 H); ^{13}C-NMR ($CDCl_3$, 100 MHz, δ [ppm]):

173.88 (s); 169.27 (s); 166.48 (s); 147.09 (s); 147.01 (s); 128.52 (s); 123.70 (s); 85.88 (s); 82.54 (s); 69.01 (s); 59.97 (s); 53.86 (s); 52.38 (s); 42.73 (s); 37.34 (s); 34.47 (s); 30.11 (s); 28.17 (s); 27.92 (s); 25.58 (s); 22.01 (s)

MS (ESI^+): m/z (%): 706.38, 707.42, 708.45 ($M+H^+$); 728.43, 729.44, 730.45 ($M+Na^+$)

*1,4-Di(acetate)-6-((5-((4-isothiocyanatobenzyl)-amino)-5-oxopentyl)-6-(amino(methyl)-(acetate)-perhydro-1,4-diazepane (**A**)*

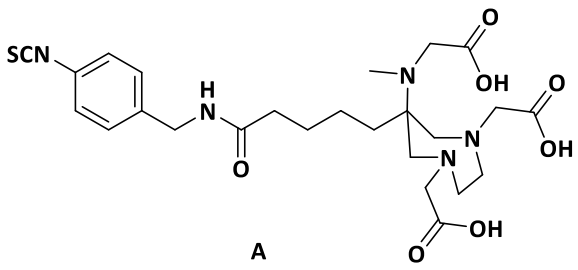

A

6 (25 mg; 0,035 mmol) was dissolved in tetrahydrofuran (2 mL) and suspended with Raney®Nickel 2800®. The suspension was flushed with and kept under hydrogen for 5 h at room temperature. After completion the mixture was filtrated over celite/sand, the celite was washed twice with methanol (5 mL) and the organic layer was concentrated under vacuum. The obtained product was used without further purification (21.3 mg; 0,032 mmol; 90 %). The residue was stirred at room temperature in dry dichloromethane (1 mL) and TEA (8.9 µL; 0,064 mmol) for 15 minutes. To this solution thiophosgene (3.7 µL; 0.048 mmol), dissolved in dry dichlormethane (1 mL), was added and stirred for 1 h. The solution was quenched with 1 M NaOH solution and extracted with dichloromethane. The organic layer was concentrated under vacuum and the obtained product was dissolved in dichloromethane/trifluoroacetic acid (1:1, vol%). After 5 h the solvent was removed under vacuum and the residue was purified via HPLC to obtain product **A** as colorless solid (5.3 mg ; 0.010 mmol; 28 %; t_R=11.0 min (34 % ACN (0.1 % TFA))).

^{1}H-NMR (CD_3CN, 400 MHz, δ [ppm]): 7.27 (m, 4 H); 4.28 (s, 2 H); 3.61 (s, 2 H); 3.47 (s, 4 H); 3.21 (d, J=3.21 Hz, 2 H); 2.96 – 2.84 (m, 6 H); 2.71 (s, 3 H); 2.19 (t, J=2.20 Hz, 2 H); 1.52 (m, 4 H); 1.25 (m, 2 H);

^{13}C-NMR (CD_3CN, 100 MHz, δ [ppm]): 174.35 (s); 172.81 (s); 138.92 (s); 128.71 (s); 125.85 (s); 68.16 (s); 58.47 (s), 54.41 (s); 54.28 (s); 53.50 (s); 52.25 (s); 46.37 (s); 42.02 (s); 36.93 (s); 35.15 (s); 30.15 (s); 25.98 (s); 22.13 (s)

MS (ESI^+): m/z (%): 550.2248, 551.2264, 552.2162 ($M+H^+$)

*1,4-Di(acetate)-6-((5-(2-((2-ethoxy-3,4-dioxocyclobut-1-en-1yl)aminoethyl)amino)-5-oxopentyl)-6-(amino(methyl)-acetate)-perhydro-1,4-diazepane (*DATA^{5m}-en-SA (**B**)*)*

*1,4-Di(tert-butylacetate)-6-((5-(2-((tert-butoxy-carbonyl)aminoethyl)amino)-5-oxopentyl)-6-(amino(methyl)-tert-butylacetate)-perhydro-1,4-diazepane (**7**)*

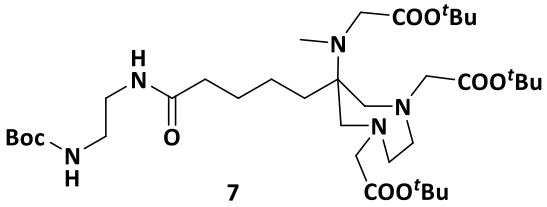

7

5 (46 mg; 0.08 mmol) was dissolved in dry acetonitrile (1 mL), combined with HATU (30 mg; 0.08 mmol), DIEA (42 µL; 0.24 mmol) and stirred for 15 min at room temperature. To this solution *tert*-butyl(2-aminoethyl)carbamate (19 µL; 0.12 mmol) was added and stirred for 1 h at room temperature. After completion of the reaction the solution was concentrated under vacuum and the residue was purified via column chromatography ($CHCl_3$/MeOH, 20:1, R_f=0.14). The product **7** was obtained as yellowish oil (46 mg; 0.06 mmol; 80 %).

^{1}H-NMR (DMSO, 400 MHz, δ [ppm]): 3.36 (s, 2 H); 3.23 (s, 4 H); 3.07-3.01 (m, 2 H); 2.97-2.91 (m, 2 H); 2.79 (d, J=13.7 Hz, 2 H); 2.72-2.67 (m, 2 H); 2.59-2.54 (m, 2 H); 2.51 (d, J=13.7 Hz, 2 H); 2.17 (s, 3 H); 2.03 (t, 2 H); 1.45-1.41 (m, 4 H); 1.40 (s, 18 H); 1.39 (s, 9 H); 1.37(s, 9 H); 1.22-1.18 (m, 2 H)

^{13}C-NMR ($CDCl_3$, 100 MHz, δ [ppm]): 172.25 (s); 171.72 (s); 170.28 (s); 169.58 (s); 155.62 (s); 80.19 (s); 80.08 (s); 77.63 (s); 62.37 (s); 61.87 (s); 61.73 (s); 58.72 (s); 56.06 (s); 51.50 (s); 37.10 (s); 35.55 (s); 28.24 (s); 27.87 (s); 27.77 (s); 26.11 (s); 25.50 (s); 21.55 (s).

MS (ESI$^+$): m/z (%): 714.42, 715.46, 716.50 (M+H$^+$); 736.48, 737.15, 737.50 (M+Na$^+$)

*1,4-Di(acetate)-6-((5-(2-((2-ethoxy-3,4-dioxo-cyclobut-1-en-1yl)aminoethyl)amino)-5-oxo-pentyl)-6-(amino(methyl)-acetate)-perhydro-1,4-diazepane (**B**)*

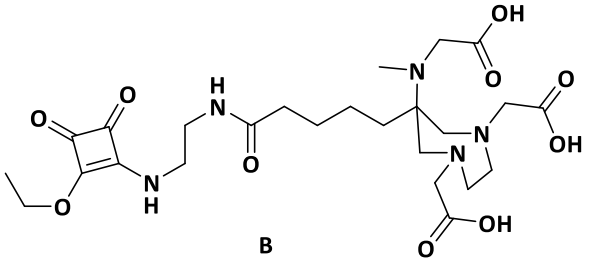

B

9 (28 mg; 0.04 mmol) was dissolved in dichloromethane/trifluoroacetic acid (1:1; vol%) and stirred for 3 h. After completion of the reaction the solvent was removed under vacuum and the residue was dissolved in 0.5 M phosphate buffer (pH 7; 3 mL). To this solution 3,4-diethoxycyclobut-3-ene-1,2-dione (16 mg; 0,03 mmol) was added, the pH was adjusted with 1 M NaOH solution to pH 7 and the reaction was stirred over night at room temperature. After completion the reaction mixture was purified via HPLC to obtain the product **B** as colourless solid (7.2 mg; 0.01 mmol; 33 %; t_R=9.4 min (12 % ACN (0.1 % TFA).

^{1}H-NMR (D_2O, 600 MHz, δ [ppm]): 4.73-4.66 (m, 2 H); 3.79 (s, 2 H); 3.70 (s, 4 H), 3.67-3.47 (m, 6 H); 3.39-3.22 (m, 6 H); 2.98 (d, J=8.7 Hz, 3 H); 2.22 (t, 2 H); 1.71-1.68 (m, 2 H); 1.53-1.48 (m, 2 H); 1.43-1.38 (m, 2 H); 1.35-1.29 (m, 2 H)

^{13}C-NMR (D_2O, 150 MHz, δ [ppm]): 188.70 (s); 183.25 (s); 177.21 (s); 176.42 (s); 173.82 (s); 170.00 (s); 117.19 (s); 115.26 (s); 70.66 (s); 68.77 (s); 54.14 (s); 43.89 (s); 39.22 (s); 37.76 (s); 35.09 (s); 29.53 (s); 25.69 (s); 25.54 (s); 22.09 (s); 15.03 (s); 14.94 (s).
HRMS (ESI$^+$): m/z (%): 570.2778, 571.2919, 572.2980 ($M+H^+$)

*1,4-Di(acetate)-6-(1-azido-13-oxo-3,6,9-trioxa-12-azadecan-12-yl)amino)-5-oxopentyl)-6-(amino-(methyl)-acetate)-perhydro-1,4-diazepane (*DATA^{5m}-TEG-N_3 (**C**))

*1,4-Di(acetate)-6-(1-azido-3,6,9-trioxa-12-azadecan-12-yl)-amino)-5-oxopentyl)-6-(amino(methyl)-acetate)-perhydro-1,4-diazepane (**C**)*

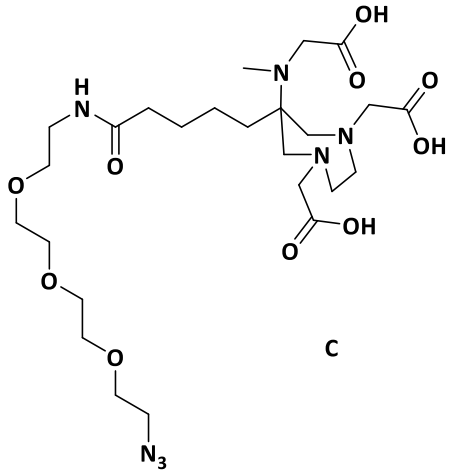

C

5 (32 mg; 0.06 mmol) was dissolved in dry acetonitrile (1 mL), combined with HOBt (8.3 mg; 0.06 mmol), EDC·HCl (11.8 mg, 0.06 mmol) and DIEA (19 µL; 0.11 mmol) and stirred for 15 min at room temperature. To this solution 11-azido-3,6,9-trioxa-undecan-1-amine (12.3 µL; 0.06 mmol) was added and stirred for 1 h at room temperature. After completion of the reaction the solution was concentrated under vacuum and the residue was dissolved in dichloromethane/trifluoroacetic acid (1:1; vol %). After 3 h at room temperature the solution was concentrated under vacuum and the residue was purified via HPLC to obtain product **C** as colourless solid (11.3 mg; 0.02 mmol; 33 %; t_R=10.0 min (15 % ACN (0.1 % TFA))).
^{1}H-NMR ($CDCl_3$, 400 MHz, δ [ppm]): 3.85 (s, 2 H); 3.73-3.68 (m, 14 H); 3.61 (t, 2 H); 3.56-3.49 (m, 6 H); 3.38-3.34 (m, 4 H); 3.27-3.22 (m, 2 H); 3.00 (s, 3 H); 2.27 (t, 2 H); 1.77-1.73 (m, 2 H); 1.64-1.57 (m, 2 H); 1.42-1.34 (m, 2 H); ^{13}C-NMR (D_2O, 100 MHz, δ [ppm]): 176.39 (s); 172.48 (s); 169.94 (s); 69.59 (s); 69.54 (s); 69.47 (s); 69.35 (s); 69.16 (s); 68.96 (s); 68.78 (s); 58.93 (s); 56.51 (s); 54.03 (s); 52.86 (s); 50.11 (s); 38.84 (s); 37.86 (s); 35.02 (s); 29.61 (s); 25.54 (s); 22.03 (s).
HRMS (ESI$^+$): m/z (%): 604.3314, 605.3481, 606.3568 ($M+H^+$)

*2,2'-(6-((carboxymethyl)(methyl)amino)-6-(5-((2-((2-((3-hydroxy-3,3-diphosphonopropyl)amino)-3,4-dioxocyclobut-1-en-1-yl)amino)ethyl)amino)-5-oxopentyl)-1,4-diazepane-1,4-diyl)diacetic acid (*DATA^{5m}-en-SA-PAM (**D**)*)*

B (4.7 mg; 8.2 µmol) was dissolved in Na_2HPO_4 solution (0.5 M, pH 9) and added to a solution of **PAM** (11 mg, 46.9 µmol) in Na_2HPO_4 solution, which was adjusted to pH 9 with NaOH (TraceSelect). The mixture was stirred at room temperature for 16 h. After completion of the reaction, the mixture was purified via HPLC to obtain product **D** as colourless solid (3.4 mg, 4.5 µmol, 55 %; t_R=6.5 min (12 % ACN (0.1 % TFA))).

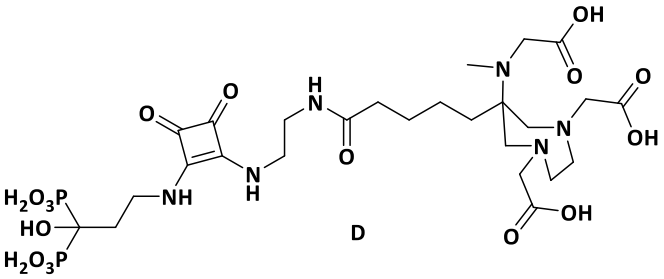

D

^{1}H-NMR ($CDCl_3$, 400 MHz, δ [ppm]): 3.73 (s, 2 H); 3.63 ((s, 4 H); 3.48-3.18 (m, 10 H); 2.20-2.12 (m, 5 H); 1.65-1.61 (m, 2 H); 1.45-1.41 (m, 2 H); 1.30-1.23 (m, 2 H)

MS (ESI$^+$): m/z (%): 759.2; 760.2; 761.3 ($M+H^+$)

Radiolabelling and *in vitro* evaluation

Kinetic studies

Following figures show the kinetic studies of the 4 derivatives with the buffer systems sodium acetate (NaOAc, 0.25 M, pH 4.5), ammonium acetate (AmOAc, 0.25 M, pH 5.5) and *N*-2-hydroxyethyl piperazine-*N'*-2-ethanesulfonic acid (HEPES, 0.25 M and 0.025 M, pH 4.3, respectively). All values were analysed via radio-TLC (silica gel, citrate buffer (0.01 M, pH 4) or acetone/ acetylacetone/ conc. HCl (3:3:1 vol%) as mobile phase) and verified with radio-HPLC (after 15 min labelling reaction).

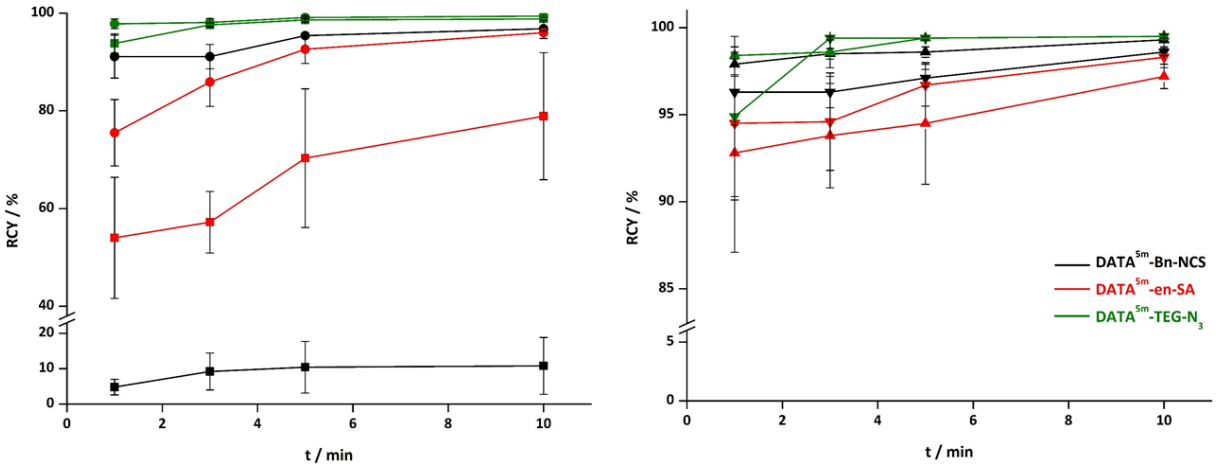

Figure 3: Radiolabelling kinetics with ^{68}Ga of the derivatives DATA^{5m}-Bz-NCS (–), DATA^{5m}-en-SA (–) and DATA^{5m}-TEG-N$_3$ (–) in NaOAc (0.25 M, pH 4.5) with 1 µM (■), 2.5 µM (●), 5 µM (▲) and 10 µM (▼) at 25 °C; n=3

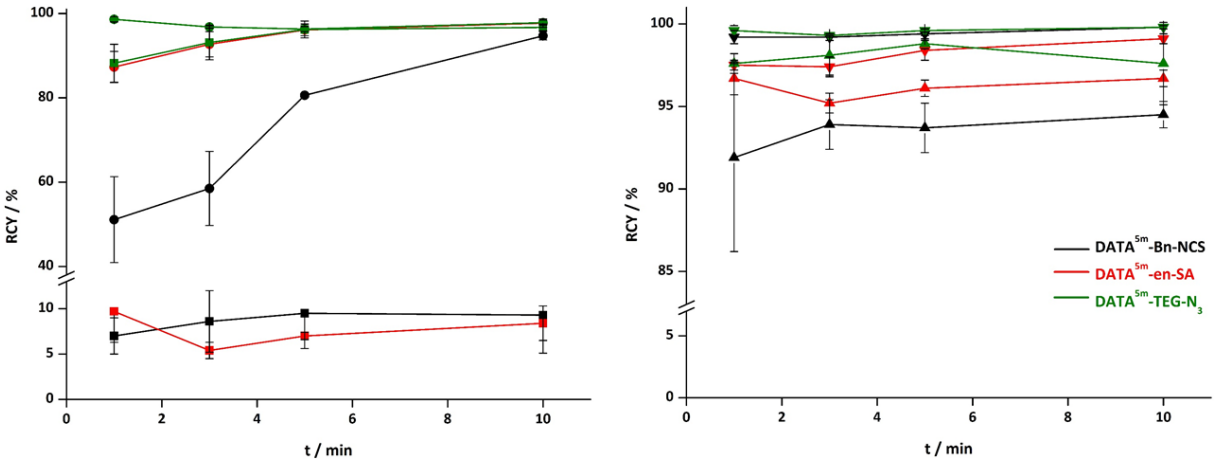

Figure 4: Radiolabelling kinetics with ^{68}Ga of the derivatives DATA^{5m}-Bz-NCS (–), DATA^{5m}-en-SA (–) and DATA^{5m}-TEG-N$_3$ (–) in AmOAc (0.25 mM, pH 5.5) with 1 µM (■), 2.5 µM (●), 5 µM (▲) and 10 µM (▼) at 25 °C; n=3

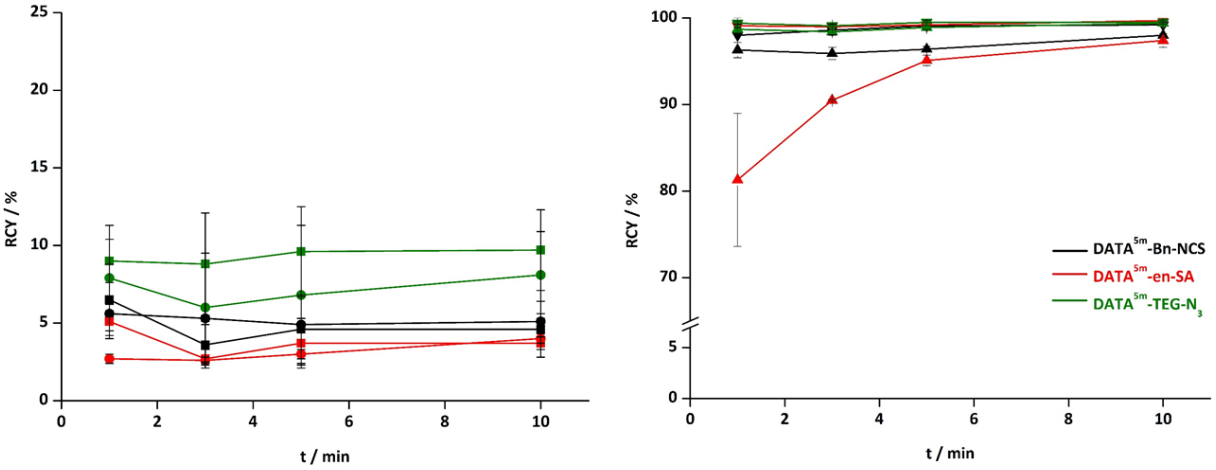

Figure 5: Radiolabelling kinetics with ^{68}Ga of the derivatives DATA^{5m}-Bz-NCS (–), DATA^{5m}-en-SA (–) and DATA^{5m}-TEG-N$_3$ (–) in HEPES (0.25 M, pH 4.3) with 1 µM (■), 2.5 µM (●), 5 µM (▲) and 10 µM (▼) at 25 °C; n=3

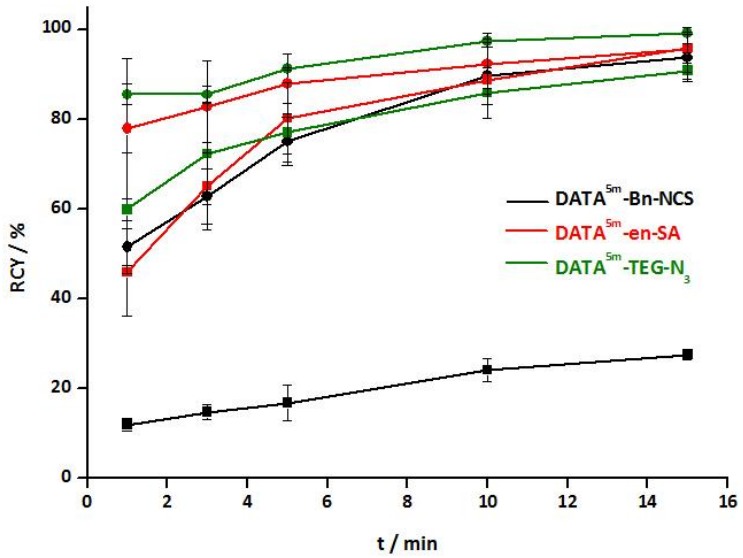

Figure 6: Radiolabelling kinetics with ^{68}Ga of the derivatives DATA^{5m}-Bz-NCS (–), DATA^{5m}-en-SA (–) and DATA^{5m}-TEG-N$_3$ (–) in HEPES (0.025 M, pH 4.3) with 1 µM (■) and 2.5 µM (●) at 25 °C; n=3

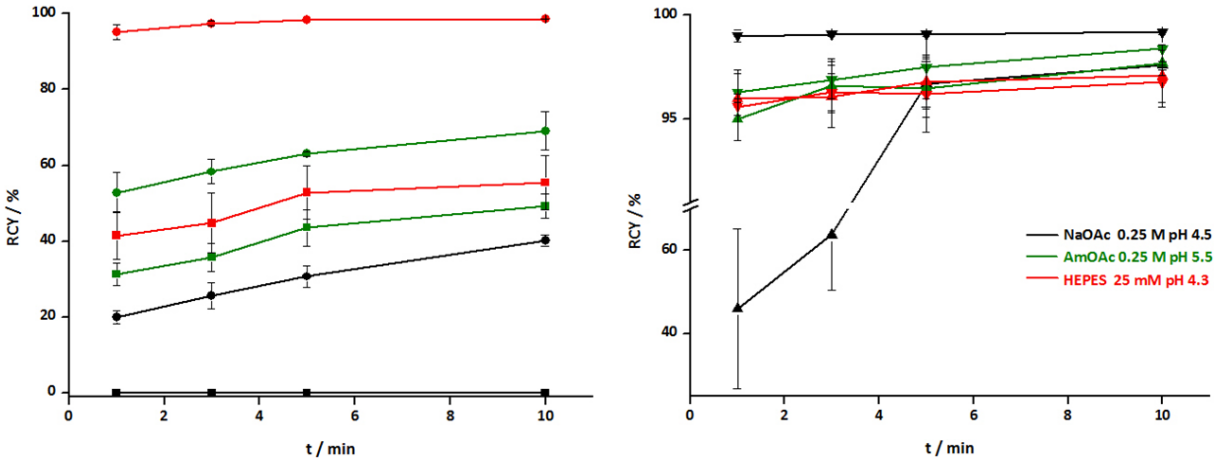

Figure 7: Radiolabelling kinetics with ^{68}Ga of the derivatives DATA^{5m}-en-QS-PAM in NaOAc (–), AmOAc (–) and HEPES (–) with 1 µM (■), 2.5 µM (●), 5 µM (▲) and 10 µM (▼) at 90 °C; n=3

Stability studies

Following figures show histograms after 1 and 2 h as well as the HPLC chromatograms after 2 h of the ligands [^{68}Ga]Ga-**A**, [^{68}Ga]Ga-**B** and [^{68}Ga]Ga-**C** in the media human serum (HS), DTPA, EDTA and PBS. All values were obtained by analysis of the ligands by means of HPLC (LaChrom (Merck), Luna 10 u (C18) 100 Å (250x10.00 mm 10 micron); gradient: 0 % ACN (0.1 % TFA) for 1 min, 15 % to 95 % ACN (0.1 % TFA) in 15 min, 95 % ACN (0.1 % TFA) for 3 min).

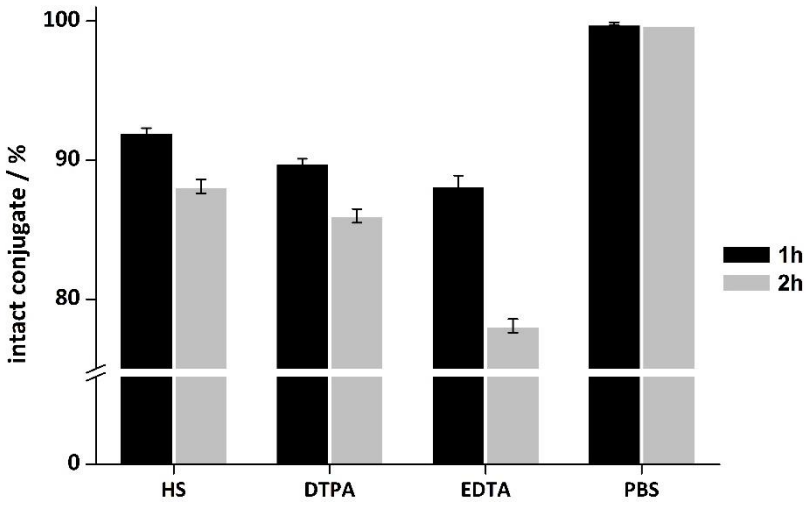

Figure 8: *In vitro* stability of [^{68}Ga]Ga-DATA^{5m}-Bz-NCS ([^{68}Ga]Ga-**A**) in HS, DTPA, EDTA and PBS after 1 h (■) and 2 h (■), n=3

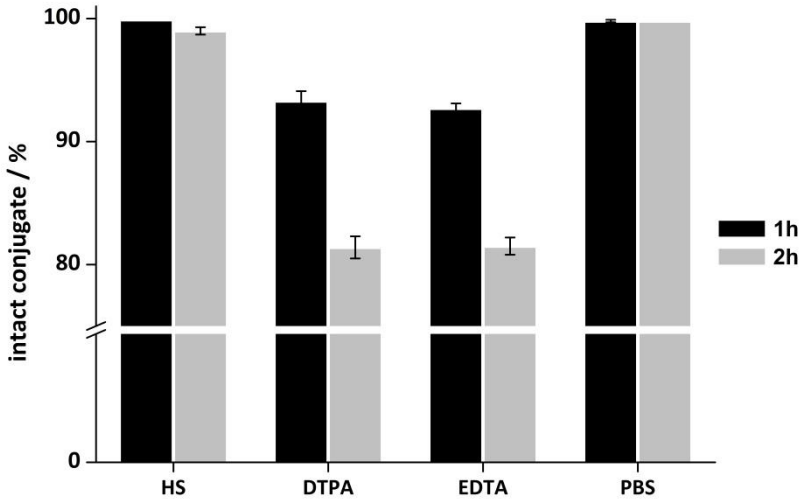

Figure 9: I*n vitro* stability of [^{68}Ga]Ga-DATA^{5m}-en-QS ([^{68}Ga]Ga-**B**) in HS, DTPA, EDTA and PBS after 1 h (■) and 2 h (■), n=3

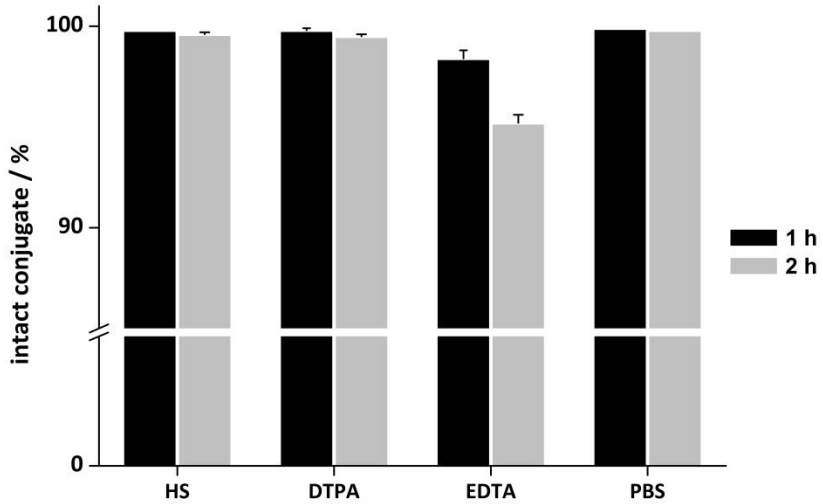

Figure 10: *In vitro* stability of [^{68}Ga]Ga-DATA^{5m}-TEG-N_3 ([^{68}Ga]Ga-**C**) in HS, DTPA, EDTA and PBS after 1 h (■) and 2 h (■); n=3

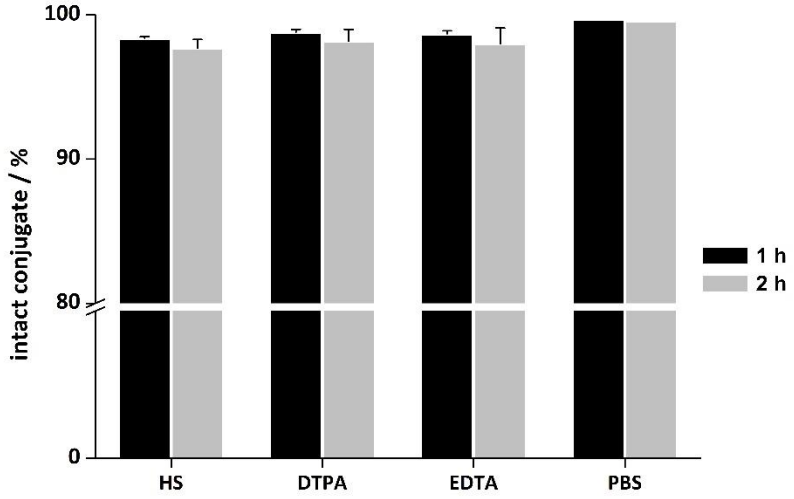

Figure 11: *In vitro* stability of [^{68}Ga]Ga-DATA^{5m}-en-QS-PAM ([^{68}Ga]Ga-**D**) in HS, DTPA, EDTA and PBS after 1 h (■) and 2 h (■); n=3

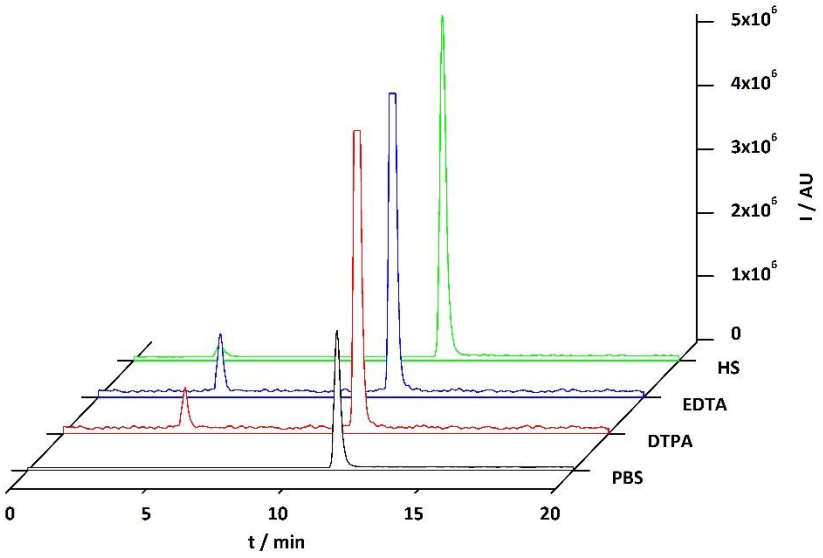

Figure 12: *In vitro* stability analysis of [^{68}Ga]Ga-**A** after 2 h in HS (–), EDTA (–), DTPA (–) and PBS (–)

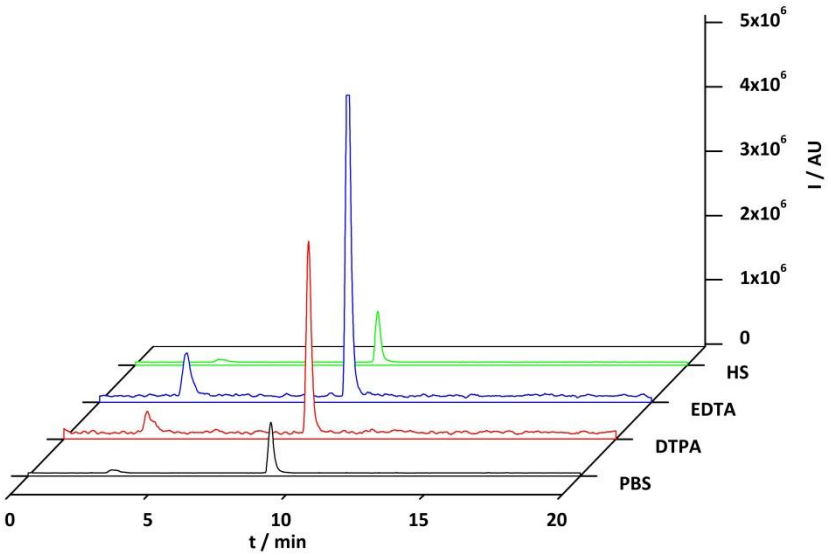

Figure 13: *In vitro* stability analysis of [^{68}Ga]Ga-**B** after 2 h in HS (–), EDTA (–), DTPA (–) and PBS (–)

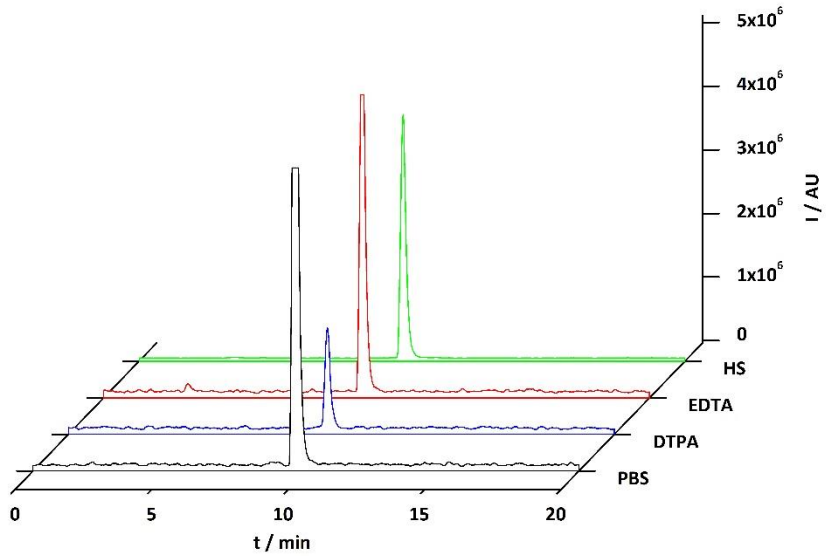

Figure 14: *In vitro* stability analysis of [^{68}Ga]Ga-**C** after 2 h in HS (–), EDTA (–), DTPA (–) and PBS (–)

REFERENCES

1. Bulman R.A. Chelating agents and the regulation of metal ions. Met. Based. Drugs. 1994; 1(7): 87–106.

2. Price E.W., Orvig C. Matching chelators to radiometals for radiopharmaceuticals. Chem. Soc. Rev. 2014; 43(1): 260–90.

3. Bailey G.A., Price E.W., Zeglis B.M., Ferreira C.L., Boros E., Lacasse M.J., Patrick B.O., Lewis J.S., Adam M.J., Orvig C. H_2azapa: A versatile acyclic multifunctional chelator for Ga-67, Cu-64, In-111, and Lu-177. Inorg. Chem. 2012; 51(22): 12575–89.

4. Price E.W., Zeglis B.M., Cawthray J.F., Ramogida C.F., Ramos N., Lewis J.S., Adam M.J., Orvig C. H_4octapa-trastuzumab: Versatile acyclic chelate system for In-111 and Lu-177 imaging and therapy. J. Am. Chem. Soc. 2013; 135(34): 12707–21.

5. Li W.P., Ma D.S., Higginbotham C., Hoffman T., Ketring A.R., Cutler C.S., Jurisson S.S. Development of an in vitro model for assessing the in vivo stability of lanthanide chelates. Nucl. Med. Biol. 2001; 28(2): 145–54.

6. Hancock R.D. Chelate ring size and metal ion selection. The basis of selectivity for metal ions in open-chain ligands and macrocycles. J. Chem. Educ. 1992; 69(8): 615–21.

7. Liu S., Edwards S.D. Bifunctional chelators for therapeutic lanthanide radiopharmaceuticals. Bioconjug. Chem. 2001; 12(1): 7–34.

8. Berry D.J., Ma Y., Ballinger J.R., Tavaré R., Koers A., Sunassee K., Zhou T., Nawaz S., Mullen G.E.D., Hider R.C., Blower P.J. Efficient bifunctional gallium-68 chelators for positron emission tomography: tris(hydroxypyridinone) ligands. Chem. Commun. 2011; 47(25): 7068–70.

9. Eder M., Wängler B., Knackmuss S., LeGall F., Little M., Haberkorn U., Mier W., Eisenhut M. Tetrafluorophenolate of HBED-CC: A versatile conjugation agent for Ga-68-labeled small recombinant antibodies. Eur. J. Nucl. Med. Mol. Imaging. 2008; 35(10): 1878–86.

10. Eder M., Neels O., Müller M., Bauder-Wüst U., Remde Y., Schäfer M., Hennrich U., Eisenhut M., Afshar-Oromieh A., Haberkorn U., Kopka K. Novel preclinical and radiopharmaceutical aspects of Ga-68-PSMA-HBED-CC: A new PET tracer for imaging of prostate cancer. Pharmaceuticals. 2014; 7(7): 779–96.

11. Boros E., Ferreira C.L., Cawthray J.F., Price E.W., Patrick B.O., Wester D.W., Adam M.J., Orvig C. Acyclic chelate with ideal properties for Ga-68 PET imaging agent elaboration. J. Am. Chem. Soc. 2010; 132(44): 15726–33.

12. Boros E., Ferreira C.L., Yapp D.T.T., Gill R.K., Price E.W., Adam M.J., Orvig C. RGD conjugates of the H_2dedpa scaffold: Synthesis, labeling and imaging with ^{68}Ga. Nucl. Med. Biol. 2012; 39(6): 785–94.

13. Waldron B.P., Parker D., Burchardt C., Yufit D.S., Zimny M., Rösch F. Structure and stability of hexadentate complexes of ligands based on AAZTA for efficient PET labelling with gallium-68. Chem. Commun. 2013; 49: 579–81.

14. Eliel E.L., Wilen S.H. Stereochemistry of Organic Compounds. 1993.

15. Hirsch J. A. Topics in Stereochemistry. 1967.

16. Farkas E., Nagel J., Waldron B.P., Parker D., Tóth I., Brücher E., Rösch F., Baranyai Z. Equilibrium, kinetic and structural properties of gallium(III)- and some divalent metal complexes formed with the new DATA^{m} and DATA^{5m} ligands. Chem. - A Eur. J. 2017 (accepted).

17. Meares C.F., McCall M.J., Reardan D.T., Goodwin D.A., Diamanti C.I., McTigue M. Conjugation of antibodies with bifunctional chelating agents: Isothiocyanate and bromoacetamide reagents, methods of analysis, and subsequent addition of metal ions. Anal. Biochem. 1984; 142(1): 68–78.

18. Brechbiel M.W., Gansow O.A., Atcher R.W., Schlom J., Esteban J., Simpson D.E., Colcher D. Synthesis of 1-(*p*-isothiocyanatobenzyl) derivatives of DTPA and EDTA. Antibody labeling and tumor-imaging studies. Inorg. Chem. 1986; 25(16): 2772–81.

19. Esteban J.M., Schlom J., Gansow O.A., Atcher R.W., Brechbiel M.W., Simpson D.E., Colcher D. New Method for the Chelation of Indium-111 to Monoclonal Antibodies : Biodistnbution and Imaging of Athymic Mice Bearing Human Colon Carcinoma Xenografts. 1987; 28(5): 861–71.

20. Halime Z., Frindel M., Camus N., Orain P.-Y., Lacombe M., Cherel M., Gestin J.-F., Faivre-Chauvet A., Tripier R. New synthesis of phenyl-isothiocyanate C-functionalised cyclams. Bioconjugation and Cu-64 phenotypic PET imaging studies of multiple myeloma with the te2a derivative. Org. Biomol. Chem. 2015; 13(46): 11302–14.

21. Tietze L.F., Arlt M., Beller M., Glüsenkamp K.-H., Jähde E., Rajewsky M.F. Anticancer Agents, 15. Squaric Acid Diethyl Ester: A New Coupling Reagent for the Formation of Drug Biopolymer Conjugates. Synthesis of Squaric Acid Ester Amides and Diamides. Chem. Ber. 1991; 124(5): 1215–21.

22. Rudd S.E., Roselt P., Cullinane C., Hicks R.J., Donnelly P.S. A desferrioxamine B squaramide ester for the incorporation of zirconium-89 into antibodies. Chem. Commun. 2016; 52: 1–4.

23. Huisgen R. 1,3-Dipolar Cycloadditions. Past and Future. Angew. Chem. Int. Ed. 1963; 2(10): 565–98.

24. Jewett J.C., Bertozzi C.R. Cu-free click cycloaddition reactions in chemical biology. Chem. Soc. Rev. 2010; 39(4): 1272–9.

25. Liu X., Hermange P., Ruiz J., Astruc D. Pd/C as an Efficient and Reusable Catalyst for the Selective N-Alkylation of Amines with Alcohols. ChemCatChem. 2016; (2 mL): 1043–5.

26. García Ruano J.L., Parra A., Alemán J., Yuste F., Mastranzo V.M. Monoalkylation of primary amines and N-sulfinylamides. Chem. Commun. (Camb). 2009; 404–6.

27. Russell H.F., Bremner J.B., Bushelle-Edghill J., Lewis M.R., Thomas S.R., Bates F. A new palladium-mediated approach to 4-N-arylamino-1-butanols from peroxidic tetrahydrofuran and primary aromatic amines. Tetrahedron Lett. 2007; 48(9): 1637–9.

28. Eisenwiener K.P., Prata M.I.M., Buschmann I., Zhang H.W., Santos A.C., Wenger S., Reubi J.C., Mäcke H.R. NODAGATOC, a new chelator-coupled somatostatin analogue labeled with Ga-67/68 and In-111 for SPECT, PET, and targeted therapeutic applications of somatostatin receptor (hsst2) expressing tumors. Bioconjug. Chem. 2002; 13(3): 530–41.

29. Velikyan I., Mäcke H.R., Langstrom B. Convenient Preparation of Temperature Ga-Based PET-Radiopharmaceuticals at Room. Bioconjug. Chem. 2008; 19: 569–73.

30. Piggot P.M.T., Hall L.A., White A.J.P., Williams D.J., Thompson L.K. Synthesis, Structure, and Magnetochemical Analysis of Selected First-Row Transition-Metal Anilino- and Anisolesquarate Compounds. Inorg. Chem. 2004; 43(3): 1167–74.

31. Alleyne B.D., St. Bernard L., Jaggernauth H., Hall L.A., Baxter I., White A.J.P., Williams D.J. Lanthanide Complexes of 3-Diphenylamino-4-hydroxycyclobut-3-ene-1,2-dione (Diphenylamino-squarate). Inorg. Chem. 1999; 38(17): 3774–8.

32. Azab H.A., Abou El Nour K.M., Sherif S. Metal ion complexes containing di-, tripeptides and biologically important zwitterionic buffers. J. Chem. Eng. Data. 2007; 52: 381–390.

33. Martins A.F., Prata M.I.M., Rodrigues S.P.J., Geraldes C.F.G.C., Riss P.J., Amor-Coarasa A., Burchardt C., Kroll C., Rösch F. Spectroscopic, radiochemical, and theoretical studies of the Ga3+-N-2-hydroxyethyl piperazine-N'-2-ethanesulfonic acid (HEPES buffer) system: Evidence for the formation of Ga^{3+}-HEPES complexes in Ga-68 labeling reactions. Contrast Media Mol. Imaging. 2013; 8(3): 265–73.

34. Holub J., Meckel M., Kubíček V., Rösch F., Hermann P. Gallium(III) complexes of NOTA-bis (phosphonate) conjugates as PET radiotracers for bone imaging. Contrast Media Mol. Imaging. 2015; 10(2): 122–34.

35. Suzuki K., Satake M., Suwada J., Oshikiri S., Ashino H., Dozono H., Hino A., Kasahara H., Minamizawa T. Synthesis and evaluation of a novel Ga-68-chelate-conjugated bisphosphonate as a bone-seeking agent for PET imaging. Nucl. Med. Biol. 2011; 38(7): 1011–8.

36. Sasson R., Vaknin D., Bross A., Lavie E. Determination of HEPES in Ga-68-labeled peptide solutions. J. Radioanal. Nucl. Chem. 2010; 283(3): 753–6.

37. Macedo S., Pechlaner M., Schmid W., Weik M., Sato K., Dennison C., Djinović-Carugo K. Can soaked-in scavengers protect metalloprotein active sites from reduction during data collection? J. Synchrotron Radiat. 2009; 16(2): 191–204.

38. de Blois E., Sze Chan H., Naidoo C., Prince D., Krenning E.P., Breeman W.A.P. Characteristics of SnO_2-based Ge-68/Ga-68 generator and aspects of radiolabelling DOTA-peptides. Appl. Radiat. Isot. 2011; 69(2): 308–15.

39. Sudbrock F., Fischer T., Zimmermanns B., Guliyev M., Dietlein M., Drzezga A., Schomäcker K. Characterization of SnO_2-based Ge-68/Ga-68 generators and Ga-68-DOTATATE preparations: radionuclide purity, radiochemical yield and long-term constancy. EJNMMI Res. 2014; 4(1): 36.

40. Simecek J., Hermann P., Wester H.J., Notni J. How is Ga-68 Labeling of Macrocyclic Chelators Influenced by Metal Ion Contaminants in Ge-68/Ga-68 Generator Eluates? ChemMedChem. 2013; 8(1): 95–103.

41. Banerjee S., Pillai M.R.A., Ramamoorthy N. Evolution of Tc-99m in diagnostic radiopharmaceuticals. Semin. Nucl. Med. 2001; 31(4): 260–77.

42. Zolle I. Technetium-99m Pharmaceuticals. 2007.

43. Zhernosekov K.P., Filosofov D. V., Baum R.P., Aschoff P., Bihl H., Razbash A., Jahn M., Jennewein M., Rösch F. Processing of generator-produced Ga-68 for medical application. J. Nucl. Med. 2007; 48(10): 1741–8.

44. Kovács R., Grün A., Németh O., Garadnay S., Greiner I., Keglevich G. The synthesis of pamidronic derivatives in different solvents: an potimization and a mechanistic study. Int. J. Nanomedicine. 2014; 25(3): 186–93.

4.5 Synthesis and radiolabelling of new AAZTA-derivatives with ^{177}Lu for mild coupling with targeting vectors

Synthesis and radiolabelling of new AAZTA-derivatives with ^{177}Lu for mild coupling with targeting vectors

J. Nagel, J. P. Sinnes, F. Rösch

Institute of Nuclear Chemistry, Johannes Gutenberg-University of Mainz, Germany

ABSTRACT

The development of new chelating agents has become an important field for nuclear medical applications. Because the beta emitting nuclide ^{177}Lu ($t_{1/2}$=6.6 d) has gathered great attention in the last years, we synthesized and characterized three new derivatives of the heptadentate ligand AAZTA (6-amino-6-methylperhydro-1,4-diazepinetetraacetic acid). The three derivatives AAZTA^5-Bz-NCS (**A**), AAZTA^5-en-SA (**B**) and AAZTA^5-TEG-N_3 (**C**) as well as an antibody conjugate of the NCS ester were radiolabelled with ^{177}Lu under different conditions (chelator-to-Lu ratio, pH, buffer) to approach kit-type labelling of ^{177}Lu at room temperature. All derivatives offered quantivative radiolabelling yields (>95 %) with a chelator-to-Lu ratio of 2:1 after 10 min. Further the stabilities were tested in different media (human serum, PBS, EDTA, DTPA). The Lu-complexes of derivatives **B** and **C** showed high stabilities within all media (>90 % after 24 h), whereas **A** showed a decreased stability, especially in HS. To test the influence on the stability of **A** by introducing a targeting vector to the ligand, **A** was coupled to a monoclonal antibody (mAb). Radiolabelling of the conjugate reached high labelling yields after 15 min (>60 %). Nevertheless, the stability of the Lu-complex could not be influenced and the Lu-conjugate was 31 % after 7 d in human serum.

In summary the new bifunctional AAZTA-based ligands **B** and **C** offer a fast and reliable radiolabelling of ^{177}Lu already at room temperature. This represents a substantial progress compared to ^{177}Lu-DOTA structures, which typically require labelling at 90 °C (or higher) [1–3] and make radiolabelling of temperature sensitive targeting vectors cumbersome. With the new coupling sites the AAZTA ligands can now be introduced to several biomolecular applications like peptides, bisphosphonates, antibodies or even nanoparticles and polymers.

Keywords: Lutetium-177, AAZTA, bifunctional chelator, radiolabelling, buffer

INTRODUCTION

Bifunctional chelators (BFC) have become of great interest for nuclear medical applications. Especially for peptide receptor radionuclide therapy (PRRT) BFCs possess a key role [4–6]. Beside the radionuclides ^{90}Y ($t_{1/2}$=64.1 h; $E_{\beta,max}$=2.27 MeV) [7,8], ^{153}Sm ($t_{1/2}$=46.3 h; $E_{\beta,max}$=0.81 MeV) [8–10] and ^{188}Re ($t_{1/2}$=16.9 h; $E_{\beta,max}$=2.12 MeV) [8,11], ^{177}Lu ($t_{1/2}$=6.71 d; $E_{\beta,max}$=0.49 MeV) has become an important nuclide in the last decades [8,10,12]. This is to the low-energy β^- particles (176 keV (12.2 %), 385 keV (9.1 %) and 498 keV (78.6 %)), the low-energy gamma photons (113 keV, 208 keV) and in particular the high yield production of n.c.a. ^{177}Lu. Therefore several BFCs (based on the DOTA or DTPA scaffold, see scheme 1) have been investigated according to their stability with ^{177}Lu [13].

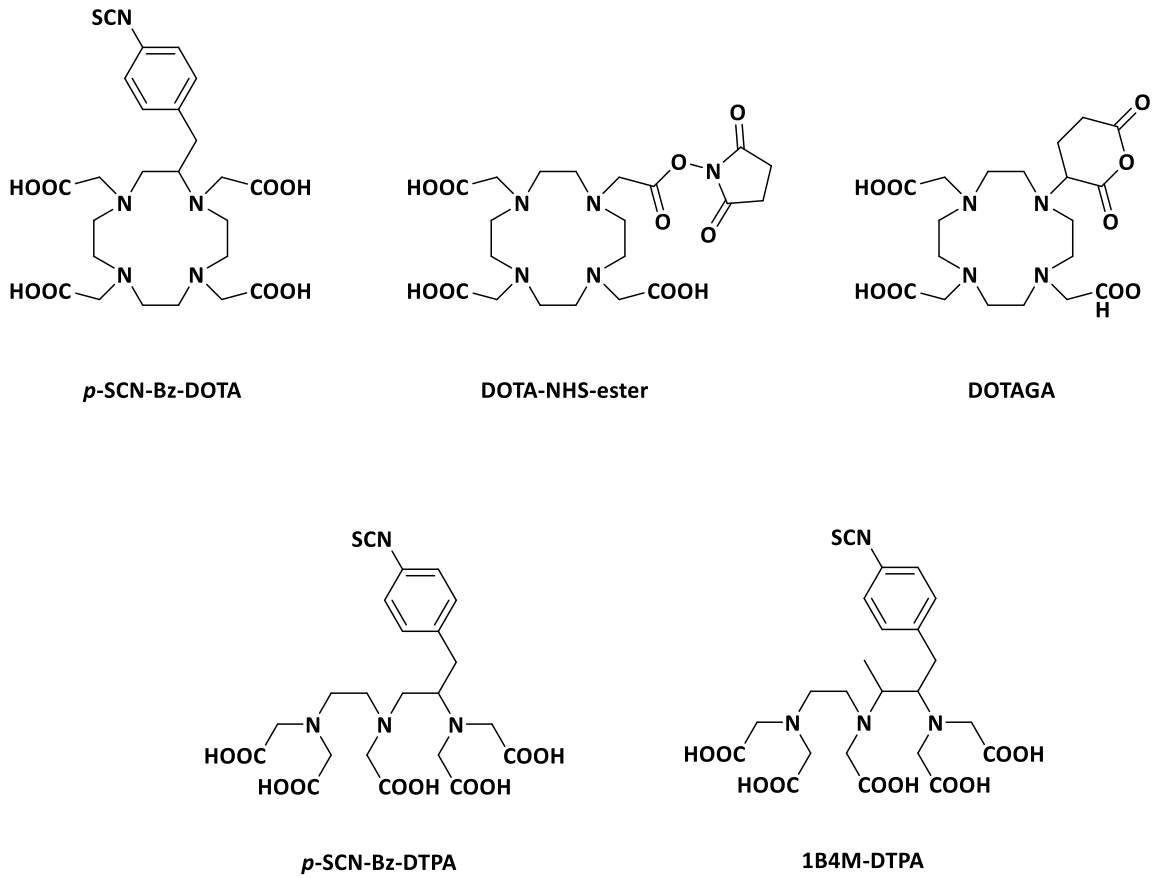

Scheme 1: Bifunctional derivatives of DOTA and DTPA for radiolabelling with ^{177}Lu

In their very beginning DOTA as well as AAZTA were used as complexing agent of Gd^{3+} for MRI imaging [14–18]. Baranyai *et al.* reported the equilibrium and kinetic properties not only of lanthanoids, but also of various divalent metal complexes of the heptadentate ligand AAZTA [19]. The results revealed the highest complex stability for Lu-AAZTA with a $\log K_{ML}$ of 21.85.

Comparing this with DOTA ($\log K_{ML}$=23.5) both complexes possess equal thermodynamic stability with Lu^{3+} [20]. The advantage of AAZTA over DOTA, however, is the fast radio-labelling under mild condi-

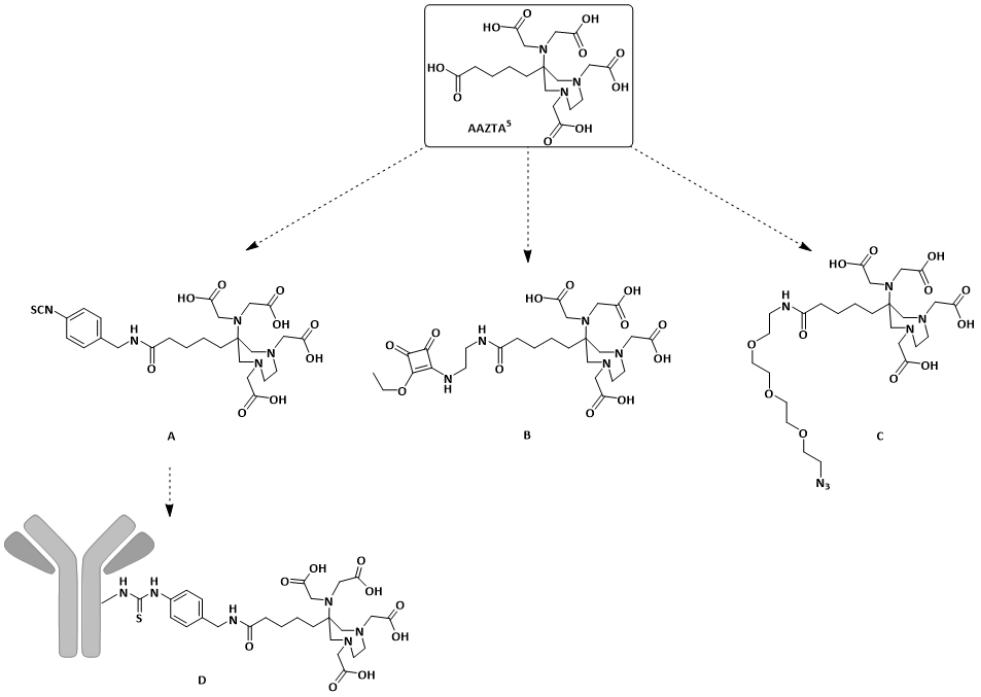

Scheme 2: AAZTA^5 and its different coupling sites: AAZTA^5-Bz-NCS (**A**), AAZTA^5-en-SA (**B**), AAZTA^5-TEG-N_3 (**C**) and AAZTA^5-Bz-NCS-mAb (**D**)

tions (RT, pH 4-5, <10 min). This offers the opportunity to radiolabel targeting vectors (TV) like antibodies, nanoparticles or polymers which are pH and heat sensitive. The AAZTA scaffold described by Baranyai *et al.* demonstrates a stand-alone chelator without a coupling site for the introduction of potential TVs.

To overcome this obstacle, we synthesized the bifunctional AAZTA^5 (scheme 2) and introduced three new coupling sites. These enable the attachment to TVs like antibodies, proteins, nanoparticles and polymers under aqueous conditions within a short time range [21–25].

Derivate **A** (AAZTA^5-Bz-NCS) can be introduced via the benzyl-isothiocyanate group to free, primary amines on polypeptides or antibodies. This coupling site was reported for different chelators like DOTA or DTPA [26–29]. Derivative **B** (AAZTA^5-en-SA) is functionalized with an ethylenediamine squaric acid derivative. This offers the attachment to amines under mild conditions (pH 7, RT) [25,30]. **C** (AAZTA^5-TEG-N_3) contains a triglycol azide linker and can be coupled to nanoparticles, polypeptides or polymers, which are attached to alkyne or ring strained systems like DBCO. This enables a mild coupling via the [1,3] dipolar cycloaddtion [31,32]. We also investigated the influence of the radiolabelling conditions (pH, buffer system, Lu-to-chelator-ratio) of these derivatives with ^{177}Lu. Additionally the stability of the radiometal-complexes in different media (human serum, EDTA, DTPA, PBS) was examined for all ligands.

RESULTS AND DISCUSSION

Organic synthesis

The *tert*-butyl-protected AAZTA^5(^{t}Bu)$_4$ (scheme 4, **4**) was synthesized over 4 steps with an overall yield of 20 %. The synthesis was started with the alkylation of *N,N'*-dibenzylethylenediamine with *tert*-butyl bromoacetate (product **1**). After deprotection of the diamine the diazepane was built by a Nitro-Mannich-reaction with formaldehyde and 2-nitrocyclohexanone to yield product **2**. The nitro group of **2** was reduced to the corresponding amine and alkylated with *tert*-butyl bromoacetate to obtain product **3**. The methyl ester was deprotected with LiOH to yield the derivative for the coupling of the linker (**4**). Starting from product **4** the linkers were coupled via the free carboxylic acid. The coupling reactions for product **5** and **6** were done under the same conditions with HATU, DIEA and ACN at room temperature. For amide bond formation of product **C** HOBt and EDC·HCl was used instead. By use of HATU the amino group of the 11-azido-3,6,9-trioxaundecan-1-amine built the guanidinium ion, which, even by using HPLC methods, could not be separated from the product.

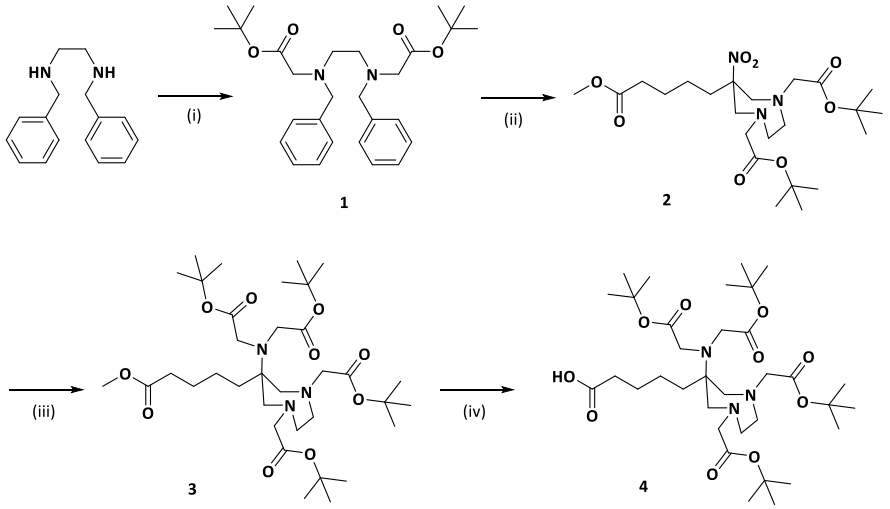

Scheme 3: Synthesis route of AAZTA^5(^{t}Bu)$_4$: (i) *tert*-butyl bromoacetate, Na_2CO_3, ACN, 95 %; (ii) a) Pd/C, EtOH, H_2, 100 %; b) paraformaldehyde, 2-nitrocyclohexanone, MeOH, 67 %; (iii) *tert*-butyl bromoacetate, DIEA, ACN, 49 %; (iv) LiOH, dioxane/H_2O, 91 %; (v) DCM/TFA, RT, 71 %

An important fact for the synthesis of the squaric acid derivative was the adjustment of the pH to 7. At lower pH no reaction occurred, whereas at higher pH two ligands were coupled to the squaric acid ester. The latter fact is going to be used for the attachment of this derivative to free amines of polypeptides or other macromolecular systems [30]. The synthesis of the aniline intermediate of product **5** was carried out in several media with different catalysts. The best system was Raney® Nickel in THF. Using Pd/C as catalyst either with ethanol or THF resulted in the addition of at least one unit of a solvent molecule to the amino group. This effect is known due to the evolution of acetaldehyde and the reductive amination with the produced amine [33,34]. Regarding the THF side product Russell *et*

al. investigated the Pd-mediated addition of peroxidic THF to aromatic amines [35]. All ligands (scheme 4) were purified by means of HPLC under isocratic conditions.

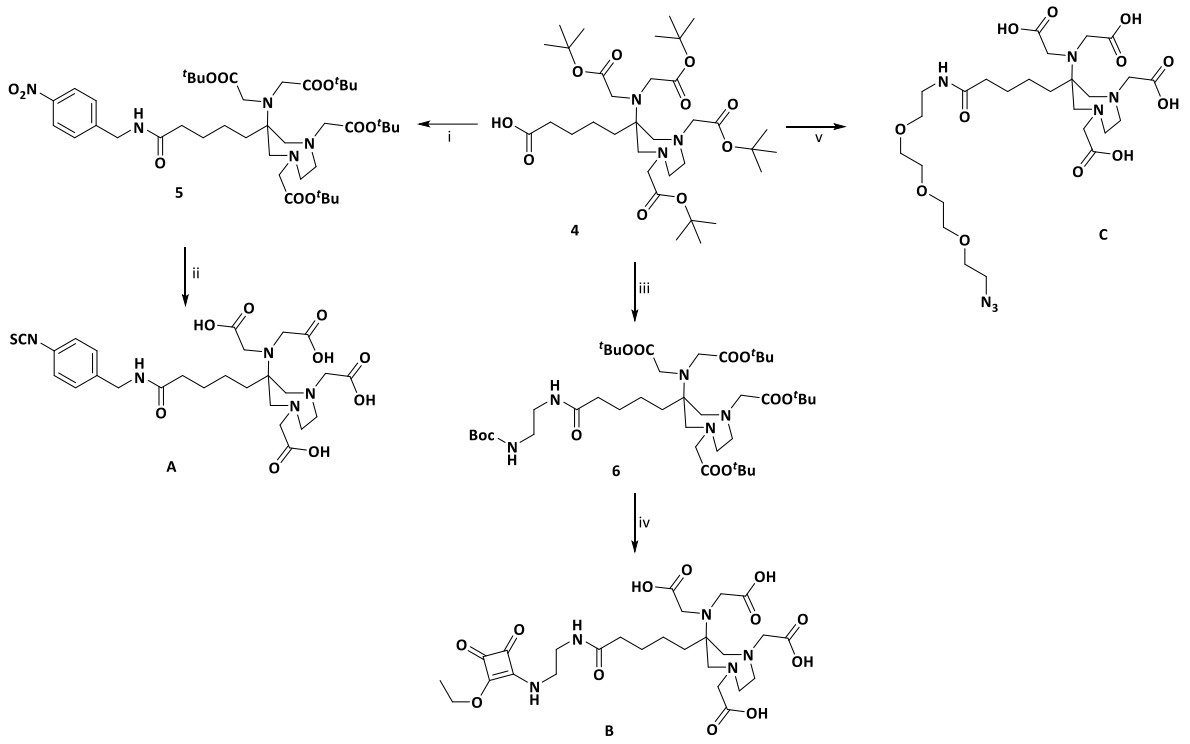

Scheme 4: Synthesis route for the 3 derivatives AAZTA^5-Bz-NCS (**A**), AAZTA^5-en-SA (**B**) and AAZTA^5-TEG-N_3 (**C**): 4-nitrobenzylamine hydrochloride, HATU, DIEA, ACN, 60 %; (ii) a) Raney®Nickel, H_2, EtOH; b) $SCCl_2$, TEA, $CHCl_3$; c) TFA/DCM, RT, 39 %; (iii) *tert*-butyl-*N*-(2-aminoethyl)carbamate, HATU, DIEA, ACN, 33 %; (iv) a) TFA/DCM, 100 %; b) 3,4-diethoxy-3-cyclobuten-1,2-dione, phosphate buffer (0.5 M, pH 7), 33 %; (v) a) 11-azido-3,6,9-trioxaundecan-1-amine, HOBt/EDC·HCl, DIEA, ACN; b) 4 M HCl in dioxane, RT, 16 %

Radiolabelling (pH- and concentration-dependence)

All three derivatives were radiolabelled with ^{177}Lu under various conditions (pH, buffer system, Lu-to-chelator-ratio). As buffer systems sodium acetate (NaOAc), ammonium acetate (AmOAc) and *N*-2-hydroxyethyl piperazine-*N'*-2-ethanesulfonic acid (HEPES) were used. These three buffer systems were chosen according to previous studies for radiolabelling with ^{177}Lu [23,2,38–41]. In table 1 the radiolabelling yields for all three derivatives **A**, **B** and **C** are listed.

Table 1: Radiolabelling yields (in %) of derivatives **A**, **B** and **C** with various buffer systems after 10 min at 25 °C (n=3; A(^{177}Lu)=30-50 MBq)

	NaOAc (0.25 M, pH 4.5)			AmOAc (0.25 M, pH 5.5)			HEPES (0.025 mM, pH 4.3)		
ligand-to-Lu	**A**	**B**	**C**	**A**	**B**	**C**	**A**	**B**	**C**
1:1	20.7 ± 1.1	17.7 ± 1.2	35.1 ± 0.6	<5 %	<5 %	<5 %	38.2 ± 0.1	39.8 ± 5.9	40.7 ± 6.2
2:1	62.5 ± 5.9	74.9 ± 3.8	91.8 ± 3.3	7.0 ± 0.3	8.5 ± 1.1	21.5 ± 4.3	96.1 ± 2.7	98.5 ± 0.0	98.0 ± 0.6
5:1	87.0 ± 3.3	96.7 ± 3.2	98.8 ± 0.2	81.6 ± 4.9	52.6 ± 6.2	86.9 ± 1.2	97.0 ± 0.4	96.1 ± 0.8	98.2 ± 0.2
10:1	94.1 ± 2.0	98.1 ± 0.3	98.7 ± 0.6	94.1 ± 0.2	98.0 ± 1.3	97.9 ± 0.2	98.7 ± 0.3	98.2 ± 0.7	99.0 ± 0.1
15:1	95.6 ± 0.7	98.4 ± 0.3	98.0 ± 0.6	97.3 ± 1.8	97.3 ± 0.3	99.0 ± 0.1	98.2 ± 0.3	96.8 ± 0.4	99.2 ± 0.3

First radiolabelling reactions were performed at room temperature with a reaction time of 10 min using a ligand-to-metal-ratio of 15:1 and 30-50 MBq (=0.062-0.0690 nmol) ^{177}Lu were used for each labelling. For all derivatives in each buffer system quantitative yields (>95 % RCY) could be obtained. Same results were observed with a ratio of 10:1 (except for the system **A** in AmOAc). According to Stimmel *et al.* ligands like DOTA, PADOTA and DTPA could be radiolabelled with equal ligand-to-metal-ratios and RCY [23]. With ratios of 5:1 quantitative labelling yields could be obtained in HEPES buffer for all ligands as well as for ligand **B** and **C** in NaOAc. In comparison with the other systems, the AmOAc buffer effects the labelling of ligand **B** resulting in a RCY <55 %. As it is known, that NH_4^+ is able to form complexes with crown ethers [42,43], the squaric acid moiety might act as complexing unit for the NH_4^+. This leads to a change in the electrostatic system of the ligand and therefore a decreased complexation ability of **B**. For ratios below 5:1, HEPES and NaOAc offer high labelling yields, whereas with ammonium acetate only yields below 30 % could be obtained. Interestingly, the labelling in HEPES resulted in yields >35 % for a 1:1 ratio between Lu and the chelator amount. This demonstrates the high affinity of the chelator AAZTA, depending on the used buffer system.

In vitro stability

For *in vivo* applications of ligands their *in vitro* stability is an important indicator. To get an insight into the kinetic stability, the radiolabelled compounds and their stability were analysed versus several media (HS, PBS, EDTA, DTPA) at different time points. Table 2 shows the percentage of intact Lu-complexes of all three derivatives after 1, 2 and 24 h.

Table 2: Stability of [^{177}Lu]Lu-**A**, [^{177}Lu]Lu-**B** and [^{177}Lu]Lu-**C** (in % intact complex) in human serum (HS), DTPA, EDTA and PBS after 1, 2 and 24 h at 37 °C

	t / h	HS	DPTA	EDTA	PBS
[^{177}Lu]Lu-A	**1**	89.6 ± 0.8	98.5 ± 0.2	98.8 ± 0.2	98.8 ± 0.1
	2	89.1 ± 0.4	98.2 ± 0.1	98.3 ± 0.2	98.8 ± 0.1
	24	50.8 ± 1.0	80.8 ± 1.2	82.7 ± 3.5	98.7 ± 0.1
[^{177}Lu]Lu-B	**1**	99.8 ± 0.0	99.8 ± 0.0	99.9 ± 0.0	98.7 ± 0.3
	2	99.9 ± 0.0	99.7 ± 0.0	99.8 ± 0.0	98.6 ± 0.2
	24	91.3 ± 1.1	94.0 ± 0.2	92.7 ± 0.1	98.5 ± 0.1
[^{177}Lu]Lu-C	**1**	99.9 ± 0.0	99.8 ± 0.0	99.8 ± 0.0	98.8 ± 0.1
	2	99.8 ± 0.0	99.9 ± 0.0	99.9 ± 0.0	98.8 ± 0.1
	24	97.8 ± 0.5	92.4 ± 0.4	91.8 ± 0.2	98.7 ± 0.2

Beside [^{177}Lu]Lu-**A**, with a 50 % intact complex after 24 h, all Lu-complexes show a high stability versus HS (>91 %). An explanation for the low stability of [^{177}Lu]Lu-**A** could be the negative influence of the conjugated amide-Bz-NCS moiety. The electron-withdrawing characteristic due to the negative inductive effects (-I) of the Bz-NCS and the amide leads to a decreased electron density at the exocyclic amine and thereby to a decreased electron density at the carboxylic groups. Since Lu needs up to 9 ligation atoms the lowered complexation ability of the exocyclic amino-diacetate group results in a labile complex and thereby to the release of ^{177}Lu [44].

The competition studies of the Lu-complexes versus DTPA and EDTA (10 mM, pH 7, respectively) show stabilities of at least >80 % for [^{177}Lu]Lu-**A** and >91 % for [^{177}Lu]Lu-**B** and [^{177}Lu]Lu-**C** after 24 h, respectively. These values are in the expected range and comparable with stability of Lu-labelled AAZTA-minigastrin described by Pfister *et al.* [45]. For comparison, same analyses were performed with PBS as media. For all three derivatives stabilities of >98 % after 24 h could be obtained. Considering the application of AAZTA-TV systems for further *in vivo* experiments, this offers the storage of the radiolabelled compounds for several hours in PBS before usage.

Coupling AAZTA^5-Bz-NCS to mAb

As proof-of-concept the ligand **A** was coupled to a monoclonal antibody (mAb) and purified according the method described by Perk *et al.* [46]. The chelator-antibody-conjugate (AAZTA^5-Bz-NCS-mAb, **A-mAb**) was radiolabelled with ^{177}Lu at room temperature and analysed due to the kinetic labelling behaviour. table 3 summarizes, that after 15 minutes a RCY over 60 % could be achieved, yielding in 73 % after 60 min. These data show, that a fast and high yielding labelling is possible with AAZTA, even if it is coupled to large targeting vectors like antibodies.

Table 3: Radiolabelling yields (in %) of derivative **A-mAb** in HEPES buffer (0.5 M, pH 7.0) at 25 °C (n=3; A(^{177}Lu)=50 MBq)

	t / min	yield / %
[^{177}Lu]Lu-A-mAb	15	63.7 ± 3.0
	30	69.3 ± 4.4
	45	70.4 ± 4.3
	60	72.7 ± 3.5

After 60 min the reaction mixture was purified via PD-10 column using NaCl solution (0.9 %) as solvent. Analysis via HPLC represents a radiolabelled conjugate with one peak (figure 5, Supporting Information).

The radiolabelled and purified conjugate was analysed according to its stability in human serum and PBS buffer over a period of 1, 2 and 24 h as well as 168 h (table 4).

Table 4: Stability of [^{177}Lu]Lu-**A**-mAb in human serum (HS) and PBS (in % intact complex) after 1, 2, 24 and 168 h at 37 °C

	t / h	HS	PBS
[^{177}Lu]Lu-A-mAb	**1**	43.0 ± 10.0	92.8 ± 1.0
	2	31.6 ± 3.7	90.9 ± 0.7
	24	29.9 ± 2.4	89.5 ± 1.6
	168	31.8 ± 6.8	91.0 ± 1.9

The conjugate shows a stability of over 90 % after even 7 days in PBS. Same results were obtained for the labelled chelator (table 2). Within human serum the conjugate and the chelator itself release the Lu. As mentioned above the benzyl group of the linking moiety seems to have a destabilizing effect on the chelator. Introducing an antibody to this chelator site in combination with competitive ligands or metals inside the HS results in the fast decomplexation of the Lu.

CONCLUSION

AAZTA^5 and its bifunctional derivatives AAZTA^5-Bz-NCS (**A**), AAZTA^5-en-SA (**B**) and AAZTA^5-TEG-N_3 (**C**) show a high potential as stable and reliable chelator for ^{177}Lu. The new coupling sites of AAZTA^5 demonstrate high stabilities (especially the squaric acid and the azide) and simultaneously offer the option to covalentely attach the ligands to targeting vectors like peptides or bisphosphonates but also to antibodies or nanodimensional systems like polymers or nanoparticles. In difference to the established DOTA-derivatives the fast radiolabelling with RCY's greater 95 % at mild conditions (RT, pH 4.5-7) broadens the field for the application of these new systems.

ACKNOWLEDGEMENT

We thank ITM (Garching, Germany) for the supply of n. c. a. ^{177}Lu for all radiolabellings performed in this work.

SUPPORTING INFORMATION

General methods:

All used chemicals were commercially available at Acros Organics, Bachem, Fluka, SigmaAldrich or VWR and were used without further purification. For radiolabellings trace metal-free salts and water were used. The measurements of ^{1}H- and ^{13}C-NMR spectra were performed on a Bruker Avance III HD 400 (400 MHz)or Avance III 600 (600 MHz). Chemical shifts are given in parts per million downfield from TMS (δ=0 ppm) referred to the solvent residual signal. Low-resolution mass spectra (LR-MS) were recorded on Agilent 6100 Series Single Quadrupole LC/MS and high-resolution mass spectra (HR-MS) were recorded on either a Micromass Quattro Micro API LC-ESI or a Finnigan MAT90-Spectrometer.

Purification and analysis of the compounds was performed on a HPLC system from Merck (LaChrom; pump: Hitachi L7100; UV-detector: L7400). Following columns were used: Luna 10 u (C18) 100 Å (250x10.00 mm 10 micron); Gemini 5 u (C18) 110 Å (250x10.00 mm 5 micron); Luna 10 u (C18) 100 Å (250x21.23 mm 10 micron). As eluent **A** (H_2O (0.1 % TFA)) and **B** (ACN (0.1 % TFA)) were used.

For radiolabelling n.c.a. ^{177}Lu (0.04 M HCl) from ITM (Garching, Germany) was used. Radiolabellings were performed in 1 mL total volume at 25 °C in a heating block at 600 rpm. Radio-TLCs were performed on Merck Silica F_{254} TLC plates with citrate buffer (0.01 M, pH 4) and analyzed with the radio detector GABI STAR from Raytest. For radio-HPLC a Chromolith Performance RP18e column (100x4.6 mm; Merck) was used with a linear **A**-**B** gradient (5 % **B** for 2 min, 5 % to 95 % **B** in 10 min, 95 % **B** for 2 min, 5 % **B** for 3 min).

Experimental Section:

AAZTA^5 synthesis

*N,N'-Dibenzyl-N,N'-di-(tert-butylacetate)-ethylendiamine (**1**)*

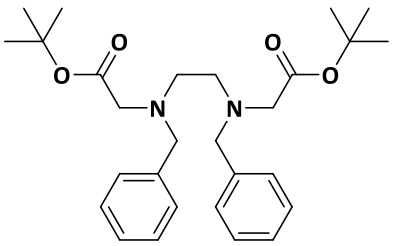

1

N,N´-dibenzylethylenediamine (3.00 g; 12.48 mmol) and Na_2CO_3 (5.12 g; 48.67 mmol) were stirred at room temperature in dry acetonitrile (50 mL) for 30 min. *Tert*-butyl bromoacetate (4.64 g; 23.72 mmol), dissolved in dry acetonitrile (10 mL), was added at room temperature over a period of 30 min. After completion the suspension was heated over night at 90 °C, filtrated and the filtrate was concentrated under vacuum. After purification via column chromatography (H/EA; 6:1; R_f=0.25) the product was obtained as colourless solid (5.56 g; 11.87 mmol; 95 %).

^{1}H-NMR ($CDCl_3$, 400 MHz, δ [ppm]): 7.34-7.21 (m, 10 H); 3.78 (s, 4 H); 3.26 (s, 4 H); 2.82 (s, 4 H); 1.44 (s, 18 H); ^{13}C-NMR ($CDCl_3$, 100 MHz, δ [ppm]): 171.03 (s); 139,18 (s); 129.05 (s); 128.30 (s); 127.10 (s); 80.86 (s); 58.39 (s); 55.27 (s); 51.73 (s); 28.24 (s)

MS (ESI$^+$): 469.28, 470.31, 471.33 (M+H$^+$); 507.32, 508.34, 509.35 (M+K$^+$)

1,4-Di(tert-butylacetate)-6-methylpentanoate-6-nitroperhydro-1,4-diazepane (**2**)

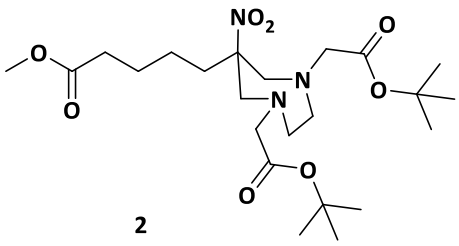

2

1 (3.28 g; 7.00 mmol) was dissolved in 20 mL abs. ethanol and formic acid (528 µL; 14.00 mmol). To this solution Pd/C (0.53 g; 16 wt%) was added and the solution was saturated and kept overnight with hydrogen. After completion the Pd/C was filtrated over celite, the filtrate was concentrated and dried. The crude product **2a** (1.99 g; 6.90 mmol; 99 %) was used without further purification. A solution of 2-nitrocyclohexanone (1 g; 6.99 mmol) and Amberlyst® A21 (2 mass-eq) in dry methanol (30 mL) was heated for 1 h. Then product **2a** (1.99 g; 6.99 mmol) and paraformaldehyde (0.76 g; 25.2 mmol) was added and the suspension was heated overnight under reflux. The suspension was filterated, the filtrate was concentrated under vacuum and purified via column chromatography (H/EA, 2:1; R_f=0.43). The product **2** was obtained as yellowish oil (2.25 g; 4.62 mmol; 66 %).

^{1}H-NMR ($CDCl_3$, 400 MHz, δ [ppm]): 3.65 (s, 3 H); 3.60 (d, J=14.6 Hz, 2 H); 3.45 (d, J=17.3 Hz, 2 H); 3.30 (d, J=17.3 Hz, 2 H); 3.12 (d, J=14.6 Hz, 2 H); 2.84 (m, 4 H); 2.27 (t, 3 H); 1.83 (m, 2 H), 1.57 (m, 2 H); 1.46 (s, 18 H); 1.18 (m, 2 H); ^{13}C-NMR ($CDCl_3$, 100 MHz, δ [ppm]): 173.73 (s); 170.92 (s); 95.12 (s); 81.31 (s); 61.57 (s); 61.18 (s); 56.87 (s); 51.68 (s); 37.27 (s); 33.71 (s); 28.35 (s); 24.82 (s); 22.99 (s)

MS (ESI$^+$): 388.14, 389.18, 390.20 (M+H$^+$); 410.15, 411.17, 412.18 (M+Na$^+$)

1,4-Di(tert-butylacetate)-6-methylpentanoate-6-amino-di(tert-butylacetate)-perhydro-1,4-diazepane (**3**)

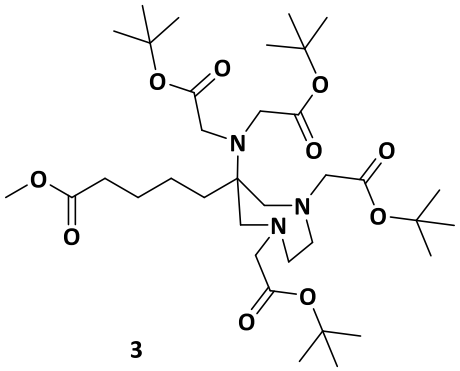

3

2 (2.25 g; 4.62 mmol) was dissolved in absolute ethanol (15 mL), combined with Raney®Nickel 2800® (0.5 g) (washed 4 times with ethanol) and the suspension was saturated with hydrogen and stirred at 40 °C for 6 h. After completion the nickel was filtrated over celite/sand, the filtrate was concentrated and dried under vacuum. The product **3a** (2.11 g; 4.62 mmol) was dissolved with diisopropylethylamine (805 µL; 4.62 mmol) in dry acetonitrile and stirred under nitrogen for 30 minutes at room temperature. *Tert*-butyl bromoacetate (1.57 mL; 10.63 mmol) was added dropwise to the solution and stirred at room temperature overnight. The solution was concentrated under vacuum and purified via column chromatorgraphy (H/EA, 3:1; R_f=0.82). The product **3** was obtained as yellow oil (2.53 g; 3.70 mmol; 49 %).

^{1}H-NMR ($CDCl_3$, 400 MHz, δ [ppm]): 3.65 (s, 4 H); 3.61 (s, 4 H); 3.22 (s, 3 H); 2.99 (d, J=14.1 Hz, 2 H);

2.85-2.65 (m, 4 H); 2.63 (d, J=14.1 Hz, 2 H); 2.31 (t, J=7.4 Hz, 2 H); 1.62-1.52 (m, 4 H); 1.44 (s, 18 H); 1.43 (s, 18 H); 1.25 (m, 2 H); ^{13}C-NMR ($CDCl_3$, 100 MHz, δ [ppm]): 174.37 (s); 172.89 (s); 170.94 (s); 80.86 (s); 80.38 (s); 65.29 (s); 63.17 (s); 62.61 (s); 59.39 (s); 52.09 (s); 51.56 (s); 37.34 (s); 34.26 (s); 28.31 (s); 28.25 (s); 25.89 (s); 21.83 (s)

MS (ESI^+): 686.60, 687.60, 688.60 ($M+H^+$)

*1,4-Di(tert-butylacetate)-6-pentanoicacid-6-(amino-di(tert-butylacetate))-perhydro-1,4-diazepane (**4**)*

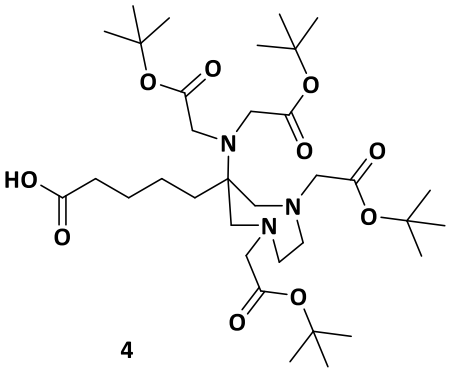

4

3 (0.67 g, 0.97 mmol) was dissolved in 1,4-dioxane/water (2:1, 14 mL), 1 M LiOH (1.46 mL, 1.46 mmol) and stirred at room temperature. After completion the solution was concentrated under vacuum and the residue extracted with $NaHCO_3$ (1M) and chloroform. The organic layer was dried over sodium sulfate, filtrated and concentrated under vacuum. The product was obtained as yellowish oil without further purification (0.84 g, 1.25 mmol, 90 %).

^{1}H-NMR ($CDCl_3$, 400 MHz, δ [ppm]): 3.60 (s, 4 H); 3.23 (s, 4 H); 3.00-2.97 (d, J=14.2 Hz, 2 H); 2.88-2.60 (m, 6 H); 2.36-2.32 (t, J=7.90 Hz, 2 H); 1.64-1.52 (m, 4 H); 1.43 (s, 18 H); 1.42 (s, 18 H); 1.24 (m, 2 H); ^{13}C-NMR ($CDCl_3$, 100 MHz, δ [ppm]): 178.92 (s); 172.93 (s); 170.87 (s); 81.04 (s); 80.54 (s); 65.10 (s); 63.10 (s); 59.35 (s); 52.16 (s); 34.20 (s); 29.82 (s); 28.32 (s); 28.22 (s); 25.62 (s); 22.81 (s); 21.87

MS (ESI^+): 672.45, 673.45, 674.46 ($M+H^+$); 694.43, 695.44, 696.45 ($M+Na^+$)

Synthesis of derivatives AAZTA^5-Bz-NCS (A), AAZTA^5-en-SA (B), AAZTA^5-TEG-N_3 (C) and AAZTA^5-Bz-NCS-mAb (D)

1,4-Di(acetate)-6-((5-((4-isothiocyanatobenzyl)amino)-5-oxopentyl)-6-(amino-di(acetate)-perhydro-1,4-diazepane (AAZTA^5-Bz-NCS (**A**))

1,4-Di(tert-butylacetate)-6-((5-((4-nitro-benzyl)amino)-5-oxopentyl)-6-(amino-di(tert-butylacetate))-perhydro-1,4-diazepane (**5**)

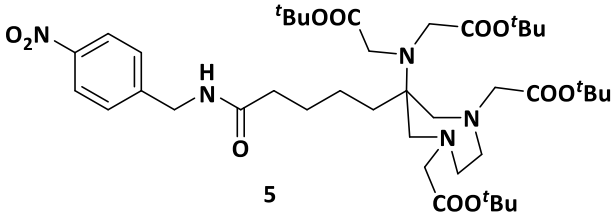

5

4 (0.30 g; 0.44 mmol) was dissolved in dry acetonitrile (1 mL), combined with HATU (0.20 g; 0.53 mmol), DIEA (230 µL; 1.32 mmol) and stirred for 15 min at room temperature. To this solution 4-nitrobenzylamine hydrochloride (0.11 g; 0.58 mmol) was added and stirred for 1 h at room temperature. After completion of the reaction the solution was concentrated under vacuum and the residue was purified via column chromatography (H/EA; 1:1; R_f=0.20). The product **5** was obtained as orange oil (0.21 g; 0.26 mmol; 60 %).

^{1}H-NMR ($CDCl_3$, 400 MHz, δ [ppm]): 8.18 (d, J=8.53 Hz, 2 H) 7.46 (d, J=8.53 Hz, 2 H); 6.51 (br, 2 H); 4.56 (d, J=6.12 Hz, 2 H); 3.60 (s, 4 H); 3.20 (s, 4 H); 2.98 (d, J=14.18 Hz, 2 H); 2.77-2.74 (m, 2 H); 2.67-2.61 (m, 4 H) 2.29 (t, 2 H); 1.71-1.66 (m, 2 H); 1.60-1.56 (m, 2 H) 1.43 (s, 18 H); 1.42 (s, 18 H) 1.28-1.23 (m, 2 H); ^{13}C-NMR ($CDCl_3$, 100 MHz, δ [ppm]): 173.58 (s); 172.93 (s); 170.89 (s); 128.37 (s); 123.94 (s); 80.96 (s); 80.52 (s); 65.20 (s); 63.18 (s); 62.57 (s); 59.44 (s); 52.32 (s); 38.75 (s); 36.95 (s); 36.66 (s); 28.34 (s); 28.24 (s); 21.86 (s).

MS (ESI$^+$): 806.48, 807.49, 808.52 (M+H$^+$); 828.45, 829.47, 830.50 (M+Na$^+$)

*1,4-Di(acetate)-6-((5-((4-isothiocyanatobenzyl)-amino)-5-oxopentyl)-6-(amino-di(acetate))-per-hydro-1,4-diazepane (**A**)*

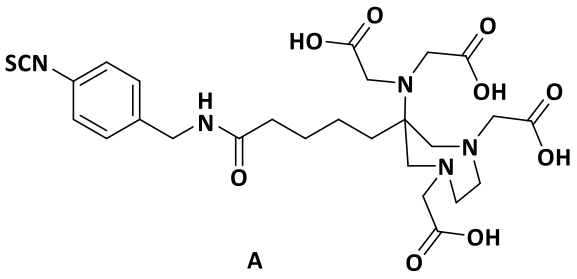

A

5 (0.21 g; 0.26 mmol) was dissolved in tetrahydrofuran (3 mL) and suspended with Raney®Nickel 2800®. The suspension was flushed with and kept under hydrogen for 5 h at room temperature. After completion the mixture was filtrated over celite/sand, the celite washed twice with methanol (5 mL) and the organic layer was concentrated under vacuum. The obtained product was used without further purification (0.20 g; 22 mmol; 85 %). The residue was stirred at room temperature in dry dichloromethane (3 mL) and TEA (57 µL; 0.44 mmol) for 15 minutes. To this solution thiophosgene (44 µL; 0.44 mmol), dissolved in dry dichlormethane (1 mL), was added and stirred for 1 h. The solution was quenched with 1 M NaOH solution and extracted with dichloromethane. The organic layer was concentrated under

vacuum and the obtained product was dissolved in dichloromethane/trifluoroacetic acid (1:1, vol%). After 5 h the solvent was removed under vacuum and the residue was purified via HPLC to obtained product **A** as colourless solid (51 mg; 0.09 mmol; 39 %; t_R=13.7 min (28 % ACN (0.1 % TFA))).

^{1}H-NMR ($CDCl_3$, 400 MHz, δ [ppm]): 7.66-7.61 (m, 4 H); 4.65 (s, 2 H); 4.03 (s, 4 H); 3.95 (s, 4 H); 3.79-3.72 (m, 2 H); 3.68-3.61 (m,4 H); 3.51 (d, J=13.53 Hz, 2 H); 2.55 (t, 2 H); 1.87-1.80 (m, 2 H); 1.75-1.71 (m, 2 H); 1.60-1.51 (m, 2 H); ^{13}C-NMR ($CDCl_3$, 100 MHz, δ [ppm]): 175.43 (s); 175.08 (s); 170.52 (s); 137.95 (s); 128.28 (s); 125.46 (s); 62.36 (s); 59.35 (s); 58.22 (s); 52.25 (s); 51.43 (s); 41.78 (s); 34.94 (s); 33.66 (s); 25.25 (s); 21.79 (s).

MS (ESI$^+$): 645.1099, 646.1092, 647.1002 ((M-4H$^+$)+Fe^{3+})

*1,4-Di(acetate)-6-((5-(2-((2-ethoxy-3,4- dioxocyclobut-1-en-1yl)aminoethyl)amino)-5-oxopentyl)-6-(amino-di(acetate))-perhydro-1,4-diazepane (**B**)*

*1,4-Di(tert-butylacetate)-6-((5-(2-((tert-butoxy-carbonyl)-amino-ethyl)amino)-5-oxopentyl)-6-(amino-di(tert-butylacetate))-per-hydro-1,4-diazepane (**6**)*

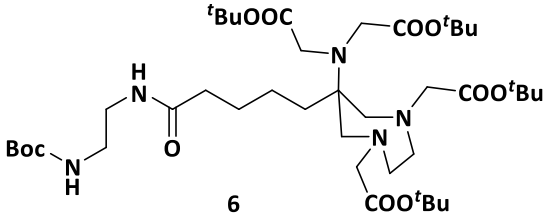

6

4 (100 mg; 0.15 mmol) was dissolved in dry acetonitrile (1 mL), combined with HATU (62 mg; 0.16 mmol), DIEA (78 µL; 0.45 mmol) and stirred for 15 min at room temperature. To this solution *tert*-butyl(2-aminoethyl)carbamate (36 µL; 0.23 mmol) was added and stirred for 1 h at room temperature. After completion of the reaction the solution was concentrated under vacuum and the residue was purified via column chromatography (H/EA, 2:1, R_f: 0.11). The product **6** was obtained as yellowish oil (40 mg; 0.05 mmol; 33 %).

^{1}H-NMR (DMSO, 400 MHz, δ [ppm]): 6.34 (br, 1 H); 5.26 (br, 1 H); 3.60 (s, 4 H); 3.38-3.34 (m, 2 H); 3.26-3.24 (m, 2 H); 3.21 (s, 4 H); 2.96 (d, J=14.1 Hz, 2 H); 2.75- 2.73 (m, 2 H); 2.66-2.63 (m, 2 H); 2.59 (d, J=14.1 Hz, 2 H); 2.19 (t, 2 H); 1.62-1.53 (m, 4 H); 1.43 (s, 18 H); 1.42 (s, 27 H); 1.28-1.20 (m, 2 H); ^{13}C-NMR ($CDCl_3$, 100 MHz, δ [ppm]): 174.38 (s); 173.31 (s); 172.80 (s); 165.88 (s); 82.85 (s); 82.77 (s); 63.44 (s); 62.48 (s); 62.05 (s); 55.48 (s); 54.47 (s); 47.11 (s); 40.81 (s); 39.87 (s); 35.55 (s); 29.82 (s); 28.53 (s); 28.32 (s); 28.14 (s); 27.91 (s); 26.17 (s); 23.41 (s).

MS (ESI$^+$): 814.53, 815.54, 816.57 (M+H$^+$); 836.454, 837.55, 838.56 (M+Na$^+$)

*1,4-Di(acetate)-6-((5-(2-((2-ethoxy-3,4-dioxocyclobut-1-en-1yl)-aminoethyl)amino)-5-oxopentyl)-6-(amino-di(acetate))-perhydro-1,4-diazepane (***B**)

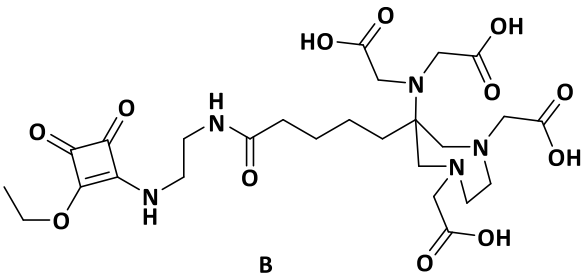

B

6 (28 mg; 0.04 mmol) was dissolved in dichloromethane/trifluoroacetic acid (1:1; vol %) and stirred for 3 h. After completion of the reaction the solvent was removed under vacuum and the residue was dissolved in 0.5 M phosphate buffer (pH 7; 3 mL). To this solution 3,4-diethoxycyclobut-3-ene-1,2-dione (16 mg; 0,03 mmol) was added, the pH was adjusted with 1 M NaOH solution to pH 7 and the reaction was stirred over night at room temperature. After completion the reaction mixture was purified via HPLC to obtain the product **B** as colourless solid (7.2 mg; 0.01 mmol; 33 %; t_R=9.4 min (12 % ACN (0.1 % TFA)).

^{1}H-NMR (D_2O, 400 MHz, δ [ppm]): 4.75-4.67 (m, 2H); 3.88 (s, 2 H); 3.76-3.66 (m, 6 H); 3.59-3.44 (m, 8 H); 3.40-3.38 (m, 2 H); 2.20 (t, 2 H); 1.52-1.45 (m, 4 H); 1.43 (t, 3 H); 1.30-1.21 (m; 2 H); ^{13}C-NMR (D_2O, 100 MHz, δ [ppm]): 176.60 (s); 176.06 (s); 175.97 (s); 173.82 (s); 170.67 (s); 70.70 (s); 70.55 (s); 62.81 (s); 59.41 (s); 58.63 (s); 52.59 (s); 52.20 (s); 43.93 (s); 39.56 (s); 39.24 (s); 35.31 (s); 33.76 (s); 25.73 (s); 22.26 (s); 15.07 (s).

MS (ESI$^+$): 665.1624, 666.1661, 667.1680 ((M-4H$^+$)+Fe^{3+})

*<u>1,4-Di(acetate)-6-(1-azido-13-oxo-3,6,9-trioxa-12-azadecan-12-yl)amino)-5-oxopentyl)-6-(amino-di(acetate))-perhydro-1,4-diazepane (**C**)</u>*

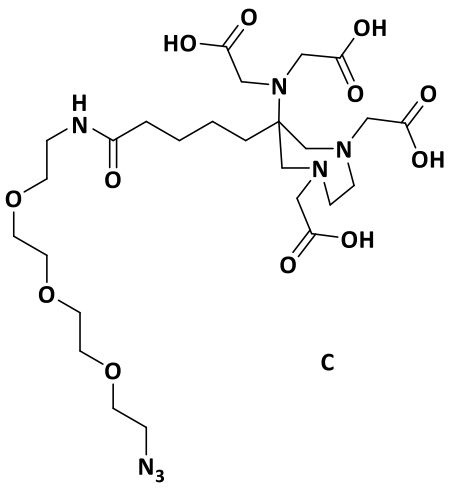

C

4 (47 mg; 0.07 mmol) was dissolved in dry acetonitrile (1 mL), combined with HOBt (18.9 mg; 0.14 mmol), EDC·HCl (20.1 mg, 0.10 mmol) and DIEA (49 µL; 0.28 mmol) and stirred for 15 min at room temperature. To this solution 11-azido-3,6,9-trioxaundecan-1-amine (15 µL; 0.07 mmol) was added and stirred for 1 h at room temperature. After completion of the reaction the solution was concentrated under vacuum and the residue was dissolved in dichloromethane/trifluoroacetic acid (1:1; vol %). After 3 h at room temperature the solution was concentrated under vacuum and the residue was purified via HPLC to obtain product **C**as yellowish oil (6.8 mg; 0.01 mmol; 16 %; t_R=8.9 (20 % ACN (0.1 % TFA))).

^{1}H-NMR (CD_3CN, 400 MHz, δ [ppm]): 3.69 (s, 4 H); 3.63-3.54 (m, 14 H) 3.48 (t, 2 H); 3.38 (t, 2 H) 3.29-3.22 (m, 8 H); 3.10 (d, J=14.6 Hz); 2.11 (t, 2 H); 1.48-1.41 (m, 2 H); 1.34-1.21 (m, 4 H); ^{13}C-NMR (CD_3CN, 100 MHz, δ [ppm]): 176.84 (s); 175.32 (s); 171.06 (s); 70.96 (s); 70.71 (s); 70.40 (s); 70.14 (s); 63.52 (s);

61.30 (s); 59.10 (s); 54.10 (s); 51.82 (s); 51.42 (s); 39.80 (s); 36.41 (s); 35.65 (s); 26.84 (s); 23.42 (s).

MS (ESI^+): 699.2148, 700.2185, 701.2201 ($(M-4H^+)+Fe^{3+}$)

*mAb-AAZTA^5-Bz-NCS (**D**)*

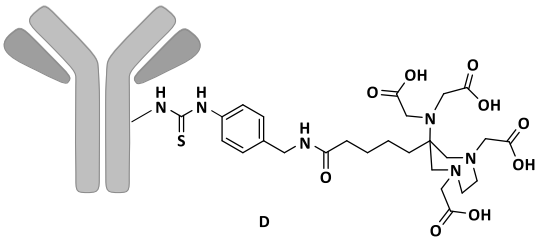

D

The antibody was coupled to **A** according to the protocol by Perk *et al.*[47] In brief, the antibody solution (2.1 mg, 14 nmol) was adjusted to pH 9 with 0.1 Na_2CO_3. To this solution **A** was added (90.2 µg, 140 nmol) and incubated for 1 h at 37 °C. After completion of the reaction the conjugate was separated with PD-10 column purification and was ready for radiolabelling.

Radiolabelling and *in vitro* evaluation

Kinetic studies and HPLC diagrams

Following figures show the kinetic studies of the 3 derivatives with the buffer systems sodium acetate (NaOAc, 0.25 M, pH 4.5), ammonium acetate (AmOAc, 0.25 M, pH 5.5) and *N*-2-hydroxyethyl piperazine-*N'*-2-ethanesulfonic acid (HEPES, 0.025 M, pH 4.3 and 0.5 M, pH 7.00) and the HPLC chromatograms of all three radiolabelled derivatives and the radiolabelled mAb conjugate. All values were analyzed via radio-TLC (silica gel, citrate buffer (0.01 M, pH 4) as mobile phase) and verified with radio-HPLC (after 15 min labelling reaction). For the systems NaOAc and HEPES the ligand-to-^{177}Lu ratios from 1:1 till 10:1 are shown, whereas for AmOAc ratios from 2:1 till 15:1 are shown.

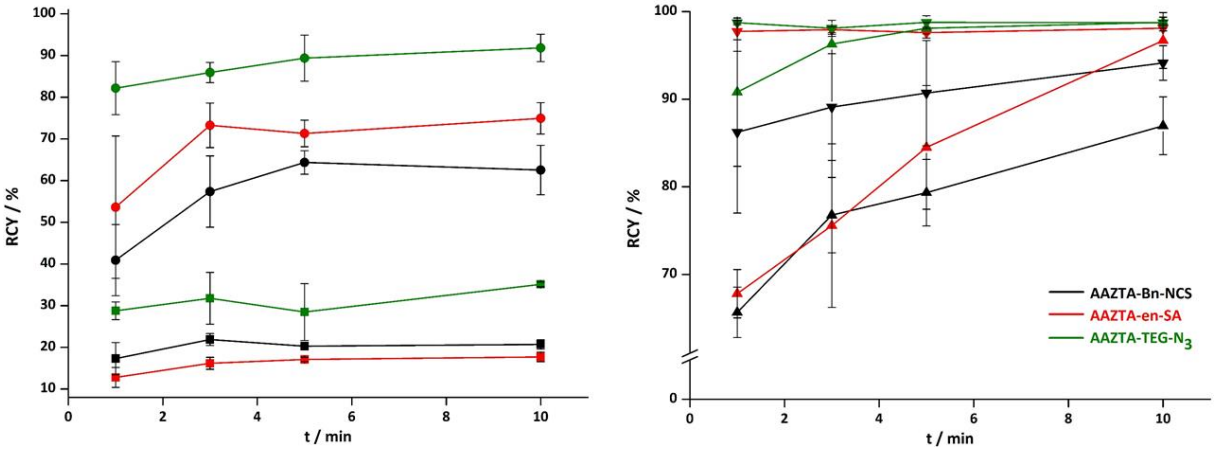

Figure 1: Radiolabelling kinetics with ^{177}Lu of the derivatives AAZTA^5-Bz-NCS (–), AAZTA^5-en-SA (–) and AAZTA^5-TEG-N_3 (–) in NaOAc (0.25 M, pH 4.5) with ligand-to-^{177}Lu ratio 1:1 (■), 2:1 (●), 5:1 (▲) and 10:1 (▼) at 25 °C; n=3

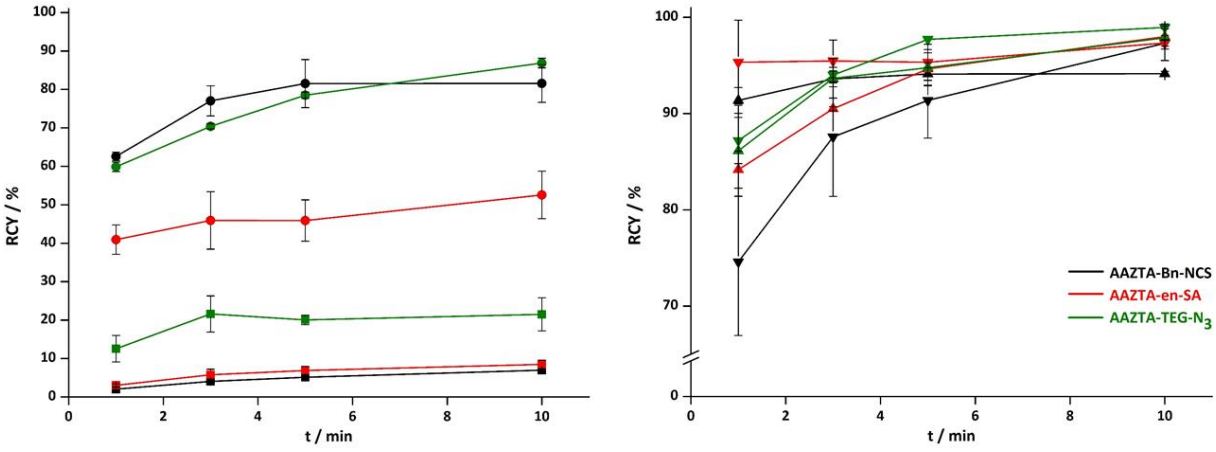

Figure 2: Radiolabelling kinetics with ^{177}Lu of the derivatives AAZTA^5-Bz-NCS (–), AAZTA^5-en-SA (–) and AAZTA^5-TEG-N_3 (–) in AmOAc (0.25 M, pH 5.5) with ligand-to-^{177}Lu ratio 2:1 (■), 5:1 (●), 10:1 (▲) and 15:1 (▼) at 25 °C; n=3

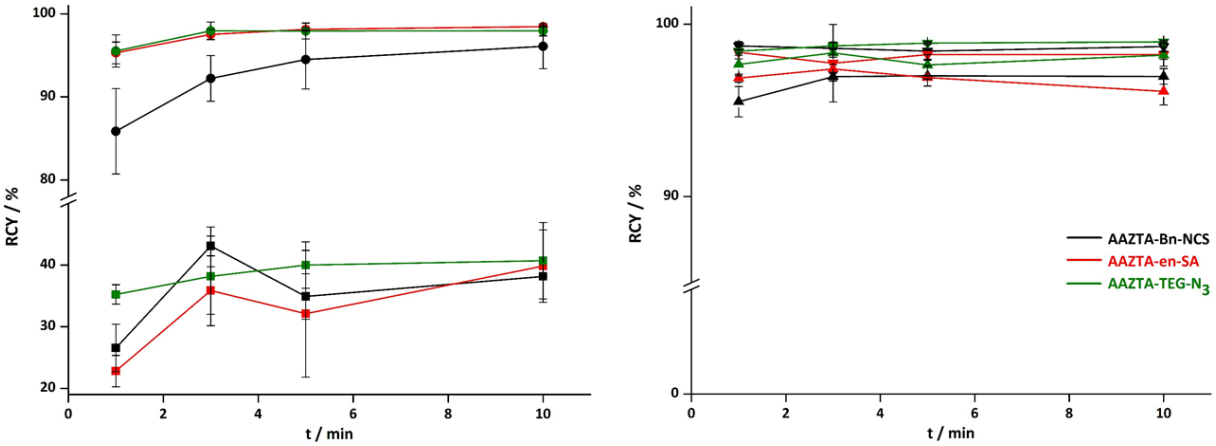

Figure 3: Radiolabelling kinetics with ^{177}Lu of the derivatives AAZTA^5-Bz-NCS (–), AAZTA^5-en-SA (–) and AAZTA^5-TEG-N_3 (–) in HEPES (0.025 M, pH 4.3) with ligand-to-^{177}Lu ratio 1:1 (■), 2:1 (●), 5:1 (▲) and 10:1 (▼) at 25 °C; n=3

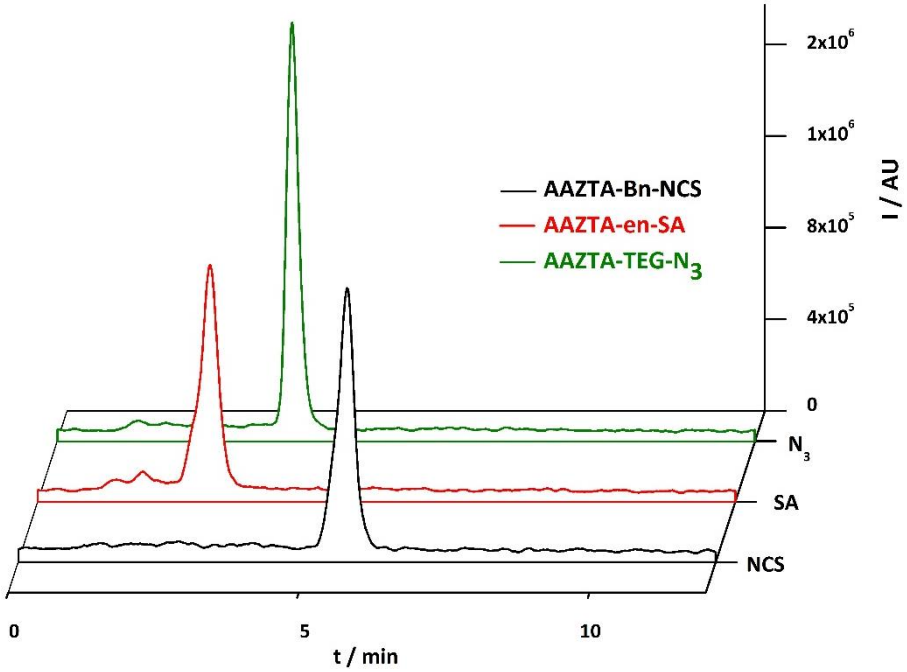

Figure 4: HPLC chromatograms of radiolabelled AAZTA^5-Bz-NCS (–), AAZTA^5-en-SA (–) and AAZTA^5-TEG-N_3 (–) after 15 min (ligand-to-^{177}Lu 10:1, NaOAc 0.25 M, pH 4.5, 25 °C)

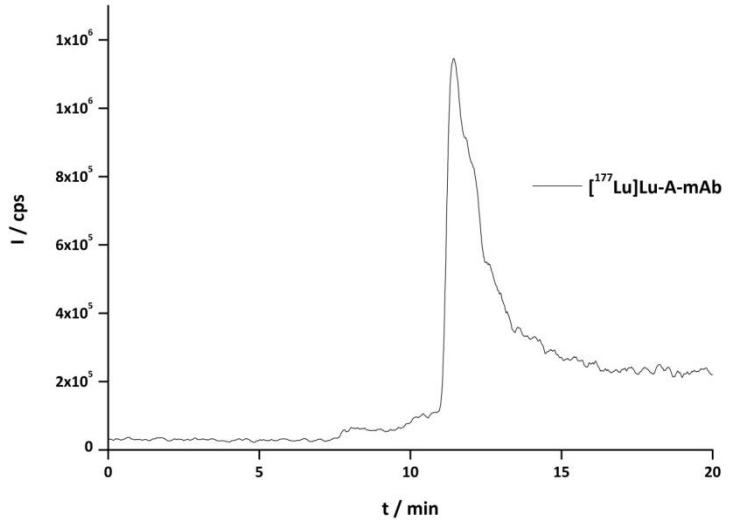

Figure 5: HPLC chromatogram of radiolabelled conjugate of AAZTA^5-BnNCS and antibody after purification

Following figures show histograms after 1, 2 and 24 h as well as the HPLC chromatograms after 2 h of the ligands [^{177}Lu]Lu-**A**, [^{177}Lu]Lu-**B** and [^{177}Lu]Lu-**C** in the media human serum (HS), DTPA, EDTA and PBS. All TLCs were analyzed with citrate buffer (0.01 M, pH 4) as eluent.

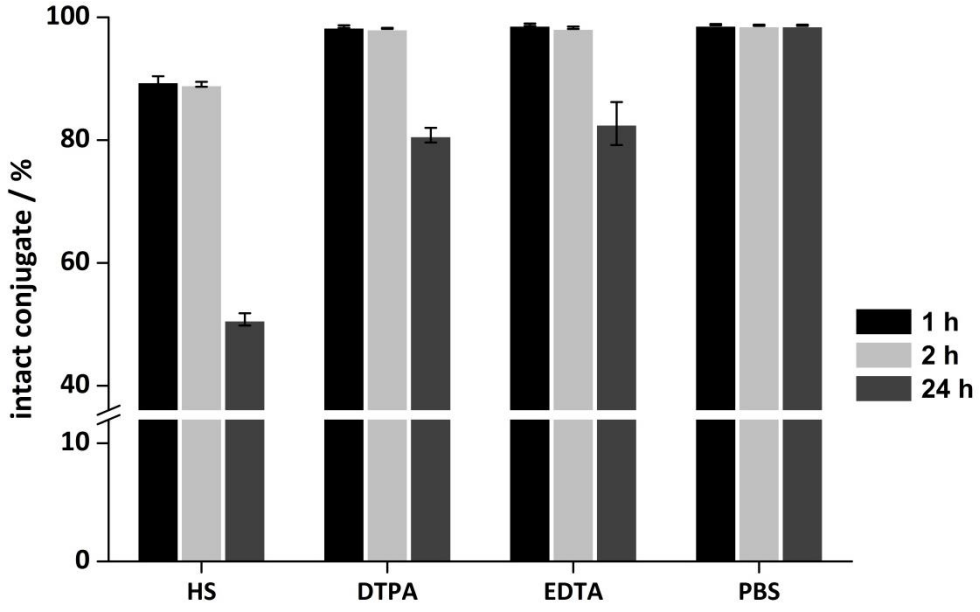

Figure 6: *In vitro* stability of [^{177}Lu]Lu-AAZTA^5-Bz-NCS ([^{177}Lu]Lu-**A**) in HS, DTPA, EDTA and PBS after 1 h (■), 2 h (■) and 24 h (■), n=3

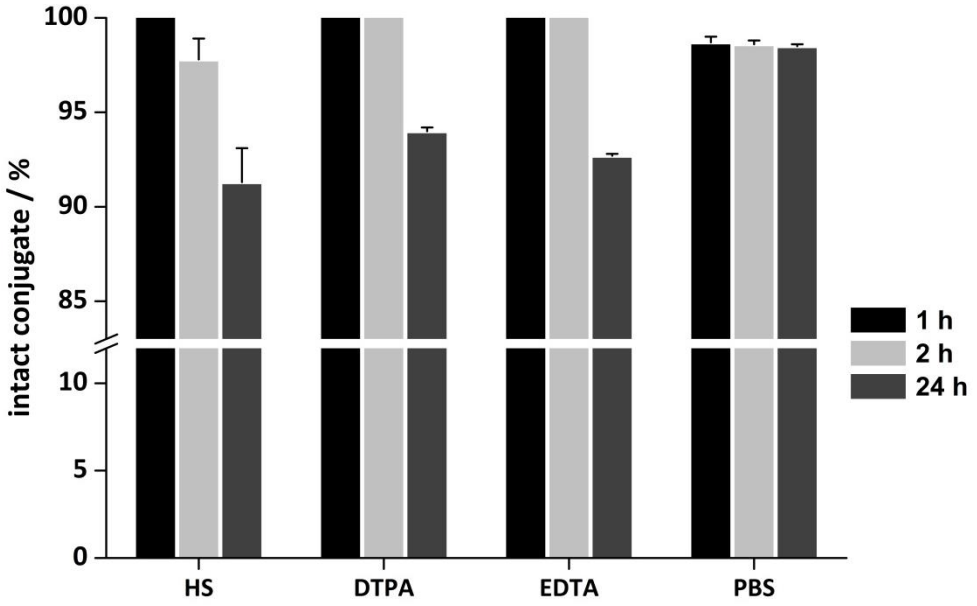

Figure 7: *In vitro* stability of [^{177}Lu]Lu-AAZTA^{5}-en-SA ([^{177}Lu]Lu-**B**) in HS, DTPA, EDTA and PBS after 1 h (■), 2 h (■) and 24 h (■), n=3

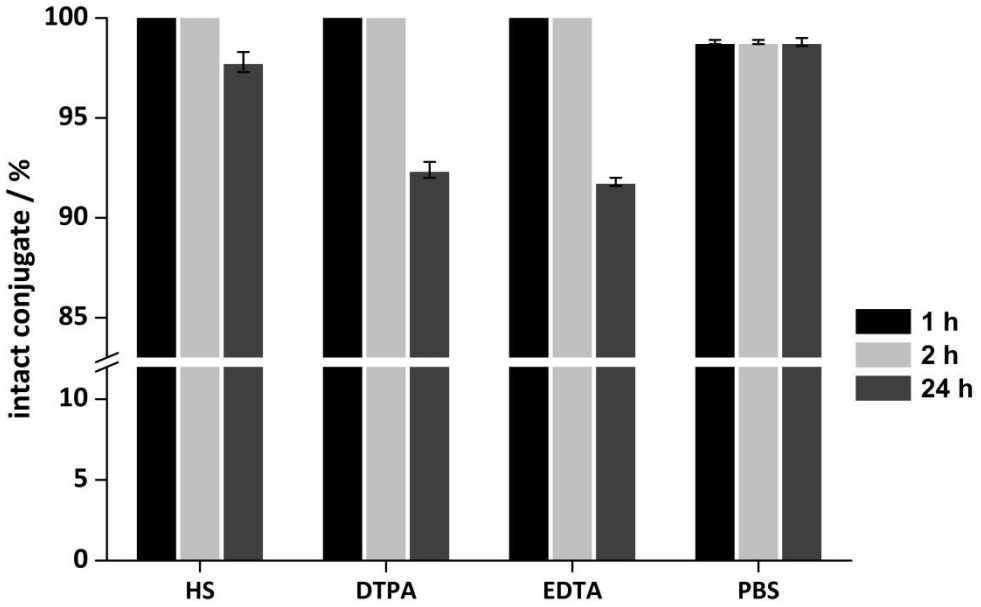

Figure 8: *In vitro* stability of [^{177}Lu]Lu-AAZTA^{5}-TEG-N_3 ([^{177}Lu]Lu-**C**) in HS, DTPA, EDTA and PBS after 1 h (■), 2 h (■) and 24 h (■), n=3

REFERENCES

1. Asti M., Tegoni M., Farioli D., Iori M., Guidotti C., Cutler C.S., Mayer P., Versari A., Salvo D. Influence of cations on the complexation yield of DOTATATE with yttrium and lutetium: A perspective study for enhancing the Y-90 and Lu-177 labeling conditions. Nucl. Med. Biol. 2012; 39(4): 509–17.

2. Breeman W.A.P., De Jong M., Visser T.J., Erion J.L., Krenning E.P. Optimising conditions for radiolabelling of DOTA-peptides with Y-90, In-111 and Lu-177 at high specific activities. Eur. J. Nucl. Med. Mol. Imaging. 2003; 30(6): 917–20.

3. Wunderlich G., Schiller E., Bergmann R., Pietzsch H.J. Comparison of the stability of Y-90-, Lu-177- and Ga-68- labeled human serum albumin microspheres (DOTA-HSAM). Nucl. Med. Biol. 2010; 37(8): 861–7.

4. Krenning E.P., Kooij P.P.M., Bakker W.H., Breeman W.A.P., Postema P.T.E., Kwekkeboom D.J., Oei H.Y., De Jong M., Visser T.J., Reijs A.E.M., Lamberts S.W.J. Radiotherapy with a radiolabeled somatostatin analogue, In-111-DTPA-[D-Phe1]-Octreotide. A case history. Ann. N. Y. Acad. Sci. 1994; 733: 496–506.

5. Valkema R., De Jong M., Bakker W.H., Breeman W.A.P., Kooij P.P.M., Lugtenburg P.J., De Jong F.H., Christiansen A., Kam B.L.R., De Herder W.W., Stridsberg M., Lindemans J., Ensing G., Krenning E.P. Phase I Study of Peptide Receptor Radionuclide Therapy With In-111-DTPA-Octreotide: The Rotterdam Experience. Semin. Nucl. Med. 2002; 32(2): 110–22.

6. Kwekkeboom D.J., Müller-Brand J., Paganelli G., Anthony L.B., Pauwels S., Kvols L.K., O'dorisio T.M., Valkema R., Bodei L., Chinol M., Mäcke H.R., Krenning E.P. Overview of results of peptide receptor radionuclide therapy with 3 radiolabeled somatostatin analogs. J Nucl Med. 2005; 46(1): 62S–66S.

7. De Jong M., Bernard B.F., De Bruin E., Van Gameren A., Bakker W.H., Visser T.J., Mäcke H.R., Krenning E.P. Internalization of radiolabelled [$DTPA^0$]octreotide and [$DOTA^0$,Try^3]octreotide: Peptides for somatostatin receptor-trageted scintigraphy and radionuclide therapy. Nucl. Med. Commun. 1998; 19: 283–8.

8. Mausner L.F., Srivastava S.C. Selection of radionuclides for radioimmunotherapy. Med. Phys. 1993; 20(2): 503–9.

9. Goeckeler W.F., Edwards B., Volkert W.A., Holmes R.A., Simon J., Wilson D. Skeletal localization of samarium-153 chelates: potential therapeutic bone agents. J. Nucl. Med. 1987; 28(4): 495–504.

10. Ma D., Ketring A., Ehrhardt G., Jia W. Production of radiolanthanides and radiotherapy research at MURR. J. Radioanal. Nucl. Chem. 1996; (206): 119–26.

11. Das T., Banerjee S., Samuel G., Sarma H.D., Ramamoorthy N., Pillai M.R.A. Re-188-ethylene dicysteine: A novel agent for possible use in endovascular radiation therapy. Nucl. Med. Commun. 2000; 21(10): 939–45.

12. Pillai M.R.A., Chakraborty S., Das T., Venkatesh M., Ramamoorthy N. Production logistics of Lu-177 for radionuclide therapy. Appl. Radiat. Isot. 2003; 59(2–3): 109–18.

13. Banerjee S., Pillai M.R.A., Knapp F.F. Lutetium-177 therapeutic radiopharmaceuticals: Linking chemistry, radiochemistry, and practical applications. Chem. Rev. 2015; 115(8): 2934–74.

14. Pulukkody K.P., Norman T.J., Parker D., Royle L., Broan C.J. Synthesis of Charged and Uncharged Complexes of Gadolinium and Yttrium with Cyclic Polyazaphosphinic Acid Ligands for in vivo Applications. J. Chem. Soc. Perkin Trans. 1993; 2.

15. Caravan P., Ellison J.J., McMurry T.J., Lauffer R.B. Gadolinium(III) Chelates as MRI Contrast Agents: Structure, Dynamics, and Applications. Chem. Rev. 1999; 99(9): 2293–352.

16. Raymond K.N., Pierre V.C. Next generation, high relaxivity gadolinium MRI agents. Bioconjug. Chem. 2005; 16(1): 3–8.

17. Aime S., Calabi L., Cavallotti C., Gianolio E., Giovenzana G.B., Losi P., Maiocchi A., Palmisano G., Sisti M. [Gd-AAZTA]$^{-}$: A new structural entry for an improved generation of MRI contrast agents. Inorg. Chem. 2004; 43(24): 7588–90.

18. Aime S., Bombieri G., Cavallotti C., Giovenzana G.B., Imperio D., Marchini N. An unusual gadolinium ten-coordinated dimeric complex in the series of MRI contrast agents: Na[Gd(H_2O)AAZTA]$_3H_2O$. Inorganica Chim. Acta. 2008; 361(5): 1534–41.

19. Baranyai Z., Uggeri F., Giovenzana G.B., Bényei A., Brücher E., Aime S. Equilibrium and kinetic properties of the lanthanoids(III) and various divalent metal complexes of the heptadentate ligand AAZTA. Chem. - A Eur. J. 2009; 15(7): 1696–705.

20. Price E.W., Orvig C. Matching chelators to radiometals for radiopharmaceuticals. Chem. Soc. Rev. 2014; 43(1): 260–90.

21. Hnatowich D.J., Rusckowski M., Brill A.B., Siebecker D.A., Misra H., Mardirossian G., Bushe H., Rescigno A., Stevens S., Griffin T.W., Johnson D.K. Pharmacokinetics in Patients of an Anti-Carcinoembryonic Antigen Antibody Radiolabeled with Indium-111 Using a Novel Diethylenetriamine Pentaacetic Acid Chelator. Cancer Res. 1990; 50(22): 7272–8.

22. Baskin J.M., Prescher J.A., Laughlin S.T., Agard N.J., Chang P. V., Miller I.A., Lo A., Codelli J.A., Bertozzi C.R. Copper-free click chemistry for dynamic in vivo imaging. Proc. Natl. Acad. Sci. U. S. A. 2007; 104(43): 16793–7.

23. Stimmel J.B., Kull F.C. Samarium-153 and Lutetium-177 chelation properties of selected macrocyclic and acyclic ligands. Nucl. Med. Biol. 1998; 25(2): 117–25.

24. Lewis M.R. Macrocyclic Radiochelates for Antibody Imaging and Therapy of Breast Cancer. 1998. p. 113.

25. Rudd S.E., Roselt P., Cullinane C., Hicks R.J., Donnelly P.S. A desferrioxamine B squaramide ester for the incorporation of zirconium-89 into antibodies. Chem. Commun. 2016; 52: 1–4.

26. Meares C.F., McCall M.J., Reardan D.T., Goodwin D.A., Diamanti C.I., McTigue M. Conjugation of antibodies with bifunctional chelating agents: Isothiocyanate and bromoacetamide reagents, methods of analysis, and subsequent addition of metal ions. Anal. Biochem. 1984; 142(1): 68–78.

27. Brechbiel M.W., Gansow O.A., Atcher R.W., Schlom J., Esteban J., Simpson D.E., Colcher D. Synthesis of 1-(p-isothiocyanatobenzyl) derivatives of DTPA and EDTA. Antibody labeling and tumor-imaging studies. Inorg. Chem. 1986; 25(16): 2772–81.

28. Esteban J.M., Schlom J., Gansow O.A., Atcher R.W., Brechbiel M.W., Simpson D.E., Colcher D. New Method for the Chelation of Indium-111 to Monoclonal Antibodies: Biodistnbution and Imaging of Athymic Mice Bearing Human Colon Carcinoma Xenografts. 1987; 28(5): 861–71.

29. Halime Z., Frindel M., Camus N., Orain P.-Y., Lacombe M., Cherel M., Gestin J.-F., Faivre-Chauvet A., Tripier R. New synthesis of phenyl-isothiocyanate C-functionalised cyclams. Bioconjugation and Cu-64 phenotypic PET imaging studies of multiple myeloma with the te2a derivative. Org. Biomol. Chem. 2015; 13(46): 11302–14.

30. Tietze L.F., Arlt M., Beller M., Glüsenkamp K.-H., Jähde E., Rajewsky M.F. Anticancer Agents, 15. Squaric Acid Diethyl Ester: A New Coupling Reagent for the Formation of Drug Biopolymer Conjugates. Synthesis of Squaric Acid Ester Amides and Diamides. Chem. Ber. 1991; 124(5): 1215–21.

31. Jewett J.C., Bertozzi C.R. Cu-free click cycloaddition reactions in chemical biology. Chem. Soc. Rev. 2010; 39(4): 1272–9.

32. Huisgen R. 1,3-Dipolar Cycloadditions. Past and Future. Angew. Chem. Int. Ed. 1963; 2(10): 565–98.

33. Liu X., Hermange P., Ruiz J., Astruc D. Pd/C as an Efficient and Reusable Catalyst for the Selective N-Alkylation of Amines with Alcohols. ChemCatChem. 2016; (2 mL): 1043–5.

34. García Ruano J.L., Parra A., Alemán J., Yuste F., Mastranzo V.M. Monoalkylation of primary amines and N-sulfinylamides. Chem. Commun. (Camb). 2009; 404–6.

35. Russell H.F., Bremner J.B., Bushelle-Edghill J., Lewis M.R., Thomas S.R., Bates F. A new palladium-mediated approach to 4-N-arylamino-1-butanols from peroxidic tetrahydrofuran and primary aromatic amines. Tetrahedron Lett. 2007; 48(9): 1637–9.

36. Donovan S.F., Pescatore M.C. Method for measuring the logarithm of the octanol-water partition coefficient by using short octadecyl-poly(vinyl alcohol) high-performance liquid chromatography columns. J. Chromatogr. A. 2002; 952(1–2): 47–61.

37. Wenzel B., Mollitor J., Deuther-Conrad W., Dukic-Stefanovic S., Kranz M., Vraka C., Teodoro R., Günther R., Donat C.K., Ludwig F.A., Fischer S., Smits R., Wadsak W., Mitterhauser M., Steinbach J., Hoepping A., Brust P. Development of a Novel Nonpeptidic 18F-Labeled Radiotracer for in Vivo Imaging of Oxytocin Receptors with Positron Emission Tomography. J. Med. Chem. 2016; 59(5): 1800–17.

38. Smith C.J., Gali H., Sieckman G.L., Hayes D.L., Owen N.K., Mazuru D.G., Volkert W.A., Hoffman T.J. Radiochemical investigations of Lu-177-DOTA-8-Aoc-BBN[7-14]NH2: An in vitro/in vivo assessment of the targeting ability of this new radiopharmaceutical for PC-3 human prostate cancer cells. Nucl. Med. Biol. 2003; 30(2): 101–9.

39. Baur B., Solbach C., Andreolli E., Winter G., Machulla H.J., Reske S.N. Synthesis, radiolabelling and in vitro characterization of the gallium-68-, yttrium-90- and lutetium-177-labelled PSMA Ligand, CHX-A"-DTPA-DUPA-Pep. Pharmaceuticals. 2014; 7(5): 517–29.

40. Kruper W.J., Fordyce W.A., Sherry A.D. Carboxamide Modified Polyamine Chelators and Radioactive Complexes thereof for Conjugation to Antibodies. 1994. p. 13.

41. Pribish J.R. Acid cleavable compounds, their Preparation and use as bifunctional acid-labile crosslinking agents. 1996. p. 15.

42. Cooper R.S. Crown Compounds: Towards Future Applications. 1992.

43. Rüdiger V., Schneider H.J., Solov'ev V.P., Kazachenko V.P., Raevsky O.A. Crown ether-ammonium complexes: Binding mechanisms and solvent effects. European J. Org. Chem. 1999; (8): 1847–56.

44. Aime S., Barge A., Botta M., Fasano M., Danilo Ayala J., Bombieri G. Crystal structure and solution dynamics of the lutetium(III) chelate of DOTA. Inorganica Chim. Acta. 1996; 246(1–2): 423–9.

45. Pfister J., Summer D., Rangger C., Petrik M., von Guggenberg E., Minazzi P., Giovenzana G.B., Aloj L., Decristoforo C. Influence of a novel, versatile bifunctional chelator on theranostic properties of a minigastrin analogue. EJNMMI Res. 2015; 5(1): 74.

46. Perk L.R., Vosjan M.J.W.D., Visser G.W.M., Budde M., Jurek P., Kiefer G.E., Van Dongen G.A.M.S. P-Isothiocyanatobenzyl-desferrioxamine: A new bifunctional chelate for facile radiolabeling of monoclonal antibodies with zirconium-89 for immuno-PET imaging. Eur. J. Nucl. Med. Mol. Imaging. 2010; 37(2): 250–9.

47. Vosjan M.J.W.D., Perk L.R., Visser G.W.M., Budde M., Jurek P., Kiefer G.E., Van Dongen G.A.M.S. Conjugation and radiolabeling of monoclonal antibodies with zirconium-89 for PET imaging using the bifunctional chelate p-isothiocyanatobenzyl-desferrioxamine. Nat. Protoc. 2010; 5(4): 739–743.

4.6 Radiolabelling, *in vitro* and *in vivo* evaluation of a novel ^{89}Zr-MUC1-antibody for ImmunoPET

Radiolabelling, *in vitro* and *in vivo* evaluation of a novel ^{89}Zr-MUC1-antibody for ImmunoPET

N. Stergiou[1], J. Nagel[2], S. Pektor[3], M. Miederer[3], H. Kunz[4], F. Rösch[2], E. Schmitt[1]

[1] Institute of Immunology, Johannes Gutenberg-University of Mainz, Germany
[2] Institute of Nuclear Chemistry, Johannes Gutenberg-University of Mainz, Germany
[3] Department of Nuclear Medicine, University Medical Center of Johannes Gutenberg-University Mainz, Germany
[4] Institute of Organic Chemistry, Johannes Gutenberg-University of Mainz, Germany

ABSTRACT

An important antigen for several tumors is the tumor-associated glycoprotein Mucin1 (TA-MUC1). Decreased activity of the β-1,6-*N*-acetylglucosamintransferase as well as increased activity of the sialyltransferase leads to shortened glycoside side chains. The aberrantly glycosylated MUC1 is overexpressed on epithelial tumor cells and provides an ideal binding motif for monoclonal antibodies (mAb). By vaccination with TA-MUC1-glycopeptide the novel mAb (GGSK-1/30) could be generated, which demonstrated high affinity to TA-MUC1 on several human breast cancer cell lines. GGSK-1/30 was coupled with Df-Bz-NCS (Df-Bz-NCS-GGSK-1/30), radiolabelled with ^{89}Zr, purified and evaluated *in vitro* (stability, immunoreactivity, cell binding) and *in vivo* (PET, *ex vivo* biodistribution) in tumor bearing mice.

[^{89}Zr]Zr-Df-Bz-NCS- GGSK-1/30 was radiolabelled with a radiochemical yield of >70 %, a radiochemical purity of > 95 % and an apparent specific activity of 6.1 GBq/µmol. After 3 d, stabilities >80 % in human serum and >90 % in sodium chloride (0.9 %) could be obtained. *In vitro* cell studies showed a high affinity to the self-generated murine mamma carcinoma cell line PyMTxhuMUC1 (15 % binding), that express human TA-MUC1, and the commercially available human mamma carcinoma cell line T47D (33 % binding). The affinity to TA-MUC1 was confirmed by *ex vivo* tumor uptake of >50 % ID/g in tumor bearing mice, which was clearly visible in small animal PET/MRI imaging.

The novel mAb GGSK-1/30 and its conjugate is a promising candidate for *in vivo* application for ImmunoPET due to its high and specific affinity to TA-MUC1.

INTRODUCTION

Monoclonal antibodies (mAb) are attractive candidates for cancer diagnosis, cancer therapy and drug delivery [1]. An important antigen for mAb is the tumor associated glycoprotein Mucin1 (TA-MUC1) [2–6]. TA-MUC1, with an aberrant glycan pattern, is strongly overexpressed on epithelial cells of tumor tissue like breast cancer as a result of changed activity of glycoltransferases in MUC1 biosynthesis [7]. The main part of MUC1 consists of an extracellular domain that contains numerous (20-120) tandem repeats of 20 aminoacids. Based on the aberrant glycan pattern Kaiser *et al.* synthesized glycopeptides as mimic for the TA-MUC1, coupled these to Tetanus toxoid (TTox) and administered the vaccines in Balb/c mice [3,4]. Analysis of mice antisera showed a high specificity as well as exclusive binding to aberrantly glycolsylated MUC1 and isolated human breast tumor tissue. Consequently, the novel IgG mAb (GGSK-1/30), isolated from mice antisera, demonstrated high affinity towards human breast cancer cells (MCF-7) [8].

With the idea to introduce antibody-based imaging systems, using single photon emission computed tomography (SPECT) or positron emission tomography (PET) [9–11], new pathways have been explored to combine the requirements of PET/SPECT application with the *in vivo* characteristics of a mAb. Due to the slow pharmacokinetics of the mAb of several days the radiolabelled derivatives have to fulfill two requirements: a high *in vivo* stability of the conjugate and a radionuclide half-life suited to the pharmacokinetics of the mAb. Important radionuclides for imaging application with mAbs/antibody fragments are listed in table 1.

Table 1: Relevant radioisotopes for the application in radioimmunoscintigraphy [12–27]

nuclide	$t_{1/2}$	application
^{64}Cu	12.8 h	PET
^{86}Y	14.7 h	
^{89}Zr	3.27 d	
^{90}Nb	14.6 h	
^{124}I	4.18 d	
^{67}Ga	3.26 d	SPECT
^{99m}Tc	6.0 h	
^{111}In	2.80 d	

The nuclides for SPECT imaging (expect ^{99m}Tc) possess half-lifes of several days, which is ideal for antibody-based imaging, but in comparison to the higher resolution of PET, SPECT imaging is of less interest. Thus, ^{64}Cu, ^{86}Y, ^{89}Zr and ^{124}I are of great interest for ImmunoPET imaging. According to the shorter half life of ^{64}Cu, ^{86}Y and ^{90}Nb (12.8 h, 14.7 h and 14.6 h, respectively), these nuclides can be used for

antibody fragments, which offer a faster pharmacokinetic behavior. ^{124}I as well as ^{89}Zr are ideal candidates for ImmunoPET. The disadvantage of ^{124}I is the low resolution due to the high energy of its positron and the dehalogenation of ^{124}I-labelled antibodies *in vivo* [21,28]. Therefore ^{89}Zr was suggested as more suitable positron emitter for labelling of antibodies by attaching chelating agents to the protein [24,29]. Baroncelli *et al.* showed a high complex stability of Zr with hydroxamate groups of desferrioxamine (Df) [30]. Based on this fact, Verel *et al.* evaluated the coupling of a bifunctional derivative of Df (TFP-*N*-suc-Df-Fe) [31]. The drawback of this method is the relatively complicated multi-step procedure, which makes its challenging with respect to Good Manufacturing Practice (GMP) compliancy. Therefore, Jurek *et al*. and Perk *et al.* established an NCS ester of Df (Df-Bz-NCS) for easy coupling to primary amines on the mAb [32,33].

Based on these perspectives we wanted to introduce the Df-Bz-NCS as chelating agent for ^{89}Zr to evaluate the mAb GGSK-1/30, which offers a specificity to TA-MUC1 and its epitope [5–8,34,35]. The radiolabelled derivative [^{89}Zr]Zr-Df-Bz-NCS-GGSK-1/30 was evaluated in first *in vitro* and *in vivo* studies using a transgenic tumor model, which was developed by crossbred of mammary tumor virus (MMTV), polyoma virus T-antigene (PyMT) and human MUC1 (MMTV-PyMTxhuMUC1).

RESULTS AND DISCUSSION

Synthesis, chelate coupling and ^{89}Zr radiolabelling of GGSK-1/30

GGSK-1/30 was generated via hybridoma technique by vaccination of mice with a synthetic glycopeptide that mimics one specific structure of TA-MUC1 on human cancer cells. The glycopeptide was coupled to Tetanus Toxoid to build the vaccine.

The conjugation of the chelate Df-Bz-NCS to the lysine side chain as well as the ^{89}Zr radiolabelling of GGSK-1/30 is shown in figure 1. The coupling of the chelate resulted in a ratio of 4.2 chelate moieties per antibody. To verify the immunoreactivity of Df-Bz-NCS-GGSK-1/30, its binding to breast cancer cells (T47D) was investigated using fluorescence-activated cell sorting (FACS) (figure 2). With a binding of more than 97 % the conjugate shows no loss towards tumor associated Mucin1. This is in agreement with previous works for DOTA-conjuagted rituximab, where no influence on immunoreactivity was reported for a chelate-to-antibody ratio of 4 [36].

The radiolabelling was performed at room temperature over 90 min and resulted in an overall yield of 73 %. Radiochemical purity of [^{89}Zr]Zr-Df-Bz-NCS-GGSK-1/30 exceeded 95 % after purification with PD-10 column with an apparent specific activity of 6.1 GBq/µmol.

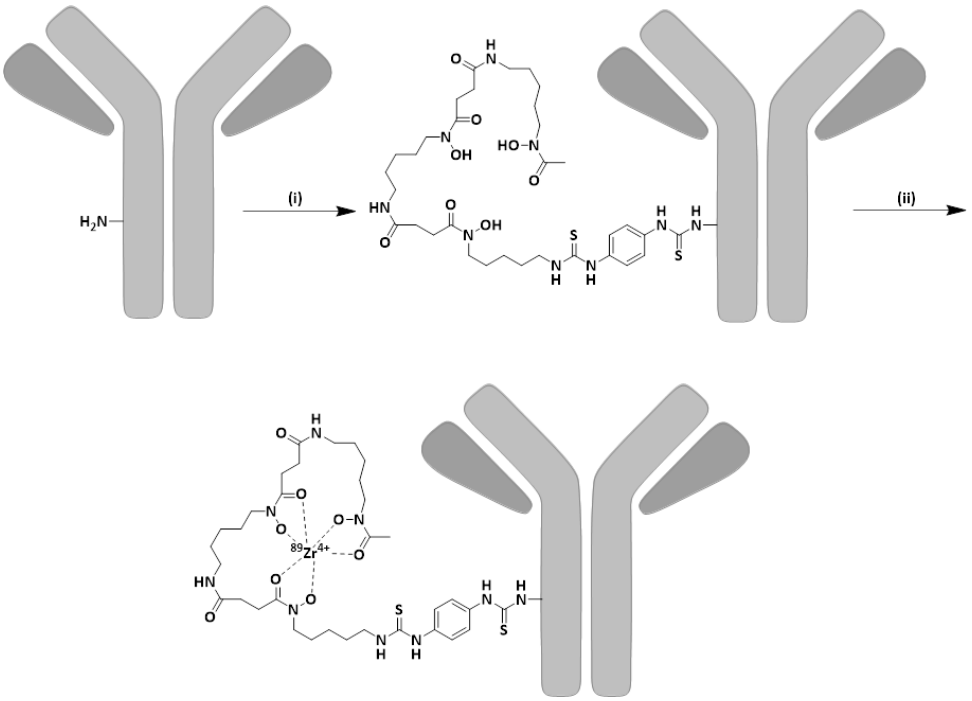

Figure 1: General coupling method of Df-Bz-NCS with antibodies; (i) pH=9.0, 37 °C, 30 min, gel filtration, (ii) pH=7.0, 25 °C, 90 min gel filtration

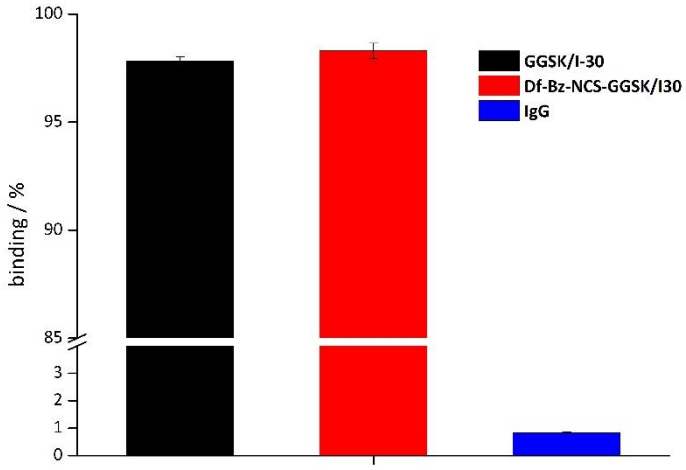

Figure 2: FACS analysis of the immunoreactivity for GGSK-1/30 (black bar), its conjugate (red bar) and a control IgG antibody (blue bar) using T47D cells

In vitro studies

Stabilities

[^{89}Zr]Zr-Df-Bz-NCS-GGSK-1/30 offers a high stability of >90 % after 3 d in human serum and sodium chloride solution (figure 9, supporting information). In PBS buffer the radioconjugate remains stable even after 3 d, while a slight decrease down to 83 % intact conjugate after 7 days is observed in human serum.

Cell binding

The binding affinity of [^{89}Zr]Zr-Df-Bz-NCS-GGSK-1/30 was evaluated towards four cell lines with different expression levels of aberrantly glycosylated MUC1. Figure 3 represents the binding profile of the radiolabelled compound as a function of the concentration of [^{89}Zr]Zr-Df-Bz-NCS-GGSK-1/30.

The affinity and specificity of the radiolabelled conjugate to TA-MUC1 human mammary epithelial cells (HMEC) that express normally glycosylated MUC1 was investigated, PyMT as murine mammary tumor cell line, that do not express human TA-MUC1, served as negative control. Less than 2 % of the applied activity for both cell lines and all concentrations were found on the cell surfaces. T47D human carcinoma cells showed the highest affinity of all cell lines towards the antibody conjugate with a binding of >30 %. The novel transgenic murine cell line PyMTxhuMUC1 offers a binding of >15 %. This cell model was used for further *in vivo* small animal studies (mice) to get an insight of this transgenic cell model as target and the radio conjugate as targeting vector.

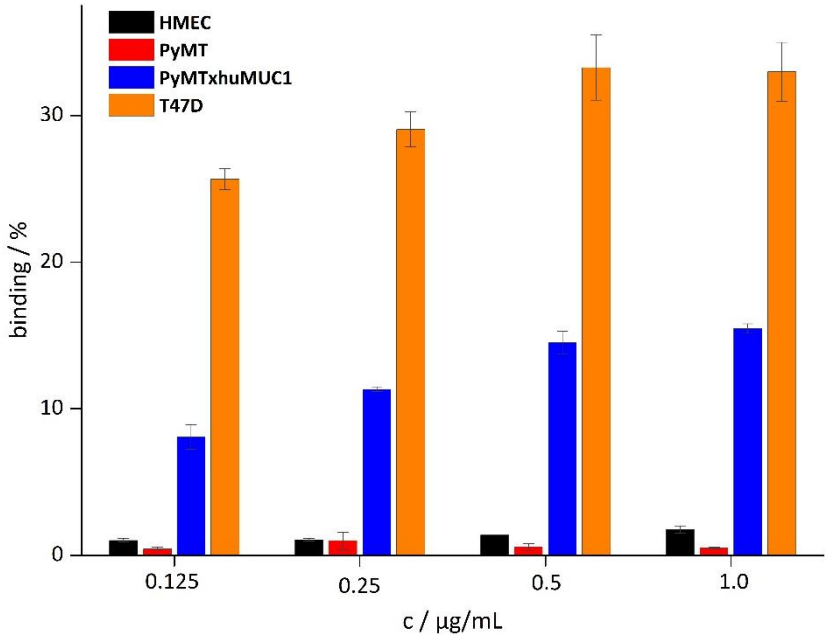

Figure 3: Cell binding profile of [^{89}Zr]Zr-Df-Bz-NCS-GGSK-1/30 with respect to the cell line and concentration of [^{89}Zr]Zr-Df-Bz-NCS- GGSK-1/30

In vivo studies

ex vivo biodistribution

To confirm the specificity of [^{89}Zr]Zr-Df-Bz-NCS-GGSK-1/30 towards TA-MUC1, the conjugate was administered in human MUC1 transgenic mice bearing PyMTxhuMUC1 tumors (positive control). For blocking, the radiolabelled conjugate was incubated with a 1200-fold molar excess of TA-MUC1-glycopeptide described by Palitzsch *et al.* [8] for 30 min before the application into the aforementioned mice model. As negative control, an IgG1-mAb with no affinity towards TA-MUC1, was radiolabelled and purified in the same manner as the GGSK-1/30. 50-80 µg of radiolabelled compounds were injected intraperitoneal (i.p.). After 72 h post injection (p.i.), the average uptake (%ID/g (tissue), mean±SD) in tumor, blood and normal tissues was determined *ex vivo*. The results of the *ex vivo* biodistribution are shown in figure 4.

[^{89}Zr]Zr-Df-Bz-NCS-GGSK-1/30 demonstrated an uptake of 53 %ID/g(tumor tissue). The blocking of GGSK-1/30 with TA-MUC1-glycopeptide resulted in decreased uptake in tumor tissue of less than 8 %ID/g(tumor tissue), reflecting the specificity of GGSK-1/30 towards TA-MUC1. With 15 %ID/g(tumor tissue) an unspecific uptake towards the target tissue was observed for [^{89}Zr]Zr-Df-Bz-NCS-IgG1. This could be explained by the *enhanced permeability and retention* (EPR) effect, which is known for macromolecular, lipophilic compounds that show a passive accumulation in solid tumor tissue [37,38].

Uptake values in normal tissue like lymph nodes, lung, blood, heart, spleen, intestines as well as muscle and mammary glands are below 10 %ID/g(tissue) for [^{89}Zr]Zr-Df-Bz-NCS-GGSK-1/30 in control and blocking studies. The uptake values in bone tissue of more than 10%ID/g(bone tissue) is the result of the slight degradation of the Zr-Df-complex *in vivo*, which is known ^{89}Zr-radiolabelled antibodies [31,39,40]. Both antibody conjugates show hepatobiliary and renal excretion with uptake values from 17 to 35 %ID/g(liver tissue) and 25 to 40 %ID/g(kidney tissue). The higher uptake in liver within the blocking and the negative control studies emphasizing the decreased affinity of the blocked [^{89}Zr]Zr-Df-Bz-NCS-GGSK-1/30 and the missing specificity of [^{89}Zr]Zr-Df-Bz-NCS-IgG1, respectively. For [^{89}Zr]Zr-Df-Bz-NCS-IgG1 the higher blood pool activity, and with this a higher activity in lung tissue, is due to a lack of a specific binding site of this antibody. The uptake in kidney, liver and spleen can be explained by a residualizing effect of the compounds by these cells [10,25]. For [^{89}Zr]Zr-Df-Bz-NCS-GGSK-1/30 an increased uptake in kidney tissue was observed.

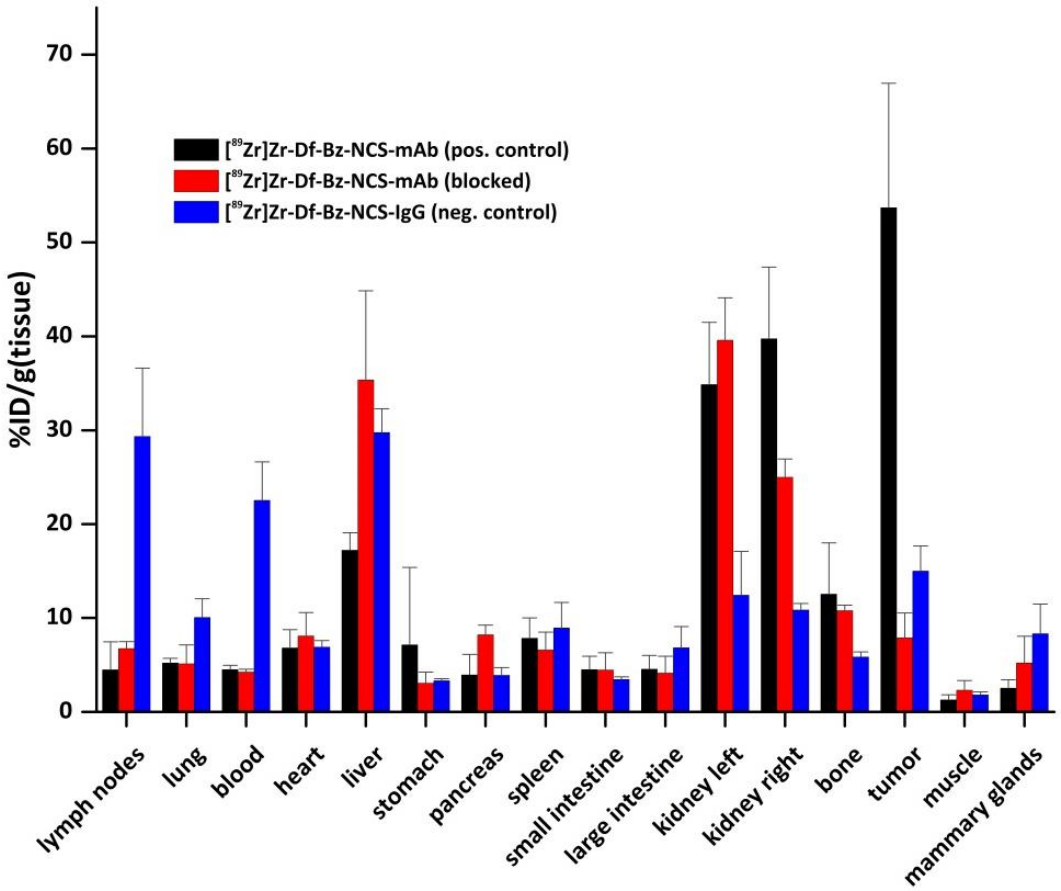

Figure 4: *ex vivo* biodistribution of radiolabelled GGSK-1/30 ([^{89}Zr]Zr-Df-Bz-NCS-GGSK-1/30) and control mAb ([^{89}Zr]Zr-Df-Bz-NCS-IgG) in C57BL/6 mice bearing PyMTxhuMUC1 tumor after 72 h; 50-80 µg (0.33-0.53 nmol, 0.5-2.5 MBq) of radiolabelled compounds were administered i.p. (n=3)

The tumor/non-target-tissue ratios of [^{89}Zr]Zr-Df-Bz-NCS-GGSK-1/30 are illustrated in figure 5. Ratios between tumor tissue and lung, blood and muscle are 3.4, 8.3 and 42.4, respectively. With this, the contrast between target and non-target tissue appear to be promising for *in vivo* PET imaging.

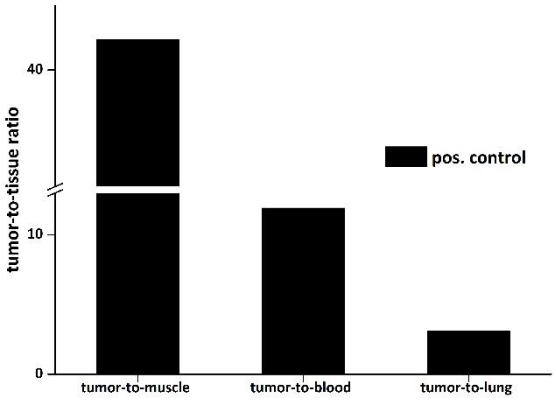

Figure 5: Tumor/non-target-tissue ratios of [^{89}Zr]Zr-Df-Bz-NCS-GGSK-1/30 after 72 h

Small animal PET studies

To verify the *ex vivo* results, small animal PET imaging studies were accomplished for [^{89}Zr]Zr-Df-Bz-NCS-GGSK-1/30) (blocked and unblocked) as well as for [^{89}Zr]Zr-Df-Bz-NCS-IgG1. The *in vivo* binding of the radioconjugates was assessed by PET imaging at 72 hours post injection (72 h p.i.) on tumor bearing mice after injection of 50-80 µg of the radiolabelled compound. [^{89}Zr]Zr-Df-Bz-NCS-GGSK-1/30 shows a clearly visible uptake in the tumor tissue (figure 6, **A**) with a renal excretion pathway. This result is consistent with the *ex vivo* biodistribution of the radio conjugate, where the main activity accumulated in the target tissue and the kidneys. In the blocking experiment a high uptake in kidney and liver with almost no accumulation of the radioconjugate in tumor tissue was observed (figure 6, **B**). The negative control evaluation with [^{89}Zr]Zr-Df-Bz-NCS-IgG1 shows a generally higher background in non-target tissue (figure 6, **C**). This finding is in agreement with the *ex vivo* data with high uptake values in lung, blood or mammary glands mammalian (figure 4) and, consequently, emphasizes the absence of the specificity of the IgG antibody.

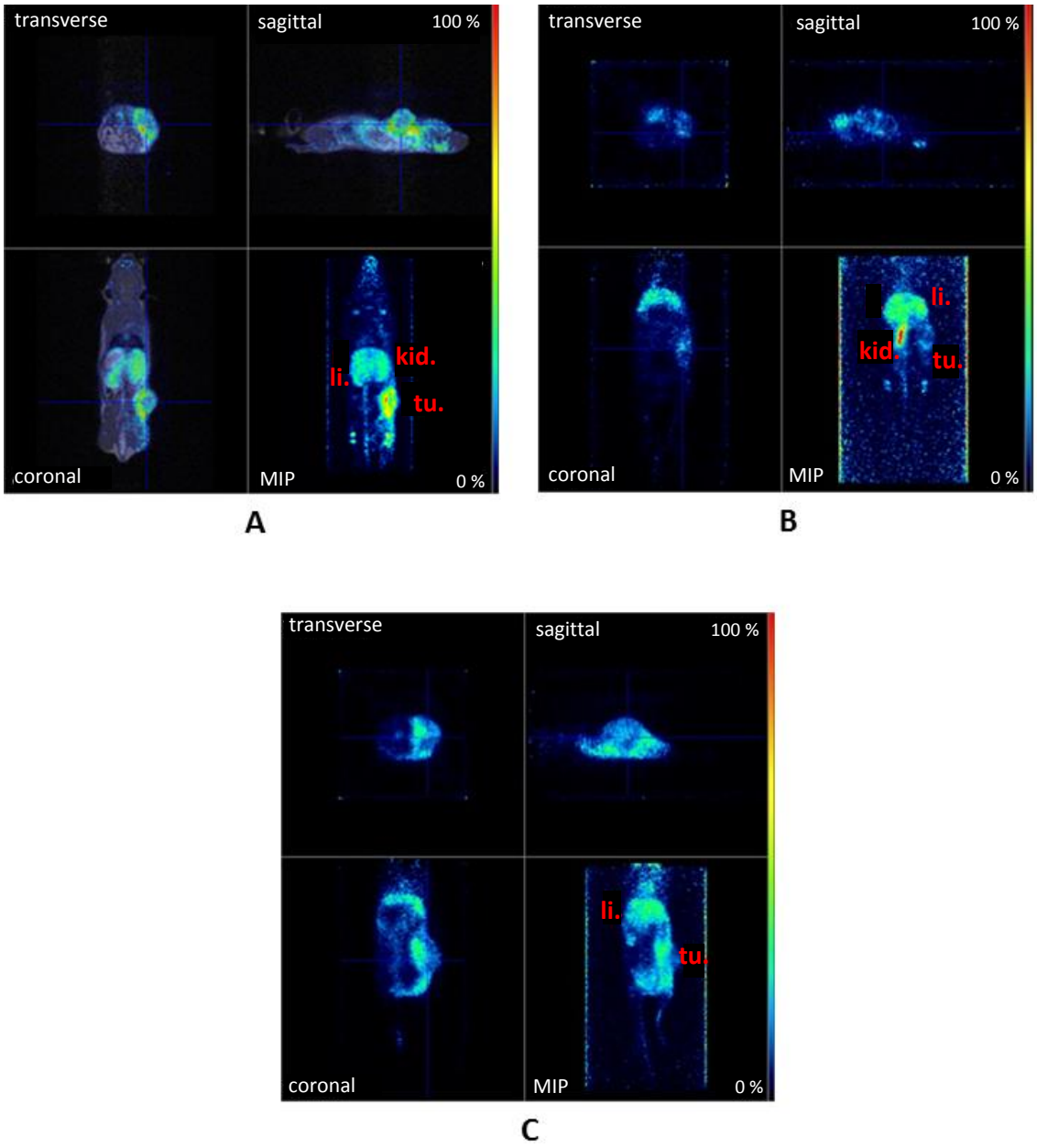

Figure 6: PET images of [^{89}Zr]Zr-Df-Bz-NCS-GGSK-1/30 (**A**), [^{89}Zr]Zr-Df-Bz-NCS-GGSK-1/30 blocked (**B**) and [^{89}Zr]Zr-Df-Bz-NCS-IgG (**C**) after 72 h in tumor bearing mice after injection of 50-80 µg (0.33-0.53 nmol, 0.5-2.5 MBq); tu.: tumor, kid.: kidney, li.: liver

CONCLUSION

Tumor-associated Mucin1 is an important antigen for targeting tumor tissue in breast cancer. In this study a stable and reproducible coupling of the long-lived positron emitter ^{89}Zr was evaluated for the novel antibody GGSK-1/30 with the chelating agent Df-Bz-NCS. After radiolabelling and purification the radioconjugate [^{89}Zr]Zr-Df-Bz-NCS-GGSK/1-30 was obtained with 95 % radiochemical purity, an apparent specific activity of 6.1 GBq/mol and a stability over in 80 % in humans serum after 3 d.

The high *in vitro* binding affinity with over 15 % binding to human TA-MUC1 expressing cells as well as the high specificity of [^{89}Zr]Zr-Df-Bz-NCS-GGSK/1-30 towards human TA-MUC1 indicates its strong potential for tumor imaging. The i*n vitro* results could be confirmed within first *in vivo* studies in tumor bearing mice. *Ex vivo* biodistribution showed a tumor uptake of >50 %ID/g and a clearly visible accumulation in PET/MR imaging.

With these characteristics GGSK-1/30 offers the application in clinical studies for molecular imaging using PET as well as for radioimmunotherapy approaches.

ACKNOWLEDGEMENT

This project was financially supported by the *Inneruniversitäre Forschungsförderung* of the JGU Mainz and the CRC1066. The authors thank Markus Glaffig for supplying the glycopeptide for blocking experiments and Nicole Bausbacher for kind help during PET/MRI studies.

SUPPORTING INFORMATION

General methods:

All used chemicals were commercially available at Acros Organics, CheMatech, Fluka, SigmaAldrich or VWR and were used without further purification. For purification of conjugated and radiolabelled antibody, PD-10 columns (GE Healthcare Life Science) were applied with 0.9 % sodium chloride (Fresenius-Kabi) solution. For radiolabellings trace metal-free salts and water (18 MΩ cm^{-1}) were used. For radiolabelling n.c.a. ^{89}Zr (1 M oxalic acid) from PerkinElmer (BV Cyclotron VU, Amsterdam, Netherlands) was used.

FACS-Analysis of the antibody binding and its conjugate to human breast cancer cells

$2 \cdot 10^5$ human breast cancer cells (T47D) were incubated with 1 µg/ml GGSK-1/30, 1 µg/ml of its conjugate and 1 µg/ml of the control IgG1 antibody for 20 min at a temperature of 4 °C. Then the cells were washed for two times with 100 µl of PBS and then incubated for 20 minutes at a temperature of 4 °C with a goat-α-mouse-IgG Alexa Fluor 488 antibody (dilution 1:1000 in PBS) and with a viability dye eFluor780 (dilution 1:1000 in PBS) to exclude the false positive dead cells. The cells were washed again two times with 100 µL PBS. The cells were then taken up in 100 µL of PBS and pipetted into a FACS tube and analyzed on a *BD Biosciences* FACSVerse machine. For each sample 10^4 cells were analyzed.

Preparation of PyMTxhuMUC1

Female mice of the mouse stem R10 (Tg(MMTVPyMT)634MuI; short: *PyMT;* kindly gift from the group of Prof. Dr. Ruf in Mainz) generate spontaneously breast cancer cells 15 weeks after birth [41]. Cross breeding of R10 mice with TG(MUC1)79.24GEND/J mice expressing human MUC1 (short: *huMUC1,* The Jackson laboratory) lead to the tumor model PyMTxhuMUC1. To obtain stable tumor cell lines of PyMT mice and PyMTxhuMUC1 mice, tumor tissues were extracted, digested by collagenase and DNAse and cultured in single cell suspension. Stable PyMT and PyMTxhuMUC1 tumor cells could be harvested after 6 weeks.

Analysis of the *in vitro* cell binding of radiolabelled GGSK-1/30 to human MUC1 expressing cell lines

The human breast cancer cell line (T47D) that express TA-MUC1 and as control the human mammary epithelial cell line (HMEC) that express normally glycosylated MUC1 as well as the murine cell lines PyMT-huMUC1 that express human TA-MUC1 and as control PyMT that do not express human TA-MUC1 were incubated for 20 minutes at 4°C. The cells were washed two times with 100 µl PBS. The washing solution was kept to detect the unbound antibody. The radioactive emission was detected of

the cells and the washing solution. The ratio cells/washing solution x 100 resulted in binding/%.

Inoculation of PyMTxhuMUC1

PyMTxhuMUC1 cells ($1x10^6$) were subcutaneously inoculated in the right flank of nine 10 weeks old TG(MUC1)79.24GEND/J mice (The Jackson Laboratory). The tumor growth was observed every 3 d. 21 d after inoculation (tumor size 40 mm^2 on average) 50-80 µg of the radioconjugate was administered i.p.

Preparation of Df-Bz-NCS-GGSK-1/30

GGSK-1/30 was coupled with Df-Bz-NCS following a known procedure (figure 1) [33]. In short, a ten-fold molar excess of Df-Bz-NCS (in 10 µL DMSO) was added to the GGSK-1/30 (2 mg/mL in 1 mL 0.1 mL $NaHCO_3$ buffer, pH 9.0) and incubated for 30 min at 37 °C. The chelator-GGSK-1/30 conjugate was purified by size exclusion chromatography (SEC) using a PD-10 column and 0.25 M sodium acetate buffer, pH 5.4 as eluent.

Determination of chelate-to-mAb ratio (CAR)

To determine the CAR the conjugate was labelled according to aforementioned procedure [33,42] with a known nanomolar excess of zirconium oxalate solution (TraceCERT®, 1000 mg/mL) spiked with ^{89}Zr. Different molar ratios between Zr and antibody were used, to investigate the number of chelates per antibody.

Preparation of [^{89}Zr]Zr-Df-Bz-NCS-GGSK-1/30

Df-Bz-NCS-GGSK-1/30 was labelled according to aforementioned method [43]. In short, Df-Bz-NCS-GGSK-1/30 was radiolabelled with ^{89}Zr in HEPES buffer (0.5 M, pH 7) at room temperature in a volume of 2.5-3 mL under gentle stirring for 90 min. The radiochemical yield (RCY) was checked by using radio thin layer chromatography (radio-TLC) and analyzed with the radio detector GABI STAR from Raytest. The radiolabelled compound was purified by PD-10 column using a 0.9 % sodium chloride solution as eluent.

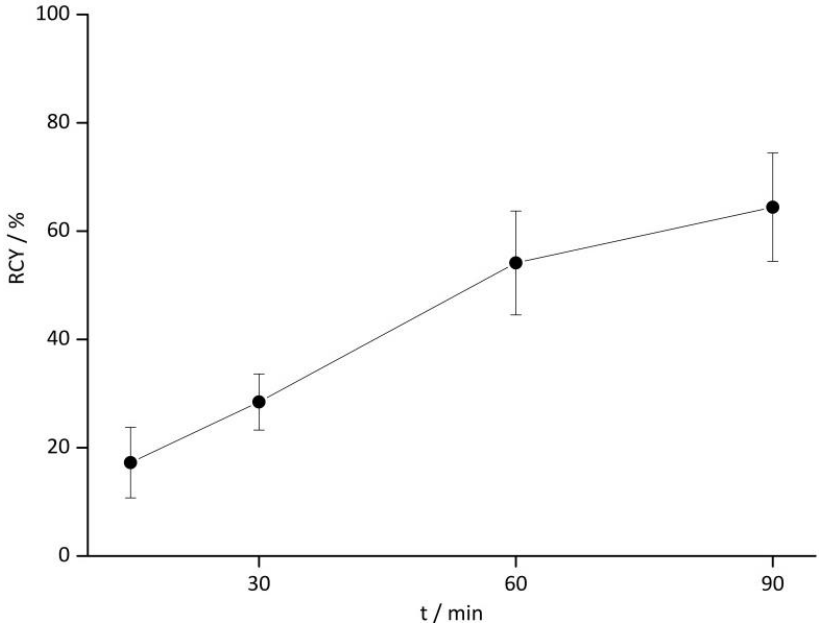

Figure 7: Radiolabelling kinetics with ^{89}Zr of Df-Bz-NCS-GGSK-1/30 in 0.5 M HEPES (pH 7)

Analytical quality control of [^{89}Zr]Zr-Df-Bz-NCS-GGSK-1/30

The purified product was analysed by radio-TLC and by high performance liquid chromatography (HPLC) for radiochemical purity. Radio-TLC analysis of [^{89}Zr]Zr-Df-Bz-NCS-GGSK-1/30 was performed using Merck Silica F_{254} TLC plates with citrate buffer (0.01 M, pH 4) and analyzed with the radio detector GABI STAR from Raytest. HPLC monitoring was performed on a HPLC system from Merck (LaChrom; pump: Hitachi L7100; UV-detector: L7400) using a BioSep SEC-S 2000 column (Phenomenex®) with 0.05 M sodium phosphate (pH 7) as mobile phase (1 mL/min).

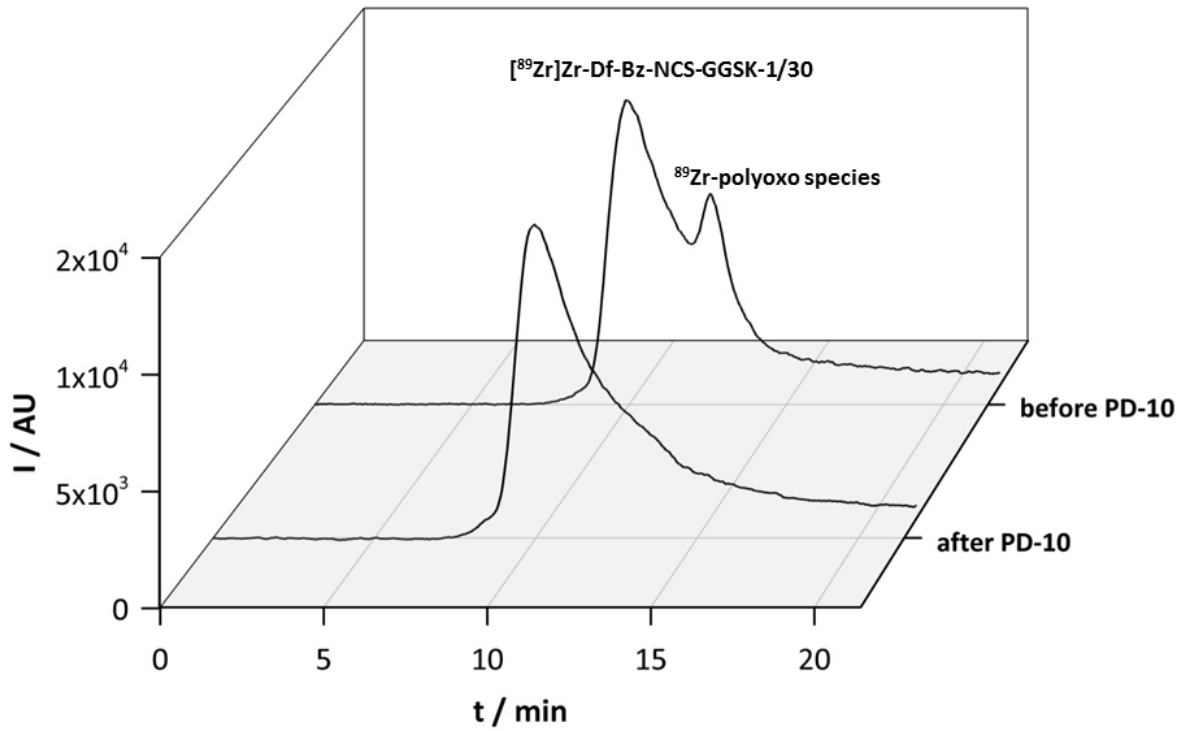

Figure 8: HPLC diagram of [^{89}Zr]Zr-Df-Bz-NCS-GGSK-1/30 using BioSep SEC-S 2000 column (Phenomenex®) with 0.05 M sodium phosphate (pH 7) as mobile phase (1 mL/min) before and after purification using size exclusion chromatography on PD-10 column

In vitro stability test of [^{89}Zr]Zr-Df-Bz-NCS-GGSK-1/30

In vitro stability studies of [^{89}Zr]Zr-Df-Bz-NCS-GGSK-1/30 were performed in human serum (Sigma-Aldrich®, from human male AB plasma) and sodium chloride (0.9 %) (n=3). The samples were incubated at 37 °C and aliquots of 2 µL were analyzed at various time points (1 d, 3 d, 7 d) via radio-TLC using citrate buffer (figure 8).

In vitro binding studies of [^{89}Zr]Zr-Df-Bz-NCS-GGSK-1/30

For *in vitro* binding studies different concentration of [^{89}Zr]Zr-Df-Bz-NCS-GGSK-1/30 (0.125-2 µg/mL) were incubated on $2 \cdot 10^5$ cells (HMEC and T47D (commercially obtained by ATCC), PyMT and PyMTxhu-MUC1 (self-made tumor cell lines from an isolated murine tumor in the lab of the Immunology department)) for 30 min at 37 °C. The supernatant was removed, the cell surface washed twice with PBS buffer and the cells cleaved for gamma counting.

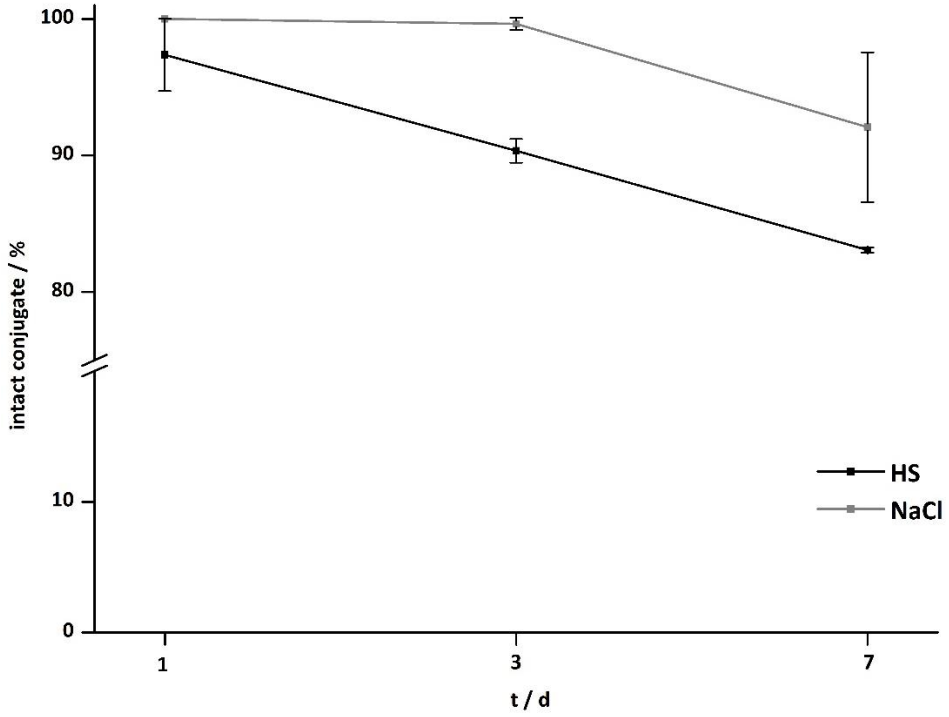

Figure 9: Stability of [^{89}Zr]Zr-Df-Bz-NCS-GGSK-1/30 in human serum (black line) and sodium chloride solution (0.9 %, gray line) after 1 d, 3 d and 7 d at 37 °C (n=3)

Ex vivo biodistribution

$1 \cdot 10^6$ PyMTxhuMUC1 cells were subcutaneously implanted in the right flank of human MUC1 transgenic mice, 10 to 13 weeks old, female. 3 weeks after tumor cell injection application of 50-80 µg of radiolabelled compound was administered i.p. For the blocking experiment [^{89}Zr]Zr-Df-Bz-NCS-GGSK-1/30 was incubated for 30 min with 1200-fold molar excess of the corresponding glycopeptide [8], that mimic the antigen for GGSK-1/30 and administered i.p. 72 h post injection, groups of 3 mice were anaesthetised, killed and dissected. Blood, tumor, normal tissue and gastrointestinal contents were weighed and the amount of radioactivity in each tissue was measured in a γ-counter (PerkinElmer Wizard^2). Radioactivity uptake was calculated as the percentage of the injected dose per gram of tissue (%ID/g(tissue)).

In vivo small animal PET studies

Small animal PET imaging was performed under general anesthesia with isoflurane inhalation (2.5 %). 50-80 µg (0.5-2.5 MBq) of radioconjugate in 230-300 µL sodium chloride solution (0.9 %) were injected intraperitoneal (i.p.) and mice were positioned 72 h p.i. in head-first-supine position in a PET scanner. PET imaging was recorded on a NanoScan PET/MRI (Mediso, Hungary) reconstructed to OSEM 2D and files were processed using Pmod 3.5.

REFERENCES

1. Wu A.M., Senter P.D. Arming antibodies: prospects and challenges for immunoconjugates. Nat. Biotechnol. 2005;23(9):1137–46.

2. Nath S., Mukherjee P. MUC1: A multifaceted oncoprotein with a key role in cancer progression. Trends Mol. Med. 2014;20(6):332–42.

3. Kaiser A., Gaidzik N., Westerlind U., Kowalczyk D., Hobel A., Schmitt E., Kunz H. A synthetic vaccine consisting of a tumor-associated sialyl-T N-MUC1 tandem-repeat glycopeptide and tetanus toxoid: induction of a strong and highly selective immune response. Angew. Chemie - Int. Ed. 2009;48(41):7551–5.

4. Gaidzik N., Kaiser A., Kowalczyk D., Westerlind U., Gerlitzki B., Sinn H.P., Schmitt E., Kunz H. Synthetic antitumor vaccines containing MUC1 glycopeptides with two immunodominant domains-induction of a strong immune response against breast tumor tissues. Angew. Chemie - Int. Ed. 2011;50(42):9977–81.

5. Taylor-Papadimitriou J., Burchell J., Miles D.W., Dalziel M. MUC1 and cancer. Biochim. Biophys. Acta - Mol. Basis Dis. 1999;1455(2–3):301–13.

6. Hanisch F.G. O-glycosylation of the mucin type. Biol. Chem. 2001;382(2):143–9.

7. Brockhausen I., Yang J.-M., Burchell J., Whitehouse C., Taylor-Papadimitriou J. Mechanisms Underlying Aberrant Glycosylation of MUC1 Mucin in Breast Cancer Cells. Eur. J. Biochem. 1995;233(2):607–17.

8. Palitzsch B., Hartmann S., Stergiou N., Glaffig M., Schmitt E., Kunz H. A fully synthetic four-component antitumor vaccine consisting of a mucin glycopeptide antigen combined with three different T-helper-cell epitopes. Angew. Chemie - Int. Ed. 2014;53(51):14245–9.

9. Parker D. Tumour targeting with radiolabelled macrocycle-antibody conjugates. Chem. Soc. Rev. 1990;19(3):271–91.

10. Verel I., Visser G.W.M., Boerman O.C., van Eerd J.E.M., Finn R., Boellaard R., Vosjan M.J.W.D., Stigter-van Walsum M., Snow G.B., Van Dongen G.A.M.S. Long-lived positron emitters zirconium-89 and iodine-124 for scouting of therapeutic radioimmunoconjugates with PET. Cancer Biother. Radiopharm. 2003;18(4):655–61.

11. Philpott G.W., Schwarz S.W., Anderson C.J., Dehdashti F., Connett J.M., Zinn K.R., Meares C.F., Cutler P.D., Welch M.J., Siegel B.A. RadioimmunoPET: detection of colorectal carcinoma with positron-emitting copper-64-labeled monoclonal antibody. J. Nucl. Med. 1995;36(10):1818–24.

12. Timmermand O. V., Ulmert D., Evans-Axelsson S., Pettersson K., Bjartell A., Lilja H., Strand S.-E.,

Tran T.A. Preclinical imaging of kallikrein-related peptidase 2 (hK2) in prostate cancer with a In-111-radiolabelled monoclonal antibody, 11B6. EJNMMI Res. 2014;4(1):51.

13. Li L., Bading J., Yazaki P.J., Ahuja A.H., Crow D., Colcher D., Williams L.E., Wong J.Y.C., Raubitschek A., Shively J.E. A versatile bifunctional chelate for radiolabeling humanized anti-CEA antibody with In-111 and Cu-64 at either thiol or amino groups: PET imaging of CEA-positive tumors with whole antibodies. Bioconjug. Chem. 2008;19(1):89–96.

14. Kim H., Chaudhuri T.R., Buchsbaum D.J., Wang D., Zinn K.R. High-resolution single-photon emission computed tomography and X-ray computed tomography imaging of Tc-99m-labeled anti-DR5 antibody in breast tumor xenografts. Mol. Cancer Ther. 2007;6(3):866–75.

15. Kipper S.L., Rypins E.B., Evans D.G., Thakur M.L., Smith T.D., Rhodes B. Neutrophil-specific Tc-99m-labeled anti-CD15 monoclonal antibody imaging for diagnosis of equivocal appendicitis. J. Nucl. Med. 2000;41(3):449–55.

16. Schuhmacher J., Matys R., Hauser H., Maier-Borst W., Matzku S. Labeling of monoclonal antibodies with a Ga-67-phenolic aminocarboxylic acid chelate. Eur. J. Nucl. Med. 1986;12(8):397–404.

17. Haisma H., Goedemans W., de Jong M., Hilkens J., Hilgers J., Dullens H., Den Otter W. Specific localization of In-111-labeled monoclonal antibody versus 67-Ga-labeled immunoglobulin in mice bearing human breast carcinoma xenografts. Cancer Immunol. Immunother. 1984;17(1):62–5.

18. Nayak T.K., Garmestani K., Baidoo K.E., Milenic D.E., Brechbiel M.W. Preparation, biological evaluation, and pharmacokinetics of the human anti-HER1 monoclonal antibody panitumumab labeled with Y-86 for quantitative PET of carcinoma. J. Nucl. Med. 2010;51(6):942–50.

19. Rogers B.E., Anderson C.J., Connett J.M., Guo L.W., Edwards W.B., Sherman E.L.C., Zinn K.R., Welch M.J. Comparison of four bifunctional chelates for radiolabeling monoclonal antibodies with copper radioisotopes: Biodistribution and metabolism. Bioconjug. Chem. 1996;7(4):511–22.

20. Anderson C.J., Schwarz S.W., Connett J.M., Cutler P.D., Guo L.W., Germain C.J., Philpott G.W., Zinn K.R., Greiner D.P., Meares C.F. Preparation, biodistribution and dosimetry of copper-64-labeled anti-colorectal carcinoma monoclonal antibody fragments 1A3-F(ab')2. J. Nucl. Med. 1995;36(5):850–8.

21. Verel I., Visser G.W.M., Vosjan M.J.W.D., Finn R., Boellaard R., Van Dongen G.A.M.S. High-quality I-124-labelled monoclonal antibodies for use as PET scouting agents prior to I-131-radioimmunotherapy. Eur. J. Nucl. Med. Mol. Imaging. 2004;31(12):1645–52.

22. Christoforidis J.B., Carlton M.M., Knopp M. V., Hinkle G.H. PET/CT imaging of I-124-radiolabeled

bevacizumab and ranibizumab after intravitreal injection in a rabbit model. Investig. Ophthalmol. Vis. Sci. 2011;52(8):5899–903.

23. Meijs W.E., Herscheid J.D.M., Haisma H.J., Pinedo H.M. Evaluation of desferal as a bifunctional chelating agent for labeling antibodies with Zr-89. Int. J. Radiat. Appl. Instrumentation. Part. 1992;43(12):1443–7.

24. Link J.M., Krohn K.A., Eary J.F., Kishore R., Lewellen T.K., Johnson M.W., Badger C.C., Richter K.Y., Nelp W.B. Zr-89 for antibody labeling and positron emission tomography. J. Label. Compd. Radiopharm. 1986;23(10):1297–8.

25. Deri M.A., Zeglis B.M., Francesconi L.C., Lewis J.S. PET imaging with Zr-89: From radiochemistry to the clinic. Nucl. Med. Biol. 2013;40(1):3–14.

26. Radchenko V., Busse S., Rösch F. Desferrioxamine as an appropriate chelator for Nb-90: Comparison of its complexation properties for M-Df-Octreotide (M=Nb, Fe, Ga, Zr). Nucl. Med. Biol. 2014;41(9):721–7.

27. Radchenko V., Bouziotis P., Tsotakos T., Paravatou-Petsotas M., la Fuente A. de, Loudos G., Harris A.L., Xanthopoulos S., Filosofov D., Hauser H., Eisenhut M., Ponsard B., Rösch F. Labeling and preliminary in vivo assessment of niobium-labeled radioactive species: A proof-of-concept study. Nucl. Med. Biol. 2016;43(5):280–7.

28. Carrasquillo J.A., Pandit-Taskar N., O'Donoghue J.A., Humm J.L., Zanzonico P., Smith-Jones P.M., Divgi C.R., Pryma D.A., Ruan S., Kemeny N.E., Fong Y., Wong D., Jaggi J.S., Scheinberg D.A., Gonen M., Panageas K.S., Ritter G., Jungbluth A.A., Old L.J., et al. I-124-huA33 Antibody PET of Colorectal Cancer. J. Nucl. Med. 2011;52(8):1173–80.

29. O'Brien H.A.J. Overview of radionuclides useful for radioimmunoimaging/radioimmunotherapy and current status of preparing radiolabeling antibodies. Radioimmunoimaging Radioimmunother. 1983;17(4).

30. Baroncelli F., Grossi G. The complexing power of hydroxamic acids and its effect on behaviour of organic extractants in the reprocessing of irradiated fuels. J. Inorg. Nucl. Chem. 1965;27(12).

31. Verel I., Visser G.W.M., Boellaard R., Walsum Stigter-Van M., Snow G.B., Van Dongen G.A.M.S. Zr-89 Immuno-PET: Comprehensive Procedures for the Production of Zr-89-Labeled Monoclonal Antibodies. J Nucl Med. 2003;44:1271–81.

32. Jurek P., Corbett R.J. Bifunctional hydroxamix acid ligands and method of synthesis. 2008. p. 26.

33. Perk L.R., Vosjan M.J.W.D., Visser G.W.M., Budde M., Jurek P., Kiefer G.E., Van Dongen G.A.M.S. P-Isothiocyanatobenzyl-desferrioxamine: A new bifunctional chelate for facile radiolabeling of monoclonal antibodies with zirconium-89 for immuno-PET imaging. Eur. J. Nucl. Med. Mol.

Imaging. 2010;37(2):250–9.

34. Kunz H., Hartmann S., Palitzsch B. Impfung gegen Tumore? Labor&More. 2012;6:16–25.

35. Gaidzik N., Westerlind U., Kunz H. The development of synthetic antitumour vaccines from mucin glycopeptide antigens. Chem. Soc. Rev. 2013;42(10):4421–42.

36. Forrer F., Chen J., Fani M., Powell P., Lohri A., Müller-Brand J., Moldenhauer G., Mäcke H.R. In vitro characterization of Lu-177-radiolabelled chimeric anti-CD20 monoclonal antibody and a pre-liminary dosimetry study. Eur. J. Nucl. Med. Mol. Imaging. 2009;36(9):1443–52.

37. Haag R., Kratz F. Polymere Therapeutika: Konzepte und Anwendungen. Angew. Chem. 2006;118(8):1218–37.

38. Maeda H., Wu J., Sawa T., Matsumura Y., Hori K. Tumor vascular permeability and the EPR effect in macromolecular therapeutics: A review. J. Control. Release. 2000;65(1–2):271–84.

39. Holland J.P., Divilov V., Bander N.H., Smith-Jones P.M., Larson S.M., Lewis J.S. Zr-89-DFO-J591 for ImmunoPET of Prostate-Specific Membrane Antigen Expression In Vivo. J. Nucl. Med. 2010;51(8):1293–300.

40. Holland J.P., Caldas-Lopes E., Divilov V., Longo V.A., Taldone T., Zatorska D., Chiosis G., Lewis J.S. Measuring the Pharmacodynamic Effects of a Novel Hsp90 Inhibitor on HER2/neu Expression in Mice Using Zr-89-DFO-Trastuzumab. PLoS One. 2010;5(1):e8859.

41. Guy C.T., Cardiff R.D., Muller W.J. Induction of mammary tumors by expression of polyomavirus middle T oncogene: a transgenic mouse model for metastatic disease. Mol. Cell. Biol. 1992;12(3):954–61.

42. Meares C.F., McCall M.J., Reardan D.T., Goodwin D.A., Diamanti C.I., McTigue M. Conjugation of antibodies with bifunctional chelating agents: Isothiocyanate and bromoacetamide reagents, methods of analysis, and subsequent addition of metal ions. Anal. Biochem. 1984;142(1):68–78.

43. Vosjan M.J.W.D., Perk L.R., Visser G.W.M., Budde M., Jurek P., Kiefer G.E., Van Dongen G.A.M.S. Conjugation and radiolabeling of monoclonal antibodies with zirconium-89 for PET imaging using the bifunctional chelate p-isothiocyanatobenzyl- desferrioxamine. Nat. Protoc. 2010;5(4):739–743.

5. Zusammenfassung

Kinetische, thermodynamische und strukturelle Eigenschaften von Ga^{3+}- und M^{2+}-Komplexen der Chelatoren $DATA^{m}$ und $DATA^{5m}$

Die Visualisierung biologischer Prozesse auf molekularer Ebene sowie deren quantitative und qualitative Bewertung ist ein wichtiges Gebiet der molekularen Bildgebung. Als bildgebendes Verfahren gewinnt die PET auf Grund der stetig wachsenden Verfügbarkeit neuer Radiopharmaka immer größeres Interesse. Ein wichtiges Radionuklid für die PET ist ^{68}Ga ($t_{1/2}$=67,7 min, $E_{\beta,max}$=1,89 MeV), welches mittels $^{68}Ge/^{68}Ga$-Generator gewonnen werden kann. Als dreiwertiges Metall wird ^{68}Ga durch Chelatoren am Targetingvektor komplexiert. Grundlegende Voraussetzungen an den ^{68}Ga-Chelator-Komplex sind eine hohe thermodynamische als auch kinetische Stabilität.

Im Rahmen dieser Arbeit wurden die Chelatoren $DATA^{m}$ und $DATA^{5m}$ (Abbildung 1) hinsichtlich ihrer thermodynamischen, kinetischen und strukturellen Eigenschaften ihrer Ga^{3+}- und M^{2+}-Komplexe untersucht und mit dem literaturbekannten Chelator AAZTA verglichen. Hierbei wurden die Protonierungskonstanten der reinen Chelatoren als auch die Stabilitätskonstanten der [^{nat}Ga]Ga-$DATA^{m}$- und [^{nat}Ga]Ga-$DATA^{5m}$-Komplexe unter Verwendung von pH-Potentiometrie, NMR-Spektroskopie als auch UV/Vis-Spektrometrie ermittelt. Zudem wurden die Stabilitäten verschiedener divalenter Metall-Komplexe beider Chelatoren untersucht. Um eine Aussage über kinetische Stabilität, welche ein Maß für die *in vivo*-Stabilität ist, zu treffen, wurden die Halbwertszeiten für die Transchelatisierung beider Ga-Komplexe gegen Transferrin überprüft.

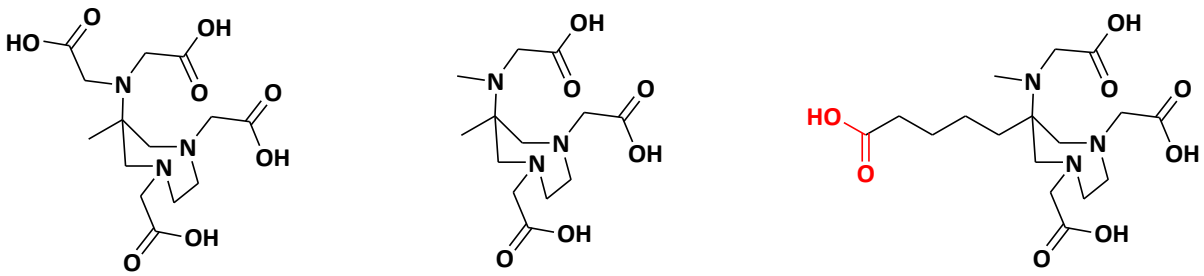

Abbildung 1: Struktur der Chelatoren AAZTA, $DATA^{m}$ und $DATA^{5m}$

Protonierungskonstanten

Die Protonierungskonstanten beider Liganden wurden pH-potentiometrisch ermittelt und sind in Tabelle 1 aufgelistet.

Tabelle 1: Protonierungskonstanten (mit jeweiliger Standardabweichung) der Chelatoren DATA^{m} und DATA^{5m} (0,15 M NaCl, 25 °C); a: $\Sigma logK_i^H$ ohne Protonierungskonstante der n-Valeriansäure, da diese nicht innerhalb der Metallbindung teilnimmt

	DATA^{m}	DATA^{5m}	AAZTA[1]
$logK_1^H$	11,27 (1)	11,39 (1)	10,06
$logK_2^H$	5,15 (2)	5,30 (2)	6,50
$logK_3^H$	3,49 (1)	4,35 (2) -COOH	3,77
$logK_4^H$	2,08 (2)	3,45 (2)	2,33
$logK_5^H$	-	2,28 (4)	1,51
$\Sigma logK_i^H$	21,99	26,77 / 22,42[a]	24,17

Stabilitätskonstanten

Die Stabilitätskonstanten der Ga-Komplexe wurden mittels pH-Potentiometrie und NMR-Spektroskopie (^{1}H/^{71}Ga) ermittelt und sind in Tabelle 2 aufgelistet.

Tabelle 2: Stabilitäts- und Protonierungskonstanten (mit jeweiliger Standardabweichung) der Ga-Komplexe von DATA^{m}, DATA^{5m} und AAZTA (0,15 M NaCl, 25 °C)

	Ga(DATA^{m})		Ga(DATA^{5m})		Ga(AAZTA)[1]
Methode	**pH-Pot.**	**^{1}H-/^{71}Ga-NMR**	**pH-Pot.**	**^{1}H-/^{71}Ga-NMR**	**pH-Pot.**
pH	12-1,7				1,7-12
$logK_{GaL}$	21.78 (2)	22.00 (4)	21.32 (2)	21.45 (5)	21.15
$logK_{GaHL}$	2.42 (2)	2.25 (9)	4.44 (3) -COOH	4.40 (4) -COOH	3.14
$logK_{GaH2L}$	-	-	2.05 (5)	-	1.14
$logK_{Ga(L)OH}$	6.25 (2)	6.38 (4)	6.31 (4)	6.25 (4)	4.60
$log\beta_{Ga(L)OH}$	15.52 (2)	15.62 (4)	15.02 (4)	15.20 (5)	16.57

Die Stabilitätskonstanten von Ga(DATA^{m}) und Ga(DATA^{5m}) sind geringfügig höher als von Ga(AAZTA). Dies ist Folge der Koordinationsgeometrie. Während beim DATA^{m} (und damit auch beim DATA^{5m}) das Ga^{3+}-Ion durch 3 Amin-Stickstoffe sowie 3 Carboxyl-Sauerstoffe in einer leicht-verzerrten Oktaedergeometrie umgeben wird [2–4], wird das Ga^{3+} beim AAZTA durch 3 Amin-Stickstoffe sowie 3 Carboxyl-Sauerstoffe (beide exozyklischen Carboxyl-Sauerstoffe und ein endozyklischer Carboxyl-Sauerstoff) in einer stärker-verzerrten und somit instabileren Geometrie umgeben [1].

Zusätzlich zu den Stabilitätskonstanten der Ga-Komplexe wurden die Stabilitätskonstanten divalenter Metall-Ionen wie Ca^{2+}, Mn^{2+}, Zn^{2+} und Cu^{2+} untersucht. Eine besonders hohe Stabilität wiesen hierbei die Zn- und Cu-Komplex für DATA^{m} und DATA^{5m} auf (Tabelle 3).

Tabelle 3: Stabilitätskonstanten (mit jeweiliger Standardabweichung) der $DATA^{m}$-, $DATA^{5m}$- und AAZTA-Komplexe mit Ca^{2+}, Mn^{2+}, Zn^{2+} und Cu^{2+} (0,15 M NaCl, 25 °C)

	$DATA^{m}$	**$DATA^{5m}$**	**AAZTA**[5]
CaL	8,7 (2)	9,09 (2)	11.75 (1)
MnL	11,43[1]	11,63 (2)	14,19[1]
ZnL	16,54 (2)	16,91 (2)	16,02 (1)
CuL	18,36 (4)	18,97 (2)	20,60 (4)

Kinetik

Um die kinetische Inertheit des Ga-Komplexes zu analysieren, wurden die Halbwertszeiten für die Transchelatisierung beider Komplexe gegen apo-Transferrin unter physiologischen Bedingungen (pH 7,4) überprüft. Der Ga($DATA^{5m}$)-Komplex zeigte hierbei die höchste kinetische Stabilität mit einer Halbwertszeit von 46 h (Tabelle 4).

Tabelle 4: Ratenkonstante (k_d) und Halbwertszeit $t_{1/2}$ der Transchelatisierungsreaktion der Komplexe Ga($DATA^{m}$), Ga($DATA^{5m}$) und Ga(AAZTA) mit Transferrin (0,15 M NaCl, 25 °C, pH=7,4)

	Ga($DATA^{m}$)	**Ga($DATA^{5m}$)**	**Ga(AAZTA)**[5]
k_d / s^{-1}	$(21\pm0,1)\cdot10^{-6}$	$(4,2\pm0,2)\cdot10^{-6}$	$8,0\cdot10^{-6}$
$t_{1/2}$ / h	9,4	46	24

Die Ergebnisse zeigten insgesamt, dass das $DATA^{5m}$ eine hohe thermodynamische Stabilität mit einem $logK_{GaL}$ von 22,0 mit einer hohen kinetischen Stabilität verbindet. Außerdem besitzt das $DATA^{5m}$ eine hohe Komplexstabilität mit dem divalenten Metallion Cu^{2+}, wodurch es durchaus möglich scheint, das Anwendungsspektrum des Chelators auf ^{64}Cu auszuweiten.

In vitro-Evaluierung von [^{nat}Ga]Ga-DATA-TOC sowie erste präklinische und klinische Studien von [^{67}Ga]/[^{68}Ga]Ga-DATA-TOC

^{68}Ga-Radiopharmaka für die molekulare Bildgebung mittels PET haben durch den klinischen Erfolg des [^{68}Ga]Ga-DOTA-TOC und [^{68}Ga]Ga-DOTA-TATE sowie der Entwicklung klinisch zugelassener ^{68}Ge/^{68}Ga-Generatoren einen großen Stellenwert in der onkologischen Radiopharmazie erhalten [6–10]. Die Entwicklung neuer bifunktioneller Chelatorsysteme für das Gallium hat in den letzten Dekaden ein breites Spektrum (makro)zyklischer und azyklischer Liganden hervorgebracht [11]. Einer dieser Vertreter basiert auf dem 6-Amino-1,4-diazapine-triacetat-Gerüst (DATA) und bietet eine Radiomarkierung von ^{68}Ga unter milden Bedingungen (pH 4-5, RT, 10 min) [12]. Die Synthese des bifunktionellen DATA^{5m} eröffnete die Ankopplung an den N-Terminus des Peptids TOC (DATA-TOC). Dieses wurden in einer ersten *proof-of-concept*-Studie unter den gleichen Bedingungen wie auch der reine Chelator mit ^{68}Ga markiert [13].

In vivo-Studien

Basierend auf diesen Grundlagen wurde in der folgenden Arbeit das Affinitätsprofil des [^{nat}Ga]Ga-DATA-TOC gegenüber den humanen Somatostatinrezeptoren (hsstr) 2, 3 und 5 untersucht und mit [^{nat}Ga]Ga-DOTA-TOC verglichen. Mit einem IC_{50}-Wert von 1,03 nM gegenüber dem hsstr 2, welcher vor allem in neuroendokrinen Tumorgewebe überexprimiert vorliegt [14], weist das [^{nat}Ga]Ga-DATA-TOC eine Affinität ähnlich des [^{nat}Ga]Ga-DOTA-TOC auf (IC_{50}(hsstr 2) = 0,21 nM; Abbildung 2).

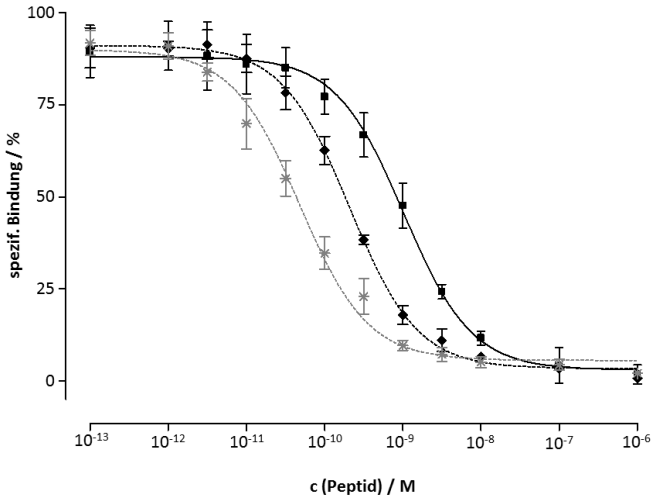

Abbildung 2: IC_{50}-Bestimmung von [^{nat}Ga]Ga-DATA-TOC (■, IC_{50}=1,03±0,08 nM), [^{nat}Ga]Ga-DOTA-TOC (◆, IC_{50}=0,21 ±0,01 nM) und [LTT]SS28 (✳,IC_{50}=0,09±0,01 nM) gegenüber hsst 2-Rezeptoren in HEK293-Zellmembranen

In vivo-/ex vivo-Studien

Des Weiteren wurden [^{67}Ga]/[^{68}Ga]Ga-DATA-TOC innerhalb von präklinischen *in vivo*- und *ex* vivo-Studien an gesunden als auch tumortragenden Tieren durchgeführt.

Für erste PET-Aufnahmen wurden [^{68}Ga]Ga-DATA-TOC als auch [^{68}Ga]Ga-DOTA-TOC in tumortragende Mäuse (MPC-mCherry, NMRI nu/nu) appliziert (Abbildung 3, B und C). Um die Spezifizität darzustellen, wurden beide Verbindungen zusätzlich mit [NaI^{3}]Octreotid koinjiziert (Abbildung 3, A und D).

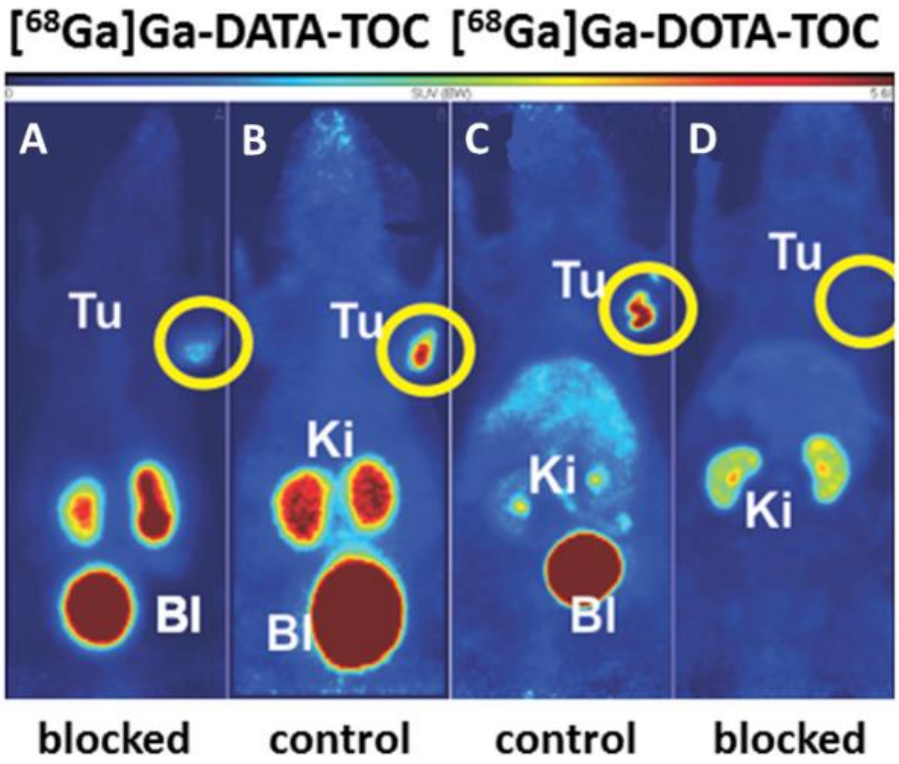

Abbildung 3: PET-Aufnahme von [^{68}Ga]Ga-DATA-TOC (A, B) und [^{68}Ga]Ga-DOTA-TOC (C, D) nach 90 min p.i.; für die Blockingexperimente wurden beide Verbindungen mit 100 µg [NaI^{3}]Octreotid koinjiziert; Tu: Tumor, Ki: Nieren, Bl: Blase

Beide Verbindungen zeigten eine deutliche Anreicherung im Zielgewebe sowie eine exklusive renale Exkretion. Durch Koninjektion des [NaI^{3}]Octreotid konnte eine deutliche Akkumulationsverringerung erzielt werden, was auf die Spezifizität beider Derivate gegenüber Somatostatinrezeptoren darlegt. Innerhalb von *in vivo*-Vergleichsstudien zwischen [^{67}Ga]Ga-DOTA-TOC und [^{67}Ga]Ga-DATA-TOC an verschiedenen Tumormodellen (AR42J und HEK293-hsst2) wurde gezeigt, dass [^{67}Ga]Ga-DATA-TOC als auch [^{67}Ga]Ga-DOTA-TOC spezifisch binden. Die Spezifizität des [^{67}Ga]Ga-DATA-TOC wurde auch hier durch die Koinjektion des Octreotids TATE durch die verringerte Tumorakkumulation nachgewiesen (Abbildung 4).

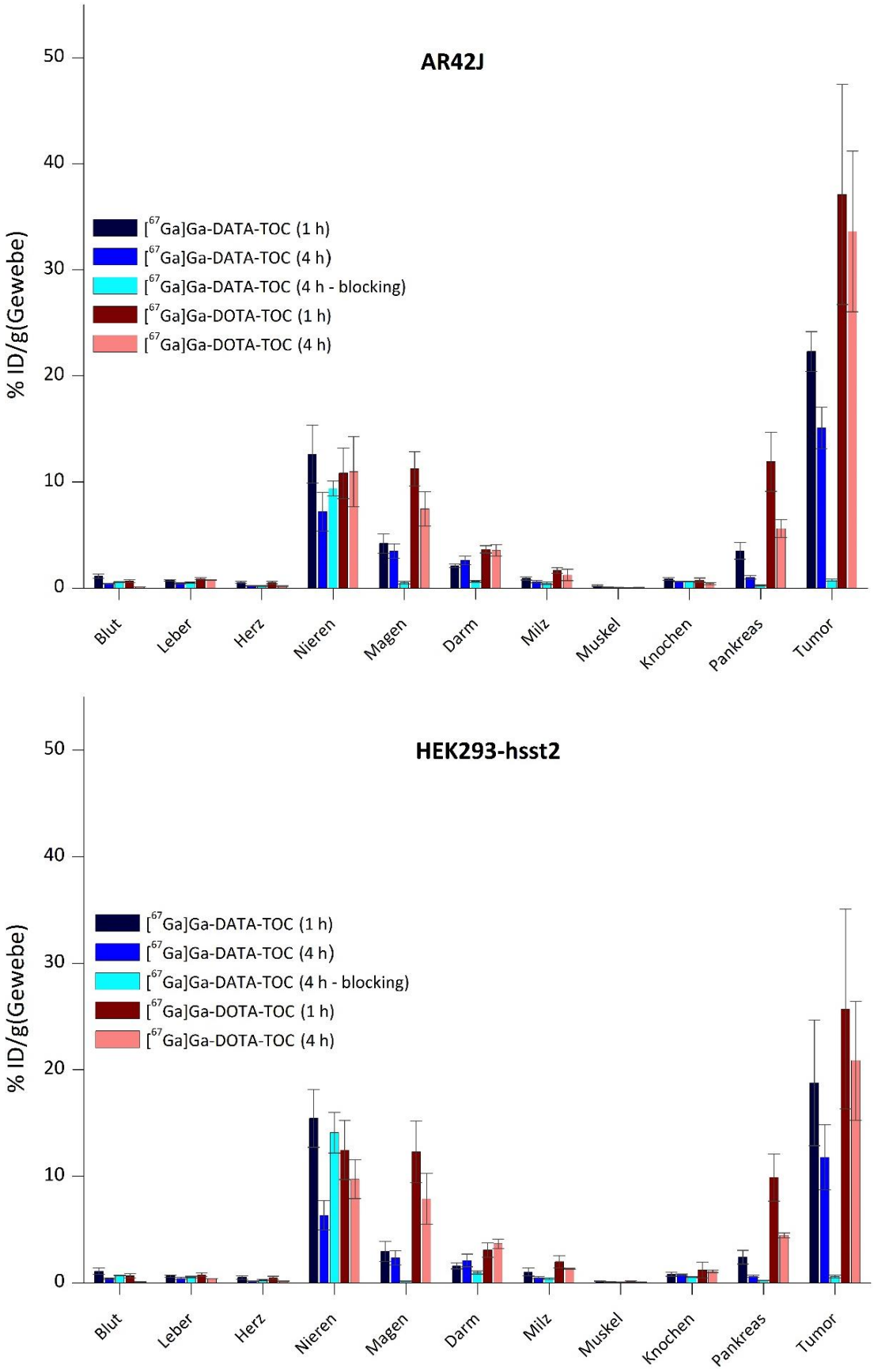

Abbildung 4: *ex vivo*-Biodistribution [^{67}Ga]Ga-DOTA-TOC und [^{67}Ga]Ga-DATA-TOC in AR42J-tumor-tragenden SCID-Mäusen (oben) und HEK293-hsst2-tumor-tragenden SCID-Mäusen (unten) nach 1 und 4 h p.i.

Das [^{67}Ga]Ga-DOTA-TOC reichert sich stärker im Zielgewebe an, jedoch erzielt das [^{67}Ga]Ga-DATA-TOC einen höheren Kontrast zwischen tumorösen und gesunden Gewebe. Dieser Effekt ist vor allem für eine klare Visualisierung neuroendokriner Tumore (wie z. B. Pankreaskrebs) von entscheidendem Vorteil.

Erste klinische Studien sowohl mit [^{68}Ga]Ga-DATA-TOC als auch mit [^{68}Ga]Ga-DOTA-TOC an einem Patienten (46 Jahre, differenzierbare neuroendokrine Tumore im Pankreas) zeigten in PET/CT-Aufnahmen, dass das [^{68}Ga]Ga-DATA-TOC auch hier zwar eine geringere Anreicherung im Tumorgewebe aufwies (SUV([^{68}Ga]Ga-DATA-TOC)=46,9; SUV([^{68}Ga]Ga-DOTA-TOC)=71,1), jedoch auf Grund der geringeren Aufnahme in er Leber einen besseren Kontrast (Tabelle 5) und damit eine bessere Differenzierung zwischen gesundem und tumorösem Gewebe bietet (Abbildung 5).

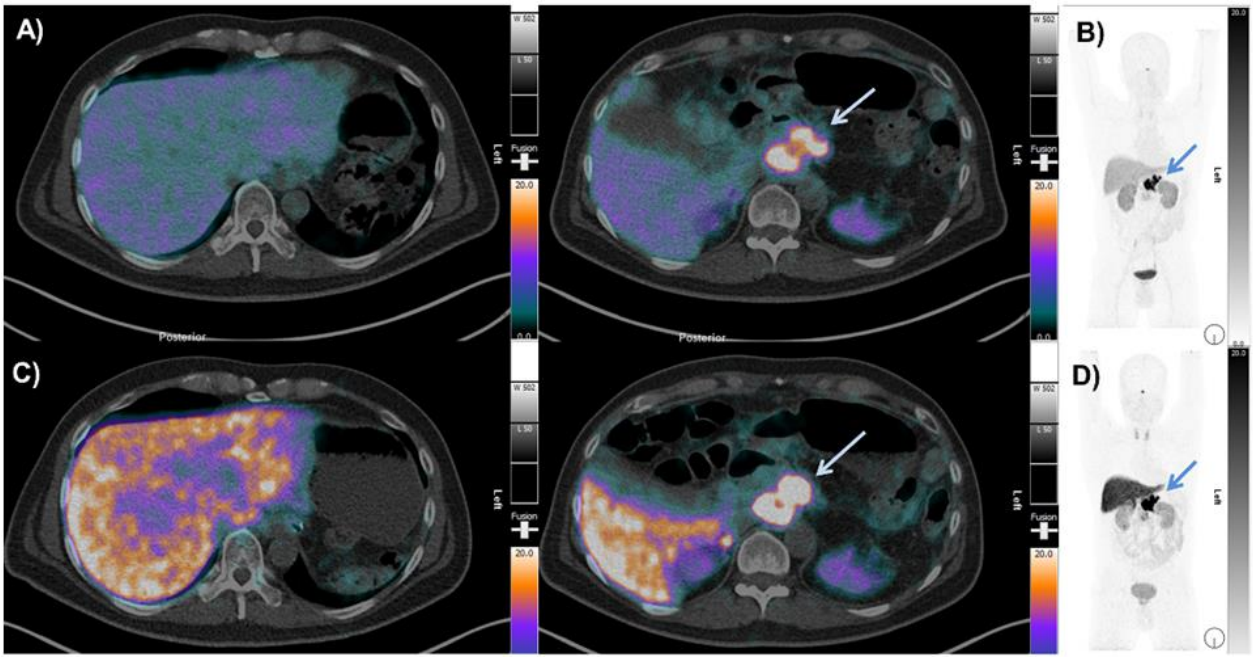

Abbildung 5: PET/CT-Aufnahmen des [^{68}Ga]Ga-DATA-TOC (A: transversale PET/CT-Fusion; B: PET-MIP) und [^{68}Ga]Ga-DATA-TOC (C: transversale PET/CT-Fusion; D: PET-MIP); die Pfeile weisen auf den neuroendokrinen Tumor im Pankreas hin

Tabelle 5: Vergleich der SUV-Werte zwischen [^{68}Ga]Ga-DATA-TOC und [^{68}Ga]Ga-DOTA-TOC in einem 46 Jahre alten, männlichen Patienten mit wohl differenzierten neuroendokrinen Tumoren im Pankreas

Gewebe	SUV	
	[^{68}Ga]Ga-DATA-TOC	[^{68}Ga]Ga -DOTA-TOC
Tumor	46,9	71,1
Leber	9,11	23,09
Verhältnis (Tumor-zu-Leber)	5,15	3,08
Hypophyse	14,57	23,69
Verhältnis (Tumor-zu-Hypophyse)	3,22	3,00

Weitere klinische Vergleichsstudien zwischen [^{68}Ga]Ga-DOTA-TOC und [^{68}Ga]Ga-DATA-TOC von Schmidt-Kreppel *et al.* zeigen eine klare Anreicherung des [^{68}Ga]Ga-DATA-TOC in Lebermetastasen (Abbildung 6) [15]. Auch hier bietet das [^{68}Ga]Ga-DATA-TOC einen höheren Kontrast trotz geringerer Aufnahmewerte im Tumorgewebe.

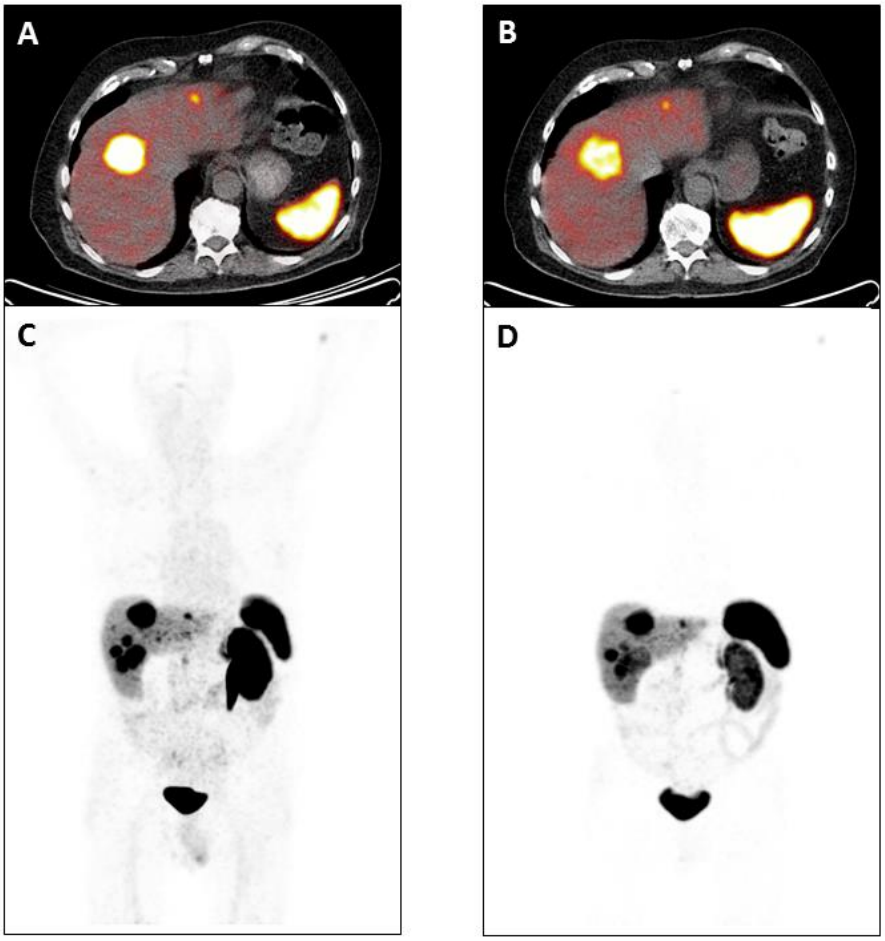

Abbildung 6: PET/CT-Aufnahmen des [^{68}Ga]Ga-DATA-TOC (A: transversale PET/CT-Fusion; C: PET-MIP) und [^{68}Ga]Ga-DATA-TOC (B: transversale PET/CT-Fusion; D: PET-MIP); Patient besaß nur eine Niere

Diese Studien konnten zeigen, das [^{nat}Ga]Ga-DATA-TOC eine hohe Affinität gegenüber hsst2-Rezeptoren mit einem IC_{50}-Wert im nanomolaren Bereich besitzt. Das [^{67}Ga]/[^{68}Ga]Ga-DATA-TOC wies in ersten präklinischen *in vivo*-Studien eine hohe Spezifizität gegenüber Tumorgewebe auf und ermöglichte im Tumormausmodell als auch am Patienten eine kontrastreiche Bildgebung, welche eine klare Differenzierung zwischen gesundem und tumorösen Gewebe ermöglicht.

Synthese und Radiomarkierung bifunktioneller DATA-Derivate mit ^{68}Ga für die Kopplung an Targetingvektoren unter milden Bedingungen

Bifunktionelle Chelatoren sind ein wichtiger Bestandteil von Radiopharmaka für die Komplexierung von Radiometallen wie dem Positronenemitter ^{68}Ga. Basierend auf dem neuartigen, bifunktionellen DATA^{5m} wurden drei Derivate synthetisiert (DATA^{5m}-Bz-NCS (**A**), DATA^{5m}-en-QS (**B**), DATA^{5m}-TEG-N_3 (**C**)), welche die Kopplung an Targetingvektoren unter milden Bedingungen ermöglichen sollen (Abbildung 7). Die Radiomarkierungen der Derivate **A**, **B** und **C** mit ^{68}Ga wurden bei Raumtemperatur durchgeführt und hinsichtlich verschiedener Variablen (pH, Puffersystem, Vorläufermenge) evaluiert. Als *proof-of-concept* wurde das Derivat **B** mit dem Bisphosphonat Pamidronat gekoppelt. Das gebildete Derivat **D** wurde bei erhöhten Temperaturen unter Variation der gleichen Parameter untersucht.

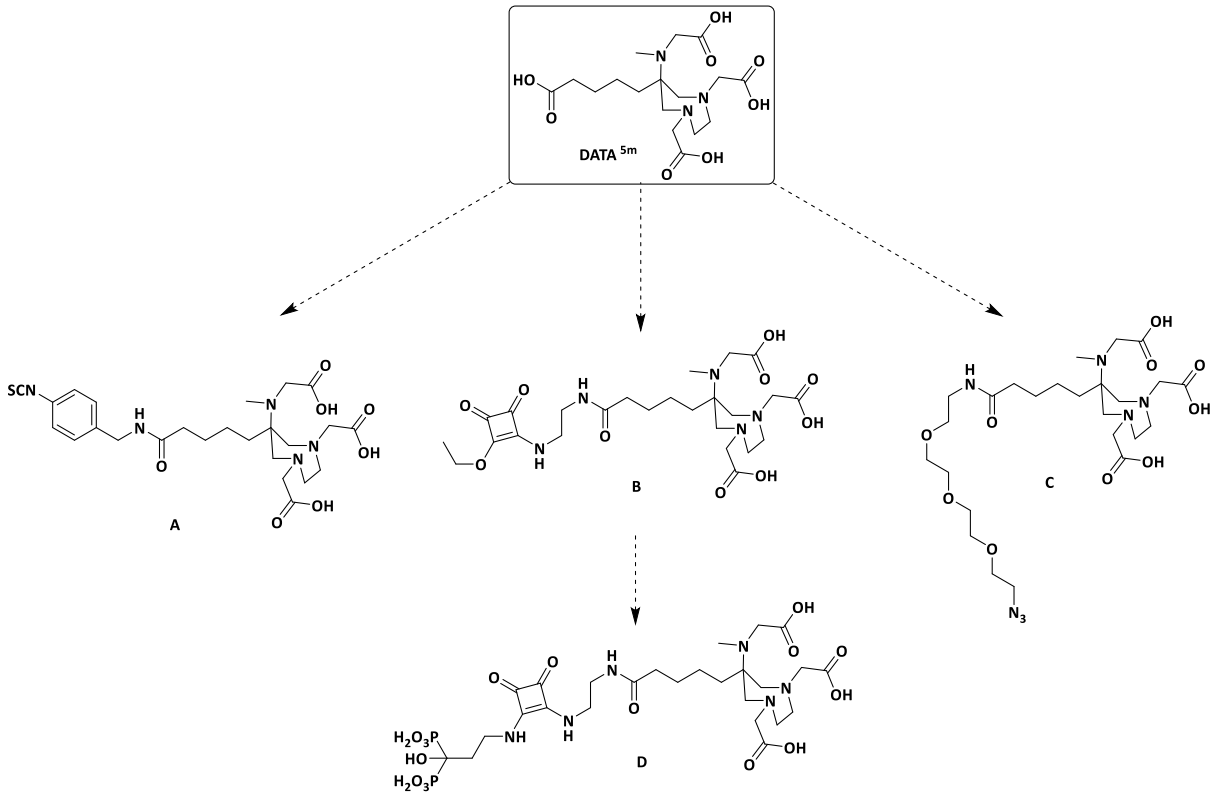

Abbildung 7: Struktur des DATA^{5m} und dessen Derivate: DATA^{5m}-Bz-NCS (**A**), DATA^{5m}-en-QS (**B**), DATA^{5m}-TEG-N_3 (**C**) und DATA^{5m}-en-SA-PAM (**D**)

Radiomarkierungen

A, **B** und **C** lieferten quantitative radiochemische Ausbeuten (>95 %) in den Puffern Natriumacetat (NaOAc), Ammoniumacetet (AmOAc) und *N*-2-hydroxyethylpiperazin-*N'*-2-ethansulfonsäure (HEPES) bei einer Konzentration von 2,5 µM und einem pH-Wertebereich zwischen 4,3 und 5,5. **B** und **C** zeigten hierbei eine sehr schnelle Markierungskinetik selbst bei geringen Vorläufermenge von 1 µM (Tabelle 6).

Tabelle 6: Radiomarkierungsausbeuten (in %) der Derivate **A**, **B** und **C** unter Verwendung verschiedener Puffer und Vorläufermengen nach 10 min bei 25 °C (n=3; A(^{68}Ga)=20-25 MBq)

	NaOAc (0,25 M, pH 4,5)			AmOAc (0,25 M, pH 5,5)			HEPES (0,025 M, pH 4,3)		
µM	**[^{68}Ga]Ga-A**	**[^{68}Ga]Ga-B**	**[^{68}Ga]Ga-C**	**[^{68}Ga]Ga-A**	**[^{68}Ga]Ga-B**	**[^{68}Ga]Ga-C**	**[^{68}Ga]Ga-A**	**[^{68}Ga]Ga-B**	**[^{68}Ga]Ga-C**
1	10,8 ± 8,0	78,9 ± 13,0	98,8 ± 0,3	55,0 ± 12,4	84,4 ± 1,9	96,7 ± 0,8	27,6 ± 1,1	95,9 ± 1,0	90,8 ± 1,8
2,5	96,8 ± 0,4	96,0 ± 1,2	99,4 ± 0,0	94,7 ± 1,0	97,7 ± 1,0	97,8 ± 0,6	93,7 ± 5,3	95,5 ± 1,2	99,2 ± 0,2
5	99,3 ± 0,1	97,2 ± 0,7	99,5 ± 0,0	94,5 ± 0,8	96,7 ± 0,5	97,6 ± 2,5	98,0 ± 0,2	97,4 ±0,8	99,4 ± 0,1
10	98,6 ± 0,2	98,3 ± 0,6	99,5 ± 0,1	99,8 ± 0,1	99,1 ± 0,3	99,8 ± 0,0	99,2 ± 0,0	99,7 ±0,1	99,5 ± 0,0

Derivat **D** wurde bei 90 °C mit ^{68}Ga markiert und wies, je nach verwendetem Puffer, ab 2,5 µM radiochemische Ausbeuten über 95 % auf (Tabelle 7).

Tabelle 7: Radiomarkierungsausbeuten (in %) des Derivats **D** unter Verwendung verschiedener Puffer und Vorläufermengen nach 10 min bei 90 °C (n=3; A(^{68}Ga)=20-25 MBq)

nmol	NaOAc (25 mM, pH 4,5)	AmOAc (25 mM, pH 5,5)	HEPES (0,025 M, pH 4,3)
1	0,0 ± 0,0	49,2 ± 3,2	55,5 ± 7,1
2,5	40,2 ± 1,5	69,1 ± 5,0	98,6 ± 0,1
5	97,6 ± 0,2	97,7 ± 0,6	97,1 ± 1,5
10	99,2 ± 0,1	98,4 ± 0,8	96,8 ± 1,0

in vitro-Stabilitäten

Ein wichtiges Kriterium für die *in vivo*-Anwendung von Chelat-Komplexen ist die Stabilität von gegenüber humanem Serum. Die 4 Ga-Komplexe wurden deshalb hinsichtlich ihrer *in vitro*-Stabilität in verschiedenen Medien untersucht (Tabelle 8). Alle Komplexe waren über den Zeitraum von 2 h mit über 99 % vollständig stabil. Transchelatisierungsversuche gegen DTPA und EDTA zeigten trotz des hohen Überschusses der kompetitiven Chelatoren weiterhin einen hohen Anteil intakter Ga-Komplexe. Zudem besaßen drei Ga-Komplexe eine Serumstabilität von 98 % nach 2 h bei 37 °C.

Tabelle 8: Stabilität von [^{68}Ga]Ga-**A**, [^{68}Ga]Ga-**B**, [^{68}Ga]Ga-**C u**nd [^{68}Ga]Ga-**D** (in % intakter Komplex) in humanem Serum (HS), DTPA, EDTA und PBS nach 1 h und 2 h bei 37 °C

	t / h	HS	DPTA	EDTA	PBS
[^{68}Ga]Ga-A	**1**	92,0 ± 0,3	89,8 ± 0,3	88,2 ± 0,7	99,8 ± 0,1
	2	88,1 ± 0,5	86,0 ± 0,5	78,1 ± 0,5	99,7 ± 0,0
[^{68}Ga]Ga-B	**1**	99,9 ± 0,0	93,3 ± 0,8	92,7 ± 0,4	99,8 ± 0,1
	2	99,0 ± 0,3	81,4 ± 0,9	81,5 ± 0,7	99,8 ± 0,0
[^{68}Ga]Ga-C	**1**	99,8 ± 0,0	99,8 ± 0,1	98,4 ± 0,4	99,9 ± 0,0
	2	99,6 ± 0,1	99,5 ± 0,1	95,2 ± 0,4	99,8 ± 0,0
[^{68}Ga]Ga-D	**1**	98,4 ± 0,1	98,7 ± 0,2	98,8 ± 0,2	99,7 ± 0,0
	2	97,7 ± 0,6	98,0 ± 1,1	98,2 ± 0,8	99,6 ± 0,0

Zusammenfassend kann festgehalten werden, dass insbesondere die Kombination aus den Derivaten **B**, **C** und **D** und dem Puffer HEPES hohe radiochemische Ausbeute bei Raumtemperatur von über 95 %

unter Einsatz von weniger als 5 µM Vorläufermenge lieferte. Die *in vitro*-Studien zeigten eine hohe kinetische Stabilität der Ga-Komplexe von **B**, **C** und **D.** Zudem konnte als *proof-of-concept*-Modell ein Targetingvektor am Derivat **B** unter milden Bedingungen (pH 9, RT) angekoppelt werden. Mit Hilfe dieser Derivate kann die Anwendung des DATA-Chelators auf ein weites Spektrum verschiedener Targetingvektoren ausgeweitet werden. Die schnelle und einfache Markierungsmethode bei Raumtemperatur, ähnlich zur kit-type-Markierung von ^{99m}Tc [16,17], eröffnet zudem den Einsatz ^{68}Ga-Radiopharmaka in der klinischen Anwendung.

Synthese und Radiomarkierung bifunktioneller AAZTA-Derivate mit ^{177}Lu für die Kopplung an Targetingvektoren unter milden Bedingungen

Bifunktionelle Chelatoren haben in den letzten Dekaden eine wichtige Rolle innerhalb der Peptidvermittelten Radiorezeptortherapie (*engl.:* peptide receptor radionuclide therapy, PRRT) eingenommen [19–20]. Neben den Nuklide wie ^{90}Y, ^{153}Sm und ^{188}Re hat ^{177}Lu ($t_{1/2}$=6.71 d; $E_{\beta,max}$=0.49 MeV) einen großen Stellenwert in diesem Bereich [21–26]. Seine niederenergetischen β^--Partikel (176 keV (12.2 %), 385 keV (9.1 %) and 498 keV (78.6 %)), die niederenergetischen Gammaphotonen (113 keV, 208 keV) und vor allem die hohen Produktionsausbeuten von trägerfreiem ^{177}Lu machen es zu einem attraktiven Nuklide für den therapeutischen Einsatz.

Ein potentieller Kandidat für eine Komplexierung des ^{177}Lu ist der heptadentale Chelator AAZTA, welcher eine Komplexstabilitätskonstante von 21,85 aufweist [27]. Als *stand-alone*-System besitzt dieser jedoch nicht die Option für die Kopplung an Targetingvektoren (TV). Bisherige bifunktionelle Systeme des AAZTAs fanden ihr Anwendungsfeld für die Komplexierung von Metalle wie Gd, ^{68}Ga oder ^{44}Sc [28–33]. Die in dieser Studie entwickelten AAZTA^5-Derivate AAZTA^5-Bz-NCS (**A**), AAZTA^5-en-QS (**B**) und AAZTA^5-TEG-N_3 (**C**), welche sich für Kopplung an TVs unter milden Bedingungen eignen (Abbildung 8), wurden mit ^{177}Lu hinsichtlich verschiedener Variablen (pH, Puffersystem, Chelator-zu-Lu-Verhältnis) radiomarkiert.

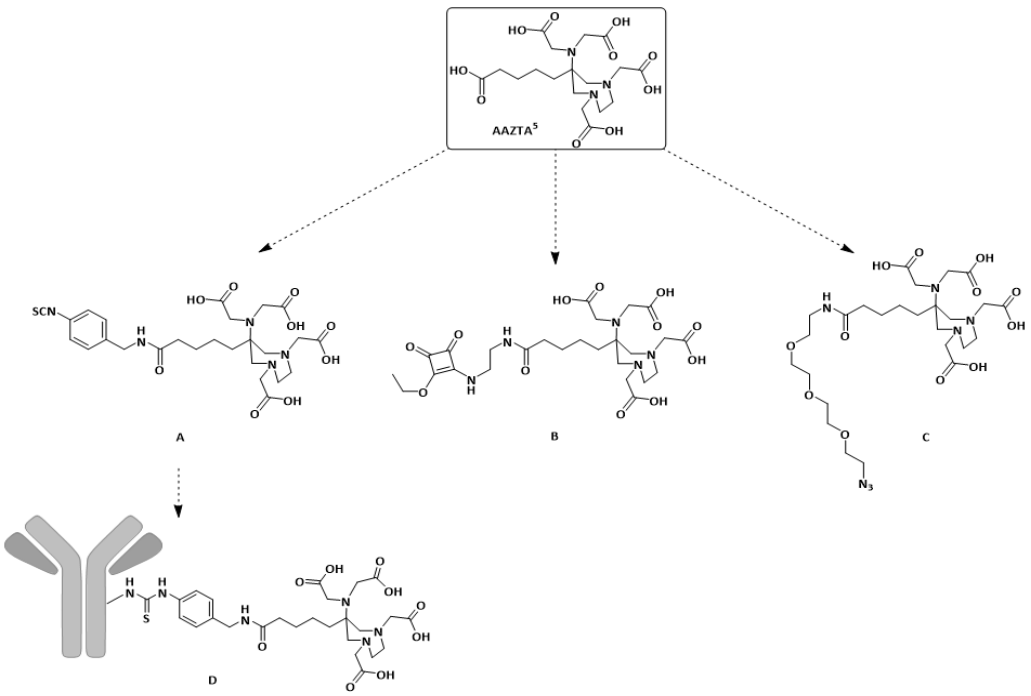

Abbildung 8: Struktur des AAZTA^5 und dessen Derivate: AAZTA^5-Bz-NCS (**A**), AAZTA^5-en-QS (**B**), AAZTA^5-TEG-N_3 (**C**) und AAZTA^5-Bz-NCS-mAb (**D**)

Als *proof-of-concept* wurde der Ligand **A** mit einem monoklonalen Antikörper (mAk) (Abbildung 7, **D**) gekoppelt und mit ^{177}Lu markiert.

Radiomarkierungen

Die Liganden **A**, **B** und **C** lieferten in Abhängigkeit vom Puffersystem und dem Chelator-zu-Lutetium-Verhältnis quantitative radiochemische Ausbeuten (>95 %) bei Raumtemperatur nach 10 min (Tabelle 9).

Tabelle 9: Radiomarkierungsausbeuten (in %) der Derivative **A**, **B** and **C** unter Verwendung verschiedener Puffer und Vorläufermengen nach 10 min bei 25 °C (n=3; A(^{177}Lu)=30-50 MBq)

	NaOAc (0,25 M, pH 4,5)			AmOAc (0,25 M, pH 5,5)			HEPES (0,025 mM, pH 4,3)		
ligand-to-Lu	**A**	**B**	**C**	**A**	**B**	**C**	**A**	**B**	**C**
1:1	20,7 ± 1,1	17,7 ± 1,2	35,1 ± 0,6	<5 %	<5 %	<5 %	38,2 ± 0,1	39,8 ± 5,9	40,7 ± 6,2
2:1	62,5 ± 5,9	74,9 ± 3,8	91,8 ± 3,3	7,0 ± 0,3	8,5 ± 1,1	21,5 ± 4,3	96,1 ± 2,7	98,5 ± 0,0	98,0 ± 0,6
5:1	87,0 ± 3,3	96,7 ± 3,2	98,8 ± 0,2	81,6 ± 4,9	52,6 ± 6,2	86,9 ± 1,2	97,0 ± 0,4	96,1 ± 0,8	98,2 ± 0,2
10:1	94,1 ± 2,0	98,1 ± 0,3	98,7 ± 0,6	94,1 ± 0,2	98,0 ± 1,3	97,9 ± 0,2	98,7 ± 0,3	98,2 ± 0,7	99,0 ± 0,1
15:1	95,6 ± 0,7	98,4 ± 0,3	98,0 ± 0,6	97,3 ± 1,8	97,3 ± 0,3	99,0 ± 0,1	98,2 ± 0,3	96,8 ± 0,4	99,2 ± 0,3

Bei einem Chelator-zu-Lutetium-Verhältnis von 15:1 liefern die Derivate in jedem Puffersystem quantitative Ausbeuten von über 95 %. Bei einem Verhältnis von 10:1 erreichte **A** in Natriumacetat (NaOAc) und Ammoniumacetat (AmOAc) noch Ausbeuten unter 95 %. Dieser Trend setzte sich für die Puffer mit sinkendem Verhältnis zwischen Chelator und Lutetium fort. Interessanterweise wurden quantitative Ausbeuten selbst mit einem Verhältnis von 2:1 mit allen Liganden im HEPES-Puffer ermittelt. Derivat **D** wurde unter milden Bedingungen über einen Zeitraum von 60 min mit ^{177}Lu markiert (Tabelle 10).

Tabelle 10: Radiomarkierungsausbeuten (in %) des Derivativs **D** in HEPES-Puffer bei 25 °C (n=3; A(^{177}Lu)=50 MBq)

	t / min	**Ausbeute / %**
[^{177}Lu]Lu-D	15	63,7 ± 3,0
	30	69,3 ± 4,4
	45	70,4 ± 4,3
	60	72,7 ± 3,5

D zeigte eine schnelle Markierung mit über 60 % radiochemischer Ausbeute nach 15 min, welche auf 73 % nach 60 min anstieg.

In vitro-Stabilitäten

Alle Lu-Komplexe wurden hinsichtlich ihrer *in vitro*-Stabilität in verschiedenen Medien bei 37 °C untersucht (Tabelle 11 und 12). Ein wichtiges Kriterium für die *in vivo*-Anwendung von Chelat-Komplexen ist die Stabilität von gegenüber humanem Serum. Die Lu-Komplexe von **B** und **C** wiesen eine Serumstabilität von über 90 % nach 24 h auf. Eine mögliche Begründung der partiellen Instabilität von [^{177}Lu]Lu-**A** sowie dem Antikörperkonjugat von **A** liegt in der NCS-Bz-Einheit und seinem negative induktiven Effekt.

Tabelle 11: Stabilität von [^{177}Lu]Lu-**A**, [^{177}Lu]Lu-**B** und [^{177}Lu]Lu-**C** (in % intakter Komplex) in humanem Serum (HS), DTPA, EDTA und PBS nach 1 h, 2 h und 24 h bei 37 °C

	t / h	HS	DPTA	EDTA	PBS
[^{177}Lu]Lu-A	**1**	89,6 ± 0,8	98,5 ± 0,2	98,8 ± 0,2	98,8 ± 0,1
	2	89,1 ± 0,4	98,2 ± 0,1	98,3 ± 0,2	98,8 ± 0,1
	24	50,8 ± 1,0	80,8 ± 1,2	82,7 ± 3,5	98,7 ± 0,1
[^{177}Lu]Lu-B	**1**	99,8 ± 0,0	99,8 ± 0,0	99,9 ± 0,0	98,7 ± 0,3
	2	99,9 ± 0,0	99,7 ± 0,0	99,8 ± 0,0	98,6 ± 0,2
	24	91,3 ± 1,1	94,0 ± 0,2	92,7 ± 0,1	98,5 ± 0,1
[^{177}Lu]Lu-C	**1**	99,9 ± 0,0	99,8 ± 0,0	99,8 ± 0,0	98,8 ± 0,1
	2	99,8 ± 0,0	99,9 ± 0,0	99,9 ± 0,0	98,8 ± 0,1
	24	97,8 ± 0,5	92,4 ± 0,4	91,8 ± 0,2	98,7 ± 0,2

Tabelle 12: Stabilität von [^{177}Lu]Lu-**D** (in % intakter Komplex) in humanem Serum (HS) und PBS nach 1 h, 2 h, 24 h und 168 h bei 37 °C

	t / h	HS	PBS
[^{177}Lu]Lu-D	**1**	43,0 ± 10,0	92,8 ± 1,0
	2	31,6 ± 3,7	90,9 ± 0,7
	24	29,9 ± 2,4	89,5 ± 1,6
	168	31,8 ± 6,8	91,0 ± 1,9

Die Studie konnte zeigen, dass die Liganden **B** und **C** in den Puffersystemen NaOAc und vor allem HEPES stabile und hohe radiochemische Ausbeuten von über 95 % bei einem Verhältnis von 5:1 oder niedriger erzielen konnten. Hinsichtlich der *in vitro*-Stabilität wiesen die Lu-Komplexe von **B** und **C** die höchste Stabilität auf, sodass das Anwendungsgebiet für *in vivo*-Studien auf diese beiden Liganden konzentriert werden sollte. Durch diese neuen Derivate und ihrer Kopplungseinheiten ist es möglich das AAZTA unter milden Bedingungen an Targetingvektoren wie Peptide, Bisphosphonate, Antikörper oder Polymere und Nanopartikel kovalent anzubinden. Die einfache und schnelle Radiomarkierung mit ^{177}Lu bei Raumtemperatur bietet zudem eine instant-kit Synthesemethode von ^{177}Lu-Radiopharmaka.

Radiomarkierung, *in vitro*- und *in vivo*-Evaluierung eines neuartigen Antikörpers für die ImmunoPET mit ^{89}Zr

Monoklonale Antikörper (mAk) stellen durch ihre hohe Spezifizität und Affinität einen attraktiven Targetingvektor für Krebstherapie und Wirkstofftransporter [34]. Mit der Einführung antikörper-basierter Systeme für die molekulare Bildgebung mittels Positronenemissionstomographie (PET) oder Einzelphotonenemissionstomographie (SPECT) [35–37] mussten zunächst die *in vivo*-Eigenschaften dieser Systeme untersucht wurden. Auf Grund der langsamen Pharmakokinetik von Antikörpern von mehreren Tagen müssen radiomarkierte Antikörperkonjugate 2 entscheidende Kriterien erfüllen: eine hohe *in vivo*-Stabilität des radiomarkierten Konjugats sowie ein Radionuklid mit einer zur Pharmakokinetik passenden Halbwertszeit. Neben den Radionukliden ^{64}Cu, ^{86}Y und ^{124}I für PET bzw. ^{67}Ga und ^{111}In für SPECT, hat das ^{89}Zr ($t_{1/2}$=3,27 d) in den letzten Jahren an wachsender Beachtung für die ImmunoPET gewonnen [38]. Ein wichtiger bifunktioneller Chelator für die Markierung von ^{89}Zr ist *p*-Isothiocyanatobenzyl-desferrioxamin (Df-Bz-NCS).

In der vorliegenden Arbeit wurde das Radiokonjugat des neuartiger Antikörpers (GGSK-1/30) [39–45], welcher eine hohe Spezifizität gegenüber Tumor-assoziiertem Mucin1 (TA-MUC1) aufweist, hinsichtlich seiner *in vitro*- und *in vivo*-Eigenschaften untersucht.

Kopplung und Radiomarkierung

Zunächst wurde der Antikörper mit Df-Bz-NCS gekoppelt (Abbildung 9), bezüglich seiner Immunoreaktivität untersucht und mit ^{89}Zr markiert.

Das Antikörper-Chelator-Konjugat (Df-Bz-NCS-mAk) wies mit 4,2 Chelator-Einheiten pro Antikörper eine Bindung an Brustkrebszellen (T47D) von über 95 % auf, was auf eine unveränderte Immunoreaktivität hindeutete. [^{89}Zr]Zr-Df-Bz-NCS-mAk demonstrierte eine Stabilität von über 90 % nach 3 d in humanem Serum als auch isotonischer Kochsalzlösung (0,9 %), womit das Konjugate als geeignet für *in vivo*-Anwendungen betrachtet werden konnte.

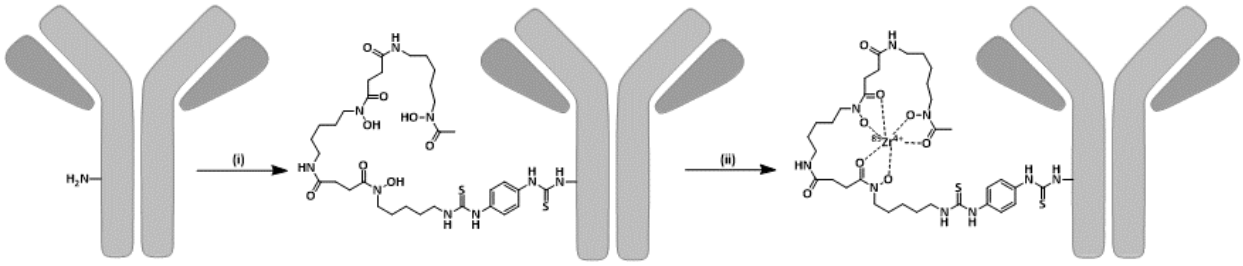

Abbildung 9: Allgemeine Kopplungsmethode von Df-Bz-NCS an Antikörper: (i) pH=9,0, 37 °C, 30 min, Gelfiltration, (ii) pH=7,0, 25 °C, 90 min Gelfiltration

In vitro-Affinitäten

Mittels Affinitätsstudien an verschiedenen Zellen (HMEC, PyMT, PyMTxhuMUC1, T47D) wurde spezifische Bindung des radiomarkierten Konjugats an TA-MUC1 untersucht (Abbildung 10). Mit über 15 % Bindung an der transgenen, humanes MUC1 exprimierenden Zelllinie PyMTxhuMUC1 wurde die Spezifizität des Antikörpers gegen TA-MUC1 belegt.

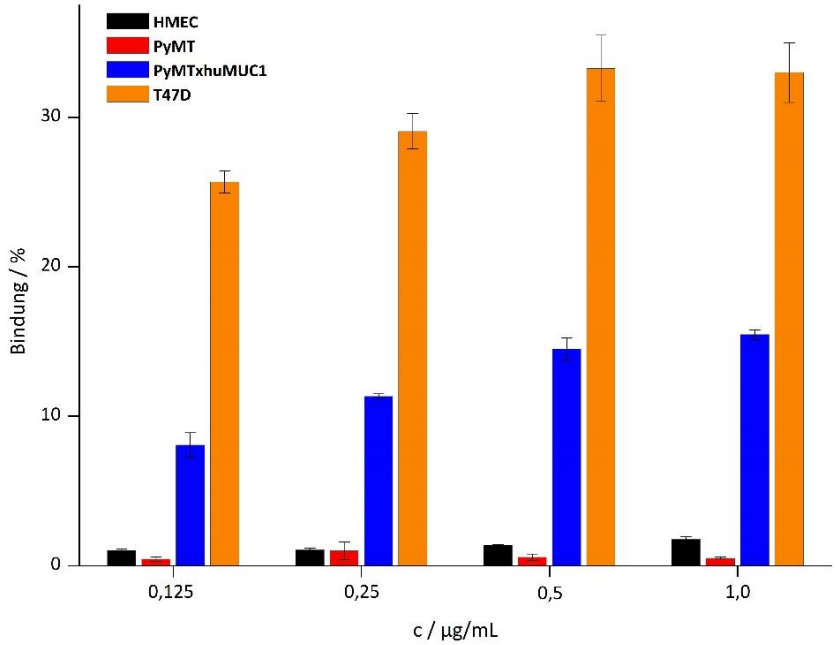

Abbildung 10: Zellbindungsprofile des [^{89}Zr]Zr-Df-Bz-NCS-mAk in Abhängigkeit von Zelllinie und Konjugatkonzentration

In vivo-Studien

Um das *in vivo*-Verhalten von [^{89}Zr]Zr-Df-Bz-NCS-mAk sowie die Spezifizität gegenüber TA-MUC1 zu untersuchen, wurde das Konjugat in tumortragenden Mäusen (PyMTxhuMUC1) appliziert und nach 72 h PET-Messungen sowie *ex vivo*-Biodistributionen durchgeführt. Sowohl PET- als auch *ex vivo*-Biodistribu-tionsstudien bestätigten die *in vitro*-Daten des Radioliganden durch spezifische Anreicherung im Tumorgewebe von über 50 %ID/g(Tumorgewebe) (Abbildung 11, links).

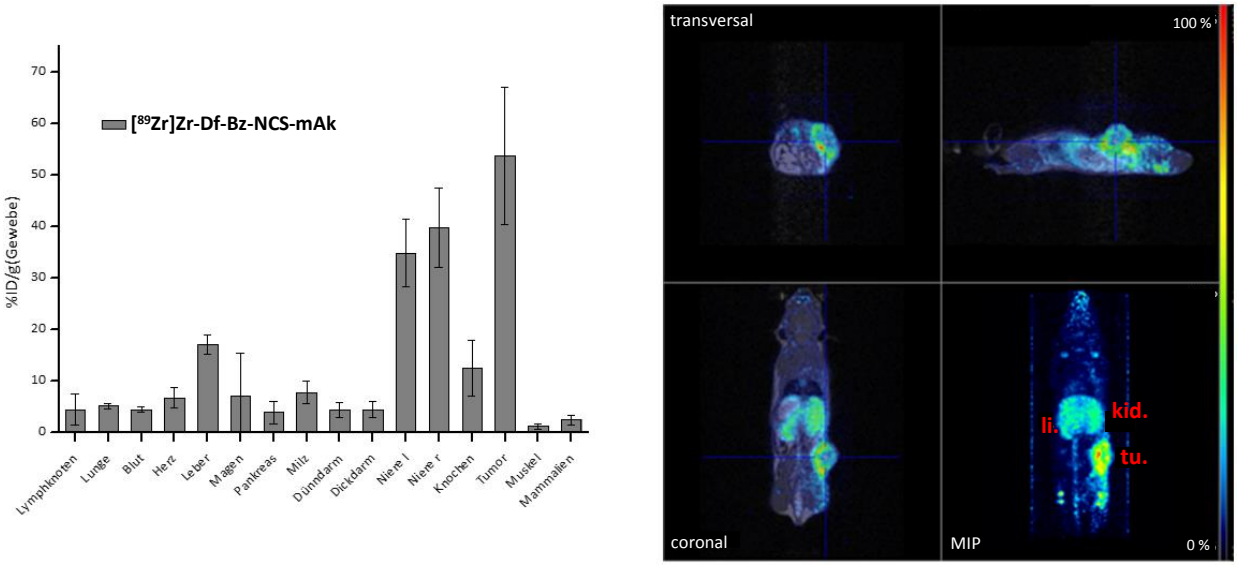

Abbildung 11: *ex vivo*-Biodistribution von [^{89}Zr]Zr-Df-Bz-NCS-mAb (links) und PET-Aufnahme nach 72 h p.i. in tumor-tragenden Mäusen (PyMTxhuMUC1); n=3, A=2,3 MBq (50 µg), tu: Tumor, kid: Niere, li: Leber

Die Studie zeigt die stabile und reproduzierbare Kopplung des bifunktionellen Chelator Df-Bz-NCS zur Radiomarkierung eines neuartigen Antikörpers mit dem Positronenemitter ^{89}Zr. Die hohe *in vitro*-Affinität als auch die hohe Spezifizität des radiomarkierten Konjugats Df-Bz-NCS-mAk gegenüber TA-MUC1 unterstreicht das hohe Potential von Df-Bz-NCS-mAk zur Tumordiagnostik, welche zudem durch erste präklinische Studien bestätigt wurde. Mit diesen Eigenschaften bietet der Antikörper GGSK-1/30 die Anwendung in ersten klinischen Studien für die Tumordiagnostik mittels PET als auch für erste Radioimmuntherapie-Ansätze.

Referenzen

1. Tei L., Gugliotta G., Fekete M., Kálmán F.K., Botta M. Mn(II) complexes of novel hexadentate AAZTA-like chelators: a solution thermodynamics and relaxometric study. Dalton Trans. 2011; 40(9): 2025–32.

2. Waldron B.P., Parker D., Burchardt C., Yufit D.S., Zimny M., Rösch F. Structure and stability of hexadentate complexes of ligands based on AAZTA for efficient PET labelling with gallium-68. Chem. Commun. 2013; 49: 579–81.

3. Parker D., Waldron B.P. Conformational analysis and synthetic approaches to polydentate perhydro-diazepine ligands for the complexation of gallium(iii). Org. Biomol. Chem. 2013; 11(17): 2827.

4. Parker D., Waldron B.P., Yufit D.S. Crystallographic and solution NMR structural analyses of four hexacoordinated gallium(III) complexes based on ligands derived from 6-amino-perhydro-1,4-diazepine. Dalton Trans. 2013; 42: 8001–8.

5. Baranyai Z., Uggeri F., Maiocchi A., Giovenzana G.B., Cavallotti C., Takács A., Tóth I., Bányai I., Bényei A., Brucher E., Aime S. Equilibrium, Kinetic and Structural Studies of AAZTA Complexes with Ga^{3+}, In^{3+} and Cu^{2+}. Eur. J. Inorg. Chem. 2013; (1): 147–62.

6. Boros E., Ferreira C.L., Cawthray J.F., Price E.W., Patrick B.O., Wester D.W., Adam M.J., Orvig C. Acyclic chelate with ideal properties for Ga-68 PET imaging agent elaboration. J. Am. Chem. Soc. 2010; 132(44): 15726–33.

7. Zhernosekov K.P., Filosofov D. V., Baum R.P., Aschoff P., Bihl H., Razbash A., Jahn M., Jennewein M., Rösch F. Processing of generator-produced Ga-68 for medical application. J. Nucl. Med. 2007; 48(10): 1741–8.

8. Müller D., Klette I., Baum R.P., Gottschaldt M., Schultz M.K., Breeman W.A.P. Simplified NaCl based Ga-68 concentration and labeling procedure for rapid synthesis of Ga-68 radiopharmaceuticals in high radiochemical purity. Bioconjug. Chem. 2012; 23(8): 1712–7.

9. Smith D.L., Breeman W.A.P., Sims-Mourtada J. The untapped potential of Gallium-68-PET: The next wave of Ga-68-agents. Appl. Radiat. Isot. 2013; 76: 14–23.

10. Eppard E., Wuttke M., Nicodemus P.L., Rosch F. Ethanol-Based Post-processing of Generator-Derived Ga-68 Toward Kit-Type Preparation of Ga-68-Radiopharmaceuticals. J Nucl Med. 2014; 55(6): 1023–8.

11. Price E.W., Orvig C. Matching chelators to radiometals for radiopharmaceuticals. Chem. Soc. Rev. 2014; 43(1): 260–90.

12. Seemann J., Waldron B.P., Rösch F., Parker D. Approaching “kit-type” labelling with Ga-68: The DATA chelators. ChemMedChem. 2015; 10(6): 1019–26.

13. Seemann J., Waldron B.P., Parker D., Rösch F. DATATOC: a novel conjugate for kit-type Ga-68 labelling of TOC at ambient temperature. EJNMMI Radiopharm. Chem. 2016; 1(1): 4.

14. Reubi J.C., Waser B., Schaer J.C., Laissue J.A. Somatostatin receptor sst1-sst5 expression in normal and neoplastic human tissues using receptor autoradiography with subtype-selective ligands. Eur. J. Nucl. Med. 2001; 28(7): 836–46.

15. Schmidt-Kreppel B., Plum T., Gärtner F. C., Eppard E., Sinnes J. P., Strunk H., Bundschuh R. A., Rösch F., Essler M. Biodistribution of [^{68}Ga]Ga-DATA-TOC in comparison with [^{68}Ga]Ga-DOTA-TOC in normal tissues and neuroendocrine tumour lessions, EANM 2017, accepted abstract (Poster)

16. Banerjee S., Pillai M.R.A., Ramamoorthy N. Evolution of Tc-99m in diagnostic radiopharmaceuticals. Semin. Nucl. Med. 2001; 31(4): 260–77.

17. Zolle I. Technetium-99m Pharmaceuticals. 2007.

18. Krenning E.P., Kooij P.P.M., Bakker W.H., Breeman W.A.P., Postema P.T.E., Kwekkeboom D.J., Oei H.Y., De Jong M., Visser T.J., Reijs A.E.M., Lamberts S.W.J. Radiotherapy with a radiolabeled somatostatin analogue, In-111-DTPA-[D-Phe1]-Octreotide. A case history. Ann. N. Y. Acad. Sci. 1994; 733: 496–506.

19. Valkema R., De Jong M., Bakker W.H., Breeman W.A.P., Kooij P.P.M., Lugtenburg P.J., De Jong F.H., Christiansen A., Kam B.L.R., De Herder W.W., Stridsberg M., Lindemans J., Ensing G., Krenning E.P. Phase I Study of Peptide Receptor Radionuclide Therapy With In-111-DTPA-Octreotide: The Rotterdam Experience. Semin. Nucl. Med. 2002; 32(2): 110–22.

20. Kwekkeboom D.J., Müller-Brand J., Paganelli G., Anthony L.B., Pauwels S., Kvols L.K., O'dorisio T.M., Valkema R., Bodei L., Chinol M., Mäcke H.R., Krenning E.P. Overview of results of peptide receptor radionuclide therapy with 3 radiolabeled somatostatin analogs. J Nucl Med. 2005; 46(1): 62S–66S.

21. De Jong M., Bernard B.F., De Bruin E., Van Gameren A., Bakker W.H., Visser T.J., Mäcke H.R., Krenning E.P. Internalization of radiolabelled [DTPA^{0}]octreotide and [DOTA^{0},Try^{3}]octreotide: Peptides for somatostatin receptor-trageted scintigraphy and radionuclide therapy. Nucl. Med. Commun. 1998; 19: 283–8.

22. Mausner L.F., Srivastava S.C. Selection of radionuclides for radioimmunotherapy. Med. Phys. 1993; 20(2): 503–9.

23. Goeckeler W.F., Edwards B., Volkert W.A., Holmes R.A., Simon J., Wilson D. Skeletal localization of samarium-153 chelates: potential therapeutic bone agents. J. Nucl. Med. 1987; 28(4): 495–504.

24. Ma D., Ketring A., Ehrhardt G., Jia W. Production of radiolanthanides and radiotherapy research at MURR. J. Radioanal. Nucl. Chem. 1996; (206): 119–26.

25. Das T., Banerjee S., Samuel G., Sarma H.D., Ramamoorthy N., Pillai M.R.A. Re-188-ethylene dicysteine: A novel agent for possible use in endovascular radiation therapy. Nucl. Med. Commun. 2000; 21(10): 939–45.

26. Pillai M.R.A., Chakraborty S., Das T., Venkatesh M., Ramamoorthy N. Production logistics of Lu-177 for radionuclide therapy. Appl. Radiat. Isot. 2003; 59(2–3): 109–18.

27. Baranyai Z., Uggeri F., Giovenzana G.B., Bényei A., Brücher E., Aime S. Equilibrium and kinetic properties of the lanthanoids(III) and various divalent metal complexes of the heptadentate ligand AAZTA. Chem. - A Eur. J. 2009; 15(7): 1696–705.

28. Aime S., Calabi L., Cavallotti C., Gianolio E., Giovenzana G.B., Losi P., Maiocchi A., Palmisano G., Sisti M. [Gd-AAZTA]$^{-}$: A new structural entry for an improved generation of MRI contrast agents. Inorg. Chem. 2004; 43(24): 7588–90.

29. Aime S., Bombieri G., Cavallotti C., Giovenzana G.B., Imperio D., Marchini N. An unusual gadolinium ten-coordinated dimeric complex in the series of MRI contrast agents: $Na[Gd(H_2O)AAZTA]_3H_2O$. Inorganica Chim. Acta. 2008; 361(5): 1534–41.

30. Manzoni L., Belvisi L., Arosio D., Bartolomeo M.P., Bianchi A., Brioschi C., Buonsanti F., Cabella C., Casagrande C., Civera M., De Matteo M., Fugazza L., Lattuada L., Maisano F., Miragoli L., Neira C., Pilkington-Miksa M., Scolastico C. Synthesis of Gd and Ga-68 Complexes in Conjugation with a Conformationally Optimized RGD Sequence as Potential MRI and PET Tumor-Imaging Probes. ChemMedChem. 2012; 7(6): 1084–93.

31. Pfister J., Summer D., Rangger C., Petrik M., von Guggenberg E., Minazzi P., Giovenzana G.B., Aloj L., Decristoforo C. Influence of a novel, versatile bifunctional chelator on theranostic properties of a minigastrin analogue. EJNMMI Res. 2015; 5(1): 74.

32. Wu Z., Zha Z., Choi S.R., Plössl K., Zhu L., Kung H.F. New Ga-68-PhenA bisphosphonates as potential bone imaging agents. Nucl. Med. Biol. 2016; 43(6): 360–71.

33. Nagy G., Szikra D., Trencsényi G., Fekete A., Garai I., Giani A.M., Negri R., Masciocchi N., Maiocchi A., Uggeri F., Tóth I., Aime S., Giovenzana G.B., Baranyai Z. AAZTA: An Ideal Chelating Agent for the Development of Sc-44 PET Imaging Agents. Angew. Chemie Int. Ed. 2017; 56: 2118–22.

34. Wu A.M., Senter P.D. Arming antibodies: prospects and challenges for immunoconjugates. Nat. Biotechnol. 2005; 23(9): 1137–46.

35. Parker D. Tumour targeting with radiolabelled macrocycle-antibody conjugates. Chem. Soc. Rev. 1990; 19(3): 271–91.

36. Verel I., Visser G.W.M., Boerman O.C., van Eerd J.E.M., Finn R., Boellaard R., Vosjan M.J.W.D., Stigter-van Walsum M., Snow G.B., Van Dongen G.A.M.S. Long-lived positron emitters zirconium-89 and iodine-124 for scouting of therapeutic radioimmunoconjugates with PET. Cancer Biother. Radiopharm. 2003; 18(4): 655–61.

37. Philpott G.W., Schwarz S.W., Anderson C.J., Dehdashti F., Connett J.M., Zinn K.R., Meares C.F., Cutler P.D., Welch M.J., Siegel B.A. RadioimmunoPET: detection of colorectal carcinoma with positron-emitting copper-64-labeled monoclonal antibody. J. Nucl. Med. 1995; 36(10): 1818–24.

38. Jurek P., Corbett R.J. Bifunctional hydroxamix acid ligands and method of synthesis. 2008. p. 26.

39. Perk L.R., Vosjan M.J.W.D., Visser G.W.M., Budde M., Jurek P., Kiefer G.E., Van Dongen G.A.M.S. P-Isothiocyanatobenzyl-desferrioxamine: A new bifunctional chelate for facile radiolabeling of monoclonal antibodies with zirconium-89 for immuno-PET imaging. Eur. J. Nucl. Med. Mol. Imaging. 2010; 37(2): 250–9.

40. Hanisch F.G. O-glycosylation of the mucin type. Biol. Chem. 2001; 382(2): 143–9.

41. Taylor-Papadimitriou J., Burchell J., Miles D.W., Dalziel M. MUC1 and cancer. Biochim. Biophys. Acta - Mol. Basis Dis. 1999; 1455(2–3): 301–13.

42. Brockhausen I., Yang J.-M., Burchell J., Whitehouse C., Taylor-Papadimitriou J. Mechanisms Underlying Aberrant Glycosylation of MUC1 Mucin in Breast Cancer Cells. Eur. J. Biochem. 1995; 233(2): 607–17.

43. Palitzsch B., Hartmann S., Stergiou N., Glaffig M., Schmitt E., Kunz H. A fully synthetic four-component antitumor vaccine consisting of a mucin glycopeptide antigen combined with three different T-helper-cell epitopes. Angew. Chemie - Int. Ed. 2014; 53(51): 14245–9.

44. Kunz H., Hartmann S., Palitzsch B. Impfung gegen Tumore? Labor&More. 2012; 6: 16–25.

45. Gaidzik N., Westerlind U., Kunz H. The development of synthetic antitumour vaccines from mucin glycopeptide antigens. Chem. Soc. Rev. 2013; 42(10): 4421–42.

6. Ausblick

Die Entwicklung neuer Liganden für die Komplexierung relevanter Radiometalle ist ein stetig wachsender Bereich in der Entwicklung von Radiopharmaka, welche in der Diagnostik als auch in der Radiotherapie ein wichtiges Werkzeug für onkologische Fragestellungen sind.

Ein Hauptziel für die in dieser Arbeit etablierten Liganden DATA^{5m} und AAZTA^{5} sollte die Kopplung an weitere Targetingstrukturen analog zum DATA-TOC sein. Die Ligand-Targetingvektor-Systeme sollten hinsichtlich ihrer Radiomarkierungs- sowie *in vitro*- und *in vivo*-Eigenschaften evaluiert und mit bekannten DOTA-und NOTA-Systemen verglichen werden. Um das Anwendungsspektrum des DATA-Chelator im Hinblick auf die Radiometalle auszuweiten, sollte die hohe Komplexstabilität des Cu-Komplex des DATA^{5m} genutzt werden, um das Potential des Liganden für die Markierung mit ^{64}Cu zu untersuchen. Die hohe Stabilität des AAZTA-Liganden mit dem Positronenemitter ^{44}Sc sollte für diesen Chelator ebenfalls berücksichtigt werden [1]. Die Verwendung des PET-Nuklids ^{44}Sc als auch des Therapienuklids ^{177}Lu ermöglichen somit den Einsatz eines AAZTA-basierenden Radiopharmakons für den theranostischen Einsatz.

Weitere Ziele für den in dieser Arbeit verwendeten Antikörper GGSK-1/30 sollten die Vervollständigung der Biodistributionsaufnahmen nach 24 h und 48 h sein, um ein Gesamtbild über die exakte Pharmakokinetik des radiomarkierten Konjugats Df-Bz-NCS-GGSK-1/30 zu erhalten. Zudem soll AAZTA^{5}-en-QS als Komplexbildner für ^{177}Lu am Antikörper angekoppelt und hinsichtlich seiner *in vitro*- und *in vivo*-Charakteristik untersucht werden. Als übergeordnetes Ziel für diese Verbindung ist die klinische Anwendung zur Diagnostik von Mammakarzinomen mittels ImmunoPET.

Referenzen

1. Nagy G., Szikra D., Trencsényi G., Fekete A., Garai I., Giani A.M., Negri R., Masciocchi N., Maiocchi A., Uggeri F., Tóth I., Aime S., Giovenzana G.B., Baranyai Z. AAZTA: An Ideal Chelating Agent for the Development of Sc-44 PET Imaging Agents. Angew. Chemie Int. Ed. 2017; 56: 2118–22.

Abkürzungsverzeichnis

α	Alpha-Zerfall
β	Beta-Zerfall
γ	Gamma-Quant
δ	chemische Verschiebung
v_e	Elektronneutrino
°C	Grad Celcius
µL	Microliter
Å	Angström
ACN	Acetonitril
AmOAc	Ammoniumacetat
BFC	bifunktioneller Chelator
CBS	Chelator-Biomolekül-System
$CDCl_3$	Deuterochloroform
$CHCl_3$	Chloroform
CT	Computertomographie
d	Tag
d	dublett (Spektroskopie)
DCM	Dichlormethan
Df	Desferrioxamin
DIEA	Diisopropylethylendiamin
DOTA	1,4,7,10-tetraazacyclododecan-1,4,7,10-tetraessigsäure
DTPA	Diethylentriaminpentaacetat
EA	Ethylacetat
EDC·HCl	1-Ethyl-3-(3-dimethylaminopropyl) carbodiimid hydrochlorid
EDTA	Ethylendiamintetraacetat
EtOH	Ethanol
$E_{\beta,max}$	Maximale Energie des Positrons
g	Gramm
h	Stunde
H	Hexan (Chromatographie)
H/H^+	Proton (Spektroskopie)
H_2	elemtarer Wasserstoff
HATU	[*O*-(7-Azabenzotriazol-1-yl)-*N*,*N*,*N*′,*N*′-< tetramethyluronium-hexafluorphosphat]
HCl	Salzsäure
HOBt	1-Hydroxybenzotriazol
HPLC	High performance liquid chromatography
Hz	Hertz
IC_{50}	mittlerer inhibitorische Konzentration
J	Kopplungskonstante
K	Gleichgewichtskonstante
kDa	Kilodalton
keV	Kiloelektronenvolt
LiOH	Lithiumhydroxid
M	Molar
m	multiplett (Spektroskopie)
MBq	Megabequerel
MeOH	Methanol
MeV	Megaelektronenvolt
mg	Milligramm
MHz	Megahertz
min	Minute
mL	Milliliter
mM	Millimolar
mm	Millimeter
mmol	Millimol
MRT	Magnetresonanztomographie
MS	Massenspektrum
N	Neutronenzahl
n. c. a.	Trägerfrei (*non carrier added*)
$n/cm^2/s$	Neutronenfluss in Neutronen in der Sekunde pro Kubizentimter

NaOAc	Natriumacetat
NaOH	Natriumhydroxid
nM	Nanomolar
nmol	Nanomol
NMR	Kernspinresonanzspektroskopie
NOTA	1,4,7-triaza-cyclo-nonane-1,4,7-triessigsäure
p. i.	post injection
Pd/C	Palladium auf Aktivkohle
PET	Positronenemssionstomographie
ppm	parts per million
PRRT	Peptidvermittelte Radiorezeptortherapie
Q	Zerfallsenergie
R_f	retarding-front; Laufstrecke einer Substanz
RT	Raumtemperatur
s	Sekunde
s	singulett (Spektroskopie)
$SCCl_2$	Thiophosgen
SPECT	Einzelphotonenemssionscomputertomographie (*single photon emission computed tomography)*
SUV	standard uptake value
t triplett	(Spektroskopie)
TEA	Triethylamin
TFA	Trifluoressigsäure
TLC	Thin-Layer-Chromatography; Dünnschichtchromatographie
t_R	Retentioinszeit
TRAP	1,4,7-triazacyclononan-1,4,7-tris [methyl(2-carboxyethyl)phosphinsäure]
vol%	Volumenprozent
Z	Ordnungszahl

Danksagung

[redacted]

Eidesstattliche Erklärung

Die vorliegende Arbeit wurde unter der Anleitung von Univ. Prof. Dr. Frank Rösch in der Zeit vom 01.09.2013 bis zum 01.07.2017 am Institut für Kernchemie der Johannes Gutenberg-Universität durchgeführt. Ich versichere, dass ich die Arbeit selbst durchgeführt und keine anderen als die in der Dissertation angegebenen Hilfsmittel und Quellen verwendet habe.

Johannes Nagel